



Universität Hamburg
DER FORSCHUNG | DER LEHRE | DER BILDUNG

Efficient Routes to Double Thermoresponsive Polymers and Degradable Hydrogels

Dissertation

in conformity with the requirements for the degree of
Doctor rerum naturalium (Dr. rer. nat)
submitted to Universität Hamburg

—

Faculty of Mathematics, Informatics, and Natural Sciences

—

Department of Chemistry

submitted by
Jingcong Xu

Hamburg, 2022

Supervisor:	Prof. Dr. Volker Abetz
1 st Referee:	Prof. Dr. Volker Abetz
2 nd Referee:	Prof. Dr. Horst Weller

Defense Committee:
Prof. Dr. Volker Abetz
Prof. Dr. Michael Steiger
Priv. Doz. Dr. Christoph Wutz

Date of Oral Defense: 15.07.2022

The study was conducted between February 2019 and April 2022 under the supervision of Prof. Dr. Volker Abetz at the Institute of Physical Chemistry, Universität Hamburg.

List of Publications

This cumulative dissertation includes three first-author publications. These publications are reprinted in the original form in Chapter 3.

1) Nonionic UCST-LCST Diblock Copolymers with Tunable Thermoresponsiveness Synthesized via PhotoRAFT Polymerization.

Jingcong Xu and Volker Abetz

Macromol. Rapid Commun. **2021**, *42*, 2000648.

DOI: 10.1002/marc.202000648

2) Double thermoresponsive graft copolymers with different chain ends: feasible precursors for covalently crosslinked hydrogels.

Jingcong Xu and Volker Abetz

Soft Matter **2022**, *18*, 2082–2091.

DOI: 10.1039/d1sm01692j

3) Synthesis of a Degradable Hydrogel Based on a Graft Copolymer with Unexpected Thermoresponsiveness.

Jingcong Xu and Volker Abetz

Macromol. Chem. Phys. **2022**, 2200058.

DOI: 10.1002/macp.202200058

Contents

Abbreviations	v
Constants and Variables	ix
Units	xi
Zusammenfassung	1
Abstract	3
Chapter 1 Introduction	5
1.1 Theoretical Background of Thermoresponsive Polymers	7
1.1.1 LCST / UCST / Cloud Points: a Terminology Issue.....	7
1.1.2 Flory-Huggins-Staverman Theory.....	9
1.1.3 Interactions in Aqueous Solutions	11
1.1.4 Summary.....	14
1.2 Synthesis of Different Chain Architectures.....	15
1.2.1 Photoiniferter RAFT Polymerization – New Roles for CTA.....	17
1.2.2 Random / Alternating / Gradient Copolymers	19
1.2.3 Block Copolymers	23
1.2.4 Graft Copolymers.....	25
1.2.5 Summary.....	27
1.3 Routes to Hydrogels.....	28
1.3.1 Physically Crosslinked Hydrogels	28
1.3.2 Chemically Crosslinked Hydrogels	30
1.3.3 Summary.....	35

1.4	Recent Advances in “Smart” Polymers	36
1.4.1	Copolymers with Tunable Cloud Points	36
1.4.2	Double Thermoresponsive Copolymers	37
1.4.3	“Smart” Hydrogels	40
1.4.4	Summary	41
	Chapter 2 Goals of The Work	43
	Chapter 3 Cumulative Part	45
3.1	Publication 1: Nonionic UCST–LCST Diblock Copolymers with Tunable Thermoresponsiveness Synthesized via PhotoRAFT Polymerization	45
3.2	Publication 2: Double Thermoresponsive Graft Copolymers with Different Chain Ends: Feasible Precursors for Covalently Crosslinked Hydrogels	53
3.3	Publication 3: Synthesis of a Degradable Hydrogel Based on a Graft Copolymer with Unexpected Thermoresponsiveness	65
	Chapter 4 Unpublished Results	77
4.1	Investigations on PMMA- <i>b</i> -POEGMA	77
4.1.1	Screening the Reaction Conditions	78
4.1.2	Synthesis of PMMA- <i>b</i> -POEGMA	83
4.1.3	Thermoresponsive Behavior of PMMA- <i>b</i> -POEGMA	84
4.1.4	Experimental Section	85
4.2	Solution Behavior of PNAGA	87
4.2.1	Synthesis of PNAGA	87
4.2.2	PNAGA Aqueous Solutions	88
4.2.3	Experimental Section	90
4.3	Influence of the End-group: Further Investigations	92

4.3.1	POEGMAs with Different Chain Ends	92
4.3.2	Experimental Section	95
Chapter 5 Discussion		97
5.1	Review of the Investigated Polymers	97
5.2	Outlook	99
Chapter 6 References		101
Chapter 7 Appendix		111
7.1	Author Contributions to the Publications	111
7.2	Supporting Information of Publication 1	113
7.3	Supporting Information of Publication 2	133
7.4	Supporting Information of Publication 3	143
7.5	Used Hazardous Substances According to GHS	155
Chapter 8 Acknowledgements		161
Chapter 9 Declaration on Oath		163

Abbreviations

AA	acrylic acid
AAm	acrylamide
AIBN	azobisisobutyronitrile
AN	acrylonitrile
ATRP	atom-transfer radical polymerization
APi	<i>N</i> -acryloylpiperidine
APy	<i>N</i> -acryloylpyrrolidine
- <i>b</i> -	- <i>block</i> -
BTPA	2-(<i>n</i> -butyltrithiocarbonate)propionic acid
BTPEMA	2-(2-(<i>n</i> -butyltrithiocarbonate)propionate)ethyl methacrylate
CDCl ₃	deuterated chloroform
CDTPA	4-cyano-4- [(dodecylsulfanylthiocarbonyl)sulfanyl]pentanoic acid
CMAM	<i>N</i> -cyanomethylacrylamide
- <i>co</i> -	- <i>copolymer</i> -
CPADB	4-cyanopentanoic acid dithiobenzoate
CPDTC	2-cyano-2-propyl dodecyl trithiocarbonate
CTA	chain transfer agent
DLS	dynamic light scattering
DMA	<i>N,N</i> -dimethylacrylamide
DMAEMA	<i>N,N</i> -(dimethylamino) ethyl methacrylate
DMF	<i>N,N</i> -dimethylformamide
DMSO	dimethyl sulfoxide
D ₂ O	deuterium oxide
DOX	1,4-dioxane
DP	degree of polymerization
DTP	2,2'-dithiodipyridine
DTT	dithiothreitol
e.g.	exempli gratia

et al.	et alia
FHS theory	Flory-Huggins-Staverman theory
FRP	free-radical polymerization
-g-	-graft-
HEMA	2-hydroxyethyl methacrylate
i.e.	id est
LAM	less activated monomer
LCST	lower critical solution temperature
LED	light-emitting diode
MAAm	methacrylamide
MAM	more activated monomer
MCDTP	methyl 4-cyano-4-(dodecylthiocarbonothioylthio)pentanoate
MEO ₂ MA	di(ethylene glycol) methyl ether methacrylate
MMA	methyl methacrylate
NAGA	<i>N</i> -acryloylglycinamide
NIPAM	<i>N</i> -isopropylacrylamide
¹ H-NMR	proton nuclear magnetic resonance
NMP	nitroxide-mediated polymerization
OEGMA	oligo(ethylene glycol) methacrylate
PAPy	poly(<i>N</i> -acryloylpyrrolidin)
PBA	poly(butyl acrylate)
PCMAm	poly(<i>N</i> -cyanomethylacrylamide)
PDMA	poly(<i>N,N</i> -dimethylacrylamide)
PDMAEMA	poly[<i>N,N</i> -(dimethylamino) ethyl methacrylate]
PDS	pyridyl disulfide
PEG	poly(ethylene)glycol
PET-RAFT	photoinduced electron/energy transfer-reversible addition-fragmentation chain transfer
PISA	polymerization-induced self-assembly
PMA	poly(methyl acrylate)
PMAAm	polymethacrylamides
PMEMA	poly[2-(<i>N</i> -morpholino)ethyl methacrylate]
PMEO ₂ MA	poly[di(ethylene glycol) methyl ether methacrylate]
PMMA	poly(methyl methacrylate)

PNAGA	poly(<i>N</i> -acryloyl)glycinamide)
PNIPAM	poly(<i>N</i> -isopropylacrylamide)
POEGMA	poly[oligo(ethylene glycol) methacrylate]
PPEGMMA	poly[poly(ethylene glycol) methyl ether methacrylate]
PS	polystyrene
- <i>r</i> -	- <i>random</i> -
RAFT	reversible addition–fragmentation chain transfer
RDRP	reversible-deactivation radical polymerization
RI	refractive index
SEC	size exclusion chromatography
Sol-gel	solution-to-gel
TCEP	tris(2-carboxyethyl)phosphine
THF	tetrahydrofuran
TTC-group	trithiocarbonate-groups
UCST	upper critical solution temperature
UV	ultraviolet
UV–vis	ultraviolet–visible

Constants and Variables

α	monomer conversion
c	concentration
\bar{D}	dispersity
f	mole fraction of comonomer in a mixture
F	mole fraction of comonomer in a copolymer
ϕ	volume fraction
ΔG_m	Gibbs free energy of mixing
ΔG_m^{cont}	contact Gibbs free energy change
ΔH_m	enthalpy of mixing
k	rate coefficient
\bar{M}_n	number average molecular weight
$\bar{M}_{n,\text{SEC}}$	number average molecular weight determined by SEC
n	number of moles
r	monomer reactivity ratio
R	ideal gas constant
R_H	hydrodynamic radius
ΔS_m	entropy of mixing
ΔS_m^{comb}	combinatorial entropy change
t	time
T	temperature
T_C	critical temperature
T_{CP}	cloud point
T_g	glass transition temperature
T_{PT}	phase transition temperature
w	interaction energy
Δw	interaction energy change
χ	interaction parameter
χ_H	enthalpic part of the interaction parameter
χ_S	entropic part of the interaction parameter

Units

°C	degree Celsius
Da	dalton
g	gram
h	hour
Hz	hertz
L	liter
m	meter
M	molar
min	minute
W	watt
% (w/w)	weight percent

Zusammenfassung

Polymerketten mit doppelter Thermoresponsivität sind in der Lage, ihre Affinität zu Lösungsmitteln bei steigender oder fallender Temperatur zweimal zu wechseln. Dank ihres hochwertigen Selbstorganisationsverhaltens in Lösungen sind diese Polymere attraktiv für Anwendungen wie Sensoren oder "intelligente" Aktoren. Die Polymere, die in wässrigen Lösungen eine doppelte Thermoresponsivität aufweisen, sind auch für biomedizinische Anwendungen wie die kontrollierte Freisetzung von Medikamenten und das *tissue engineering* interessant. In dieser Arbeit wird die Synthese und Charakterisierung neuer doppelt thermoresponsiver Polymere mit unterschiedlichen Kettenzusammensetzungen und Architekturen vorgestellt. Darüber hinaus können durch intelligentes Design der Kettenstrukturen multifunktionale Hydrogele effizient hergestellt werden.

Der erste Teil der Arbeit befasst sich mit den Diblockcopolymeren, die in reinem Wasser sowohl einen *upper critical solution temperature* (UCST)- als auch einen *lower critical solution temperature* (LCST)-Phasenübergang aufweisen. Der UCST-Block mit einem Trübungspunkt (T_{CP}) bei etwa 40 °C besteht aus einem kommerziell verfügbaren Monomer, Methacrylamid (MAAm). Der LCST-Block ist ein statistisches Copolymer aus Methacrylsäure-[2-(methoxyethoxy)-ethylester] (MEO₂MA) und Oligo(ethylenglykol)-methylether-methacrylat (OEGMA). Sein T_{CP} ist höher als der des UCST-Blocks und kann durch Änderung des molaren Verhältnisses zwischen MEO₂MA und OEGMA flexibel eingestellt werden. Die Herstellung der Diblockcopolymeren erfolgt durch kosteneffiziente *reversible addition-fragmentation chain transfer* (RAFT) Polymerisation, welche durch grünes Licht initiiert wird. Die analytischen Ergebnisse deuten darauf hin, dass die Diblockcopolymeren in wässrigen Lösungen mit steigender Temperatur einen reversiblen amphiphilen-hydrophilen-amphiphilen Übergang zeigen.

Im zweiten Teil der Arbeit werden thermoresponsive Graftcopolymeren, Poly(OEGMA)-*graft*-poly(*N*-isopropylacrylamid) (POEGMA-*g*-PNIPAM) durch einfache photoinitierte RAFT Polymerisation synthetisiert. Die beiden Komponenten zeigen LCST-Verhalten in Wasser und die Graftcopolymeren zeigen

entsprechend zwei getrennte T_{CP} s. Das POEGMA-Rückgrat, welches mit grüner Lichtbestrahlung polymerisiert wird, bewirkt eine höhere T_{CP} . Die PNIPAM-Seitenketten, die mit blauer Lichtbestrahlung polymerisiert werden, bewirken eine zweite niedrigere T_{CP} . Daher kollabieren die Seitenketten beim Erhitzen zuerst, was zur Bildung von blumenartigen Mizellen führt. Aufgrund der starken intramolekularen Wechselwirkungen in den Graftcopolymeren ist die Aggregationszahl der gebildeten Mizellen allerdings signifikant begrenzt. Darüber hinaus hat die Endgruppe am α -Ende des Rückgrats einen großen Einfluss auf das Selbstorganisationsverhalten der Polymere in verdünnten Lösungen. Eine einzelne hydrophile Carboxylgruppe am Kettenende behindert die Agglomeration von Mizellen erheblich, selbst wenn sowohl das Rückgrat als auch die Seitenketten oberhalb der zweiten T_{CP} hydrophob werden.

Zum Vergleich wird ein weiteres Graftcopolymer, Poly(MEO₂MA)-*graft*-poly(*N,N*-dimethylacrylamid) (PMEO₂MA-*g*-PDMA), in dieser Arbeit präsentiert. Im Gegensatz zu POEGMA-*g*-PNIPAM bildet PME₂O₂MA-*g*-PDMA sternförmige Mizellen oberhalb der ersten T_{CP} , die durch das PME₂O₂MA-Rückgrat bedingt ist. Die Stabilität der Mizellen in der Lösung hängt vom Gleichgewicht zwischen hydrophobem Rückgrat und hydrophilen Seitenketten ab. Das Gleichgewicht wird durch die weitere Erhöhung der Temperatur gestört, was zu einer weiteren Aggregation von Mizellen und der zweiten T_{CP} führt. Deshalb ist das Graftcopolymer auch doppelt thermoresponsive, obwohl das Homopolymer PDMA bei Normaldruck sehr gut wasserlöslich und nicht thermoresponsiv ist.

Zusätzlich zu den freien Polymerketten befasst sich diese Arbeit mit der effizienten Synthese von thermoresponsiven Hydrogelen. Aufgrund der photoinitierten RAFT Polymerisation besitzt jede Kette der präsentierten Graftcopolymere mehrere thiocarbonylthiohaltige Endgruppen. Durch Aminolyse in Gegenwart von 2,2'-Dithiodipyridin (DTP) können diese Endgruppen direkt in thiolreaktive Pyridyldisulfid (PDS)-Gruppen umgewandelt werden. Dies ermöglicht es einzelne Polymerketten unter milden Bedingungen über eine Dithiobindung miteinander zu vernetzen. Die Netzpunkte des erhaltenen thermoresponsiven Hydrogels können aufgrund der Redoxsensitivität der Disulfidbindungen bei Raumtemperatur wieder gespalten werden. Die Multifunktionalität kann die Attraktivität der Hydrogele für biomedizinische Anwendungen wie zum Beispiel kontrollierte Wirkstofffreisetzung.

Abstract

Polymer chains with double thermoresponsiveness are able to switch their affinity for solvents twice as the temperature rises or drops. Thanks to their sophisticated self-assembling behavior in solutions, these polymers are attractive for applications like sensors or “smart” actuators. The polymers exhibiting double thermoresponsiveness in aqueous solutions are also intriguing for biomedical applications, such as controlled drug release and tissue engineering. This work presents the synthesis and characterization of new double thermoresponsive polymers with different chain compositions and architectures. Moreover, thanks to the rational design of the chain structures, multifunctional hydrogels can be efficiently prepared with these thermoresponsive polymers as precursors.

The first part of the thesis focuses on the diblock copolymers showing both upper critical solution temperature (UCST) and lower critical solution temperature (LCST) phase transitions in pure water. The UCST block with a cloud point (T_{CP}) at around 40 °C consists of a commercially available monomer, methacrylamide (MAAm). The LCST block is a random copolymer of di(ethylene glycol) methyl ether methacrylate (MEO₂MA) and oligo(ethylene glycol) methacrylate (OEGMA). Its T_{CP} is higher than that of the UCST block and can be flexibly adjusted by changing the molar ratio between MEO₂MA and OEGMA. The preparation of the diblock copolymers is accomplished through cost-effective photoiniferter reversible addition–fragmentation chain transfer (RAFT) polymerization mediated by green light irradiation. The analytical results suggest that the diblock copolymers undergo a reversible amphiphilic-hydrophilic-amphiphilic transition in aqueous solutions.

In the second part, double thermoresponsive graft copolymers, poly(OEGMA)-*graft*-poly(*N*-isopropylacrylamide) (POEGMA-*g*-PNIPAM), with two separate LCST-type T_{CP} s in water are synthesized through photoiniferter RAFT. The POEGMA backbone polymerized under green light irradiation results in the higher T_{CP} , while the PNIPAM side chains polymerized under blue light irradiation are responsible for the lower T_{CP} . Therefore, the side chains collapse first during heating, leading to the formation of flower-like micelles. Due to the unique

intramolecular interactions in the graft copolymers, the aggregation number of the formed micelles is restrained and the hydrodynamic radii are thus relatively small. The end-group at the α -terminal of the backbone has an immense impact on the polymers' self-assembling behaviors in dilute solutions. A single hydrophilic carboxyl group at the chain end hinders the agglomeration of micelles significantly even when the backbone and side chains both become hydrophobic above the second LCST-type T_{CP} .

For comparison, another graft copolymer, poly(MEO₂MA)-*graft*-poly(*N,N*-dimethylacrylamide) (PMEO₂MA-*g*-PDMA), is presented in this thesis. Unlike POEGMA-*g*-PNIPAM, PMEO₂MA-*g*-PDMA forms star-like micelles in water above the first T_{CP} caused by the PMEO₂MA backbone. The stability of the micelles in the solution depends on the balance between hydrophobic PMEO₂MA backbones and hydrophilic PDMA side chains. The balance can be disrupted by the further increase of temperature, leading to another aggregation of micelles and the emergence of the second LCST-type T_{CP} . The graft copolymer is thus also double thermoresponsive, although the homopolymer PDMA is excellently water-soluble and not thermoresponsive at normal pressure,

In addition to free polymer chains, this work also includes thermoresponsive hydrogels that are efficiently synthesized. Benefitting from the photoiniferter RAFT approach, every side chain of the presented graft copolymers in this thesis possesses a thiocarbonylthio-containing end-group. Through aminolysis in the presence of 2,2'-dithiodipyridine (DTP), those end-groups can be directly converted into thiol reactive pyridyl disulfide (PDS) groups, enabling crosslinking with a dithiol based crosslinker under mild conditions. The obtained thermoresponsive hydrogel can undergo redox-sensitive degradation at room temperature due to the disulfide linkages, which may enhance its versatility in biomedical applications, such as controlled drug delivery.

Chapter 1

Introduction

Thermoresponsive polymers are capable of changing their physicochemical properties rapidly in response to temperature variations. This thesis discusses thermoresponsive polymer chains showing rapid, reversible phase transitions in aqueous solutions. The thermoresponsive behaviors can be divided into two types. The polymer chains with a lower critical solution temperature (LCST) turn from a hydrophilic into a hydrophobic state upon heating. In contrast, those polymers becoming hydrophilic upon heating exhibit an upper critical solution temperature (UCST).

As the most comprehensively investigated thermoresponsive polymer, poly(*N*-isopropylacrylamide) (PNIPAM) was reported to show thermoresponsiveness in an aqueous solution for the first time in 1967.^[1] In the following decades, its promising LCST-type phase transition temperature (about 32 °C) close to body temperature helped PNIPAM establish a vital status in the field of biomedical applications, such as drug delivery and tissue engineering.^[2-6] However, its potential depolymerization under physiological conditions and the relatively toxic monomer may hamper the translation of research output into practice.^[7] These drawbacks of PNIPAM have motivated polymer scientists worldwide to endeavor to modify the properties of PNIPAM-containing materials or seek alternatives. Compared with LCST polymers, UCST polymers are studied for a shorter time. The first molecular-level study on a hydrogen bonding-based UCST polymer was conducted in 2018.^[8] Due to the shorter history plus their high sensitivity in pure water (see Section 1.1.3), less application-oriented research about UCST polymers exists and more explorations are required.^[9]

With the advent of various living/controlled radical polymerization techniques, such as nitroxide-mediated polymerization (NMP), atom-transfer radical

polymerization (ATRP), and reversible addition–fragmentation chain transfer polymerization (RAFT), the research area of thermoresponsive materials expanded easily from homopolymers to copolymers with more complex compositions and architectures. Different kinds of copolymers, such as random, block, and graft copolymers, can now be synthesized more conveniently (see Section 1.2), promoting the design of more sophisticated thermoresponsive properties, including double thermoresponsiveness studied in this work.^[10-20] The access to well-defined polymer chains also benefits the synthesis of “smart” hydrogels (see Section 1.3). A quick search in “Web of Science” with the keywords “thermoresponsive polymer” and “temperature responsive polymer” unveils the thriving research activities regarding these materials in the past two decades (**Figure 1**). Various double thermoresponsive polymers are also covered in many of these publications (see Section 1.4.2).

In this work, three publications in Chapter 3 demonstrate the synthesis and distinct properties of thermoresponsive polymers with different compositions and architectures, including free chains and networks. The theoretical background related to these publications is explained in the following sections.

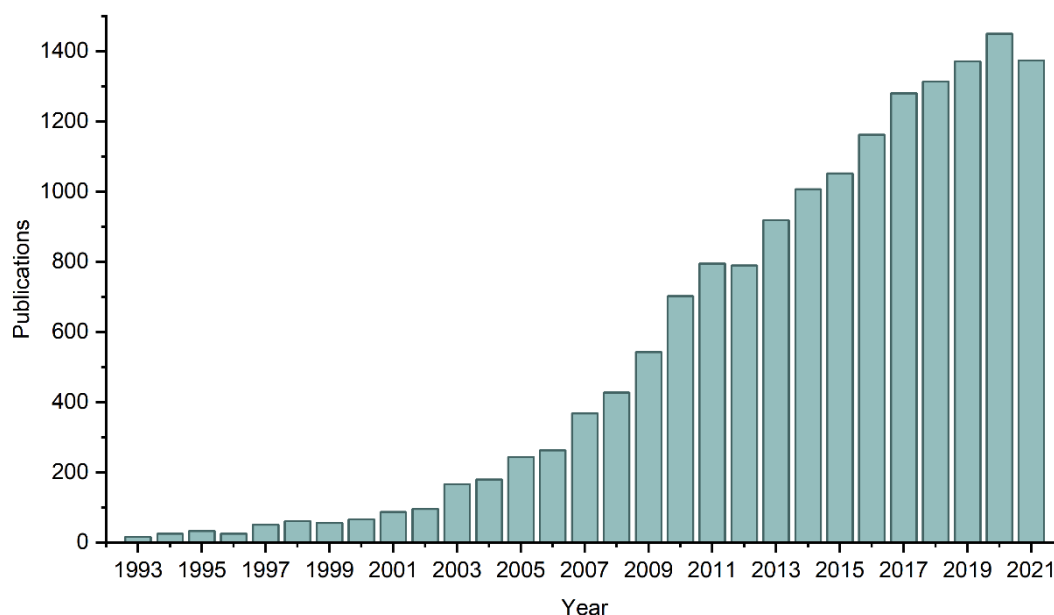


Figure 1. The number of publications about thermoresponsive and temperature responsive polymers from 1993 to 2021 (Web of Science).

1.1 Theoretical Background of Thermoresponsive Polymers

1.1.1 LCST / UCST / Cloud Points: a Terminology Issue

Figure 2 shows two simplified experimentally determined phase transition curves of polymer solutions exhibiting LCST- and UCST-type behaviors. The common methods for measuring these miscibility gaps include turbidimetry and light scattering. The orange dots represent the temperatures called LCST-type cloud points (T_{CP}) below which the polymer–solvent system is considered miscible at specific concentrations, while the blue dots denote the UCST-type T_{CP} above which the system is miscible. As the phase transitions do not necessarily cause cloudiness, T_{CP} is sometimes also called phase transition temperature (T_{PT}) in research. For simplicity, this chapter will treat these two terms equally and only mention T_{CP} in the following text.

In scientific reports, the distinction between the terms “ T_{CP} ” and “LCST” or “UCST” deserves proper attention. According to the theoretical phase diagrams of polymer solutions, LCST is generally defined as the critical temperature (T_C) corresponding to the intersection point (or common minimum) of the binodal and spinodal curves (**Figure 3**).^[21] The polymer solution is metastable between the binodal and spinodal curves. Below LCST, the polymer–solvent system exhibits one phase independent of the concentration. The situation for the system with UCST is the opposite. T_{CP} , however, is not a maximum or minimum value but a concentration-dependent value.

Besides, the experimentally observed curves in **Figure 2** may differ from the binodal curves (or coexistence curves) in the theoretical phase diagrams in **Figure 3**. The binodal curves describe the states of thermodynamic equilibrium in which the solutions are stable, while turbidimetry and light scattering methods usually require a certain degree of cloudiness or heterogeneity (i.e., the formation of polymer aggregates) in the solutions to detect the phase transition curves. Hence, the theoretical and experimental values of LCST or UCST should be distinguished.

Moreover, the determination of T_{CP} is sensitive to experimental conditions, such as heating/cooling rates, sample preparation, and criteria for identification.^[22-26] Therefore, to avoid confusion, one should state the measuring conditions explicitly and choose the terminology rationally when presenting the characterization results.

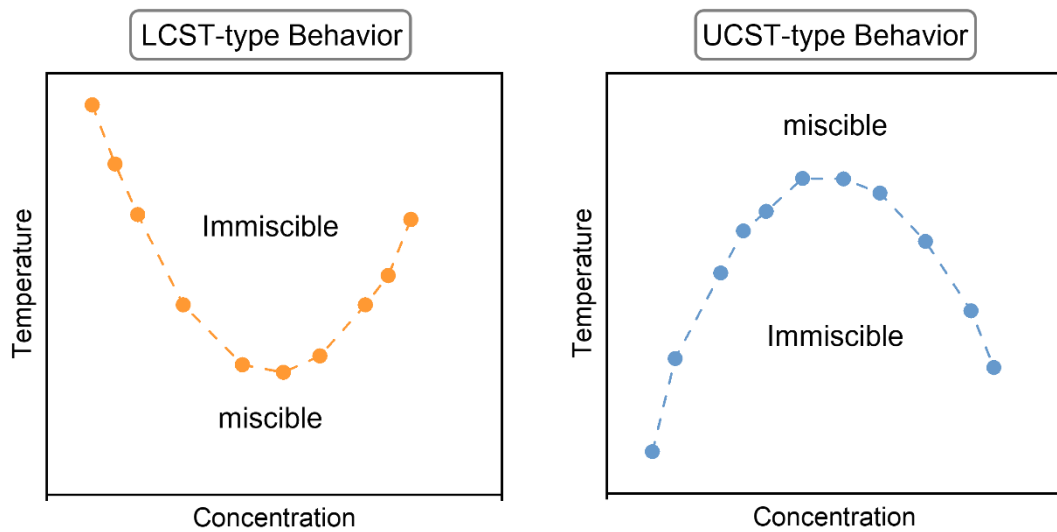


Figure 2. Simplified experimentally observed phase transition curves of polymer solutions exhibiting LCST-type (left) and UCST-type (right) behaviors. The cloud points (orange or blue dots) vary with the polymer concentration. The chains are considered miscible with the solvents below the LCST-type curve or above the UCST-type curve.

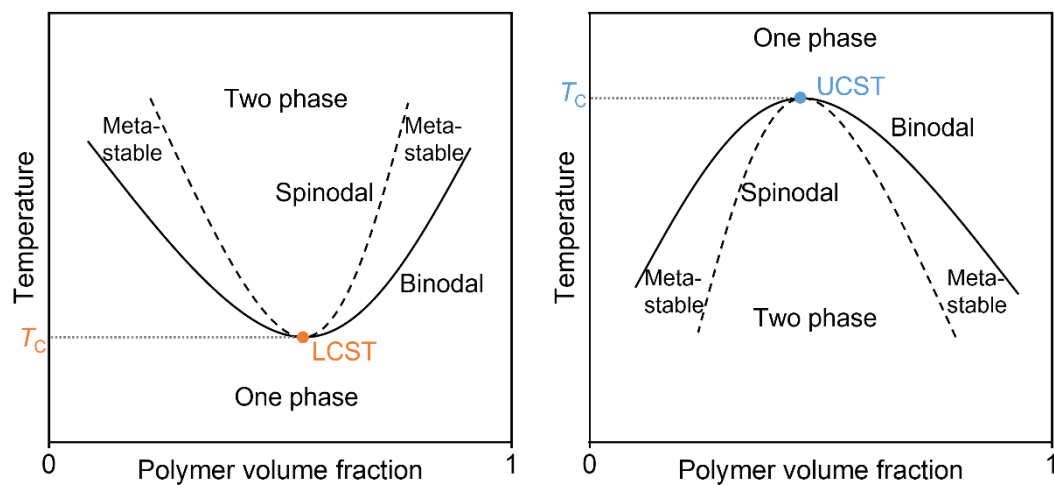


Figure 3. Simplified illustration of phase diagrams of polymer solutions with LCST (left) and UCST (right). The binodal curves are the full lines, while the spinodal curves are the dashed lines. The systems are metastable between the binodal and spinodal curves. The common minimum of binodal and spinodal is marked as LCST. The common maximum of binodal and spinodal is marked as UCST.

1.1.2 Flory-Huggins-Staverman Theory

In the last section, two types of thermoresponsive behaviors are distinguished. One classic theoretical model accounting for such phase separation of polymer solutions is the Flory-Huggins-Staverman theory (FHS theory) which was independently derived by three groups in the 1940s.^[27-32]

The FHS theory describes the Gibbs free energy of mixing (ΔG_m) for the dissolution of polymer chains in solvents by combining the entropy of mixing (ΔS_m) and the enthalpy of mixing (ΔH_m):

$$\Delta G_m = \Delta H_m - T\Delta S_m \quad (1)$$

where T is temperature. ΔS_m involves only the combinatorial entropy change ΔS_m^{comb} and can be expressed as

$$\Delta S_m = \Delta S_m^{\text{comb}} = -R(n_1 \ln \phi_1 + n_2 \ln \phi_2) \quad (2)$$

where R is the ideal gas constant, n represents the number of moles of the respective component (the subscript 1 denotes solvent, 2 denotes polymer), and ϕ stands for their volume fractions. As the sum of ϕ_1 and ϕ_2 is equal to unity, the sign of ΔS_m^{comb} is always positive and thus promotes miscibility.

On the other hand, ΔH_m considers enthalpy change caused by intermolecular contact interactions and can be given by

$$\Delta H_m = RT\chi n_1 \phi_2 \quad (3)$$

where χ represents the polymer-solvent interaction parameter and is proportional to $\Delta w/T$. Δw represents the energy change. As ΔH_m considers different types of contact interaction energies: solvent-solvent (w_{11}), polymer-solvent (w_{12}), and polymer-polymer interactions (w_{22}), Δw can be expressed as $(w_{12} - 1/2w_{11} - 1/2w_{22})$. Based on the Berthelot rule, Δw can also be written as

$$\Delta w = 1/2(\sqrt{|w_{11}|} - \sqrt{|w_{22}|})^2 \quad (4)$$

Now it is apparent that the sign of Δw is always positive, which means that χ as well as ΔH_m are always positive, thereby suppressing the miscibility. Writing Equations (1) to (3) together gives

$$\Delta G_m = RT(n_1 \ln \phi_1 + n_2 \ln \phi_2 + \chi n_1 \phi_2) \quad (5)$$

As ΔS_m^{comb} and ΔH_m made opposite contributions to ΔG_m , the original FHS theory can successfully explain the UCST-type phase separation through the balance between ΔS_m^{comb} and ΔH_m . However, as mentioned above, χ is positive and inversely proportional to temperature. The $T\chi$ term as well as ΔH_m are thus always positive and temperature-independent, excluding the possibility of LCST. This prediction apparently conflicted with the experimental findings.

The limitation of the theory can partially be attributed to the simplified assumption for ΔS_m and ΔH_m . In this theoretical model, all the contact interactions are assumed to be isotropic. There are, however, also various strong anisotropic interactions in reality, like hydrogen bonding and permanent dipoles. Moreover, these directional interactions bring about additional orientational degrees of freedom and make an entropic contribution that is not included in ΔS_m^{comb} . Therefore, both enthalpic and entropic changes should be considered for the contact interactions. One popular approach to address this issue is to resolve χ into two parts:^[33]

$$\chi = \chi_H + \chi_S \quad (6)$$

where the enthalpic part $\chi_H = A/T$ and the entropic part $\chi_S = B$. Here, A and B are two temperature-independent parameters and each of them may be positive or negative. Negative A in this function suggests the existence of specific attractive polymer–solvent interactions like hydrogen-bonding, favoring the miscibility of solvent and solute at low temperatures. χ thus may be negative. The prediction of the sign of B (reflecting the states of molecular packing) is more complex because the lattice model used in the FHS theory does not consider the anisotropic molecules in real cases.^[33] Its value needs to be determined experimentally. Nevertheless, after the modification of χ , the LCST-type phase separation can be explained as a result of negative A and positive B . In some textbooks, ΔH_m is rewritten as contact Gibbs free energy change (ΔG_m^{cont}) because of the additional entropic part in χ .

Another limitation of the FHS theory originates from the assumption that no volume change would occur during mixing. In real systems, the volume contraction associated with mixing makes a negative contribution to entropy

change, which can induce LCST-type phase separation.^[21] There are also other deficiencies in the FHS theory causing unprecise prediction of phase separation. For instance, the parameter χ has been reported to be concentration-dependent.^[34-36] Furthermore, the lattice model assumes that the segments of polymer chains are uniformly distributed in the solvent, which is unrealistic, especially for dilute solutions. Despite these deficiencies, the FHS theory is still a helpful tool providing thermodynamic insights into thermoresponsive behaviors. The theory is also the foundation of many more advanced theories involving more interactions and other factors. In the next section, the influences of specific interactions on ΔH_m and ΔS_m in aqueous solutions are introduced.

1.1.3 Interactions in Aqueous Solutions

In aqueous solutions, thermoresponsiveness can be treated as a consequence of the competition between polymer–water and polymer–polymer interactions. Despite the great effort made to modify the theoretical models, a quantitative prediction of the miscibility gap of an aqueous polymer solution containing a massive number of polar groups is still challenging. Thus, this section aims to give a qualitative description of the contributions made by different interactions to phase transitions.

Interactions Promoting LCST-type Phase Transition

Homopolymers exhibiting LCST-type phase transitions in pure water are usually amphiphilic. The hydrophilic moieties (e.g., amide groups) in those chains are able to establish attractive interactions like hydrogen bonding with water molecules, making a negative contribution to the ΔH_m and thus increasing the solubility (**Figure 4**). Surrounding the hydrophobic groups (e.g., methyl groups) of the chains, water molecules connect with each other via hydrogen bonding to form a hydration shell. Thus, the hydrated polymer is water-soluble below T_{CP} . However, the well-ordered shell structure limits the motion of water molecules in the shell, making a negative contribution to ΔS_m . When the temperature is higher than T_{CP} , the entropic term overpowers the enthalpic term. The rearrangement of water molecules occurs, leading to the exposure of the hydrophobic groups. The hydrophobic interactions then predominate and result in the collapse of the chains.

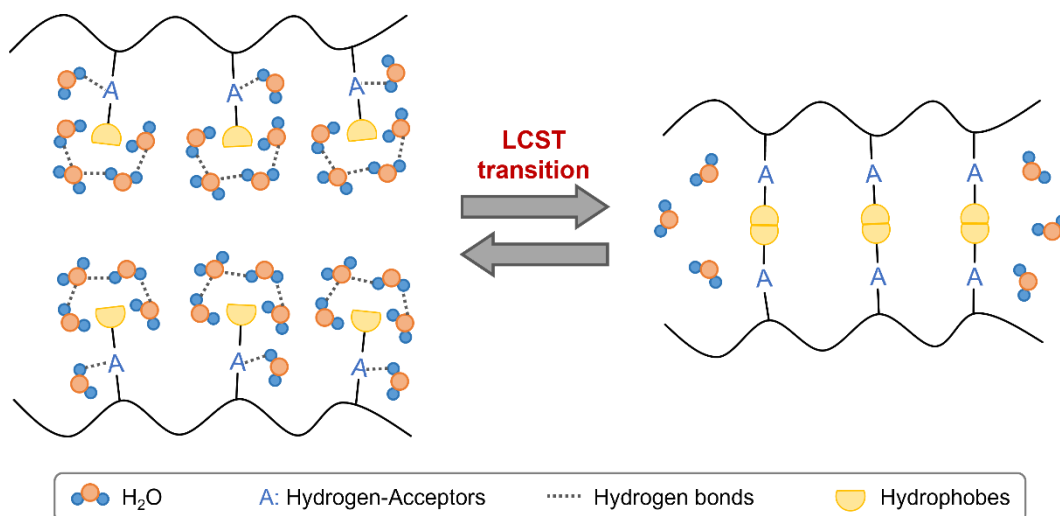


Figure 4. Simplified illustration of a typical reversible LCST transition. The exemplary amphiphilic monomer forming the chains possesses a hydrogen-acceptor and a hydrophobic moiety.

From this qualitative perspective, the phase transitions of an extensive range of LCST polymers can be generally interpreted. Since it is driven by the rearrangement of water molecules, the LCST transition upon heating is regarded as an entropic-driven transition. For the LCST transition of PNIPAM in water, several more detailed and quantitative reports combining experimental investigations and theoretical simulations are available in the literature.^[37-40] These reports manifest the crucial roles of the hydration shell and hydrophobic interactions during the LCST transition.

Interactions Promoting UCST-type Phase Transition

UCST-type phase transitions are based on strong intra- and interchain interactions of polymers. Two common interactions leading to UCST transitions are ionic interactions and hydrogen bonding (**Figure 5**).

Polymers built of monomers with both positively and negatively charged groups in water are known as zwitterionic polymers (**Figure 5a**). The dissolution of these polymers requires the breakage of the strong Coulomb attraction between opposite charges, resulting in a large positive contribution to ΔH_m . Thus, the UCST polymers are water-insoluble at low temperatures. On the other hand, ΔS_m^{comb} still makes a positive contribution to ΔS_m , favoring the polymer solubility. Hence, a UCST-type T_{CP} can be expected. As typical zwitterionic polymers,

different poly(sulfobetaine)s have now been widely investigated for their thermoresponsiveness in water. The monomers of poly(sulfobetaine)s possess an ammonium and a sulfonate group.^[10] An example is shown in **Figure 5a**. As the electrolytes can screen the attractive ionic interactions between cationic and anionic groups in poly(sulfobetaine)s, their UCST-type T_{CP} can be tuned with the ionic strength of the aqueous solution.^[41-43]

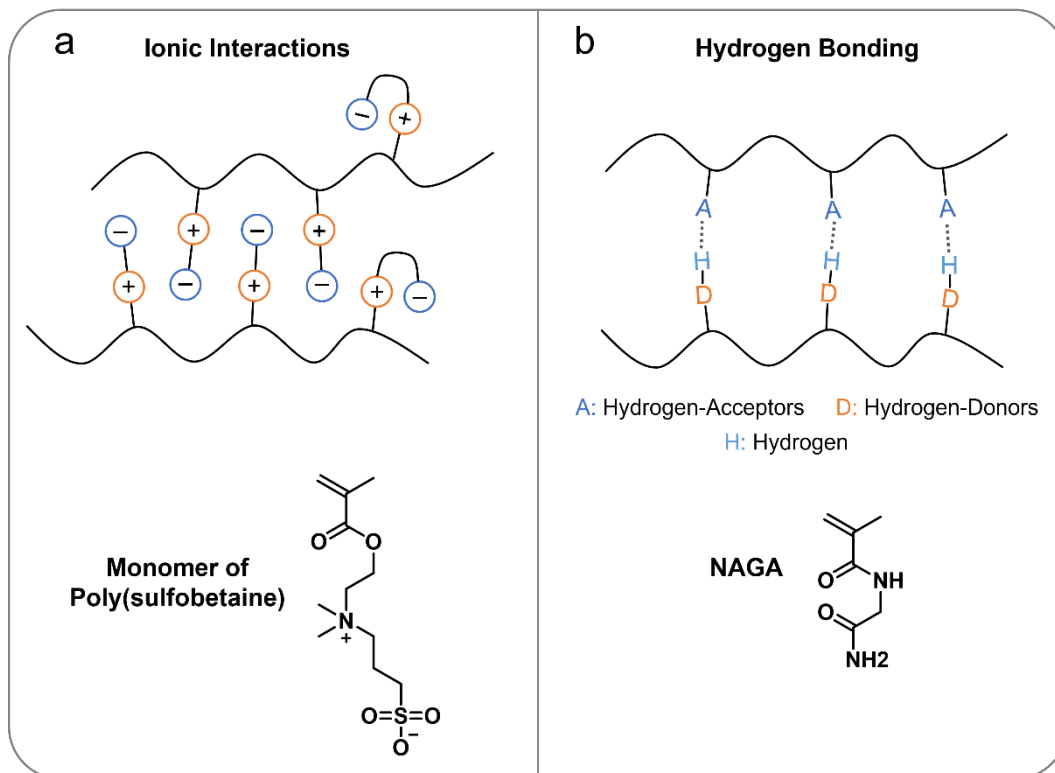


Figure 5. (a) Attractive intra- and interchain ionic interactions reducing the polymer solubility at low temperatures. An example of the monomer for poly(sulfobetaine) exhibiting UCST in water is shown; (b) Hydrogen-bonding between the polymer chains (intrachain hydrogen-bonding is not shown for simplicity), and the structure of the monomer *N*-acryloylglycinamide (NAGA).

In the cases of polymers with both good hydrogen-donors and hydrogen-acceptors, intra- and interchain hydrogen bonds can be formed in preference to polymer–water hydrogen bonds at low temperatures. Similar to the ionic interactions from the zwitterionic polymers, the formed hydrogen bonds also make a positive contribution to ΔH_m . Due to the decisive role of the polymer–polymer interaction and ΔH_m , the UCST transition is seen as mainly driven by the

enthalpic effect. Poly(*N*-acryloylglycinamide) (PNAGA), a nonionic UCST polymer, has attracted much attention since the report of Seuring and Agarwal in 2010 (the monomer is shown in **Figure 5b**).^[44] Surprisingly, although the UCST transition of PNAGA results from the reversible hydrogen bonding, the T_{CP} turned out to be highly sensitive to the ionic groups. Traces of ionic groups brought by end-groups or hydrolysis in aqueous solutions can suppress the T_{CP} to a great extent and make the polymer excellently water-soluble.^[17, 45] This phenomenon can be correlated with the low endothermic heat of the UCST transition. While the polymer–polymer hydrogen bonds make a relatively small positive contribution to ΔH_m , the hydration of ionic groups can lower the ΔH_m quite substantially.^[20] Due to the enormous impact of ionic groups, the sample synthesis and the procedure for measuring UCST-type T_{CP} based on hydrogen bonding should be prudently planned.

1.1.4 Summary

To sum up, interactions responsible for the thermoresponsiveness of aqueous polymer solutions are discussed from the thermodynamic perspective. With the help of this knowledge, the thermoresponsive behavior of polymers with more complex compositions and architectures can also be better understood and predicted. To date, various types of thermoresponsive copolymers have been reported in the literature, including random, block, and graft copolymers. These different polymer structures are often required for double thermoresponsive polymers and multifunctional hydrogels (see Section 1.4).

Before analyzing these more complicated thermoresponsive copolymers and hydrogels, it is usually essential to ensure that samples with well-defined structures are obtained. Thus, the synthetic strategy plays a crucial role in the research. In the next section, the polymerization methods used in this work will be introduced.

1.2 Synthesis of Different Chain Architectures

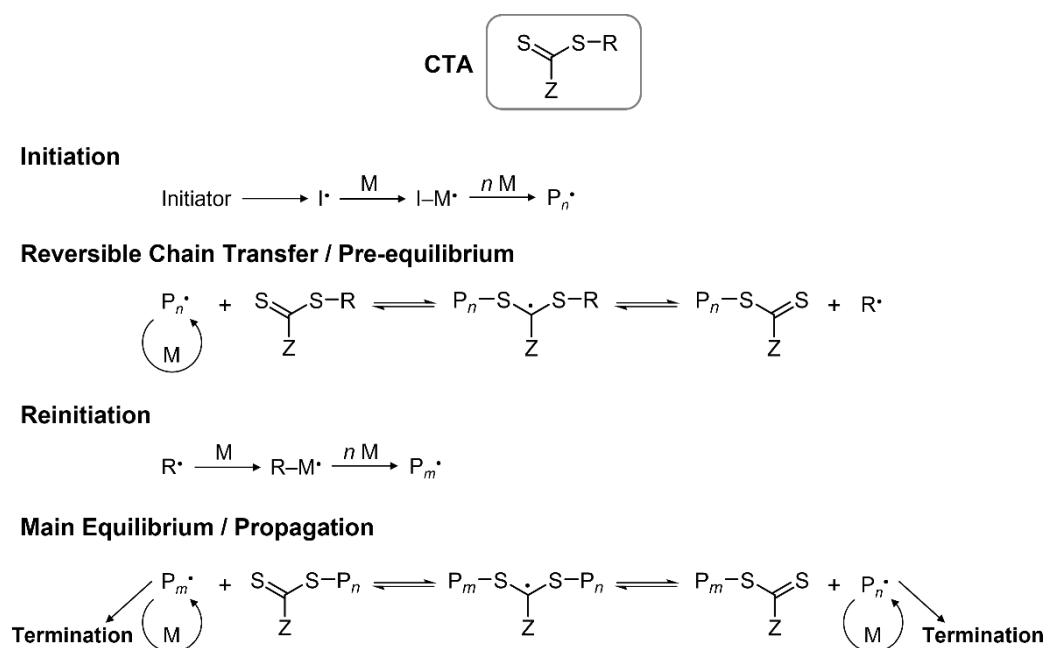
Radical polymerization is an exceptionally versatile approach for the polymerization of olefinic monomers. Highly reactive free radicals are generated through an initiator at the beginning of the polymerization. The radicals then attack the π -bonds of the unsaturated monomers, initiating chain propagation. As abundant thermoresponsive polymers are based on olefinic monomers, radical polymerization is widely used in this field. However, irreversible termination (e.g., bimolecular combination and disproportionation) is inevitable in conventional free-radical polymerizations (FRP), which broadens the molecular weight distributions of the obtained polymers and excludes the possibility of chain extension. The chains are referred to as “dead” chains after polymerization. It was thus quite challenging to synthesize well-defined polymers with complex structures with FRP. Fortunately, this obstacle has largely been overcome with the rapid development of several kinds of reversible-deactivation radical polymerization (RDRP) techniques, such as NMP, ATRP, and RAFT, since the mid-1980s.^[46-51] RDRP succeeded in reducing the probability of termination during polymerization and imparting the “living” feature to radical polymerization.

All the strategies of RDRP follow similar basic principles. By activating and deactivating chain-radicals in the presence of a selective trapping agent reversibly at a high rate, the chance of termination during polymerization is significantly reduced and the polymer’s molecular weight distribution gets narrower. As the chains stay “living” and can be released from the end-trapping agent again after polymerization, it is possible to extend the chains with another monomer to obtain a block copolymer.

In 1998, Moad and co-coworkers published a four-page communication about a new RDRP process designated RAFT polymerization.^[52] The excellent livingness of the RAFT-synthesized polymers is fulfilled by adopting the degenerative transfer approach. The mechanism of the conventional RAFT polymerization is shown in **Scheme 1**. First, an appropriate thiocarbonylthio-containing chain transfer agent (CTA, or RAFT agent) is necessary for successful polymerization. The general structure of a CTA with a stabilizing Z-group and a leaving R-group is also depicted in **Scheme 1**. The polymerization starts with the initiation step with an initiator, which is similar to that in FRP. The initiated oligomeric radical P_n^\bullet then reacts with the CTA to form an intermediate radical that subsequently

fragments to a dormant oligomeric species and a new radical R^\bullet . After reinitiating the monomers, a new propagating radical P_m^\bullet is generated. The addition of P_m^\bullet to the dormant oligomeric species affords again an intermediate radical. The followed fragmentation releases the P_n^\bullet , allowing further propagation. When the initiator concentration is significantly lower than the CTA concentration, most chains are in the dormant state during the polymerization. Since the addition–fragmentation cycles run rapidly, every chain grows with a similar opportunity.^[53] The degree of polymerization (DP) and the average molecular weight should increase almost linearly with the monomer conversion. The fast chain transfer process in the main equilibrium step also reduces the probability of termination, providing the “living” character for the polymerization.

Compared with other RDRP strategies (e.g., NMP and ATRP), the rate of RAFT polymerization is not significantly sacrificed thanks to the degenerative transfer process. Assuming that the probability of termination is ignorable and no retardation is caused by addition–fragmentation, the concentration of active free radicals should not be suppressed by the CTA and should stay constant during chain propagation.^[54] Furthermore, by choosing an adequate CTA, RAFT polymerization can be compatible with a broader range of monomers.



Scheme 1. Mechanism of the conventional RAFT polymerization.

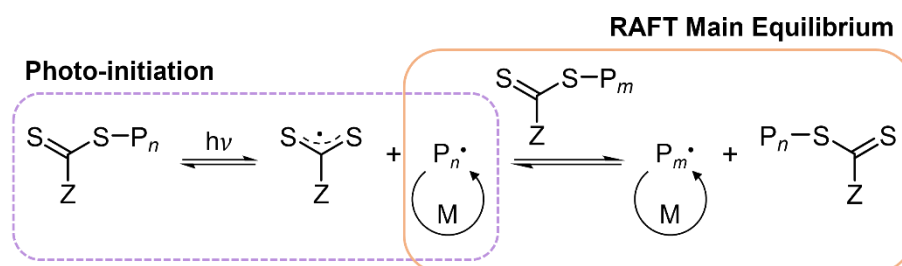
Up to now, abundant efficient CTAs have been synthesized and reported in the literature. The selection of CTAs mainly depends on the character of the used monomer (more activated (MAM) or less activated (LAM) monomer). Comprehensive guidelines for selecting CTAs can be found in the reviews of Moad et al.^[54-57] There are also studies devoted to developing universal CTAs suitable for both MAMs and LAMs.^[58, 59] Moreover, using CTAs of specific shapes, like star-shape or multiblock-shape, star or multiblock polymers can be easily obtained.^[60]

1.2.1 Photoiniferter RAFT Polymerization – New Roles for CTA

As mentioned above, thiocarbonylthio-containing CTAs play a decisive role in the conventional RAFT process. The rapid exchange between dormant and active chains leads to outstanding control over the polymers' chain length. However, as CTAs do not consume the radicals generated by the initiator, the remaining propagating radicals will end up being irreversibly terminated once polymerization is stopped, causing a loss of livingness. The polymers' livingness can be predicted and tuned through the molar ratio between CTA and the initiator.^[61] A lower initiator concentration usually means fewer “dead” chains but leads to a lower polymerization rate. The more detailed mathematical prediction of livingness can be found in various reviews about RAFT polymerization.^[53, 55, 61] Also, as some of the chains directly grow from I^{\bullet} , the initiator structure affects the end-group fidelity, which can, for example, cause the disappearance of UCST-type T_{CP} as mentioned in Section 1.1.3.^[17] Although this issue can be avoided by using an initiator with the same fragment as R-group when synthesizing a homopolymer, the impact on the synthesis of block copolymers is hard to avoid. Homopolymers will also be produced during chain extension.^[53] Additionally, as the initiation is accomplished through the initiator in the first step, no spatial or temporal control of the radical generation can be achieved afterward.^[62] Due to these disadvantages, initiation strategies without exogenous initiators were established.^[63]

Among the initiator-free strategies, photoiniferter RAFT polymerization (or photoRAFT) driven by light can be seen as an elegant technique that is easy to operate. The term “iniferter” (initiator/transfer agent/terminator) indicates the new roles assigned to CTAs.^[64] As shown in **Scheme 2**, radicals are generated directly through the β -cleavage of the CTA without any additives under light

irradiation, ensuring a high end-group fidelity. The active radical species can either participate in the chain propagation in the normal degenerative transfer approach or recombine with the stable thiocarbonylthio radical species. This recombination can deactivate propagating radicals if light irradiation pauses, offering spatial or temporal control.



Scheme 2. Mechanism of photoiniferter RAFT polymerization. After photolysis, the rapid chain transfer process between propagating radicals can take place.

The light sources for photoiniferter RAFT should be selected based on the properties of CTAs. **Figure 6** shows the absorption bands of the carbon-sulfur double bond in a typical CTA.^[65-67] The intensive band in the UV region corresponds to the spin-allowed $\pi \rightarrow \pi^*$ transition. The weak band in the visible light region is ascribed to the spin-forbidden $n \rightarrow \pi^*$ transition, which also reflects the color of CTAs.^[68] According to these two absorption bands, the CTA can be excited by both UV and visible light, causing homolytic dissociation of the weak carbon-sulfur bond and the release of R-groups. However, it should be noted that the absorption bands may shift after the insertion of the first monomer unit, which can affect the photolysis and terminate the polymerization.^[69]

Many publications have reported successful well-controlled photoiniferter RAFT polymerizations. Different CTAs, including dithiocarbamate,^[70] xanthate,^[71] and trithiocarbonate,^[72-75] have been proven to be qualified candidates in UV-mediated RAFT polymerizations. Visible light controlled polymerizations were first reported in 2015.^[62, 67] With the help of trithiocarbonate with different R-groups, well-defined poly(methyl acrylate) (PMA) and poly(methyl methacrylate) (PMMA) were synthesized under blue and green light irradiation, respectively. In 2017, an ultrafast polymerization of poly(butyl acrylate) (PBA) was achieved with xanthate under purple light irradiation.^[76] The polymerization could even tolerate oxygen in the reaction mixture.

The use of photoiniferter RAFT polymerization eludes the disadvantages caused by exogenous initiators. It not only allows spatial and temporal control but also increases the end-group fidelity of the obtained chains. The publications in Chapter 3 emphasize the exclusive advantages of visible light-controlled polymerizations concretely.

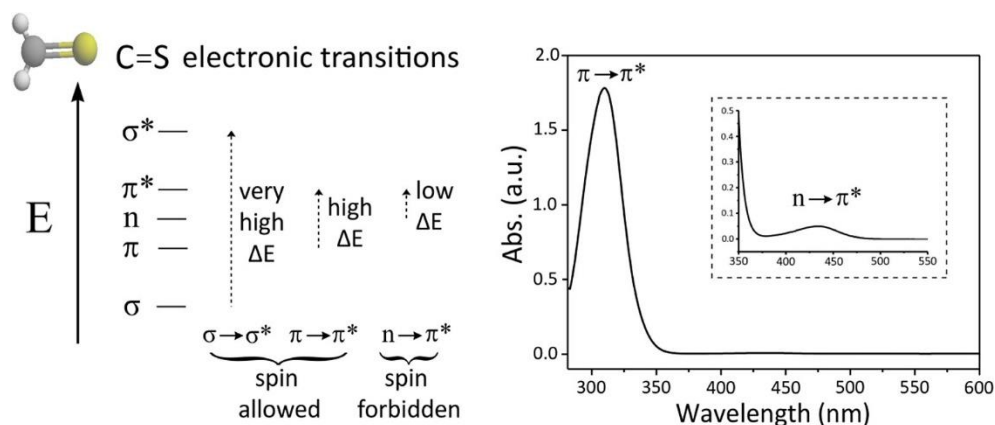


Figure 6. Simplified illustration of electronic energy levels of thiocarbonyl compounds and a representative absorbance spectrum of trithiocarbonate. Reprinted with permission.^[67] Copyright 2015, American Chemical Society.

1.2.2 Random / Alternating / Gradient Copolymers

When two monomers participate in polymerization simultaneously, RAFT polymerization delivers copolymer chains sharing not only a similar DP but also a similar composition and sequence distribution. Depending on the reactivity ratios of the monomers, random, alternating or gradient copolymers can be fabricated (Figure 7).

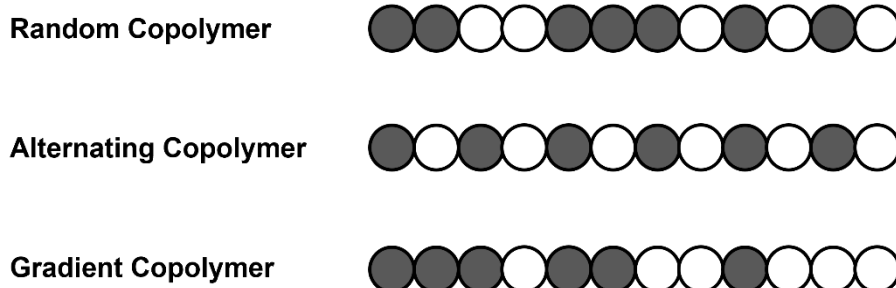
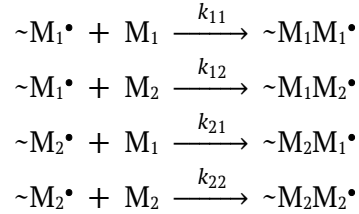


Figure 7. Simplified illustration of random, alternating, and gradient copolymer chains consisting of two monomers.

To predict the monomer addition in copolymer chains at a certain instant during simultaneous copolymerization, a simple kinetics model considering only two types of active free radicals ($\sim M_1\cdot$ and $\sim M_2\cdot$ initiated from two monomers, M_1 and M_2 , respectively) was proposed.^[77, 78] Four possible chain propagation steps are given in this model:



In these reactions, k_{11} and k_{22} are the rate coefficients of homopropagation, while k_{12} and k_{21} are the rate coefficients of cross-propagation. Based on these reaction steps, the rates of consumption of two monomers ($d[M_1]$ and $d[M_2]$) are written as

$$-\frac{d[M_1]}{dt} = k_{11} [M_1\cdot][M_1] + k_{21} [M_2\cdot][M_1] \quad (7)$$

$$-\frac{d[M_2]}{dt} = k_{22} [M_2\cdot][M_2] + k_{12} [M_1\cdot][M_2] \quad (8)$$

where t denotes time, $[M_1]$ and $[M_2]$ are the concentrations of two monomers in the reaction mixture. Assuming that a steady-state is quickly met and maintained, the copolymerization equation (or the Mayo–Lewis equation) can be yielded from Equation (7) and (8):

$$\frac{d[M_1]}{d[M_2]} = \frac{[M_1]}{[M_2]} \left(\frac{r_1 [M_1] + [M_2]}{[M_1] + r_2 [M_2]} \right) \quad (9)$$

r_1 and r_2 are the monomer reactivity ratios that are defined as

$$r_1 = \frac{k_{11}}{k_{12}}, \text{ and } r_2 = \frac{k_{22}}{k_{21}} \quad (10)$$

A reactivity ratio larger than unity indicates that the corresponding monomer prefers homopropagation, while a reactivity ratio smaller than unity means that the monomer prefers cross-propagation. The detailed deducing steps for

Equation (9) are not shown here and can be found in the original work of Mayo and Lewis.^[78] Equation (9) can also be written in the form of mole fractions. The mole fractions of M_1 and M_2 in the mixture (f_1 and f_2 , respectively) can be expressed as

$$f_1 = \frac{[M_1]}{[M_1] + [M_2]}, \text{ and } f_2 = \frac{[M_2]}{[M_1] + [M_2]} \quad (11)$$

The sum of f_1 and f_2 is unity. On the other hand, the mole fractions of M_1 and M_2 added to the copolymer chains at a certain instant (F_1 and F_2 , respectively) can be expressed as

$$F_1 = \frac{d[M_1]}{d[M_1] + d[M_2]}, \text{ and } F_2 = \frac{d[M_2]}{d[M_1] + d[M_2]} \quad (12)$$

Also, F_2 is equal to $1 - F_1$. Equation (9) can then be rearranged in terms of F_1 :

$$F_1 = \frac{r_1 f_1^2 + f_1 f_2}{r_1 f_1^2 + 2 f_1 f_2 + r_2 f_2^2} \quad (13)$$

Now with known r_1 and r_2 , F_1 can be plotted as a function of f_1 . **Figure 8** shows the relationship between F_1 and f_1 for different pairs of assumed r_1, r_2 values. These curves can help estimate F_1 or F_2 from f_1 . However, the estimation is only valid in a pretty short time interval. In most cases, comonomers are not consumed at the same rate because of different reactivities or steric effects, leading to the change of f_1 with conversion. Consequently, copolymer composition drift governed by r_1 and r_2 occurs as the overall conversion increases. In FRP, new copolymer chains with disparate compositions will be formed at different polymerization stages due to the drift of f_1 . In the end, a polymer blend will be obtained.^[55] The situations in RAFT and other living polymerizations are quite different. CTAs for RAFT polymerization do not affect r_1 and r_2 . However, since every chain grows with equal probability and stays “living” throughout the polymerization, the copolymer composition drift will only take place within the chains. Therefore, copolymer chains sharing similar compositions instead of blends are produced.

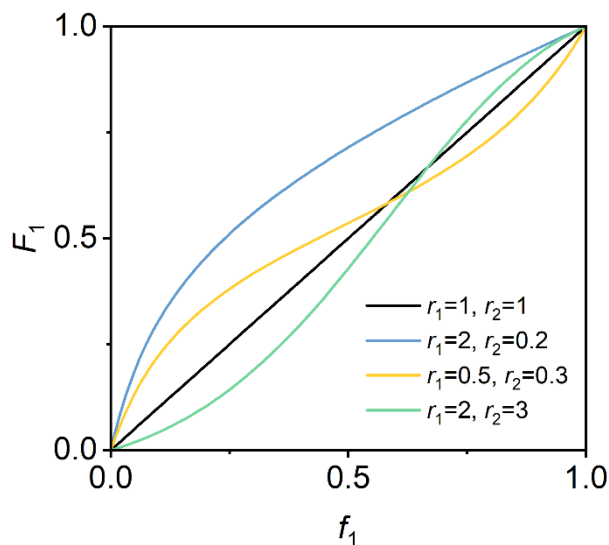


Figure 8. Plots of Equation (13) based on different pairs of assumed r_1 and r_2 values.

As reflected in **Figure 8**, r_1 and r_2 are two core parameters determining the sequence distribution of comonomers. In order to synthesize the tailored copolymers shown in **Figure 7** via living radical polymerization, particular requirements on r_1 and r_2 need to be met, which will be discussed below.

Random copolymers can be synthesized in ideal cases, i.e., when $r_1 = r_2 = 1$. Under this condition, M_1 and M_2 show no difference in terms of chain propagation. Their probabilities of being captured by both types of active radicals are equal. Thus, the comonomers are randomly distributed in the chains. Such copolymerizations are usually observed when the comonomers have similar structures.

When $r_1 \ll 1$ and $r_2 \ll 1$, both monomers prefer cross-propagation immensely, leading to the formation of alternating structures. Intriguing alternating copolymers can be obtained, for example, from monomer pairs, styrene/*N*-phenylmaleimide and styrene/maleic anhydride.^[55, 79] In contrast, when $r_1 > 1$ and $r_2 > 1$, both monomers tend to homopropagation. Hence, a blocky structure will be formed. This case, however, is rarely observed in practice.

Another special case is $r_1 > 1$ and $r_2 < 1$, i.e., M_1 is more prone to react with both types of active radicals. As M_1 is consumed preferentially, f_1 , as well as F_1 , will decrease as copolymerization progresses. As mentioned above, a polymer blend results from this drift in FRP. Living polymerization, on the other hand, provides chains with a similar composition and limits the composition drift within the

macromolecule. The yielded chains are thus rich in M_1 at one end and rich in M_2 at the other. Such copolymers are named gradient (or tapered) copolymers. The situation of $r_1 < 1$ and $r_2 > 1$ can be analyzed similarly. A gradient copolymer can be formed, for example, from the monomer pair, methyl acrylate/vinyl acetate, via RAFT polymerization.^[55] In essence, the possibility to attain gradient copolymers is also an exclusive advantage for living polymerization techniques.^[80]

1.2.3 Block Copolymers

RAFT polymerization is also a powerful tool for synthesizing diblock copolymers (**Figure 9**). The copolymerization is usually performed successively. In other words, the second block in the copolymer is prepared through chain extension after initiating the first block with a high livingness. In this two-step process, the order in which the blocks are polymerized is of great importance. To achieve efficient reinitiation of the monomer forming the second block, the propagating radical from the first block should be a better leaving group than that from the second block in the pre-equilibrium step of conventional RAFT (**Scheme 1**). Otherwise, the fragmentation to form the macro-R group radical may be hindered. For instance, methacrylates should be polymerized as the first block prior to the chain extension with acrylates or acrylamides because poly(methacrylate)s are better leaving groups.

Block Copolymer



Figure 9. Simplified illustration of a block copolymer chain consisting of two monomers.

However, it is possible to overcome the restriction on the blocking order by using photoiniferter RAFT polymerization. Recently, the group of Sumerlin has reported an inspiring study describing a successful chain extension with MMA from the homopolymer poly(*N,N*-dimethylacrylamide) (PDMA).^[81] As shown in **Figure 10**, in the conventional RAFT process, the fragmentation of the intermediate radical species to the PDMA macro-radical (secondary carbon radical) group is not favored after the addition of an MMA unit, i.e., $k_{\text{add}} \gg k_{\beta}$. Thus, the fragmentation occurs backward, leading to the homopolymerization of PMMA. After the polymerization, the authors observed a mixture of PMMA and PDMA. In the case of the photoiniferter process, the initiation of the PDMA

macro-radical was realized directly through the β -cleavage of the weak carbon-sulfur bond under UV light irradiation. The propagating radical then reinitiated MMA, resulting in the formation of a well-defined diblock copolymer.

However, the authors also showed that this method depended strongly on the Z-group of the used CTA. The chain extension was successful with xanthate but failed with trithiocarbonate.^[81] The authors attributed this result to the slower photolysis in the case of trithiocarbonate.

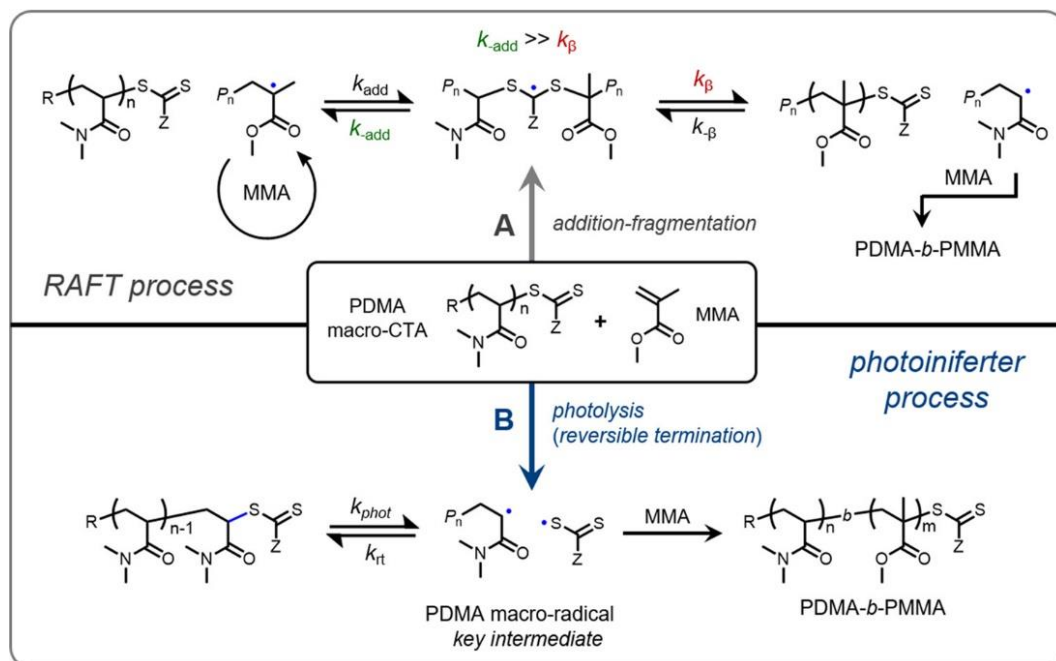


Figure 10. Mechanism of chain extension with MMA from PDMA via the conventional (top) and photoiniferter (bottom) RAFT process. Reprinted with permission.^[81] Copyright 2019, American Chemical Society.

Besides the ability to invert the blocking order, photoiniferter RAFT can also provide other advantages. Without an external initiator, the propagation of the second block can only be initiated by the radical from the first block, providing a higher chain end fidelity. Furthermore, RAFT polymerization is compatible with surfactant-free polymerization-induced self-assembly (PISA) which is a convenient process for preparing amphiphilic diblock copolymers in emulsion or dispersion.^[82] In waterborne PISA processes, a hydrophilic block is synthesized in the first step. This block then serves as a stabilizing agent during chain extension

with a hydrophobic block in emulsion or dispersion. Comprehensive reviews about RAFT-mediated PISA are present in the literature.^[85-87] A bonus provided by the photoiniferter process for PISA is that the reaction temperature of the chain extension can be selected more flexibly. Without a thermal initiator, it is possible to perform chain extensions at low temperatures, which means that the first block can be an LCST polymer with a relatively low T_{CP} , like poly(*N*-acryloylpyrrolidin) (PAPy) with a T_{CP} around 50°C.^[74] After chain extension in water at a temperature below T_{CP} , amphiphilic diblock copolymers can be yielded in the form of uniformly distributed micelles.

Furthermore, in order to obtain a block copolymer with a high molecular weight, RAFT can be combined with anionic polymerization. Although RAFT polymerization is compatible with a large range of monomers, the synthesis of polymers with high molecular weights is challenging, particularly for the monomers with slow propagation rates.^[88] On the other hand, anionic polymerization is capable of delivering well-defined long chains due to the fast polymerization rate. In 2016, Eggers et al. reported the synthesis of a stimuli-responsive diblock copolymer with a high molecular weight.^[89] The major hydrophobic polystyrene (PS) block was polymerized first through anionic polymerization. After modifying the chain end, the minor stimuli-responsive poly[2-(*N*-morpholino)ethyl methacrylate] (PMEMA) block was obtained via RAFT.

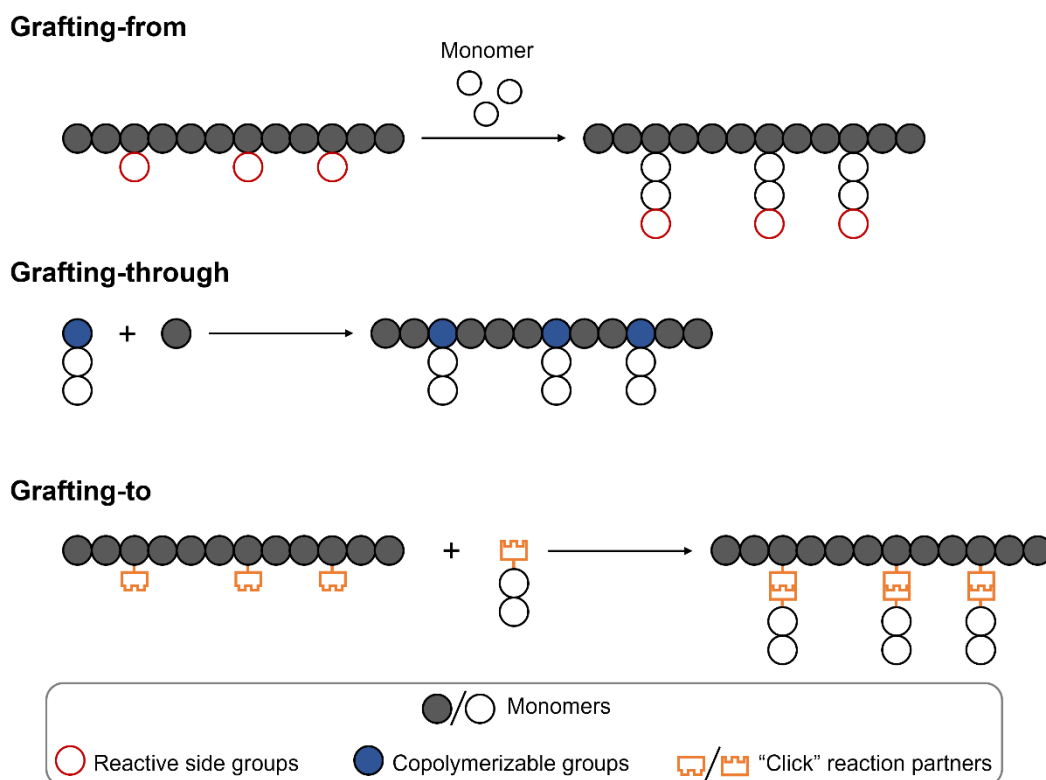
1.2.4 Graft Copolymers

A graft copolymer chain typically consists of a backbone and several side chains. The approaches to synthesizing graft copolymers can generally be classified into three types, namely grafting-from, grafting-through, and grafting-to approaches (**Scheme 3**).

The grafting-from approach utilizes a pre-formed backbone with reactive sites that are able to generate propagating radicals for the monomers forming side chains. The ongoing development of different RDRP techniques has increased the versatility of this approach to a great extent. Typically, well-defined backbones and side chains can be prepared via two different RDRP techniques free of mutual interference. For example, the method combining RAFT and ATRP has been well established.^[90, 91] Simultaneous copolymerization via RAFT with a comonomer

containing a pendant ATRP initiating group allows incorporating a certain amount of reactive sites into the backbone. The ATRP initiating groups stay dormant during RAFT polymerization, ensuring the achievement of a linear backbone. Before starting ATRP, the thiocarbonylthio group from the CTA at the chain end should be deactivated to avoid interference (the deactivation method will be discussed in more detail in Section 1.3.2). At last, side chains can grow from the pendant reactive sites via ATRP.

In 2018, Matyjaszewski and coworkers showed that the grafting-from approach does not necessarily require two different RDRP techniques.^[69] The backbone and side chains were polymerized via photoiniferter RAFT under green and blue light irradiation, respectively. Between two synthetic steps, no deactivation of the chain end was necessary. This convenient method was also employed in Publication 2 and 3 in Chapter 3. More details of the polymerization are discussed in these publications.



Scheme 3. Three approaches to synthesizing graft copolymers.

Another study from the group of Boyer is also worth mentioning for the grafting-from approach.^[92] The backbone and side chains were also polymerized via RAFT under different light sources. However, instead of photoiniferter RAFT, photoinduced electron/energy transfer-RAFT (PET-RAFT) was used in that work. Therefore, not only different light sources but also different photoredox catalysts needed to be used to synthesize the backbone and side chains.

The grafting-through approach involves a macromonomer containing a suitable polymerizable group at the chain end (**Scheme 3**). After preparing the macromonomer (e.g., through ring-opening polymerization), the copolymerization can be carried out via RAFT.^[93] The last approach is the grafting-to approach. Due to the high versatility, RAFT copolymerization can easily incorporate monomers with functional groups supporting “click” chemistry into the backbone. The pre-formed side chains with corresponding functionalities at the chain end can then be attached to the backbone through “click” reactions.^[94] Alternatively, the R-groups of CTAs can be modified to support “click” reactions. In this case, the RAFT-synthesized chains are grafted onto the backbone as side chains.^[95, 96]

1.2.5 Summary

In summary, the development of RAFT polymerization offers tremendous convenience to the synthesis of different chain architectures. The development of photoiniferter RAFT has overcome some shortcomings of the conventional RAFT process. The advantages brought by photoiniferter RAFT are shown in publications in Chapter 3 vividly. The benefit of RAFT polymerization is not just limited to narrowing the molecular weight distribution and delivering complicated chain architectures. In the next section, the preparation of hydrogels, especially thermoresponsive hydrogels, based on RAFT-synthesized polymers will be introduced.

1.3 Routes to Hydrogels

Natural hydrogels are an indispensable building block for life on earth. In human history, the applications of natural hydrogels, like gelatine and agar, in food can be traced back a long time ago.^[97] With the development of polymerization techniques, synthetic hydrogels have become popular as their structures can be better controlled. According to the crosslinking methods utilized in synthesis, the obtained hydrogels can be classified into physically and chemically crosslinked hydrogels. These two types of hydrogels will be described in the following sections.

1.3.1 Physically Crosslinked Hydrogels

Physically crosslinked hydrogels are fixed by junctions resulting from interchain interactions, such as hydrophobic interaction, hydrogen bonding, ionic interaction and host–guest interaction.^[98-102] As introduced in Section 1.1.3, some of these reversible interchain interactions are also the driving force of UCST and LCST transitions in water. Therefore, thermoresponsive polymers are capable of forming reversible crosslinking sites in hydrogels. The hydrogels purely based on these interactions can undergo reversible solution-to-gel (sol-gel) transitions in response to temperature change when the proper polymer concentrations are reached.

A common way to prepare hydrogels featuring an efficient thermoresponsive sol-gel transition is to synthesize a triblock or a multiblock polymer. In the presence of a symmetric difunctional CTA, an ABA triblock polymer can be synthesized conveniently. To enable thermogelation in aqueous solutions, block A is usually thermoresponsive. When the polymer concentration is sufficiently high, a three-dimensional network can be formed once block A turns hydrophobic (**Figure 11**). Block B is usually highly hydrophilic to bridge the hydrophobic domains (physical crosslinks) and keep the formed network stable. An example of thermoreversible hydrogel based on UCST transition was reported by Zhao et al.^[103] In that study, block A was a random copolymer of acrylamide (AAm) and acrylonitrile (AN), which exhibited UCST transition in water. Block B was water-soluble poly[poly(ethylene glycol) methyl ether methacrylate] (PPEGMMA). With an appropriate block ratio, the sol-gel transition could be triggered at a concentration of 5% (w/w) upon cooling.

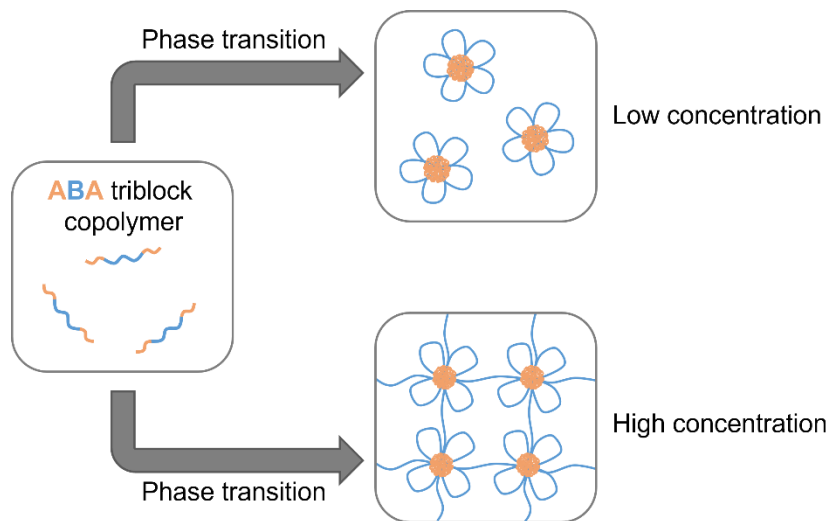


Figure 11. Thermoresponsive behavior of a hydrophilic ABA triblock copolymer in aqueous solutions. When A block becomes hydrophobic after phase transition, flower-like micelles can be formed if the polymer concentration is low. If a critical concentration is reached, a three-dimensional hydrogel can be formed.

Chen et al. synthesized an ABC triblock terpolymer to study its LCST-induced gelation.^[104] The terpolymer was synthesized via RAFT consecutively in three steps. Block A was permanently hydrophobic PMMA. The middle block B was poly[*N,N*-(dimethylamino) ethyl methacrylate] (PDMAEMA), which is excellently water-soluble under acidic conditions. The last C block was a typical LCST polymer, PNIPAM. The authors could already observe a sol-gel transition in the acidic aqueous solution with a low polymer concentration of 2% (w/w) upon heating. Besides triblock terpolymers, tetrablock terpolymers that are able to form physically crosslinked hydrogels were reported by Georgiou et al.^[105, 106] The relationship between the blocking sequence and gelling behavior was investigated in detail in their research.

In terms of biomedical applications, temperature-induced gelation makes the hydrogels injectable because of their low viscosity in a solution state, which is an attractive feature for controlled drug delivery and tissue engineering.^[107-109] At last, it is worth noticing that the gelation behavior of block polymers can be affected by many factors, such as asymmetry,^[110] hydrophilicity of monomers,^[111-114] and block lengths.^[115-117] Therefore, the sol-gel transition can be altered and optimized from different aspects.

1.3.2 Chemically Crosslinked Hydrogels

Unlike physically crosslinked hydrogels, chemically crosslinked hydrogels are polymer networks fixed through covalent bonds. These hydrogels thus usually show improved stability. RAFT polymerization can provide well-defined polymer precursors for chemically crosslinked hydrogels. Those RAFT-synthesized polymer chains have one thing in common: they all possess at least one thiocarbonylthio group stemming from CTAs. Also, the thiocarbonylthio groups are located at the chain end in many cases. Considering that a wealth of methods have been established to modify these end-groups after polymerization, it should be cost-effective to generate reactive functions for chemical crosslinking directly from these end-groups. Before showing the common crosslinking reaction types, the standard end-group modification methods for RAFT-synthesized polymers are introduced.

End-group Modification

Figure 12 summarizes the widely used pathways to the end-group transformation of RAFT-synthesized chains.^[118] First, thermolysis can lead to desulfurization of the chain and leaves an unsaturated end-group.^[119] Radical-induced reactions also allow the removal of thiocarbonylthio groups and are usually carried out with an initiator, like azobisisobutyronitrile (AIBN). With excess radicals generated from the initiator, the end-group of the polymer can be replaced by the initiator fragment.^[120, 121] By adding a hydrogen atom donor together with an initiator, the polymer chain can be capped by a single hydrogen atom rather than the initiator fragment.^[122] Moreover, heating the polymer with AIBN in air and then treating the solution with a reducing agent can produce a hydroxyl-terminated chain.^[123] The end-group can also be removed in a catalytic chain transfer process with a square planar Co^{II} complex, which delivers the same product as thermolysis.^[118] Treating the polymer with a nitroxide can produce an end-group enabling chain extension via NMP.^[124] The end-groups with electron-withdrawing Z-groups can also undergo hetero-Diels–Alder reactions with dienes.^[125] Block or even star polymers can be yielded in this way. Last but not least, the end-group can react with nucleophiles or ionic reducing agents to give a reactive thiol group.^[126]

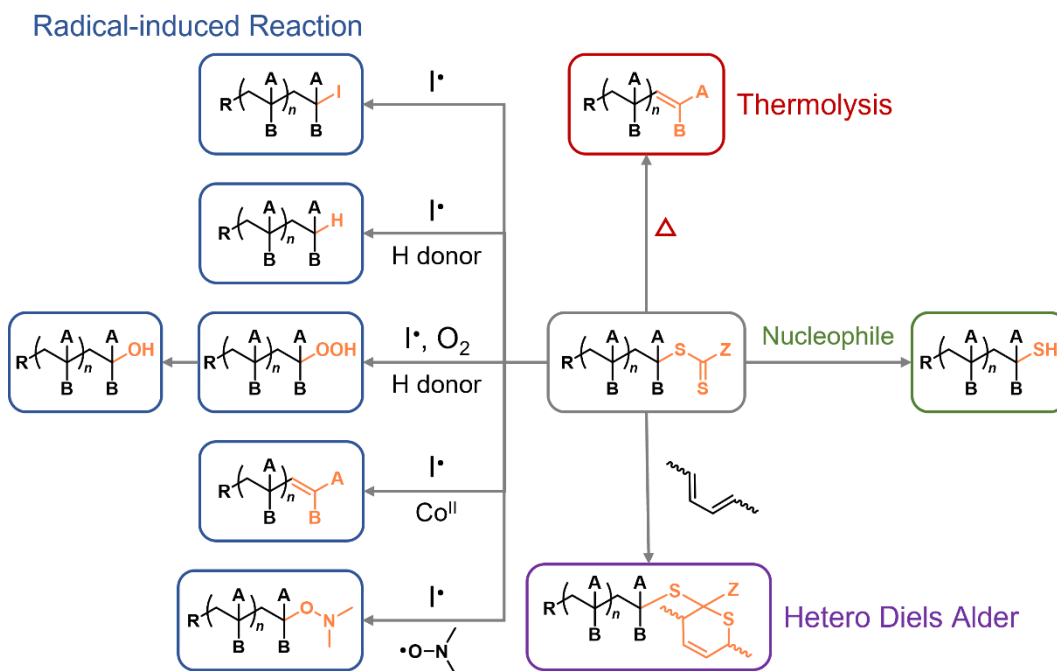


Figure 12. Commonly used pathways to end-group transformation.^[118]

It is well-known that thiol-based chemistry is a powerful toolbox. The involved reactions are usually efficient and selective even under mild conditions, causing fewer side reactions. Since the thiocarbonylthio group can be converted into a thiol group, as mentioned above, thiol-chemistry is an excellent complement to RAFT polymerization.^[127] In this context, the end-group modification approaches to obtaining thiol groups at the chain end deserve more introduction.

The modification procedure with an amine (e.g., butylamine or hexylamine) as a nucleophile is named aminolysis. The reaction can be accomplished at room temperature. However, the oxidative coupling between the formed thiol groups may occur without specific treatments. The caused disulfide bridge will broaden the molecular weight distribution and reduce the end-group fidelity of the modified polymer. The oxidation can be mitigated by degassing the reaction mixture or adding a reducing agent, such as sodium bisulfite or tris(2-carboxyethyl)phosphine (TCEP).^[128, 129] In 2010, hydrazine, as an effective nucleophile, was found to provide rapid and clean removal of thiocarbonylthio groups even without degassing.^[130] Another strategy to avoid the formation of unwanted disulfide is to add a thiol-trapping agent (**Figure 13**). The trapping reactions should not participate in the aminolysis so that the removal and

trapping processes can be performed simultaneously. (Meth)acrylates and (meth)acrylamide with activated alkenes (i.e., Michael acceptors) are widely used as trapping agents as they are readily available and support one-pot thiol-ene “click” reactions under mild conditions.^[131-135] Moreover, different thiosulfonates and α -bromoesters can be employed as trapping agents supporting thiol-disulfide exchange and thiol-bromo reactions.^[136, 137] Through aminolysis in the presence of 2,2'-dithiodipyridine (DTP), the thiocarbonylthio groups can easily be converted to stable pyridyl disulfide (PDS)-functions.^[138] This convenient approach was also used in Publication 2 and 3 in Chapter 3. Certainly, the oxidative coupling of thiol groups is not totally worthless, either. It is possible to synthesize ultra-high molecular weight block polymers through intentional chain coupling during aminolysis in the presence of oxygen.^[139]

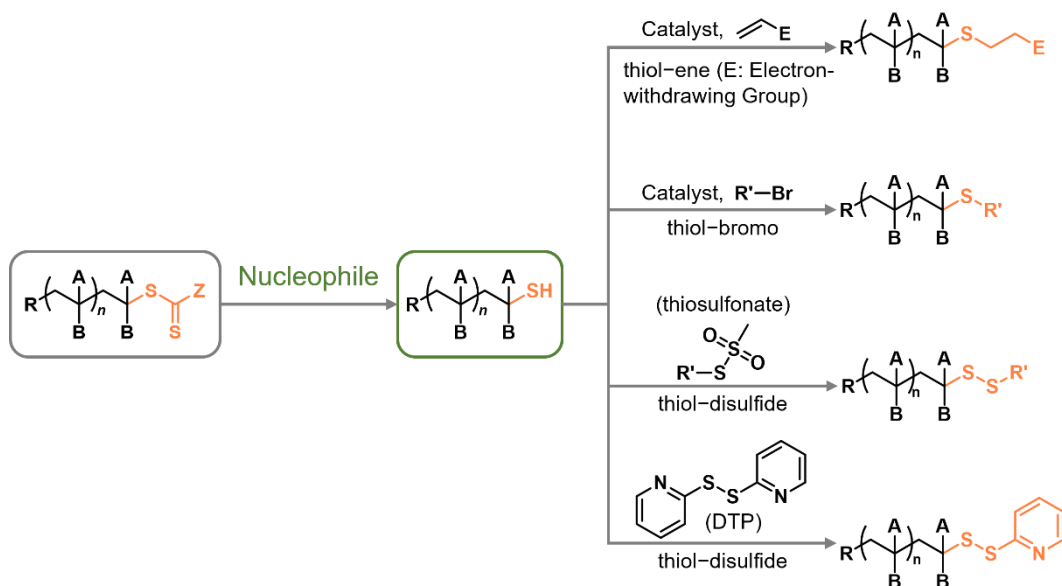


Figure 13. Commonly used trapping reactions using thiol “click” chemistry.^[118]

These diverse trapping reactions not just provide large numbers of options to restrain the side reactions but also reveal the high versatility of thiol chemistry. It is thus not surprising that thiol chemistry is also widely used in crosslinking processes.^[140] The following section gives a few examples of crosslinking. However, instead of listing the employment of different “click” reactions exhaustively, it is intended to focus on the methods making use of end-group modification (aminolysis) of RAFT-synthesized polymers.

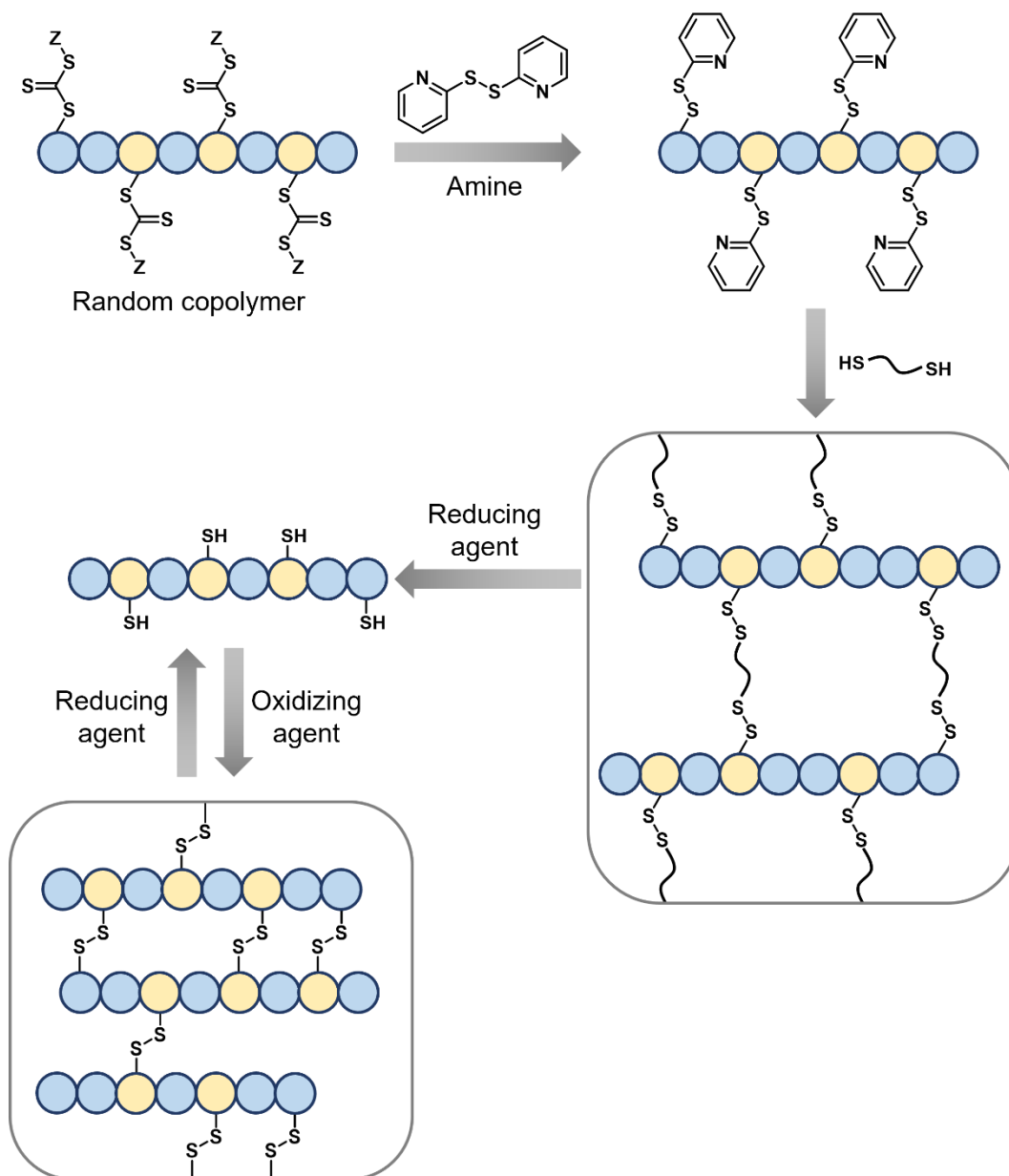
Crosslinking Promoted by Aminolysis

An example of crosslinking methods involving aminolysis was presented by Konkolewicz et al.^[141] The thiocarbonylthio groups along the chains and at the ω -terminal were converted to thiol groups with isopropylamine. Subsequently, a bismaleimide crosslinker was added to connect the chains via the thiol–Michael reaction. The formed thiol–Michael linkages showed dynamic character at elevated temperatures. Although the final product in that research was not hydrogel, the crosslinking strategy is still instructive. Recently, the group of Sanyal has reported an *in situ* crosslinking process upon aminolysis.^[142] A thiosulfonate-containing monomer was copolymerized with a hydrophilic monomer via RAFT polymerization. The obtained copolymer was then incubated with amylamine in water at room temperature to liberate thiol end-groups. These thiol groups initiated the crosslinking process immediately in the solution through the thiol–disulfide exchange reaction with thiosulfonate side groups. A free-standing hydrogel was observed within a relatively short time.

The crosslinking strategies mentioned above exploit the inherent reactivity of thiol groups generated by aminolysis. Furthermore, aminolysis can facilitate crosslinking by cooperating with the thiol-trapping agents containing specific functional groups. An advantage of the crosslinking strategies with trapping agents lies in the protected thiol groups which give the modified polymers longer shelf life. The crosslinking reactions can then be performed at a later stage. For instance, the hydrogels reported by Peng et al. were formed by the photo-initiated thiol–ene reaction.^[143] The authors synthesized linear PNIPAM with trithiocarbonate (TTC)-groups at both α - and ω -terminals as precursors. After aminolysis in the presence of a bisacrylamide trapping agent and a catalyst, a telechelic alkene end-functionalized PNIPAM was yielded. This modified polymer enabled a further thiol–ene crosslinking reaction with a four-arm thiol-terminated crosslinker under UV light.

As the thiol–ene reaction still requires a catalyst or a light source, DTP as a trapping agent appears to be a more elegant alternative. As mentioned above, aminolysis with DTP produces thiol-reactive PDS-groups. Therefore, hydrogels can be formed through the catalyst-free exchange reaction between PDS-group and thiol-based crosslinkers. An overview of a proposed reaction route is shown in **Scheme 4**. The TTC-groups can be incorporated into the chain through copolymerization. More interestingly, the network obtained in this approach is

redox-sensitive. The disulfide linkages are cleavable with a reducing agent (e.g., dithiothreitol (DTT)), liberating thiol-functions which enables a reversible sol-gel transition in response to redox variations later. This crosslinking strategy was used in Publication 2 and 3 in Chapter 3. More experimental details are explained in these publications.



Scheme 4. Schematic illustration of the crosslinking strategy using PDS-functionalized copolymer chains as a precursor.

1.3.3 Summary

This section shows how RAFT-synthesized polymer chains can serve as precursors for physically and chemically crosslinked networks. The advantages of the crosslinking methods involving thiol chemistry are stressed with examples. In the next section, the recent advances in thermoresponsive (“smart”) polymers with different tailored structures and properties, including chemically crosslinked “smart” hydrogels, will be introduced. Their representative application possibilities will also be mentioned.

1.4 Recent Advances in “Smart” Polymers

The thermoresponsive behaviors of polymers depend strongly on the chain structure and composition. For instance, simultaneous copolymerization can predictably tune the LCST- and UCST-type T_{CP} s. By connecting two thermoresponsive polymer blocks with different T_{CP} s, double thermoresponsive polymers can be obtained. The development of RDRP techniques eases the synthesis of complicated polymer chains and networks to a great extent, thereby benefitting the design of polymers with more sophisticated functions. Recent advances in these “smart” polymers will be introduced.

1.4.1 Copolymers with Tunable Cloud Points

Both LCST- and UCST-type T_{CP} s of the chains can be tuned through copolymerization. In principle, a hydrophobic comonomer can lower the LCST-type T_{CP} and elevate the UCST-type T_{CP} in aqueous solutions. **Figure 14** shows the examples of comonomer pairs usually used to tune the T_{CP} s in specific ranges.

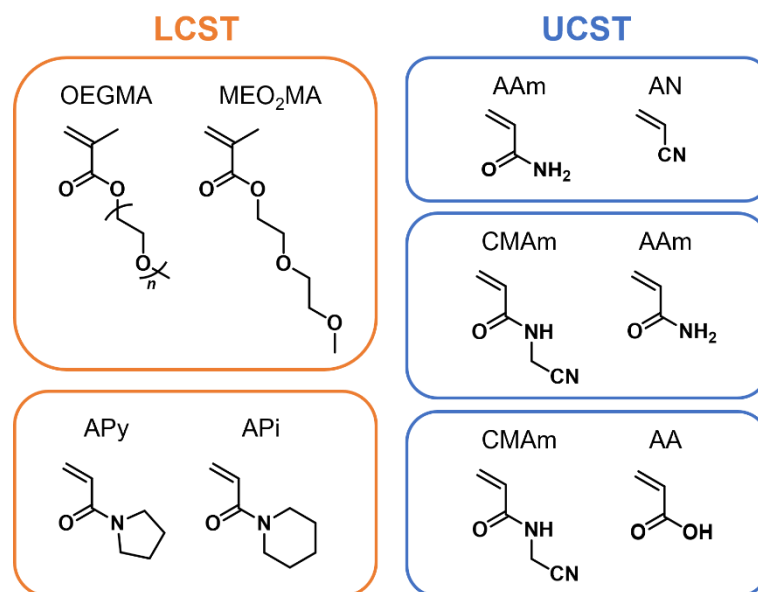


Figure 14. Comonomer pairs found in the literature for tunable LCST transition,^[74, 144] and UCST transition.^[45, 145]

The first example is oligo(ethylene glycol) methacrylate (OEGMA) with an average molecular weight of around 500 Da and di(ethylene glycol) methyl ether methacrylate (MEO₂MA). It is evident that MEO₂MA is more hydrophobic. The LCST-type T_{CP} s of the homopolymers POEGMA and PMEO₂MA are around 95 °C and 28 °C, respectively. The two monomers can readily be polymerized via radical polymerization. The T_{CP} of their copolymer can be adjusted through the comonomer ratio. Interestingly, according to the previous research, when the molar fraction of OEGMA does not exceed 30%, the T_{CP} increases almost linearly with the DP of OEGMA.^[144] With a suitable comonomer ratio and overall DP, a T_{CP} close to body temperature can be reached. Thus, these poly(ethylene)glycol (PEG)-based monomers are regarded as a potential alternative to NIPAM.^[146] This monomer pair was also used in Publication 1 in Chapter 3.

The second example for tunable LCST shown in **Figure 14** is an acrylamide monomer pair, *N*-acryloylpiperidine (APi)/*N*-acryloylpyrrolidine (APy). Their reactivity ratios were determined in the previous study.^[147, 148] The results suggest that the copolymerization of APi and APy gave almost random copolymers. The LCST-type T_{CP} of the copolymer decreased from 47 °C to 3 °C linearly with the increasing molar fraction of APi. Therefore, the T_{CP} adjustment was predictable.

UCST-type T_{CP} s of the polymer chains also allow being flexibly tuned through copolymerization. The first example depicted in **Figure 14** is AAm/AN. AAm is highly hydrophilic, while AN is hydrophobic. By adjusting the balance between two monomers in the copolymer, the T_{CP} can be controlled between 6 °C and 60 °C.^[45] Recently, Audureau et al. reported the UCST transition of homopolymer poly(*N*-cyanomethylacrylamide) (PCMAM) for the first time.^[145] Through RAFT copolymerization with AAm or acrylic acid (AA), the UCST-type T_{CP} could be altered between 22 °C to 85 °C. The analysis of the copolymer composition suggested a random copolymerization mechanism.

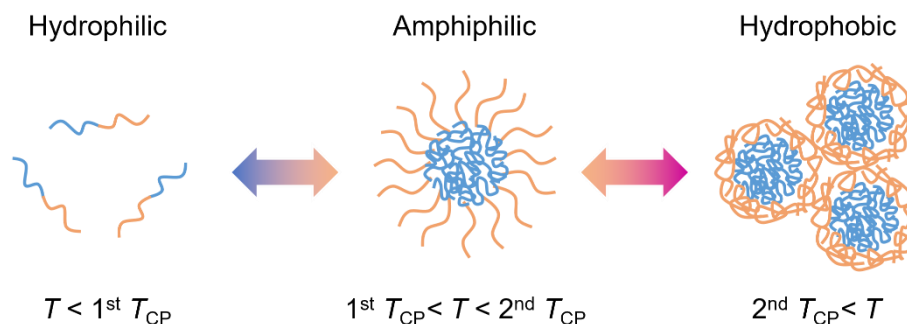
1.4.2 Double Thermoresponsive Copolymers

The polymers exhibiting two separate T_{CP} s can adopt more conformational states in solutions. These materials are currently of great interest in biomedical areas.^[149] A straightforward way to prepare a double thermoresponsive polymer is to combine two monomers of different natures in a block copolymer. This thesis

deals with two types of double thermoresponsive polymer systems: LCST–LCST and UCST–LCST polymer systems.

LCST–LCST Polymer Systems

LCST–LCST polymers typically contain two LCST polymer blocks. As shown in **Scheme 5**, an ideal linear LCST–LCST diblock polymer exhibits a hydrophilic-amphiphilic-hydrophobic transition in water during heating. The polymer chains can self-assemble into amphiphilic micelles when the first T_{CP} is reached. Above the second T_{CP} , larger aggregates or even precipitation can be observed. For the polymerization of such block polymers, monomers like DMAEMA, MEO₂MA, NIPAM, and OEGMA have been proven to be good candidates.^[150–153] Publication 2 and 3 in Chapter 3 focus on the LCST–LCST transitions of graft copolymers which differ significantly from those of diblock copolymers.



Scheme 5. Schematic illustration for the two-step phase transition of an ideal LCST–LCST diblock copolymer in water.

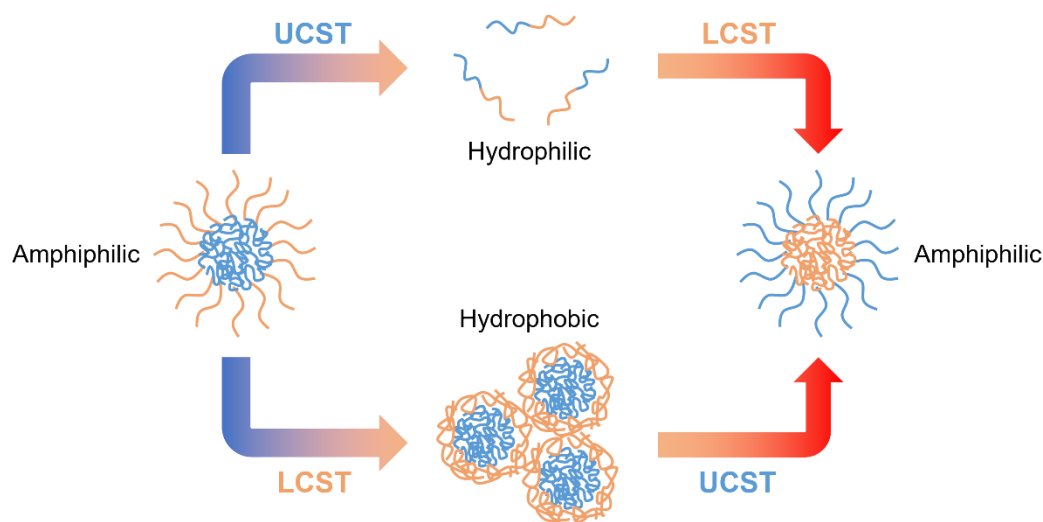
LCST polymers have the potential to be applied as sensors or biosensors due to their rapid phase transition in response to temperature variation.^[154, 155] With two T_{CP} s, the LCST–LCST polymers can provide a more precise temperature diagnosis and be used for a larger test range.^[149]

UCST–LCST Polymer Systems

Polymers with both UCST and LCST properties sometimes are also named schizophrenic polymers.^[156] When the UCST-type T_{CP} is lower than the LCST-type T_{CP} in water, an ideal UCST–LCST diblock polymer exhibits an amphiphilic-hydrophilic-amphiphilic transition during heating (**Scheme 6**, top). The two-step phase transition can lead to structure inversion of the micelles formed by the

diblock copolymer. A series of such polymers have been synthesized by Papadakis et al.^[157-160] The authors thoroughly characterized the self-assembling behaviors of the polymer chains in different environments. Besides linear structures, a UCST–LCST graft polymer was reported by the group of Tenhu.^[161] The poly(sulfobetaine) backbone with zwitterionic groups was responsible for the UCST transition. The LCST transition was rendered by the side chains of P(OEGMA-*co*-MEO₂MA). The thermoresponsive behavior of the graft polymer depended significantly on the length of side chains. However, all the UCST blocks in the copolymers mentioned above comprised zwitterionic monomers. The UCST–LCST diblock polymer systems consisting of nonionic LCST as well as UCST blocks are rare, which is partially attributed to the lack of nonionic UCST monomers.

An example of uncharged diblock polymers exhibiting both UCST and LCST transitions in pure water was reported by Zhao et al.^[162] The diblock polymer was synthesized via RAFT polymerization. The UCST block is the copolymer of AAm and AN, and the LCST block is PDMAEMA. Publication 1 in Chapter 3 also shows the synthesis and characterization of a nonionic UCST–LCST diblock polymer. The advantages of the investigated system are mentioned in that publication.



Scheme 6. Two possible pathways to the structure inversion of micelles formed by ideal UCST–LCST diblock copolymers in water.

The other type of UCST–LCST diblock polymers undergoes an LCST transition first during heating and is even more sparsely reported (**Scheme 6**, bottom). The polymer chains exhibit an amphiphilic-hydrophobic-amphiphilic transition during heating. An example was published by Agarwal et al.^[163] The UCST block was again the copolymer of AAm and AN. The LCST block was PEG stemming from a macro-azoinitiator.

By virtue of the temperature-induced core-shell inversion of their micellar structures, the schizophrenic polymers can be used as nanocarriers in biomedical applications.^[156] The UCST–LCST polymers can also be used to modify the surface of enzymes.^[164] The produced bioconjugates showed improved stability in harsh environments.

1.4.3 “Smart” Hydrogels

“Smart” hydrogels based on thermoresponsive polymers have also been broadly investigated due to their broad application possibilities. With the temperature-induced swelling and deswelling behaviors, thermoresponsive hydrogels can be used as artificial actuators that transform temperature stimulus into motions, like bending, folding or twisting motions.^[165, 166] Several PNIPAM-based hydrogels with characteristic crosslinking density and components have been reported to display anisotropic deformation upon temperature changes.^[167-172] As the volume change of the thermoresponsive hydrogel is sometimes also associated with transparency change, the hydrogels can also be used for optical applications, such as smart windows and responsive photonic crystals.^[173-178] These “smart” materials may help reduce global energy consumption.^[179]

Thermoresponsive hydrogels are also promising platforms in biomedical applications. For drug delivery systems, the pores in the crosslinked polymer networks can load the small drug molecules through hydration. The drug-loaded hydrogels based on LCST polymers can release the small molecules during deswelling at high temperatures.^[180] Karbarz et al. prepared a PNIPAM-based nanogel to encapsulate the drug doxorubicin.^[181] Thus, drug release could be observed at 37 °C. Moreover, the authors used a crosslinker containing disulfide bonds, leading to the degradation of the nanogel and faster drug release in a reducing environment. Another PNIPAM-based nanogel with both thermo- and redox-sensitivity was also reported by Zhan et al.^[182] In addition, “smart”

hydrogels have the potential to serve as tissue engineering scaffolds. For example, Kim et al. developed a photo-crosslinked PNIPAM nanofiber that was able to encapsulate and release cells efficiently in response to temperature changes.^[183]

1.4.4 Summary

This section introduces the recent advances in thermoresponsive polymers with different compositions and structures. Target T_{CP} can be realized through simultaneous copolymerization. Double thermoresponsive polymers have drawn attention from different fields due to their two-step phase transitions. After crosslinking, the application areas of these materials can be further expanded. The goals of this work are synthesizing and characterizing different thermoresponsive polymers with unique peculiarities, including free chains and hydrogels, which will be discussed in the next chapter.

Chapter 2

Goals of The Work

Double thermoresponsive polymers have gained significant attention in polymer research as particles with distinct morphologies can be formed in polymer solutions at different stages during heating or cooling. The synthesis of these polymers seems to be straightforward. With RDRP techniques, polymer blocks with different properties can be combined, e.g., through block copolymerization or graft copolymerization. However, the reality is not always so simple. The character of monomers, block length, end-group, the architecture of chains, and interactions between blocks may all influence the T_{CPs} . It is necessary to take these issues into account before copolymerization in order to get two separated T_{CPs} . Therefore, one main goal of this work is to develop efficient strategies for synthesizing new double thermoresponsive polymers. Meanwhile, the unique self-assembling behaviors of the synthesized polymers in water will be analyzed by various methods.

Linear UCST–LCST Diblock copolymers

The first part of this work deals with synthesizing well-defined nonionic UCST–LCST diblock copolymers via cost-effective photoiniferter RAFT polymerization, which is challenging and sparsely reported in the literature. The difficulty of the synthesis results mainly from the UCST block. First, the previously reported UCST polymers always comprise monomers that are highly toxic or require complicated synthesis and purification. Second, the solubility of the UCST polymers in organic solvents is usually rather limited, restricting the selection of the polymerization medium. To address these issues, Publication 1 in Chapter 3 attempts to use a commercially available monomer, which is water-soluble, solid and easy to handle, for the UCST block. Like other monomers forming the

hydrogen bonding-based UCST polymers, the selected monomer owns both an excellent hydrogen-donor and hydrogen-acceptor. Since the LCST blocks are also water-soluble below the LCST-type T_{CPs} , the study endeavors to prepare UCST blocks through chain extension from LCST blocks in water, a truly eco-friendly solvent.

LCST–LCST Graft Copolymers

The second part of the work concerns LCST–LCST polymers. Considering that the vast majority of the previously reported LCST–LCST polymer systems adopt linear structures, this work aims to synthesize and investigate the LCST–LCST polymers with graft structures. Regarding the synthetic method, the study tries to implement a convenient two-step photoiniferter RAFT strategy belonging to the grafting-from approach. The backbones and side chains will be polymerized with different light sources. The LCST–LCST graft copolymers can be generally divided into two types according to whether the LCST-type T_{CP} of the backbone is higher or lower than that of the side chains. Publication 2 and 3 in Chapter 3 are intended to carefully analyze and compare the thermoresponsive behaviors of the aqueous solutions of these two copolymer types.

“Smart” Hydrogels

In addition to the free polymeric chains, thermoresponsive networks are also attractive. Hence, another goal of this work is to propose a simple method to synthesize multifunctional hydrogels from well-defined thermoresponsive polymers. The desired hydrogel should exhibit distinct water capacities at high and low temperatures and be fully degradable in specific environments. In the case of chemically crosslinked hydrogels, the on-demand degradability requires the linkages fixing the networks to be stimuli-responsive. Publication 2 and 3 endeavor to synthesize and characterize such “smart” hydrogels based on the LCST–LCST graft polymers. The presented synthetic method may hopefully inspire other scientists to prepare multifunctional materials for different applications, such as biomedical applications.

Chapter 3

Cumulative Part

This chapter contains three whole first-author papers published during this work. A short synopsis is written for every publication, emphasizing the central theme of the study.

3.1 Publication 1: Nonionic UCST–LCST Diblock Copolymers with Tunable Thermoresponsiveness Synthesized via PhotoRAFT Polymerization

This publication concisely describes the synthesis and characterization of nonionic diblock copolymers with both UCST and LCST in pure water. The random copolymers of MEO₂MA and OEGMA are responsible for the LCST transition. The nonionic monomer methacrylamide (MAAm) forms the UCST blocks. Compared with AAm and AN mentioned in Section 1.4.1, MAAm is much less toxic. Compared with NAGA, MAAm with high purity can be bought at a fair price, saving the elaborate synthetic steps.

The RAFT polymerization of polymethacrylamide (PMAAm) is, however, not trivial. As PMAAm is exclusively soluble in water at high temperatures, water is the best solvent for the polymerization, not to mention its low hazard. On the other hand, when performing RAFT polymerization of MAAm with an external initiator, the CTAs and initiators containing ionic groups should be avoided as they can suppress UCST. Then the options of chemicals become pretty narrow because most nonionic CTAs and initiators are water-insoluble. This

contradiction was addressed in the following publication by using initiator-free photoiniferter RAFT polymerization. The LCST blocks were prepared first, followed by the chain extension with MAAm in water below the LCST-type T_{CPs} under green light irradiation. The UCST–LCST transitions of the obtained diblock copolymers were confirmed by turbidimetry and dynamic light scattering (DLS) measurements.

The publication is reprinted with permission from J. Xu and V. Abetz, *Macromol. Rapid Commun.* **2021**, *42*, 2000648 – published by Wiley-VCH GmbH. The related supporting information is available in Section 7.2.



Nonionic UCST–LCST Diblock Copolymers with Tunable Thermoresponsiveness Synthesized via PhotoRAFT Polymerization

Jingcong Xu and Volker Abetz*

Nonionic double thermoresponsive diblock copolymers with both upper critical solution temperature (UCST) and lower critical solution temperature (LCST) phase transitions are synthesized via eco-friendly photoiniferter reversible addition–fragmentation chain transfer polymerization. While the biocompatible random copolymer of di(ethylene glycol) methyl ether methacrylate and oligo(ethylene glycol) methacrylate accounts for the LCST transition, the block of polymethacrylamide from an easily accessible monomer with low health hazard is responsible for the UCST transition. Temperature-dependent dynamic light scattering measurements confirm the formation of micellar aggregates in water at the temperatures below UCST- and above LCST-type cloud points. Additionally, the temperature interval between UCST and LCST, where both blocks are dissolved, can be tailored by varying the comonomer ratio in the random copolymer block. With these unique advantages, the presented work introduces a new polymer system for the design of schizophrenic polymers.

Thermo-responsive polymers have become one of the most intriguing “smart” materials in polymer chemistry due to their easily switchable solubility in aqueous or organic solutions upon the change of temperature.^[1–3] The rapid and reversible phase transitions taking place in these polymer solutions can be divided into two types: entropically controlled lower critical solution temperature (LCST) transitions and enthalpically controlled upper critical solution temperature (UCST) transitions.^[4–6] The polymer chains exhibiting an LCST transition are soluble and in a coiled state (which causes entropy loss) due

to the attractive polymer–solvent interactions below the cloud point temperature T_{CP} . Once the temperature rises above T_{CP} , the chains collapse and turn into a globular state while setting free the absorbed solvent molecules.^[6] Conversely, UCST polymers are insoluble below T_{CP} due to strong enthalpic intra- and intermolecular polymer–polymer interactions like hydrogen bonding or ionic interactions.^[4] These interactions are disrupted at elevated temperatures, leading to the dissolution of the polymers.

Polymers with LCST transitions in water have been extensively studied as they can be applied for many applications, like the development of drug delivery,^[7–9] gating membranes,^[10–13] and polymeric thermometers.^[14–16] Among the abundant choices for LCST polymers, poly[oligo(ethylene glycol) methacrylate]s

(POEGMAs) with different lengths of side chains have some superior features. For instance, in comparison with amide-based polymers, the LCST transitions of POEGMAs generally exhibit less apparent hysteresis.^[17] Furthermore, POEGMA with an average repeating unit weight of 500 Da (**Scheme 1**) displays an LCST-type T_{CP} at about 95 °C. By copolymerization with di(ethylene glycol) methyl ether methacrylate (MEO₂MA), the T_{CP} can precisely be adjusted between 28 and 95 °C.^[18] Additionally, the biocompatibility of POEGMAs makes applications in biomedical areas conceivable.^[19,20]

In contrast to the LCST polymers, UCST polymers, especially nonionic UCST polymers, in pure water are much less reported, which could be attributed to their susceptibility to impurities and hydrolysis.^[21–24] The hydrogen bonding based UCST transition of polymethacrylamide (PMAAm) was first reported by Seuring et al.^[25] The polymer was synthesized via conventional free radical polymerization in that study. Recently, our group has reported a green approach to the synthesis of PMAAm via photoiniferter reversible addition–fragmentation chain transfer polymerization (photoRAFT) under UV light irradiation.^[26] The obtained polymers show reversible UCST transitions in mixtures of water and ethanol. In comparison with other UCST monomers, MAAm is also much less toxic.

Apart from the polymers with either an LCST or a UCST transition, schizophrenic polymers combining both LCST and UCST transitions in water have drawn great attention.^[27,28] A straightforward pathway to such polymers is the fabrication

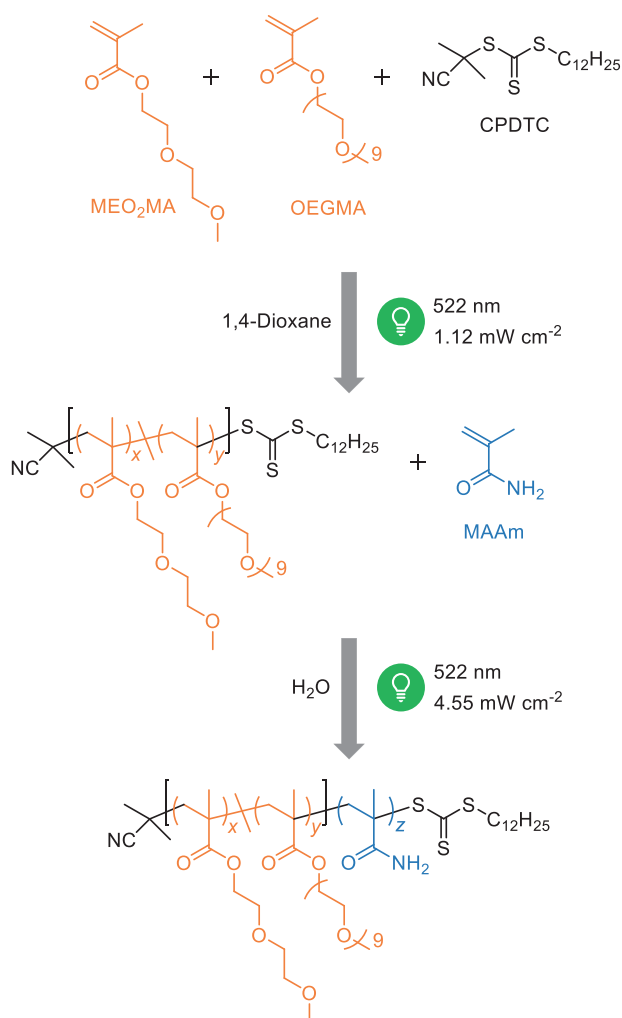
J. Xu, Prof. V. Abetz
 Institute of Physical Chemistry
 Universität Hamburg
 Grindelallee 117, Hamburg 20146, Germany
 E-mail: volker.abetz@hzg.de

Prof. V. Abetz
 Institute of Polymer Research
 Helmholtz-Zentrum Geesthacht
 Max-Planck-Straße 1, Geesthacht 21502, Germany

The ORCID identification number(s) for the author(s) of this article can be found under <https://doi.org/10.1002/marc.202000648>.

© 2021 The Authors. Macromolecular Rapid Communications published by Wiley-VCH GmbH. This is an open access article under the terms of the Creative Commons Attribution License, which permits use, distribution and reproduction in any medium, provided the original work is properly cited.

DOI: 10.1002/marc.202000648



Scheme 1. Two-step photoRAFT polymerization of a P(MEO₂MA-*r*-OEGMA)-*b*-PMAAm diblock copolymer.

of diblock copolymers with both LCST and UCST blocks. The amphiphilic nature of the diblock copolymers in specific temperature ranges leads to the formation of micelles which can undergo structure inversion during both heating and cooling processes. To date, most reported schizophrenic polymers contain polysulfobetaines as UCST blocks.^[29–34] The systems with nonionic UCST blocks are rather scarce. In those few instances, monomers which are either hard accessible or highly toxic were

employed.^[35,36] Because the UCST of a nonionic block is less prone to be disturbed by external conditions,^[25] the exploration of novel nonionic schizophrenic polymers is highly motivated.

In this study, we present a novel nonionic diblock copolymer P(MEO₂MA-*r*-OEGMA)-*b*-PMAAm with both LCST and UCST transitions. All the investigated polymers were synthesized via photoRAFT without any catalysts or initiators, which leads to high chain-end fidelity and avoids the potential influence of end groups of initiators on UCST transitions. As shown in Scheme 1, a nonionic RAFT agent like 2-cyano-2-propyl dodecyl trithiocarbonate (CPDTC) was required for the emergence of the UCST transition of PMAAm.^[25] The light absorption of CPDTC in the region between 400 and 560 nm enables photolysis under both blue and green light (Figure S2, Supporting Information). Based on a previous study by Shanmugam et al.,^[37] green light emitting diodes, which show a peak at 522 nm in the emission spectrum, were chosen to initiate the polymerization as they provide better control for monomers like methacrylates or methacrylamides. The light intensity was set to 1.12 mW cm⁻². Assuming that the reactivities of MEO₂MA and OEGMA are similar,^[38] three random copolymers P(MEO₂MA-*r*-OEGMA) (Table 1) with similar chain lengths were polymerized in the first step. To achieve high chain-end fidelities, the monomer conversions α were all kept at an intermediate level. The kinetic studies shown in Figure S5 (Supporting Information) indicate smooth chain growths with different feed comonomer molar ratios ($R_{\text{ME/OE}}$) after short inhibition periods. The extremely similar rates of polymerization show ignorable influences of $R_{\text{ME/OE}}$. The molar ratios between MEO₂MA and OEGMA in the products ($F_{\text{ME/OE}}$) are calculated from ¹H-NMR spectra (Figures S6–S8, Supporting Information). The results are all in good agreement with $R_{\text{ME/OE}}$ indicating an ideal copolymerization. The relatively narrow dispersities (D) measured by size exclusion chromatography (SEC) manifest successful photoRAFT polymerizations. Number average molecular weights of the macro-RAFTs after purification were also determined by end-group analysis with UV-vis spectroscopy which is supposed to be more accurate than SEC measurements without appropriate calibration standards. The absorbance of the thiocarbonyl group at the ω -terminal at about 308 nm was used.^[39] The obtained values $\bar{M}_{n,\text{end-group}}$ exhibit deviations from the theoretical number average molecular weights $\bar{M}_{n,\text{th}}$. This result is not surprising as a certain portion of short chains was lost after precipitation in *n*-hexane, leading to an increment in the average molecular weight. The relatively low degrees of polymerization and the oily shape of the products promoted this loss even more.

Table 1. Analytical results of P(MEO₂MA-*r*-OEGMA) that were used as macro-RAFTs.

Macro-RAFT ^{a)}	$R_{\text{ME/OE}}$	$F_{\text{ME/OE}}^{\text{b)}$	$\alpha^{\text{c)}$ [%]	$\bar{M}_{n,\text{th}}^{\text{d)}$ [kDa]	$\bar{M}_{n,\text{SEC}}^{\text{e),g)}$ [kDa]	$\bar{M}_{n,\text{end-group}}^{\text{f)}$ [kDa]	$D^{\text{g)}$	$T_{\text{CP}}^{\text{h)}$ [°C]
P(60/40) ₂₇	60/40	60/40	53	8.7	10.9	14.4	1.30	64
P(53/47) ₂₀	50/50	53/47	40	7.3	10.7	13.8	1.33	70
P(46/54) ₂₂	45/55	46/54	44	8.3	11.1	14.3	1.37	73

^{a)}Numbers in parentheses represent comonomer ratios in the products ($F_{\text{ME/OE}}$). Subscripts denote degrees of polymerization based on monomer conversions; ^{b)} $F_{\text{ME/OE}}$ calculated from ¹H-NMR spectra; ^{c)}monomer conversion calculated from ¹H-NMR spectra with reference signal of dimethylformamide (DMF); ^{d)}theoretical number average molecular weight calculated from monomer conversion; ^{e),g)}determined by SEC in tetrahydrofuran (THF) relative to poly(methyl methacrylate) standards; ^{f)}determined by UV-vis analysis in methylene chloride with the absorption coefficient ϵ of 10 400 L mol⁻¹ cm⁻¹ of the model RAFT agent: methyl 2-(butylsulfanylthiocarbonylsulfanyl)-2-methyl propionate^[39]; ^{h)}cloud point determined by DLS measurement.

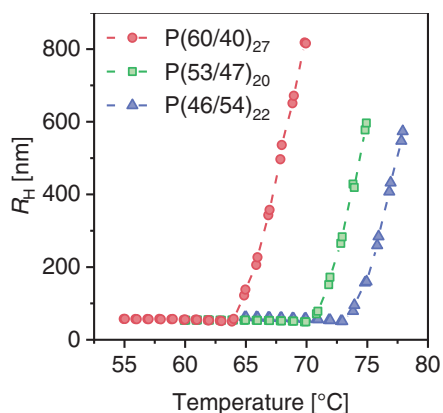


Figure 1. Evolution of hydrodynamic radius (R_H) of macro-RAFTs in aqueous solutions ($c = 0.1\%$ [w/w]) during the heating processes of temperature-dependent DLS measurements. The temperature step was 1°C and two measurements were conducted at each temperature. The obtained intensity correlation functions were fitted by using the cumulant approach (Equations (S1) and (S2), Supporting Information).

Despite the deviations, these three macro-RAFTs still have comparable molecular weights. Hence, their thermoresponsiveness in water can be analyzed together.

The LCST-type T_{CP} of the yielded macro-RAFTs in water were determined by temperature-dependent dynamic light scattering (DLS) measurements so that the change in particle sizes can also be followed (Figure 1). The T_{CP} are determined as the onsets of the abrupt increase in hydrodynamic radius (R_H) during heating (Table 1). The cooling processes can be found in the Supporting Information (Figures S11–S13, Supporting Information). As expected, T_{CP} increases with the OEGMA content in the random copolymer. However, the R_H of about 50 nm below the T_{CP} are much larger than the previously reported values.^[38] The random copolymer of MEO₂MA and OEGMA prepared by atom transfer radical polymerization (ATRP) was reported to have an R_H of about 20 nm which is in accordance with the sizes of unimers in an aqueous solution. Therefore, micelles could already be formed below T_{CP} in our case. This result is actually reasonable considering the hydrophobic dodecyl group at the ω -terminal of the polymers. A similar phenomenon was also described by Lauterbach et al. in a previous study.^[40] In that work it was found that even a butyl group at the end of a via photoRAFT synthesized LCST polymer, poly(*N*-acryloylpyrrolidin), caused formation of micelles below T_{CP} . In addition, these micelles with hydrophilic shells were well stabilized in water and could still be initiated by UV light for chain extensions. Therefore, water, an eco-friendly solvent, has gained the chance to become the solvent in the second step of the polymerization in this work, as well, with green light still serving as the light source.

The choice of the polymerization temperature (T) for the chain extension with MAAM was not trivial. To ensure sufficient solubility of the macro-RAFTs, T was controlled at about 10°C below their T_{CP} . On the other hand, T should also be higher than the predicted UCST-type T_{CP} (40°C according to the literature^[25]) of the PMAAm block, preventing macroscopic phase separation and elevating the polymerization rate. Therefore, the polymerizations were performed at either 55 or 60°C

Table 2. Polymerization temperatures and analytical results of the diblock copolymers.

Diblock copolymers ^{a)}	T [$^\circ\text{C}$]	α^b [%]	$\bar{M}_{n,th}^c$ [kDa]	W_{MAAm}^d [%]
P(60/40) ₂₇ - <i>b</i> -PMAAm ₄₄₀	55	55	46.1	81
P(53/47) ₂₀ - <i>b</i> -PMAAm ₃₅₂	60	44	37.3	80
P(46/54) ₂₂ - <i>b</i> -PMAAm ₂₉₆	60	49	33.5	75
P(46/54) ₂₂ - <i>b</i> -PMAAm ₃₆₁	60	52	39.0	79

^{a)}Numbers in parentheses represent comonomer ratios in the products (FME/OE). Subscripts denote degrees of polymerization based on monomer conversions; ^{b)}monomer conversion calculated from ¹H-NMR spectra with reference signal of DMF; ^{c)}theoretical number average molecular weight calculated from monomer conversion; ^{d)}weight percentage of PMAAm in the product.

(Table 2). As the RAFT polymerization of methacrylamides is usually known to proceed at a slower rate,^[41] the light intensity was increased to 4.55 mW cm^{-2} to raise the radical concentration and accelerate the polymerization.

To prove a good control over the chain extension, an “on–off” kinetic experiment was first performed. The result (Figure 2a) indicates that the polymerization paused when the light went off and was able to continue when the irradiation proceeded. This behavior reveals the recombination of thiyl radicals with

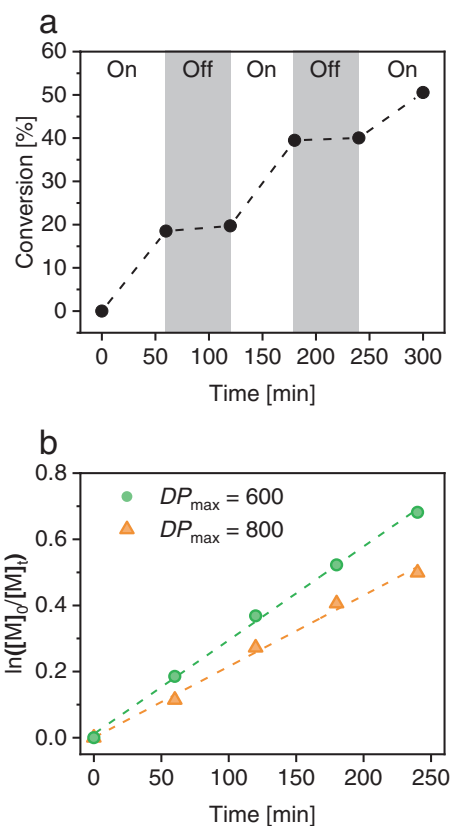


Figure 2. a) “On–off” kinetic plot of a chain extension with MAAM from P(60/40)₂₇ at 55°C in water with a solid concentration of 10% (w/w) and a maximum degree of polymerization (DP_{max}) of 400. The light was turned off in the second and fourth hours; b) pseudo first-order kinetic plots of the chain extensions with MAAM from P(46/54)₂₂ at 60°C in water with different DP_{max} .

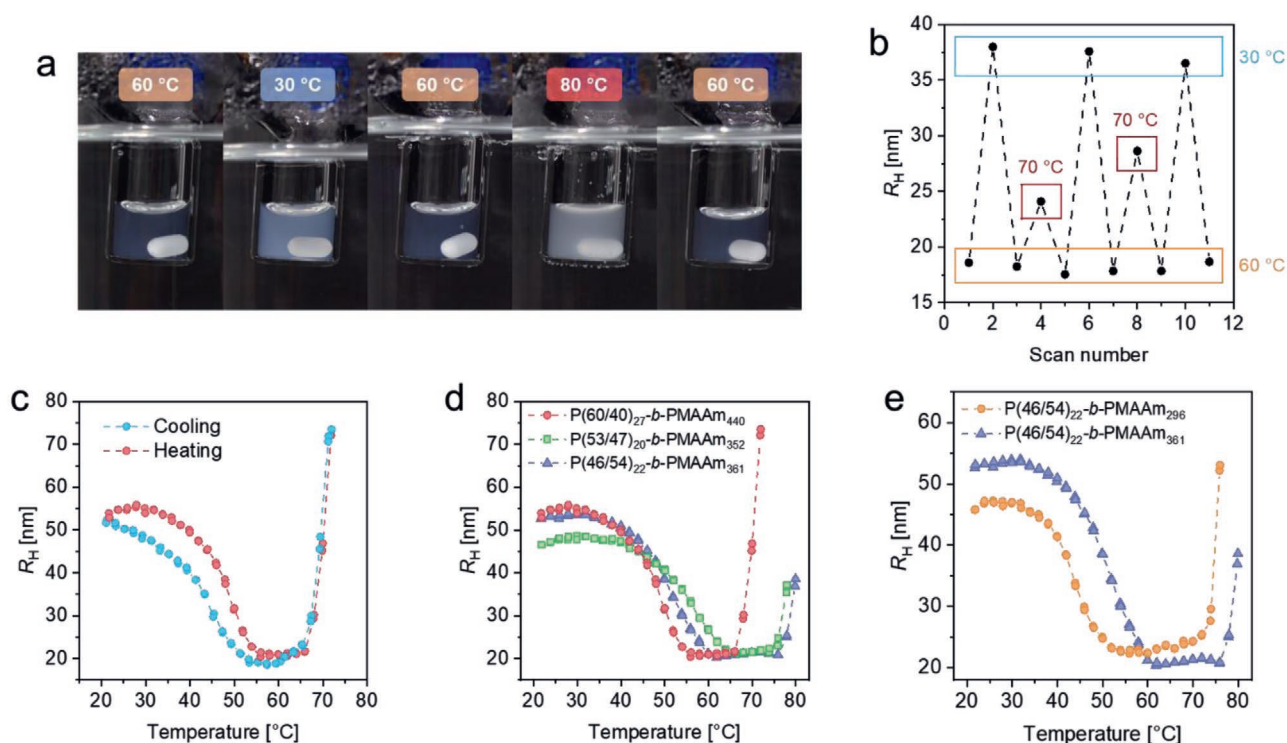


Figure 3. a) Visual turbidimetry of an aqueous solution of P(60/40)₂₇-b-PMAAm₄₄₀ ($c = 2\%$ [w/w]) in a water bath at different temperatures; b) hydrodynamic radii (R_H) of P(60/40)₂₇-b-PMAAm₄₄₀ in an aqueous solution ($c = 0.5\%$ [w/w]) at different temperatures obtained by DLS measurements. The solution was cooled or heated directly to the target temperatures (30, 60, and 70 °C); c) evolution of R_H of P(60/40)₂₇-b-PMAAm₄₄₀ in an aqueous solution ($c = 0.5\%$ [w/w]) obtained by temperature-dependent DLS measurements. The measurement started with a cooling process from 60 to 20 °C, followed by a heating process till 72 °C. Last, the solution was cooled to 60 °C. The temperature step was 2 °C and two measurements were conducted at each temperature; d) comparison of the thermoresponsive behavior of samples with similar contents of PMAAm (W_{PMAAm}) during heating; e) comparison of the thermoresponsive behavior of samples with the same first block but different lengths of the second block during heating. All the obtained intensity correlation functions were fitted by using the cumulant approach.

the propagating radical species without a light source.^[42] Meanwhile, the high livingness of the chains was maintained in dark so that they could be reinitiated rapidly.

Furthermore, the influence of the theoretical maximum degree of polymerization (DP_{max}) on the rate of a photoRAFT polymerization is also an evidence for a good control. Figure 2b displays the kinetic plots of two polymerizations with different DP_{max} . Both of them could be referred to as a pseudo-first order reaction within 240 min, indicating a constant concentration of propagating radical species during the reactions. The apparent propagation rate constants (k_p^{app}) are determined with the linear regression slopes. It is obvious that the reaction with a higher DP_{max} demonstrates a lower k_p^{app} ($k_p^{\text{app}} = 2.1 \text{ min}^{-1}$ for $DP_{\text{max}} = 800$ and $k_p^{\text{app}} = 2.8 \text{ min}^{-1}$ for $DP_{\text{max}} = 600$), which confirms that the chain initiation was a result of photolysis of the macro-RAFT. Given that the solid concentrations (10% [w/w]) in both reaction solutions were identical, the concentration of the macro-RAFT decreased with increasing DP_{max} , leading to a decrease in the radical concentration.

Finally, five yielded diblock copolymers are listed in Table 2. To minimize the influence of the dodecyl group at the ω -terminal on the solubilities of the copolymers in water, relatively long PMAAm blocks were polymerized. The monomer conversions were also kept at an intermediate level to reduce

the chance for chain termination. The combination of UCST and LCST transitions was first tested visually (Figure 3a). An aqueous solution of P(60/40)₂₇-b-PMAAm₄₄₀ ($c = 2\%$ [w/w]) with very low turbidity could be achieved at 60 °C. When cooling the water bath to room temperature gradually, the solution turned white. Micellar aggregates with PMAAm in the core and P(60/40)₂₇ block in the shell are expected to be formed. The sample could be dissolved again at 60 °C, implying a reversible UCST transition. Meanwhile, the LCST transition was still maintained. The solution became white again at 80 °C. At this stage, the micellar structure should be inverted, that is, P(60/40)₂₇ block is now forming the core. With PMAAm block as a stabilizing agent, no macroscopic precipitation was observed up to 80 °C. Next, the transmittance of the solution at different temperatures was quantitatively examined (Figure S10, Supporting Information). The curve of the heating process clearly shows a UCST transition. However, the value of transmittance could not reach 100% even when the temperature was above 60 °C, suggesting that the impact of the hydrophobic dodecyl group on the solubility still plays a role at this concentration.

Apart from the change in solubility, unfortunately, the promising UCST transition also brings troubles for SEC measurements.^[43] The PMAAm block is insoluble in virtually all common

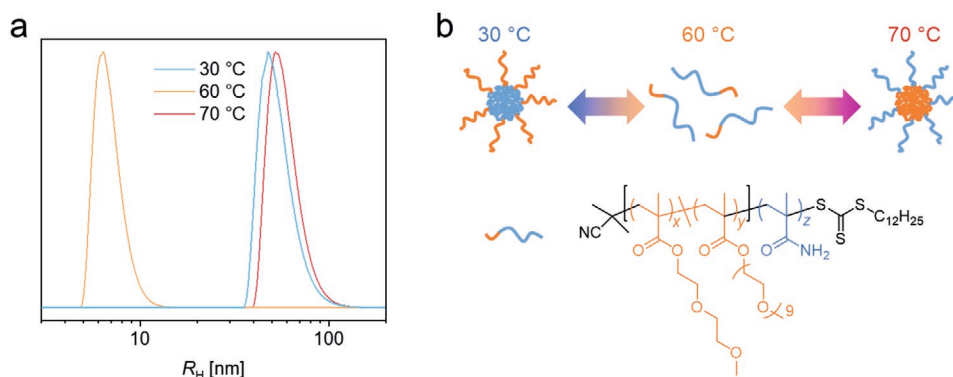


Figure 4. a) Intensity-weighted size distribution of $\text{P}(60/40)_{27}\text{-}b\text{-PMAAm}_{440}$ in an aqueous solution ($c = 0.5\%$ [w/w]) at representative temperatures obtained by CONTIN analysis on the DLS data; b) schematic illustration of the structure inversion of the micelle formed by macromolecules of a diblock copolymer in a dilute aqueous solution.

organic solvents which can be used as eluents for SEC, such as THF, dimethylacetamide, DMF, chloroform and dimethyl sulfoxide. It is exclusively soluble in water at elevated temperatures. It is also rather difficult to hydrolyze the polymer completely to make water become a suitable eluent at lower temperatures.^[44] However, even without SEC results, the kinetic studies demonstrated in Figure 2 are convincing enough to exclude the possibilities of significant chain termination, unexpected chain transfer and self-polymerization taking place during the polymerizations.

After concluding the successful chain extensions and the double thermoresponsiveness, the reversibility of the phase transitions can be resolved by DLS measurements more clearly. To avoid multiple scattering, the aqueous solution was diluted to 0.5% (w/w) before the measurements. The result (Figure 3b) agrees well with the visual turbidimetry. The polymer chains were capable of aggregating below the UCST-type and above the LCST-type T_{CP} . The UCST transition, which is usually more precious than LCST transitions, could successfully be repeated at least three times.

Although the solution ($c = 0.5\%$ [w/w]) was then too dilute for the transmittance measurement (Figure S10, Supporting Information), more details of phase transitions as well as the evolution of R_H can be delivered by temperature-dependent DLS measurements (Figure 3c). As the UCST transition of PMAAm is sensitive to hydrolysis,^[26] the temperature step of cooling and heating was fixed at 2 °C to reduce the time consumption. Consequently, a reversible UCST transition can be observed between 20 and 56 °C. The UCST-type T_{CP} can now be determined as the offset of the heating process, which is about 56 °C. Due to the lower chain mobility of the PMAAm block, which is reflected by its high glass transition temperature,^[25,45] the UCST transition exhibits an evident hysteresis. It is worth noticing that the R_H at 30 °C in Figure 3b is smaller than that in Figure 3c, which is attributed to the faster cooling rate in the former case. In order to avoid the formation of oversize agglomerates without stirring during the measurement, the heating process was stopped at 72 °C. The LCST-type T_{CP} can be found at about 66 °C, which is only marginally higher than that of $\text{P}(60/40)_{27}$. In comparison with the UCST transition, the much sharper LCST transition originates from its entropic-driven feature.^[4,46] A more elaborate CONTIN analysis on the

DLS data confirms the change of the particle sizes at different temperatures (Figure 4a). According to the intensity-weighted size distribution (Figure 4a), most of the polymers were dissolved to unimers with R_H below 10 nm. Therefore, structure inversion of the formed micelles in a dilute aqueous solution can be expected (Figure 4b).

The double thermoresponsiveness can be found in other samples in Table 2 as well. The thermoresponsive behavior of three samples with similar W_{MAAm} is compared in Figure 3d. For simplicity, only the heating processes are displayed. The steepness of the UCST transitions of the three solutions varies. The UCST transition of $\text{P}(53/47)_{20}\text{-}b\text{-PMAAm}_{352}$ is not as sharp as those of the other two samples. This probably results from different degrees of interference like attraction between two blocks as the components of the macro-RAFTs are different from each other. However, considering that the UCST transition of PMAAm itself is broad, the distinction between the UCST transitions of $\text{P}(60/40)_{27}\text{-}b\text{-PMAAm}_{440}$ and $\text{P}(46/54)_{22}\text{-}b\text{-PMAAm}_{361}$ is overall not significant. As for the LCST transitions, the trend of T_{CP} from the macro-RAFTs is maintained. Therefore, it is possible to tune the region between UCST and LCST, where the polymer is completely dissolved, by varying $F_{\text{ME/OE}}$ in the first block. Furthermore, the influence of the chain length of PMAAm was investigated (Figure 3e). With a shorter PMAAm block, the micelles formed by $\text{P}(46/54)_{22}\text{-}b\text{-PMAAm}_{296}$ at low temperatures are clearly smaller. On the other hand, the LCST-type T_{CP} decreases, implying an increased hydrophobicity due to a lower W_{MAAm} .

In summary, we successfully synthesized and characterized novel nonionic diblock copolymers featuring both UCST and LCST. The kinetic studies proved that both polymerization steps were well controlled under green light irradiation. The double thermoresponsiveness of the obtained diblock copolymers is pronounced and exhibits excellent reversibility. The polymers can be completely dissolved between two types of transitions in dilute solutions. At low and elevated temperatures, micellar aggregates with reversed cores and shells can be formed. Eventually, the low toxicity of the monomers and polymers along with the green synthetic approach make this polymer system very appealing to applications in biomedical areas or in thermoresponsive membranes and coating materials.

Supporting Information

Supporting Information is available from the Wiley Online Library or from the author.

Acknowledgements

The work is financially supported by Universität Hamburg and a collaborative project funded by the Helmholtz Association and the Russian Science Foundation. The authors would like to thank Tilman Eckert, Felix Lauterbach, and Niklas Lucht for their constructive advice and Martin Kehden for his help with SEC measurements.

Open access funding enabled and organized by Projekt DEAL.

Conflict of Interest

The authors declare no conflict of interest.

Keywords

lower critical solution temperature, photoiniferter reversible addition-fragmentation chain transfer polymerization, schizophrenic polymers, thermoresponsive diblock copolymers, upper critical solution temperature

Received: October 31, 2020

Revised: December 6, 2020

Published online: January 15, 2021

-
- [1] G. Vancoillie, D. Frank, R. Hoogenboom, *Prog. Polym. Sci.* **2014**, *39*, 1074.
- [2] X. Xu, Y. Liu, W. Fu, M. Yao, Z. Ding, J. Xuan, D. Li, S. Wang, Y. Xia, M. Cao, *Polymers* **2020**, *12*, 580.
- [3] D. Mukherji, C. M. Marques, K. Kremer, *Annu. Rev. Condens. Matter Phys.* **2020**, *11*, 271.
- [4] C. Zhao, Z. Ma, X. X. Zhu, *Prog. Polym. Sci.* **2019**, *90*, 269.
- [5] Y. Kotsuchibashi, M. Ebara, T. Aoyagi, R. Narain, *Polymers* **2016**, *8*, 380.
- [6] S. Eggers, B. Fischer, V. Abetz, *Macromol. Chem. Phys.* **2016**, *217*, 735.
- [7] H. Wei, S.-X. Cheng, X.-Z. Zhang, R.-X. Zhuo, *Prog. Polym. Sci.* **2009**, *34*, 893.
- [8] Y. Chen, Y. Gao, L. P. da Silva, R. P. Pirraco, M. Ma, L. Yang, R. L. Reis, J. Chen, *Polym. Chem.* **2018**, *9*, 4063.
- [9] G.-F. Luo, W.-H. Chen, X.-Z. Zhang, *ACS Macro Lett.* **2020**, *9*, 872.
- [10] Y.-C. Chen, R. Xie, L.-Y. Chu, *J. Membr. Sci.* **2013**, *442*, 206.
- [11] J. I. Clodt, V. Filiz, S. Rangou, K. Buhr, C. Abetz, D. Höche, J. Hahn, A. Jung, V. Abetz, *Adv. Funct. Mater.* **2013**, *23*, 731.
- [12] F. Schacher, T. Rudolph, F. Wieberger, M. Ulbricht, A. H. E. Müller, *ACS Appl. Mater. Interfaces* **2009**, *1*, 1492.
- [13] T. P. T. Dao, L. Vezekov, G. Subra, M. Amblard, M. In, J.-F. Le Meins, F. Aubrit, M.-A. Moradi, V. Ladmiral, M. Semsarilar, *Macromolecules* **2020**, *53*, 7034.
- [14] L. Sambe, V. R. de La Rosa, K. Belal, F. Stoffelbach, J. Lyskawa, F. Delattre, M. Bria, G. Cooke, R. Hoogenboom, P. Woisel, *Angew. Chem., Int. Ed.* **2014**, *53*, 5044.
- [15] G. Vancoillie, J. F. R. Van Guyse, L. Voorhaar, S. Maji, D. Frank, E. Holder, R. Hoogenboom, *Polym. Chem.* **2019**, *10*, 5778.
- [16] R. París, I. Quijada-Garrido, O. García, M. Liras, *Macromolecules* **2011**, *44*, 80.
- [17] J. F. Lutz, Ö. Akdemir, A. Hoth, *J. Am. Chem. Soc.* **2006**, *128*, 13046.
- [18] J. F. Lutz, A. Hoth, *Macromolecules* **2006**, *39*, 893.
- [19] N. Badi, J. F. Lutz, *J. Controlled Release* **2009**, *140*, 224.
- [20] J. F. Lutz, J. Andrieu, S. Üzgün, C. Rudolph, S. Agarwal, *Macromolecules* **2007**, *40*, 8540.
- [21] J. Seuring, F. M. Bayer, K. Huber, S. Agarwal, *Macromolecules* **2012**, *45*, 374.
- [22] B. A. Pineda-Contreras, F. Liu, S. Agarwal, *J. Polym. Sci., Part A: Polym. Chem.* **2014**, *52*, 1878.
- [23] J. Seuring, S. Agarwal, *Macromol. Rapid Commun.* **2012**, *33*, 1898.
- [24] Z. Xu, W. Liu, *Chem. Commun.* **2018**, *54*, 10540.
- [25] J. Seuring, S. Agarwal, *Macromolecules* **2012**, *45*, 3910.
- [26] T. Eckert, V. Abetz, *J. Polym. Sci.* **2020**, *58*, 3050.
- [27] C. M. Papadakis, P. Müller-Buschbaum, A. Laschewsky, *Langmuir* **2019**, *35*, 9660.
- [28] Y. Kotsuchibashi, *Polym. J.* **2020**, *52*, 681.
- [29] N. S. Vishnevetskaya, V. Hildebrand, M. A. Dyakonova, B.-J. Niebuur, K. Kyriakos, K. N. Raftopoulos, Z. Di, P. Müller-Buschbaum, A. Laschewsky, C. M. Papadakis, *Macromolecules* **2018**, *51*, 2604.
- [30] N. S. Vishnevetskaya, V. Hildebrand, N. M. Nizardo, C.-H. Ko, Z. Di, A. Radulescu, L. C. Barnsley, P. Müller-Buschbaum, A. Laschewsky, C. M. Papadakis, *Langmuir* **2019**, *35*, 6441.
- [31] J. V. M. Weaver, S. P. Armes, V. Bütün, *Chem. Commun.* **2002**, *2002*, 2122.
- [32] J. Virtanen, M. Arotçaréna, B. Heise, S. Ishaya, A. Laschewsky, H. Tenhu, *Langmuir* **2002**, *18*, 5360.
- [33] M. Arotçaréna, B. Heise, S. Ishaya, A. Laschewsky, *J. Am. Chem. Soc.* **2002**, *124*, 3787.
- [34] Y. Maeda, H. Mochiduki, I. Ikeda, *Macromol. Rapid Commun.* **2004**, *25*, 1330.
- [35] L. Mäkinen, D. Varadharajan, H. Tenhu, S. Hietala, *Macromolecules* **2016**, *49*, 986.
- [36] H. Zhang, X. Tong, Y. Zhao, *Langmuir* **2014**, *30*, 11433.
- [37] S. Shanmugam, J. Cuthbert, T. Kowalewski, C. Boyer, K. Matyjaszewski, *Macromolecules* **2018**, *51*, 7776.
- [38] M. Bozorg, B. Hankiewicz, V. Abetz, *Soft Matter* **2020**, *16*, 1066.
- [39] K. Skrabania, A. Miasnikova, A. M. Bivigou-Koumba, D. Zehm, A. Laschewsky, *Polym. Chem.* **2011**, *2*, 2074.
- [40] F. Lauterbach, V. Abetz, *Soft Matter* **2020**, *16*, 2321.
- [41] Z. Zhang, H. Li, S. Kasmi, S. Van Herck, K. Deswarte, B. N. Lambrecht, R. Hoogenboom, L. Nuhn, B. G. De Geest, *Angew. Chem., Int. Ed.* **2019**, *58*, 7866.
- [42] J. Luo, M. Li, M. Xin, W. Sun, W. Xiao, *Macromol. Chem. Phys.* **2016**, *217*, 1777.
- [43] J. Seuring, Ph.D. Thesis, University of Marburg, Marburg, **2012**.
- [44] V. F. Kurenkov, H.-G. Hartan, F. I. Lobanov, *Russ. J. Appl. Chem.* **2001**, *74*, 543.
- [45] F. Käfer, M. Pretschner, S. Agarwal, *Macromol. Rapid Commun.* **2018**, *39*, 1800640.
- [46] C. Pietsch, R. Hoogenboom, U. S. Schubert, *Polym. Chem.* **2010**, *1*, 1005.

3.2 Publication 2: Double Thermoresponsive Graft Copolymers with Different Chain Ends: Feasible Precursors for Covalently Crosslinked Hydrogels

After discussing the linear UCST–LCST diblock copolymers, this publication presents the LCST–LCST graft copolymers and a chemical crosslinking strategy enabled by aminolysis of the TTC-groups.

The graft copolymers were prepared solely through photoiniferter RAFT polymerization. Green and blue light-emitting diodes (LEDs) were used to initiate the growths of the POEGMA backbones and PNIPAM side chains, respectively. Investigating the influence of the chain end on the copolymers' thermoresponsive behaviors revealed the importance of a rational CTA selection for the polymerization of backbones. A hydrophilic end-group brought by CTA can hinder the chains' aggregation to a great extent. The graft copolymers were observed to form particles with a small hydrodynamic radius (R_H) and low aggregation number in dilute aqueous solutions above the first T_{CP} (i.e., when the PNIPAM side chains became hydrophobic), which can be attributed to the intramolecular interaction of the graft structure.

Unlike the UCST–LCST copolymers, the LCST–LCST copolymers are excellently soluble in many organic solvents. Moreover, the chains prepared through this photoiniferter RAFT approach possess multiple TTC-groups, enabling simple post-polymerization modification aiming for chemical crosslinking. Therefore, these copolymers are regarded as feasible precursors for thermoresponsive hydrogels.

The publication is reprinted with permission from J. Xu and V. Abetz, *Soft Matter* **2022**, *18*, 2082–2091 – published by The Royal Society of Chemistry. The related supporting information is available in Section 7.3.



Cite this: *Soft Matter*, 2022, 18, 2082

Double thermoresponsive graft copolymers with different chain ends: feasible precursors for covalently crosslinked hydrogels†

Jingcong Xu ^a and Volker Abetz ^{*ab}

The tailored synthesis of graft copolymers from acrylic and methacrylic monomers can be accomplished solely through photoiniferter reversible addition–fragmentation chain transfer (RAFT) polymerization. Samples with poly[oligo(ethylene glycol) methacrylate] (POEGMA) backbones synthesized under green light irradiation and poly(*N*-isopropylacrylamide) (PNIPAM) side chains growing under blue light irradiation are presented. As monitored by temperature-dependent dynamic light scattering (DLS) measurements and temperature-variable nuclear magnetic resonance (NMR) spectroscopy, the architecture of the graft copolymers allows unique two-step lower critical solution temperature (LCST) transitions in aqueous solutions. Meanwhile, different end-groups introduced by the corresponding RAFT agents affect the detailed thermoresponsive behavior remarkably. This RAFT strategy shows more advantages when the multiple trithiocarbonate groups are converted into thiol reactive pyridyl disulfide (PDS) groups *via* a facile post-polymerization modification. The PDS-terminated graft copolymer can then be regarded as a usable precursor for various applications, such as thermoresponsive hydrogels.

Received 29th November 2021,
Accepted 17th February 2022

DOI: 10.1039/d1sm01692j

rsc.li/soft-matter-journal

Introduction

Thermoresponsive polymers can reversibly change their solubility in specific solvents in response to temperature changes. Thermoresponsive homopolymers with a lower critical solution temperature (LCST) in water turn from a hydrophilic into a hydrophobic state once the solutions are heated beyond their cloud points (or phase transition temperatures) (T_{PT}). When two blocks of LCST polymers are coupled together, double thermoresponsiveness can be expected when the concentrations meet the critical aggregation concentration.^{1–3} To date, a variety of linear block copolymers with two LCST-type T_{PT} have been reported. Their potential applications in biomedical areas were highlighted in recent reviews.^{4–6} In contrast to linear architectures, multi-thermoresponsive graft copolymers remained sparsely investigated, which is surprising as graft copolymers with stimuli-responsive backbones or side chains usually show unique self-assembling behavior and rheological properties in water due to their confined structures and additional intramolecular interactions.^{7,8} In this contribution, we present double thermoresponsive graft copolymers with

poly[oligo(ethylene glycol) methacrylate] (POEGMA) as their backbones and poly(*N*-isopropylacrylamide) (PNIPAM) as the side chains. As POEGMA and PNIPAM are both commonly used LCST polymers with wide applications in biomedical areas,^{9–16} the study of the thermoresponsiveness of their graft copolymers is particularly appealing.

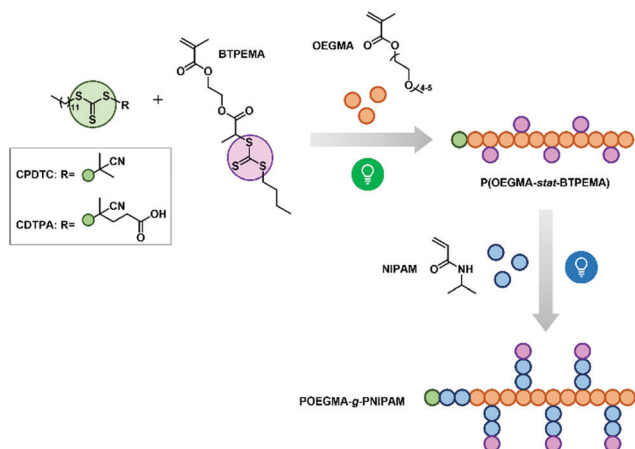
The development of different reversible deactivation radical polymerization (RDRP) techniques provides facile and versatile routes for the synthesis of graft copolymers.^{17,18} However, the polymerization often requires the combination of two RDRP methods, like reversible addition–fragmentation chain transfer (RAFT) polymerization and atom transfer radical polymerization (ATRP).^{19,20} These methods could lead to laborious synthetic and purification steps. Recently, photoiniferter polymerization was found to be a more efficient route for the preparation of polymers with graft or brush structures.^{21–24} In 2018, a catalyst-free photoiniferter RAFT polymerization that was selectively initiated by two kinds of visible light irradiation was introduced for the preparation of graft copolymers.²² In that study, methyl methacrylate (backbone) was polymerized *via* photoiniferter RAFT under green light irradiation, while *N,N*-dimethylacrylamide (side chains) was polymerized under blue light irradiation. The same two-step synthetic route could also be applied to our work. As shown in Scheme 1, the copolymerization of OEGMA and the RAFT inimer, 2-(2-(*n*-butyltrithiocarbonate)propionate)ethyl methacrylate (BTPEMA), was performed in the first step. The polymerization was mediated either by 2-cyano-2-propyl dodecyl trithiocarbonate

^a Institute of Physical Chemistry, Universität Hamburg, Grindelallee 117, 20146 Hamburg, Germany

^b Institute of Membrane Research, Helmholtz-Zentrum Hereon, Max-Planck-Straße 1, 21502 Geesthacht, Germany. E-mail: volker.abetz@hereon.de

† Electronic supplementary information (ESI) available. See DOI: 10.1039/d1sm01692j





Scheme 1 Synthetic route for graft copolymers, and used monomers and RAFT agents in this study.

(CPDTC) or 4-cyano-4-[(dodecylsulfanylthiocarbonyl)sulfanyl]penta-*noic* acid (CDTPA). These two RAFT agents with distinct R-groups can both provide good control for the polymerization of methacrylates under green light irradiation (515 nm).^{22,25} BTPEMA, on the other hand, shows no absorption in the green light region, preventing the photolysis of the trithiocarbonate (TTC) pendant groups (marked in lilac). In addition, the fragmentation to secondary carbon radical R-groups is not favored in the RAFT pre-equilibrium step (*i.e.*, in the chain transfer process).²² BTPEMA thus made no contribution to the radical propagation under green light, enabling the achievement of linear statistical copolymers P(OEGMA-*stat*-BTPEMA) that bore different functions at α -terminals. In the second synthetic step, all the TTC-groups along the chain could be activated by blue light irradiation (467 nm). They served as branching points from which PNIPAM side chains grew simultaneously under good control. The aim of using two different RAFT agents in the first step was to examine the influence of end-group on the thermoresponsive behavior of polymers in aqueous solutions. Previously, it was reported that the functionality at the chain end of linear LCST polymers sometimes affects the self-assembly of chains to a great extent.^{26–29} In this work, it was discovered that it plays a crucial role in the synthesized graft copolymers as well. The intriguing self-assembling behaviors of different samples in dilute solutions will be discussed in the following section.

Besides the convenient accessibility, another compelling advantage of the graft copolymers fabricated solely through the photoiniferter RAFT approach is that all the TTC-groups can undergo various kinds of modifications. In the past decades, abundant processes have been developed to remove the thiocarbonylthio moieties of polymers synthesized by RAFT polymerization for various purposes.^{30–40} The TTC-group can be converted to thiol functionality when reacting with suitable primary amines.³⁰ By treating the RAFT-synthesized polymers with an amine and 2,2'-dithiodipyridine (DTP) simultaneously, stable pyridyl disulfide (PDS)-terminated polymers can be generated directly. In the field of polymer therapeutics, the PDS-group is known for its thiol reactivity under mild

conditions.^{41–45} Thus, the PDS-functionalized polymers have an enormous potential for further modifications according to specific applications. Herein, we present exemplarily an efficient way to afford a covalently crosslinked hydrogel from PDS-terminated graft polymers.

Experimental

Materials

CPDTC (abcr, 97%), CDTPA (abcr, 97%), DTP (TCI, 98%), 2,2'-(ethylenedioxy)diethanethiol (EDT, Sigma Aldrich, 95%), hexylamine (Sigma Aldrich, 99%). BTPEMA was synthesized according to the literature.²² All the solvents were used as received. OEGMA (Sigma Aldrich, $\bar{M}_n = 300$ Da) was passed through activated basic alumina prior to the polymerizations. NIPAM (TCI, 98%) was recrystallized twice from *n*-hexane and stored at -30 °C.

Procedure for the polymerization of backbones

In a typical photoiniferter RAFT polymerization of P(OEGMA-*stat*-BTPEMA), OEGMA, BTPEMA and RAFT agent ([OEGMA]/[BTPEMA]/[CPDTC or CDTPA] = 390/10/1) were dissolved in 1,4-dioxane in a polymerization vial. Dimethylformamide (DMF) was added as an internal standard for calculation of conversion. The total solid (RAFT agent plus the monomers) concentration was kept at 20% (w/w). The polymerization vial was purged with nitrogen for 15 min and the reaction was subsequently carried out at 70 °C under green light irradiation (515 nm) of 1.13 mW cm⁻². After 3 h, the polymerization was stopped by exposing the mixture to air and cooling with an ice bath. Conversion was determined by nuclear magnetic resonance (NMR) spectroscopy. The polymer was then purified through precipitation in an excess amount of *n*-hexane three times. The purified product was dried *in vacuo* at 40 °C for 24 h.

Procedure for the polymerization of POEGMA-*g*-PNIPAM graft copolymers

In a typical photoiniferter RAFT polymerization of POEGMA-*g*-PNIPAM, NIPAM and the POEGMA backbone ([NIPAM]/[P(OEGMA-*stat*-BTPEMA)] = 560/1, [NIPAM]/[TTC] = 80/1) were dissolved in 1,4-dioxane in a polymerization vial. DMF was then added as an internal standard for calculation of conversion. The total solid (P(OEGMA-*stat*-BTPEMA) plus NIPAM) concentration was kept at 15% (w/w). The polymerization vial was purged with nitrogen for 15 min and the reaction was subsequently carried out at 70 °C under blue light irradiation (467 nm) of 3.86 mW cm⁻². After 4 h, the polymerization was stopped by exposing the mixture to air and cooling with an ice bath. Conversion was determined by NMR. The polymer was then purified through precipitation in an excess amount of diethyl ether three times. The purified product was dried *in vacuo* at room temperature for 24 h. For the kinetic study, aliquots of the reaction mixture were taken at specific moments during the polymerization and directly diluted with deuterated



chloroform to determine monomer conversions through $^1\text{H-NMR}$ spectra.

Procedure for the post-polymerization modification of graft copolymers

POEGMA-*g*-PNIPAM ($\bar{M}_{n,\text{th}} = 93.1$ kDa, 7 TTC-functions per chain) (210 mg, 0.016 mmol TTC-functions) and DTP (173 mg, 50-fold molar excess with respect to TTC) was dissolved in 4 mL 1,4-dioxane. The solution was purged with nitrogen for 15 min to remove oxygen. Afterwards, 0.1 mL of the hexylamine solution (0.1 mL hexylamine dilute in 2 mL 1,4-dioxane) (2.5-fold molar excess with respect to TTC) was added under the protection of nitrogen. The reaction mixture stayed yellow and was stirred overnight at room temperature. After precipitation in diethyl ether (4 times), a white PDS-functionalized polymer, POEGMA-*g*-PNIPAM-PDS, was recovered.

Procedure for hydrogel preparation

POEGMA-*g*-PNIPAM-PDS ($\bar{M}_{n,\text{th}} = 92.8$ kDa, 7 PDS-functions per chain) (162 mg, 0.012 mmol PDS-functions) was dissolved in 0.4 mL DMF in a glass vial. Afterwards, 0.02 mL of the EDT solution (0.1 mL EDT dilute in 2 mL DMF) (0.011 mmol thiol-functions) was added quickly. After shaking for seconds, the reaction mixture turned uniformly yellow immediately. In a few minutes, a free-standing gel with yellow color could be observed. The vial was then put aside at room temperature for 30 min to allow further gelation. Afterwards, the gel was immersed in tetrahydrofuran (THF) to remove the crosslinker, uncrosslinked polymer chains, DMF and other small molecules. When the gel became colorless, the residual THF was allowed to evaporate at room temperature. Finally, the gel was dried *in vacuo*.

Analytics

Nuclear magnetic resonance (NMR) spectroscopy. Standard $^1\text{H-NMR}$ spectra were recorded with a BRUKER AVANCE II 400 MHz instrument at a temperature of 300 K. For temperature-variable $^1\text{H-NMR}$ spectra, 2 mg sample were dissolved in 0.7 mL D_2O . The spectra were measured with an increment of 10 °C and normalized by the integrated intensity of the solvent peak.

Size exclusion chromatography (SEC). For the statistical copolymers of OEGMA and BTPEMA, THF was used as the mobile phase with a flow rate of 1.0 mL min^{-1} at 30 °C. The measurements were conducted on an AGILENT 1260 INFINITY system containing PSS SDV separation columns and a refractive index (RI) detector. For the graft copolymers, *N,N*-dimethylacetamide (DMAc) with 0.1 M LiCl was used as the eluent at a flow rate of 1.0 mL min^{-1} . The measurements were performed with PSS GRAM columns at a temperature of 50 °C. For the determination of molecular weights and dispersities of the polymers, the SEC systems were calibrated with narrowly distributed poly(methyl methacrylate) (PMMA) standards.

Ultraviolet-visible (UV-vis) spectroscopy. The UV-vis spectra were recorded with a spectrophotometer UV5 from METTLER TOLEDO at room temperature.

Dynamic light scattering (DLS) measurements. The aqueous solutions were prepared by stirring the samples in Milli-Q[®]

water for 24 h before the measurements. The measurements were performed by using an ALV/CGS-3 Compact Goniometer-System with an ALV/LSE-5004 Multiple Tau Digital Correlator and a Nd:YAG laser (532 nm, 400 mW). The measuring angle was 90° for all measurements. The duration of every measurement was 60 s. The viscosity and refractive index of water at each temperature were automatically corrected in the ALV Digital Correlator Software 3.0. The solution in a glass vial was put into a toluene bath. The temperature step of heating and cooling processes was controlled at 1 °C by a Julabo F25 thermostat, whose temperature accuracy was set to 1 °C. The DLS results were evaluated by using a program written by Felix Lauterbach based on a cumulant approach.⁴⁶

Static light scattering (SLS) measurements. The same instrument was used for DLS and SLS measurements. The aqueous solution was filtered through a microporous (200 nm) regenerated cellulose filter prior to the measurement. The range of the measuring angles was from 30° to 150°. The weight average molecular weight (\bar{M}_w) was estimated through the partial Zimm analysis (see eqn (S8), ESI[†]) in the software ALVStat. The aggregation number (N_{agg}) of the formed micelles above T_{PT} was estimated as $\bar{M}_{w,\text{agg}}/\bar{M}_{w,\text{uni}}$, where $\bar{M}_{w,\text{agg}}$ and $\bar{M}_{w,\text{uni}}$ are the weight average molecular weights of the micelles and the unimers, respectively.

Turbidity measurements. The temperature dependence of the transmittance of the sample solutions was measured on the spectrophotometer UV5 at 500 nm. The samples were dissolved in Milli-Q[®] water. The solutions were heated with a temperature step of 1 °C under the control of a thermostat accessory CuveT (METTLER TOLEDO).

Macroscopic test on thermoresponsiveness of hydrogel. A piece of hydrogel sample was immersed in deionized water overnight at room temperature before the test. The swollen sample in a Petri dish was placed on a warm hot plate (60 °C) for 10 min and a photo was taken. Afterwards, the hot plate was removed again.

Determination of swelling ratios. The temperature dependence of the swelling ratio was determined gravimetrically. The hydrogel sample was immersed in deionized water overnight at room temperature before tests. The swollen sample was then immersed in water at the target temperatures for 30 min. The surface of the wet sample was carefully dried with a soft precision wipe. The swelling ratio was determined as follows:

$$\text{Swelling ratio} = (W_s - W_d)/W_d,$$

where W_s represents the weight of the swollen hydrogel at the target temperature and W_d denotes the weight of the dry sample.

Results and discussion

Polymerization of the graft copolymers

As mentioned before, the two RAFT agents, CPDTC and CDTPA (Scheme 1), were used to synthesize the backbones of graft copolymers. After the first synthetic step under the green light,



two statistical copolymers, $P(O_{245}B_6)$ and $P(O_{234}B_6)-COOH$, were yielded. For the nomenclature of the samples, “O” and “B” stand for OEGMA and BTPEMA, respectively. The subscripts denote the number of the respective monomers in the statistical copolymers based on conversions. The degree of polymerization (DP) is the sum of subscripts. In comparison with the homopolymer POEGMA ($PO_{234}-COOH$), the statistical copolymers exhibit similar number average molecular weights ($\bar{M}_{n,SEC}$) and dispersities (\mathcal{D}) (Table 1). The relatively narrow monomodal molecular weight distributions shown in Fig. 1a suggest successful polymerizations of linear backbones. The similar molar ratios between OEGMA and BTPEMA in the copolymers (OEGMA/BTPEMA [mol]) confirm that the average number of BTPEMA units per chain of the two samples were comparable, *i.e.*, the average number of branching points per backbone were comparable. It can be calculated that both samples own not only one TTC-function at the ω -terminal, but also six pendant ones along every chain.

The PNIPAM side chains, as shown in Scheme 1, were synthesized *via* blue light irradiation. The DP of PNIPAM per side chain was controlled at about 40 for each polymerization. Kinetic studies were performed during two typical chain extensions (see Fig. S8, ESI†). It is obvious that the rate of chain extension was higher from the backbone $P(O_{234}B_6)-COOH$ than from the homopolymer $PO_{234}-COOH$, which makes sense as more TTC-groups (branching points) could be initiated in the backbone by blue light irradiation, leading to a higher radical concentration. Therefore, graft copolymers instead of linear block copolymers result from the statistical copolymers.

Eventually, two samples with PNIPAM side chains, $PO_{245}(PN_{40})_7$ and $PO_{234}(PN_{43})_7-COOH$, were obtained from $P(O_{245}B_6)$ and $P(O_{234}B_6)-COOH$, respectively. For the nomenclature of the graft copolymers, “(PN_m)₇” means that from the 7 TTC-functions (including those from “B”) of every chain, 7 PNIPAM segments with a DP of “m” were synthesized. The ¹H-NMR results reveal that the molar ratios between OEGMA and NIPAM (OEGMA/NIPAM [mol]) in these two graft copolymers are nearly identical and agree well with the theoretical values (Table 1). According to the results of SEC analysis, these two

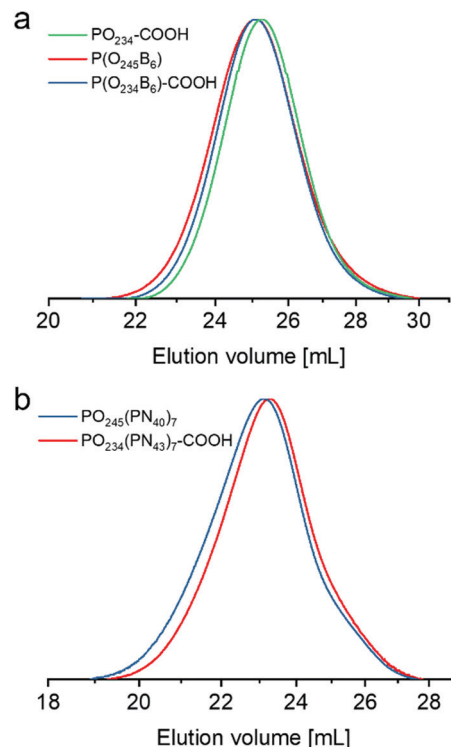


Fig. 1 SEC curves of (a) linear polymers measured with THF as the mobile phase and (b) graft copolymers measured with DMAc as the mobile phase.

graft copolymers also have similar molecular weights (Fig. 1b), enabling further investigations on the influence of the end-group.

Thermoresponsive behavior in dilute aqueous solutions

The dilute aqueous solutions ($c = 0.1\%$ [w/w]) of two linear backbone samples were first prepared for temperature-dependent DLS measurements. The results of both samples exhibit reversible LCST transitions with minor hysteresis during heating and cooling (Fig. 2a and b). The LCST-type T_{PT} of $P(O_{245}B_6)$ and $P(O_{234}B_6)-COOH$, which are determined as the onset of the increase in the hydrodynamic radius (R_H) during heating, are $59\text{ }^\circ\text{C}$ and $60\text{ }^\circ\text{C}$, respectively. The ignorable difference between T_{PT} corresponds well to our expectation, considering their similar $\bar{M}_{n,SEC}$ and \mathcal{D} . However, it is quite surprising that there is a huge difference in their detailed self-assembling behaviors in water. While both backbones could be dissolved in water in the form of unimers with $R_H < 10\text{ nm}$ below T_{PT} , the sizes of formed aggregates above T_{PT} differed remarkably.

In the case of $P(O_{245}B_6)$ (Fig. 2a), the polymer chains became hydrophobic and started to agglomerate at T_{PT} . The R_H of the particles increased to approximately 800 nm at $62\text{ }^\circ\text{C}$ and remained relatively constant at higher temperatures. For $P(O_{234}B_6)-COOH$ (Fig. 2b), the polymeric aggregates also started growing at T_{PT} , yet the growth ceased already when R_H was only around 200 nm . To elucidate this difference reasonably, the mechanism behind the LCST transition of POEGMA

Table 1 Analytical results of the polymers

Sample name ^a	OEGMA/ BTPE MA ^b [mol]	OEGMA/ NIPAM ^b [mol]	α^c [%]	$\bar{M}_{n,th}^d$ [kDa]	$\bar{M}_{n,SEC}^e$ [kDa]	\mathcal{D}^e
$PO_{234}-COOH$	—	—	60	70.6	38.8	1.30
$P(O_{245}B_6)$	39/1	—	63	75.9	41.3	1.37
$P(O_{234}B_6)-COOH$	41/1	—	60	72.8	41.6	1.31
$PO_{245}(PN_{40})_7$	39/1	45/55	50	107.3	96.2	1.47
$PO_{234}(PN_{43})_7-COOH$	41/1	45/55	54	106.9	87.6	1.42

^a Subscripts following O, B and N denote DP of different monomers based on conversion; for graft copolymers, subscripts following the parentheses denote the number of PNIPAM segments per chain. ^b Molar ratio between monomers in products calculated from ¹H-NMR spectra (see Fig. S4–S7, ESI). ^c Monomer conversion calculated from ¹H-NMR spectra with reference signal of DMF. ^d Number average molecular weight calculated from monomer conversion. ^e Determined by SEC in THF or DMAc relative to PMMA standards.



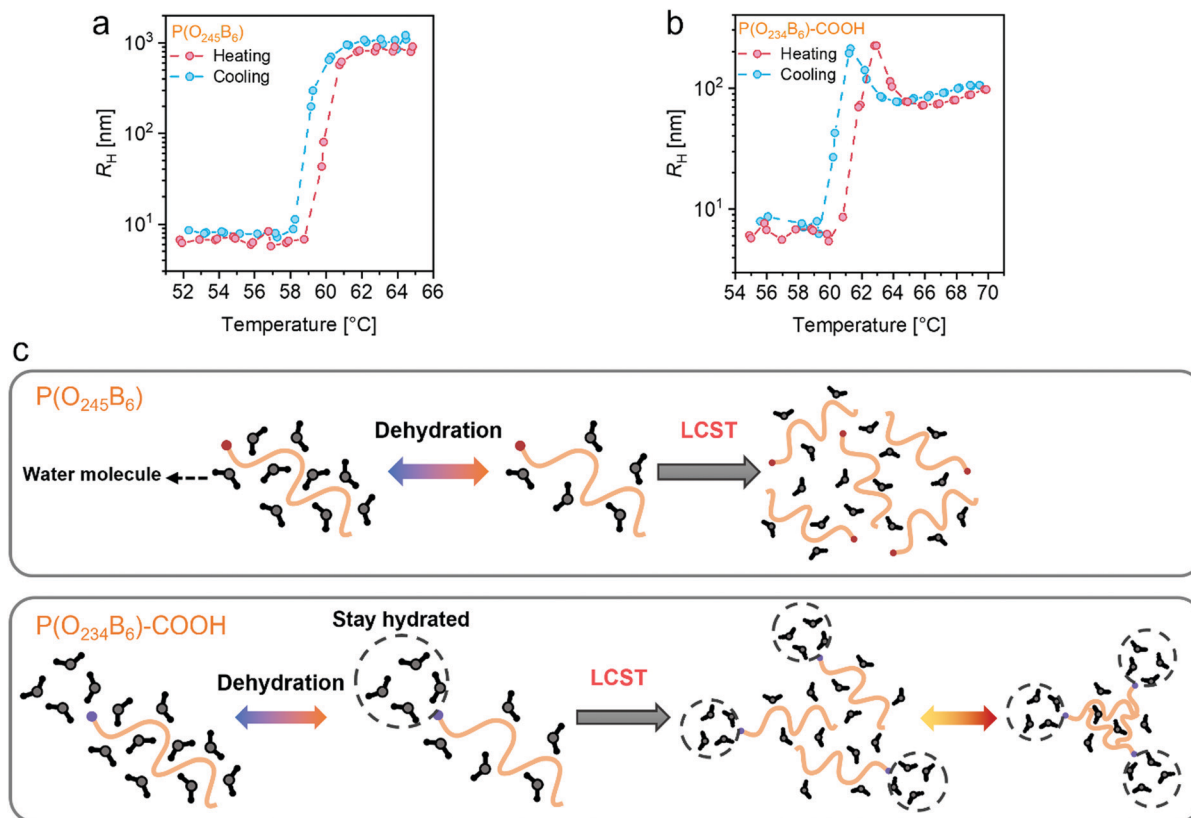


Fig. 2 Evolution of R_H of (a) $P(O_{245}B_6)$ or (b) $P(O_{234}B_6)-COOH$ in dilute aqueous solutions during heating (red dots) and cooling (blue dots) monitored by DLS; (c) assumed self-assembling processes of $P(O_{245}B_6)$ and $P(O_{234}B_6)-COOH$ chains at different stages (BTPEMA and the oxyethylene brushes are not shown in the illustrations for simplicity).

must be taken into account. A molecule of homo-POEGMA can basically be divided into two parts: the coiled backbone-like hydrophobic moiety and the pendant oxyethylene brushes. As shown in Fig. 2c, the solubility of the polymers in water below T_{PT} results from the hydration shell formed *via* the hydrogen bonds between water molecules and the ether oxygen groups of the brushes (brushes are not shown for simplicity). During heating the hydrogen bonds can be disrupted, causing the conformational changes of the oxyethylene brushes and the dehydration of the chains. According to previous research,⁴⁷ the conformation of the coiled hydrophobic moiety of POEGMA barely changes during the dehydration process. Additionally, the ether oxygen groups of the distorted brushes are still exposed to water molecules to some extent. Therefore, the large aggregates during the LCST transition are mainly formed by the “hydrogen bond bridges” among multiple chains and their structures should be relatively loose. The DLS result of $P(O_{245}B_6)$ corresponds well to the mechanism. However, the self-assembling behavior of $P(O_{234}B_6)-COOH$ could be disturbed by the carboxyl group which is also supposed to be surrounded by a hydration shell in water.⁴⁸ This extra hydration shell might not be significantly affected by the LCST transition, and the carboxyl group could stay hydrated during the whole heating process. The bulky hydration shell at the chain end could then hinder the bridging between chains, leading to a

smaller size of the aggregates. When heating the $P(O_{234}B_6)-COOH$ solution higher than 63 °C, “hydrogen bond bridges” were shortened and water was expelled from the loose aggregates, as reflected by the decrease in R_H .⁴⁷ Moreover, the coiled hydrophobic moiety could start collapsing slowly at higher temperatures due to weak van der Waals interactions.^{47,49} In principle, the decrease in R_H following the rapid phase transition should also be observed in the $P(O_{245}B_6)$ solution. The absence of the contraction of $P(O_{245}B_6)$ aggregates could be owing to the compensation from more continuously bound free chains.

Through the comparison of these results, it can be found that the end-group plays an important role in the thermoresponsive behaviors of the POEGMA backbones. Subsequently, the aqueous solutions of two different graft copolymers were analyzed by DLS measurements. The end-group again made an immense difference in the sizes of polymeric aggregates at high temperatures.

The DLS result of the $PO_{234}(PN_{43})_7-COOH$ solution ($c = 0.1\%$ [w/w]) is easier to interpret (Fig. 3a). All the obtained intensity correlation functions could be fitted by using the standard cumulant approach (see eqn (S9), ESI†). Apparently, a reversible two-step LCST transition occurred during the measurement. It is well-known that homopolymers of PNIPAM possess an LCST-type T_{PT} of about 32 °C.⁵⁰ Therefore, the PNIPAM side chains



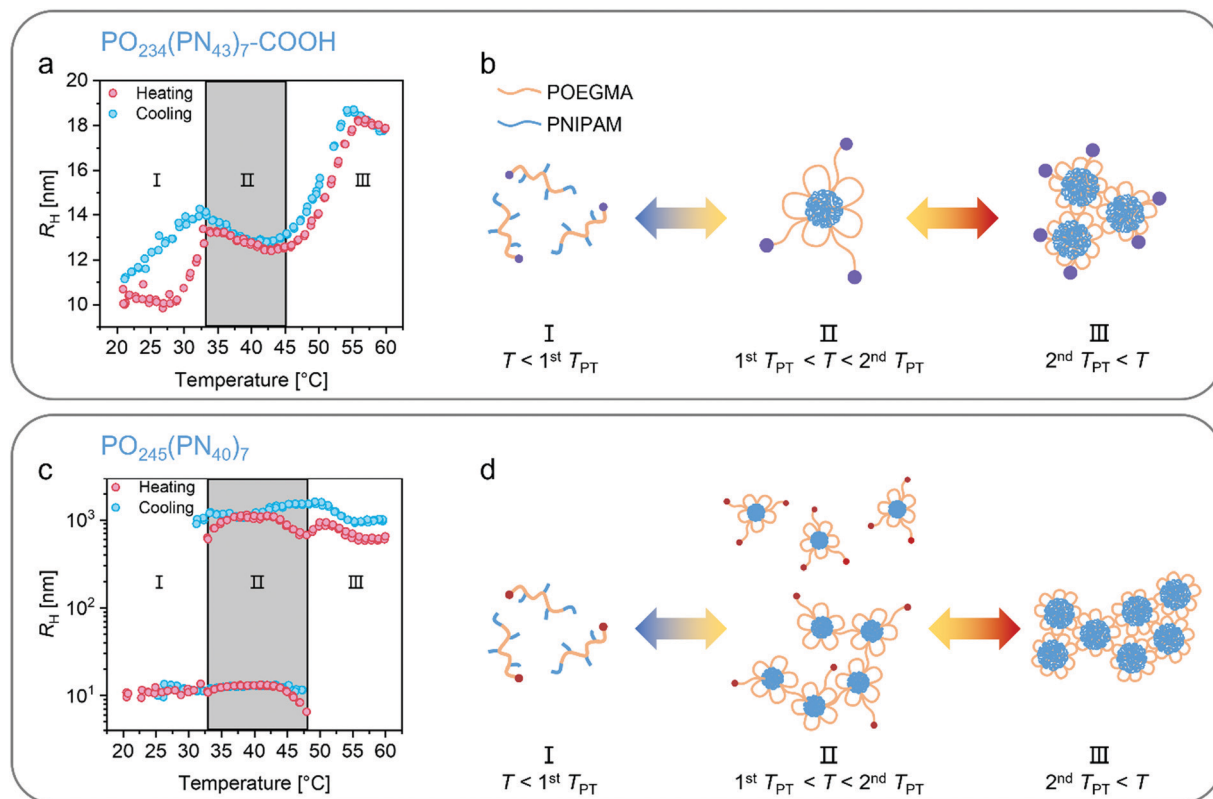


Fig. 3 Evolution of R_H of (a) $\text{PO}_{234}(\text{PN}_{43})_7\text{-COOH}$ or (c) $\text{PO}_{245}(\text{PN}_{40})_7$ in dilute aqueous solutions during heating (red dots) and cooling (blue dots) monitored by DLS; assumed self-assembling process of (b) $\text{PO}_{234}(\text{PN}_{43})_7\text{-COOH}$ or (d) $\text{PO}_{245}(\text{PN}_{40})_7$ at different temperatures.

are, most likely, responsible for the first increase in R_H at 30 °C during heating. Above the first T_{PT} , the side chains turned hydrophobic and are expected to form cores of the micelles. However, the R_H of the micelles between 30 °C and 50 °C (region II) was still less than 14 nm. Such a compact dimension can be legitimately explained from two perspectives. First, while the side chains combined together in the core, the hydrophilic backbones consisting of POEGMA were folded on the periphery so that flower-like micelles with thin shells were generated in this temperature region (Fig. 3b).^{51,52} The strong intramolecular interaction may have limited the N_{agg} of the macromolecules in a micelle.⁵³ In addition, the hydrated carboxyl groups remaining outside could prevent the formation of larger aggregates. To estimate the N_{agg} of these compact micelles, SLS measurements were conducted with the same concentration at 25 °C and 40 °C (below and above the first T_{PT}). After fitting the SLS data by the partial Zimm approach (see Fig. S9, ESI[†]), the N_{agg} was calculated to be about 2.4, which is indeed quite low and in accordance with the DLS result. Regarding the second LCST transition, the T_{PT} of the POEGMA backbone was lowered to about 45 °C, indicating enhanced polymer–polymer interactions due to the higher density of the chains in the shells. Different from the cases of the statistical copolymers, a slight precontraction (decrease in R_H) before the second LCST transition can be observed in region II during heating, corresponding to the dehydration process inside the shells of the amphiphilic micelles. Next, a

rapid agglomeration of the micelles occurred based on the mechanism explained in Fig. 2c. Yet, the R_H of less than 20 nm at about 55 °C was still relatively small, which can also be attributed to the bulky hydration shells around the carboxyl groups. Above 55 °C (region III), a gradual decrease in R_H took place but was less evident than that of $\text{P}(\text{O}_{234}\text{B}_6)\text{-COOH}$ at high temperatures. The reason could be that the micelles were already relatively dense due to the precontraction before aggregation. The more elaborate CONTIN analysis on the DLS data at three representative temperatures shown in Fig. 4a confirms the two-step LCST transition and the compact sizes of the particles.

As for $\text{PO}_{245}(\text{PN}_{40})_7$, its DLS result was more complicated to evaluate. The measurement was initially also performed at a concentration of 0.1% (w/w). However, it was difficult to fit the intensity correlation functions reasonably well through the cumulant approach. Excessively large aggregates could be formed in the solution at high temperatures. To avoid such aggregations, the concentration was lowered to 0.05% (w/w). The result of the DLS measurement is shown in Fig. 3c. Below the T_{PT} (region I) from PNIPAM, the DLS data could still be well fitted through the standard cumulant approach, implying that all the polymer chains were dissolved in the form of unimers like $\text{PO}_{234}(\text{PN}_{43})_7\text{-COOH}$. For the data obtained between 32 °C and 48 °C (region II) (exemplarily shown in Fig. S10, ESI[†]), however, it was more suitable to fit them by the sum of two exponential decay functions (see eqn (S11), ESI[†]),⁵⁴ which



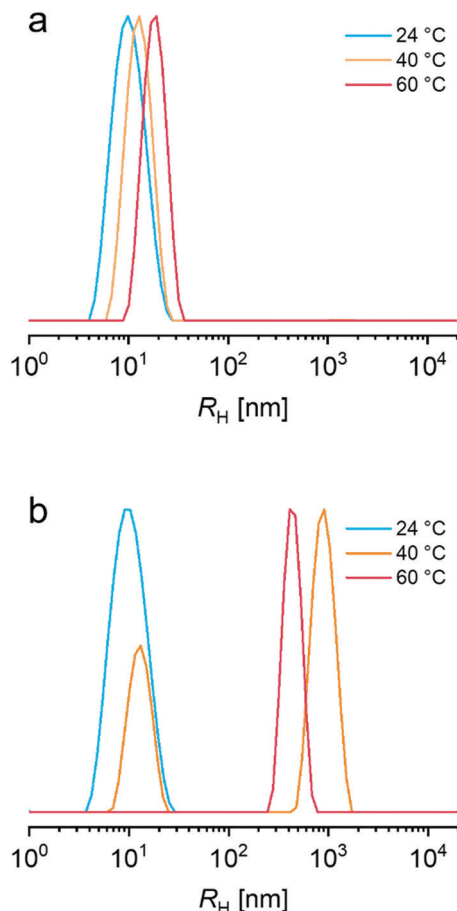


Fig. 4 Intensity-weighted size distributions of the particles formed by (a) $\text{PO}_{234}(\text{PN}_{43})_7\text{-COOH}$ or (b) $\text{PO}_{245}(\text{PN}_{40})_7$ at representative temperatures obtained by CONTIN analysis on DLS data.

means that two particle species emerged when the side chains became hydrophobic. The R_H of the smaller species in Fig. 3c and the micelles of $\text{PO}_{234}(\text{PN}_{43})_7\text{-COOH}$ in region II were alike. With the help of the CONTIN analysis, the size distributions of the particles formed at representative temperatures were calculated. As presented in Fig. 4b, a bimodal size distribution was measured in the solution at 40 °C. Considering that the scattering intensity is proportional to R_H^6 , the smaller species still dominated in the solution, which means that the N_{agg} of most micelles was limited by the intramolecular interaction. The formation of larger aggregates ($R_H > 1000$ nm) could result from the hydrophobic end-group. Unlike that of $\text{PO}_{234}(\text{PN}_{43})_7\text{-COOH}$, the α -terminal of $\text{PO}_{245}(\text{PN}_{40})_7$ could not separate all the particles. The flower-like micelles thus had the chance to link with each other through the hydrophobic interaction between the PNIPAM cores (Fig. 3d). The formation of large aggregates became inevitable despite a lower concentration (0.05% [w/w]). In temperature region II (Fig. 3c), it is also worth noticing that the R_H of both particle species started falling off when the solution was heated to 43 °C, indicating the dehydration of the looped PEOGMA chains. When the balance between hydrophilic and hydrophobic interactions was disrupted at the second

T_{PT} , numerous micelles could agglomerate together to form larger clusters in the absence of carboxyl groups and the small particles disappeared. After reaching its maximum value in region III, the R_H of the clusters tended to decrease gradually with the increasing temperature, which resembles the behavior of $\text{PO}_{234}(\text{PN}_{43})_7\text{-COOH}$. After heating, the solution was cooled to room temperature (25 °C). Although the temperature step was controlled at 1 °C by the thermostat during the whole measurement, the cooling rate was almost twice as fast as the heating rate. Besides, no stirring was allowed for the DLS measurements. It was, therefore, reasonable that the LCST transitions involving the hydrophobic particles with complex structures were not completely reversible. Nevertheless, the chains could still be fully redissolved at room temperature.

Apart from the DLS measurements, the temperature-variable $^1\text{H-NMR}$ spectra of the graft copolymers in D_2O also confirm the profound influence of the end-group. Fig. 5a and b show the characteristic peaks belonging to PEOGMA backbones and PNIPAM side chains at different temperatures. The decline of the signal of PNIPAM at 35 °C was most significant in both samples, revealing the main driving force of the first LCST transition. At 40 °C, the signal of PNIPAM became hardly detectable. Interestingly, from the spectra at 55 °C, it can be noted that the signal of PEOGMA in $\text{PO}_{245}(\text{PN}_{40})_7$ was much flatter than that in $\text{PO}_{234}(\text{PN}_{43})_7\text{-COOH}$, suggesting a higher degree of phase separation of $\text{PO}_{245}(\text{PN}_{40})_7$ at this temperature. This difference is in good agreement with the DLS results.

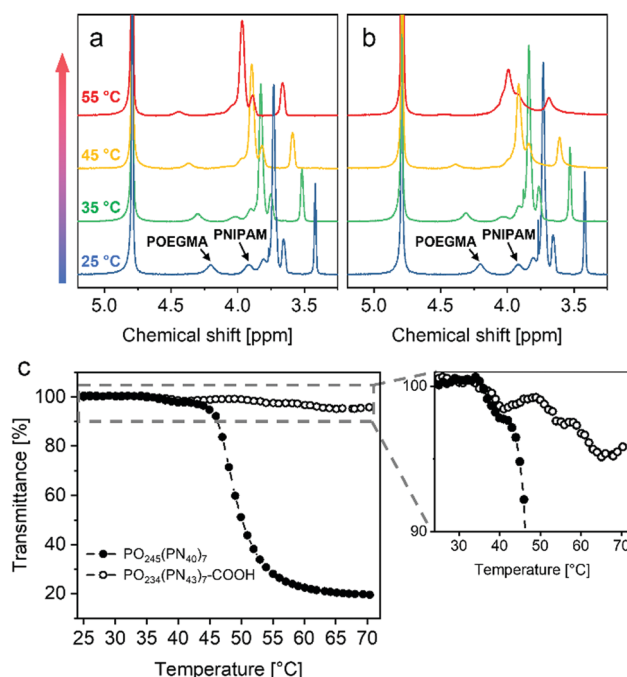


Fig. 5 Normalized temperature-variable $^1\text{H-NMR}$ spectra of (a) $\text{PO}_{234}(\text{PN}_{43})_7\text{-COOH}$ and (b) $\text{PO}_{245}(\text{PN}_{40})_7$ measured in D_2O ; (c) left: temperature dependence of the transmittance measured for the aqueous solutions of $\text{PO}_{234}(\text{PN}_{43})_7\text{-COOH}$ (0.1% [w/w]) and $\text{PO}_{245}(\text{PN}_{40})_7$ (0.05% [w/w]); right: enlarged image of the measurements.



Furthermore, the temperature dependence of the transmittance of the sample solutions is plotted in Fig. 5c. Apparently, the $\text{PO}_{245}(\text{PN}_{40})_7$ solution became much more turbid at high temperatures even with a lower concentration. Through the enlarged image of the results, a slight drop of the transmittance can be noticed for both samples at around 35 °C. The second drop of the transmittance of $\text{PO}_{245}(\text{PN}_{40})_7$ solution starting at about 43 °C was drastic, while the change of turbidity of $\text{PO}_{234}(\text{PN}_{43})_7\text{-COOH}$ solution in the rest of the heating process was still very small. Although the random error of the measurement caused some fluctuations, the result of $\text{PO}_{234}(\text{PN}_{43})_7\text{-COOH}$ still shows a two-step transition roughly.

All these results above demonstrate that both graft copolymers display a two-step LCST transition originating from PEOGMA and PNIPAM. Without the carboxyl groups at the chain end, significantly larger particles arise at high temperatures.

Modification of end-group

In this section, the end-group modification aiming for further chemical crosslinking is discussed. In order to minimize side reactions, a well-defined graft copolymer $\text{PO}_{218}(\text{PN}_{32})_7$ without carboxyl groups was prepared. According to the DLS result in Fig. S11 (ESI†) and Fig. 3c, $\text{PO}_{218}(\text{PN}_{32})_7$ and $\text{PO}_{245}(\text{PN}_{40})_7$ show a similar two-step LCST transition in water. The major difference is that the first LCST transition of $\text{PO}_{218}(\text{PN}_{32})_7$ occurred at a higher temperature, which can be ascribed to the shorter PNIPAM side chains, *i.e.*, the weaker polymer–polymer interaction.⁵⁵ After confirming the reproducibility of the LCST transitions, the polymer was subjected to chemical modification.

In the presence of excess DTP and hexylamine, the TTC-groups could be replaced by PDS-groups. The modified sample, $\text{PO}_{218}(\text{PN}_{32})_7\text{-PDS}$, was first characterized by SEC and UV–vis spectroscopy (Fig. 6). The molecular distribution is slightly broadened after modification, which could be due to the undesired oxidation between thiol groups during the aminolysis.⁵⁶ Since the oxidation just produces disulfide and the goal of the modification was chemical crosslinking, the impact of this side reaction is trivial in this work. In Fig. 6b, the absorbance of TTC-groups at about 308 nm disappears after modification, manifesting nearly complete removal of TTC-groups.

Crosslinking of the graft copolymer

Since the thiol reactive PDS-groups can react with thiol groups at ambient temperature without any catalysts, a dithiol based crosslinker, EDT, was used to obtain a covalently crosslinked hydrogel (Scheme 2).

Fig. 7a shows the procedure for the preparation of a polymeric gel briefly. The yellow color of the gel caused by the small molecule, 2-mercaptopyridine, released after crosslinking proved a successful reaction between PDS- and thiol groups. Ultimately, a colorless free-standing gel was formed after purification. After removing the organic solvents, the thermo-responsiveness of the PEOGMA–PNIPAM hydrogel was visually

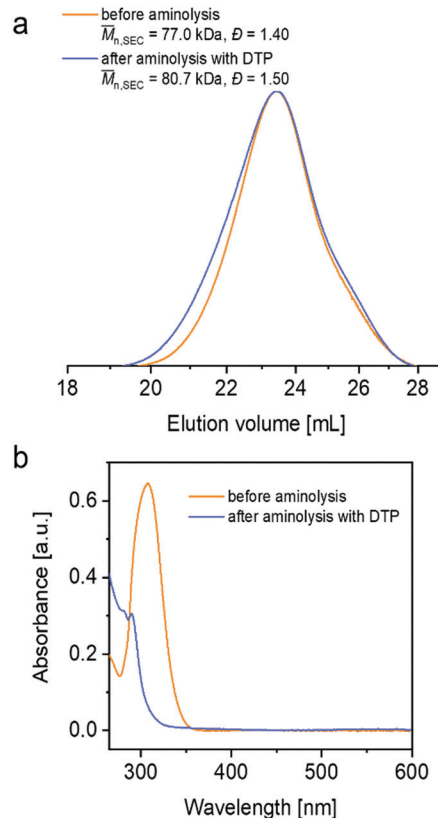
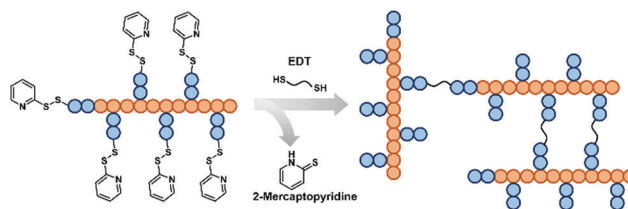


Fig. 6 (a) SEC curves measured before aminolysis and after aminolysis with DTP; (b) UV–vis spectra measured before and after aminolysis in 1,4-dioxane.



Scheme 2 Schematic illustration for chemical crosslinking of PEOGMA-g-PNIPAM-PDS with the crosslinker, EDT.

tested (Fig. 7b). The hydrogel was fully swollen and transparent at room temperature. At 60 °C, water was squeezed out of the network drastically and the hydrogel became opaque. Once it was allowed to cool down, the hydrogel regained its transparency.

The swelling ratios of the hydrogel at different temperatures were also determined quantitatively by gravimetry. Because the intensive shrinkage at a high temperature could cause splits in the sample and affect the result, the highest target temperature was lower than 50 °C. As depicted in Fig. 8, the swelling ratio of the hydrogel started to decline below 33 °C, which is lower than the T_{PT} of PNIPAM before crosslinking. This could be correlated with the high local concentration of chains within the network. Moreover, the network had a more confined and complex



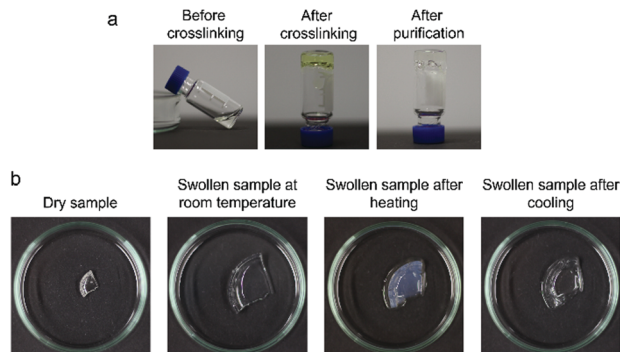


Fig. 7 (a) General procedure for the preparation of POEGMA–PNIPAM hydrogel; (b) macroscopic test on the thermoresponsiveness of the hydrogel.

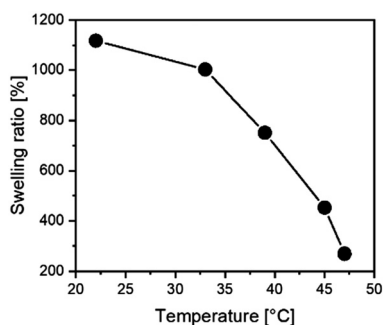


Fig. 8 Temperature dependence of the swelling ratio of the hydrogel sample.

internal structure than the free polymer chains. After the contraction of PNIPAM chains, the density of POEGMA chains became even higher, which could lead to a huge decrease in the T_{PT} . The phase transitions of PNIPAM and POEGMA could be overlapped. It was thus difficult to distinguish the LCSTs of POEGMA and PNIPAM. Instead, the hydrogel kept shrinking within a relatively broad temperature range.

Conclusions

In conclusion, two well-defined graft copolymers differing merely in the end-group were synthesized by sequentially switching the wavelengths of the light source for photoiniferter RAFT polymerization. Both polymers exhibit a two-step LCST transition in water originating from the backbone and the side chains. However, the sizes of their aggregates formed above each LCST-type T_{PT} are significantly different. Without the carboxyl group at the α -terminal, polymeric aggregates with larger R_H were detected by DLS measurements. Furthermore, multiple TTC-groups along the polymer chains were successfully converted into thiol reactive PDS-groups after polymerization by aminolysis in the presence of DTP, enabling simple chemical crosslinking at room temperature without other additives. The obtained thermoresponsive hydrogel may have

potential in various fields of applications, like controlled drug release in biomedical applications. Apart from the reaction with a crosslinker, it is also possible to use the reactive thiol groups for attachment of other functional molecules like enzymes which are then shielded or unshielded from substrates as a function of temperature.

Conflicts of interest

There are no conflicts of interest to declare.

Acknowledgements

The work is financially supported by Universität Hamburg, a collaborative project funded by Helmholtz Association and Russian Science Foundation (grant number HRSF-0075) and by the Deutsche Forschungsgemeinschaft (DFG, German Research Foundation) - GRK 2536. The authors would like to thank Felix Lauterbach and Birgit Hankiewicz for providing the programs attaining convenient fitting of the DLS results. The authors would also like to thank Martin Kehden for his help with SEC measurements.

Notes and references

- Q. Li, C. Gao, S. Li, F. Huo and W. Zhang, *Polym. Chem.*, 2014, **5**, 2961–2972.
- Y. Huang, P. Yong, Y. Chen, Y. Gao, W. Xu, Y. Lv, L. Yang, R. L. Reis, R. P. Pirraco and J. Chen, *RSC Adv.*, 2017, **7**, 28711–28722.
- Q. Zhang, J.-D. Hong and R. Hoogenboom, *Polym. Chem.*, 2013, **4**, 4322–4325.
- L. Johnson, D. M. Gray, E. Niezabitowska and T. O. McDonald, *Nanoscale*, 2021, **13**, 7879–7896.
- Y. Kotsuchibashi, *Polym. J.*, 2020, **52**, 681–689.
- Y. Kotsuchibashi, M. Ebara, T. Aoyagi and R. Narain, *Polymers*, 2016, **8**, 380.
- T. Jiang, V. Aseyev, J. Niskanen, S. Hietala, Q. Zhang and H. Tenhu, *Macromolecules*, 2020, **53**, 8267–8275.
- L. Lauber, J. Depoorter, T. Nicolai, C. Chassenieux and O. Colombani, *Macromolecules*, 2017, **50**, 8178–8184.
- X. Xu, Y. Liu, W. Fu, M. Yao, Z. Ding, J. Xuan, D. Li, S. Wang, Y. Xia and M. Cao, *Polymers*, 2020, **12**, 580.
- G.-F. Luo, W.-H. Chen and X.-Z. Zhang, *ACS Macro Lett.*, 2020, **9**, 872–881.
- L. Tang, L. Wang, X. Yang, Y. Feng, Y. Li and W. Feng, *Prog. Mater. Sci.*, 2021, **115**, 100702.
- S. H. Yu, F. Ercole, N. A. Veldhuis, M. R. Whittaker, T. P. Davis and J. F. Quinn, *Polym. Chem.*, 2017, **8**, 6362–6367.
- Y. Ling, J. Ren, T. Li, Y. Zhao and C. Wu, *Chem. Commun.*, 2016, **52**, 4533–4536.
- E. Ellis, K. Zhang, Q. Lin, E. Ye, A. Poma, G. Battaglia, X. J. Loh and T.-C. Lee, *J. Mater. Chem. B*, 2017, **5**, 4421–4425.



- 15 J. Teo, J. A. McCarroll, C. Boyer, J. Youkhana, S. M. Sagnella, H. T. Duong, J. Liu, G. Sharbeen, D. Goldstein, T. P. Davis, M. Kavallaris and P. A. Phillips, *Biomacromolecules*, 2016, **17**, 2337–2351.
- 16 M. Bozorg, B. Hankiewicz and V. Abetz, *Soft Matter*, 2020, **16**, 1066–1081.
- 17 S. Pearson, C. St Thomas, R. Guerrero-Santos and F. D'Agosto, *Polym. Chem.*, 2017, **8**, 4916–4946.
- 18 M. Semsarilar and V. Abetz, *Macromol. Chem. Phys.*, 2021, **222**, 2000311.
- 19 D. Shen, B. Xu, X. Huang, Q. Zhuang and S. Lin, *Polym. Chem.*, 2018, **9**, 2821–2829.
- 20 A. Ding, J. Xu, G. Gu, G. Lu and X. Huang, *Sci. Rep.*, 2017, **7**, 12601.
- 21 K. J. Arrington and J. B. Matson, *Polym. Chem.*, 2017, **8**, 7452–7456.
- 22 S. Shanmugam, J. Cuthbert, T. Kowalewski, C. Boyer and K. Matyjaszewski, *Macromolecules*, 2018, **51**, 7776–7784.
- 23 N. Corrigan, F. J. Trujillo, J. Xu, G. Moad, C. J. Hawker and C. Boyer, *Macromolecules*, 2021, **54**, 3430–3446.
- 24 M. Hartlieb, *Macromol. Rapid Commun.*, 2021, 2100514.
- 25 J. Xu and V. Abetz, *Macromol. Rapid Commun.*, 2021, **42**, 2000648.
- 26 M. L. Ohnsorg, J. M. Ting, S. D. Jones, S. Jung, F. S. Bates and T. M. Reineke, *Polym. Chem.*, 2019, **10**, 3469–3479.
- 27 F. Lauterbach and V. Abetz, *Soft Matter*, 2020, **16**, 2321–2331.
- 28 S. Furyk, Y. Zhang, D. Ortiz-Acosta, P. S. Cremer and D. E. Bergbreiter, *J. Polym. Sci., Part A: Polym. Chem.*, 2006, **44**, 1492–1501.
- 29 P. Kujawa, F. Segui, S. Shaban, C. Diab, Y. Okada, F. Tanaka and F. M. Winnik, *Macromolecules*, 2006, **39**, 341–348.
- 30 G. Moad, E. Rizzardo and S. H. Thang, *Polym. Int.*, 2011, **60**, 9–25.
- 31 H. Willcock and R. K. O'Reilly, *Polym. Chem.*, 2010, **1**, 149–157.
- 32 R. N. Carmean, C. A. Figg, G. M. Scheutz, T. Kubo and B. S. Sumerlin, *ACS Macro Lett.*, 2017, **6**, 185–189.
- 33 V. H. Dao, N. R. Cameron and K. Saito, *Polym. Chem.*, 2017, **8**, 6834–6843.
- 34 B. A. Abel and C. L. McCormick, *Macromolecules*, 2016, **49**, 6193–6202.
- 35 R. Nicolaÿ, *Macromolecules*, 2012, **45**, 821–827.
- 36 M. R. Newman, S. G. Russell, C. S. Schmitt, I. A. Marozas, T.-J. Sheu, J. E. Puzas and D. S. W. Benoit, *Biomacromolecules*, 2018, **19**, 71–84.
- 37 P. Chakma, Z. A. Digby, J. Via, M. P. Shulman, J. L. Sparks and D. Konkolewicz, *Polym. Chem.*, 2018, **9**, 4744–4756.
- 38 E. H. Discekici, S. L. Shankel, A. Anastasaki, B. Oschmann, I.-H. Lee, J. Niu, A. J. McGrath, P. G. Clark, D. S. Laitar, J. R. de Alaniz, C. J. Hawker and D. J. Lunn, *Chem. Commun.*, 2017, **53**, 1888–1891.
- 39 A. Hess, B. V. K. J. Schmidt and H. Schlaad, *Polym. Chem.*, 2020, **11**, 7677–7684.
- 40 H. W. Ooi, K. S. Jack, A. K. Whittaker and H. Peng, *J. Polym. Sci., Part A: Polym. Chem.*, 2013, **51**, 4626–4636.
- 41 C. Boyer, V. Bulmus and T. P. Davis, *Macromol. Rapid Commun.*, 2009, **30**, 493–497.
- 42 B. Sui, C. Cheng and P. Xu, *Adv. Therap.*, 2019, **2**, 1900062.
- 43 D. Bontempo, K. L. Heredia, B. A. Fish and H. D. Maynard, *J. Am. Chem. Soc.*, 2004, **126**, 15372–15373.
- 44 I. Altinbasak, M. Arslan, R. Sanyal and A. Sanyal, *Polym. Chem.*, 2020, **11**, 7603–7624.
- 45 Q. Song, J. Yang, S. C. L. Hall, P. Gurnani and S. Perrier, *ACS Macro Lett.*, 2019, **8**, 1347–1352.
- 46 F. Lauterbach, Advances in RAFT polymerization process design and analysis, *Dissertation*, Universität Hamburg, 2020.
- 47 S. Sun and P. Wu, *Macromolecules*, 2013, **46**, 236–246.
- 48 M. Di Gioacchino, F. Bruni, S. Imberti and M. A. Ricci, *J. Phys. Chem. B*, 2020, **124**, 4358–4364.
- 49 J.-F. Lutz, K. Weichenhan, Ö. Akdemir and A. Hoth, *Macromolecules*, 2007, **40**, 2503–2508.
- 50 J.-F. Lutz, Ö. Akdemir and A. Hoth, *J. Am. Chem. Soc.*, 2006, **128**, 13046–13047.
- 51 L. I. Atanase, J. Desbrieres and G. Riess, *Prog. Polym. Sci.*, 2017, **73**, 32–60.
- 52 Z. Tuzar and P. Kratochvíl, *Adv. Colloid Interface Sci.*, 1976, **6**, 201–232.
- 53 F. Bougard, C. Giacomelli, L. Mespouille, R. Borsali, P. Dubois and R. Lazzaroni, *Langmuir*, 2008, **24**, 8272–8279.
- 54 S. Eggers, B. Fischer and V. Abetz, *Macromol. Chem. Phys.*, 2016, **217**, 735–747.
- 55 Y. Xia, X. Yin, N. A. D. Burke and H. D. H. Stöver, *Macromolecules*, 2005, **38**, 5937–5943.
- 56 X.-P. Qiu and F. M. Winnik, *Macromolecules*, 2007, **40**, 872–878.



3.3 Publication 3: Synthesis of a Degradable Hydrogel Based on a Graft Copolymer with Unexpected Thermoresponsiveness

Publication 3 continues to discuss a graft copolymer's LCST–LCST transition and the properties of the hydrogel generated from it. The copolymers and hydrogels in Publication 2 and 3 were prepared with the same approach. As Publication 2 already mentioned that the end-group at the α -terminal has a massive impact on the thermoresponsive behavior, this publication used a symmetric CTA to prepare the backbone, unifying the nature of the chain's α - and ω -terminals.

In contrast to the case in Publication 2, the first T_{CP} of the copolymer solution in this publication was mainly caused by the dehydration of the backbone (PMEO₂MA). The second T_{CP} observed by the DLS measurement and turbidimetry was unexpected as the PDMA side chains should be highly hydrophilic. According to the subsequent temperature-variable proton nuclear magnetic resonance (¹H-NMR) measurement, the second T_{CP} was most likely driven by the gradual contraction of PMEO₂MA after the first LCST transition.

In addition, the advantages of fabricating networks based on the graft copolymers were presented more thoroughly in this publication. The obtained hydrogel is not only thermoresponsive but also degradable in a reducing environment.

The publication is reprinted with permission from J. Xu and V. Abetz, *Macromol. Chem. Phys.* **2022**, 2200058 – published by Wiley-VCH GmbH. The related supporting information is available in Section 7.4.

Synthesis of a Degradable Hydrogel Based on a Graft Copolymer with Unexpected Thermoresponsiveness

Jingcong Xu and Volker Abetz*

Incorporating multiple pyridyl disulfide (PDS) moieties into polymer chains allows the fabrication of a chemically cross-linked hydrogel through the rapid thiol–disulfide exchange reaction. By aminolysis in the presence of 2,2'-dithiodipyridine (DTP), the end groups of polymers synthesized via reversible addition–fragmentation chain transfer (RAFT) polymerization can readily be converted into PDS-groups. In this contribution, a RAFT-synthesized graft copolymer with thermoresponsive poly[di(ethylene glycol) methyl ether methacrylate] forming the backbone and hydrophilic poly(*N,N*-dimethylacrylamide) as the side chains is presented. The copolymer chains exhibit surprisingly a two-step lower critical solution temperature transition in aqueous solutions. After modification of the end groups of the backbone and side chains, the PDS-terminated chains can react with a dithiol cross-linker to form a thermoresponsive hydrogel. In a reducing environment, the cleavable disulfide linkages lead to on-demand dissolution of the hydrogel. The resulting thiol-terminated chains undergo a reversible sol–gel transition in response to redox variations, expanding the potential application areas of such a polymer system.

ionic interactions.^[5–8] These polymer systems can rapidly undergo reversible sol–gel transitions between different environments and play an important role as injectable hydrogels in biomedical research.^[9,10] On the other hand, chemically cross-linked hydrogels are fixed by covalent bonds between polymeric chains. Up to now, abundant chemical cross-linking methods have been developed. Cross-linkers such as ethylene glycol dimethacrylate and *N,N'*-methylenebisacrylamide can directly be incorporated into macromolecular chains during free radical polymerizations.^[11–13] Alternatively, the functionalized chains can be cross-linked by various types of “click” chemical reactions after polymerization. The most popular reactions comprise thiol–disulfide exchange, thiol–ene reaction, Diels–Alder reaction, hydrazone formation, and oxime formation.^[14–20] In comparison with the physically cross-linked

hydrogels, most chemically cross-linked hydrogels show improved stability and a flexibly adjustable swelling ratio.^[21–23] More interestingly, utilizing dynamic covalent bonds like disulfide bonds and imine bonds for cross-linking imparts reversible linkages to the hydrogels, combining the advantages of chemical and physical cross-links.^[24]

Chemically cross-linked stimuli-responsive hydrogels are of great interest in polymer science due to their tunable water capacity in response to environmental changes, like temperature or pH-value. The most widely investigated thermoresponsive hydrogel with a lower critical solution temperature (LCST) transition is based on poly(*N*-isopropylacrylamide) (PNIPAM). Due to the contraction at the temperature close to body temperature, PNIPAM hydrogels can be utilized in drug delivery systems, tissue engineering, and smart actuators.^[25–28] Recently, our group has shown an efficient route to prepare a thermoresponsive hydrogel from a well-defined graft copolymer with poly[oligo(ethylene glycol) methacrylate] (POEGMA) backbone and PNIPAM side chains.^[29] The graft copolymer itself is double thermoresponsive in aqueous solutions. The LCST-type cloud point (T_{CP}) of the backbone is higher than that of the side chains. After aminolysis with 2,2'-dithiodipyridine (DTP), the copolymer became pyridyl disulfide (PDS)-terminated, enabling cross-linking through a thiol–disulfide exchange reaction. In this study, we further demonstrate the versatility of this approach in preparing multifunctional hydrogels based on intriguing precursors.

1. Introduction

Hydrogels are three-dimensional networks featuring high water absorbency.^[1,2] Based on the synthetic strategies, hydrogels can be classified into physically and chemically cross-linked hydrogels.^[3,4] Physically cross-linked hydrogels are usually formed by intermolecular interactions such as hydrogen bonding, hydrophobic interactions, host–guest interactions, and

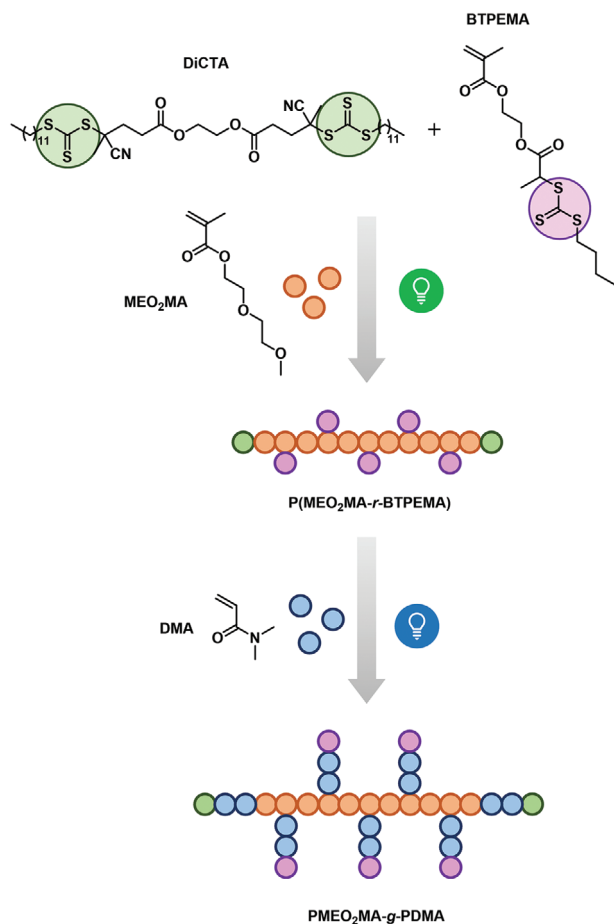
J. Xu, V. Abetz
 Institute of Physical Chemistry
 Universität Hamburg
 Grindelallee 117, Hamburg 20146, Germany
 E-mail: volker.abetz@hereon.de

V. Abetz
 Institute of Membrane Research
 Helmholtz-Zentrum Hereon
 Max-Planck-Straße 1, Geesthacht 21502, Germany

 The ORCID identification number(s) for the author(s) of this article can be found under <https://doi.org/10.1002/macp.202200058>

© 2022 The Authors. Macromolecular Chemistry and Physics published by Wiley-VCH GmbH. This is an open access article under the terms of the Creative Commons Attribution License, which permits use, distribution and reproduction in any medium, provided the original work is properly cited.

DOI: 10.1002/macp.202200058



Scheme 1. Photoiniferter RAFT polymerization of PMEO₂MA-*g*-PDMA graft copolymer.

The presented work can be divided into two parts. First, a thermoresponsive graft copolymer of di(ethylene glycol) methyl ether methacrylate (MEO₂MA) and *N,N*-dimethylacrylamide (DMA) was synthesized as a precursor for the hydrogel. In contrast to our recent work,^[29] the LCST of PDMA side chains is supposed to be much higher than that of the PMEO₂MA backbone in water.^[30,31] Inspired by the report of Shanmugam et al.,^[32] the graft copolymer was synthesized via photoiniferter reversible addition–fragmentation chain transfer (RAFT) polymerization in this work (Scheme 1). In order to prevent the difference in the end-groups at α - and ω -terminals from affecting the thermoresponsive properties of the chains, a symmetric difunctional chain transfer agent, DiCTA, was employed as an iniferter in the first synthetic step. 2-(2-(*n*-butyltrithiocarbonate)propionate)ethyl methacrylate (BTPEMA) was copolymerized simultaneously with MEO₂MA to provide the reactive sites for synthesizing side chains. As mentioned in ref. [32], BTPEMA shows no absorption in the green light region and thus was not activated by green light in the first synthetic step. Moreover, releasing the leaving group linked to the trithiocarbonate (TTC)-group (marked in lilac in Scheme 1) in BTPEMA will generate a secondary carbon radical, which is not favored when polymerizing methacrylates. Therefore, a linear random copoly-

mer, P(MEO₂MA-*r*-BTPEMA), was obtained under green light irradiation in the first step. In the second synthetic step, all the TTC-groups were activated under blue light irradiation so that PDMA side chains could be synthesized. Due to its branched structure, the graft copolymer exhibits unexpected LCST transitions in aqueous solutions, which will be discussed in detail in the following section. The second part of the article is focused on the cross-linking of the graft copolymer PMEO₂MA-*g*-PDMA and the obtained hydrogel. The copolymer was also cross-linked by the thiol–disulfide exchange reaction involving a dithiol-based cross-linker and PDS-groups. The water capacity and thermoresponsiveness of the hydrogel were thoroughly tested. Furthermore, as the polymer chains were fixed by disulfide bonds which are cleavable in a reducing environment, the hydrogel also features redox-sensitive degradability.

2. Results and Discussion

2.1. Polymerization and Characterization of the Backbone

The chain transfer agents (CTAs) 4-cyano-4-[(dodecylsulfanylthiocarbonyl)sulfanyl]pentanoic acid (CDTPA), as the precursor of DiCTA, and 2-cyano-2-propyl dodecyl trithiocarbonate (CPDTC) were proven to provide good control for the polymerization of methacrylates under green light irradiation.^[32,33] Since the absorption spectra of DiCTA and CDTPA are almost identical (Figure S2, Supporting Information), green light was used to initiate the first synthetic step (simultaneous copolymerization) shown in Scheme 1. As a control, an additional homopolymer of MEO₂MA was synthesized with the commercially available CPDTC under the same reaction conditions (Figure 1a). When the monomer conversions (α) were comparable (about 60%), the polymerizations mediated by DiCTA and CPDTC delivered the products with similar molecular weight distributions (Figure 1b). The relatively narrow dispersities ($\mathcal{D} \leq 1.40$) of the size exclusion chromatography (SEC) curves suggest successful polymerizations of a homopolymer PM₂₁₁ and a random copolymer P(M₂₁₅B₁₁). For the nomenclature, “M” and “B” stand for MEO₂MA and BTPEMA, respectively. The subscripts represent the number of the repeating units in the polymers calculated based on the conversion α (Figure S3, Supporting Information). The name of the random copolymer also indicates that the feed molar ratio between MEO₂MA and BTPEMA ($f_{M/B}$) was 19/1 before the polymerization. The actual comonomer ratio ($F_{M/B}$) in the purified product is allowed to be determined by integrating intensities of the corresponding signals in the proton nuclear magnetic resonance (¹H-NMR) spectrum (Figure S4, Supporting Information). According to Equation (S3) (Supporting Information), $F_{M/B}$ of the copolymer was about 21/1, which agrees well with $f_{M/B}$. Furthermore, $F_{M/B}$ shows no notable dependence on α (Table S1, Supporting Information), manifesting that BTPEMA was randomly distributed in the linear chains. Therefore, according to the α , P(M₂₁₅B₁₁) was regarded as a backbone with a total of 13 TTC-groups (including 11 ones from the BTPEMA units and two others at α - and ω -terminals), i.e., a backbone with 13 branching points for the propagation of side chains.

After the polymerization, the LCST transitions of the homopolymer and the copolymer in aqueous solutions were

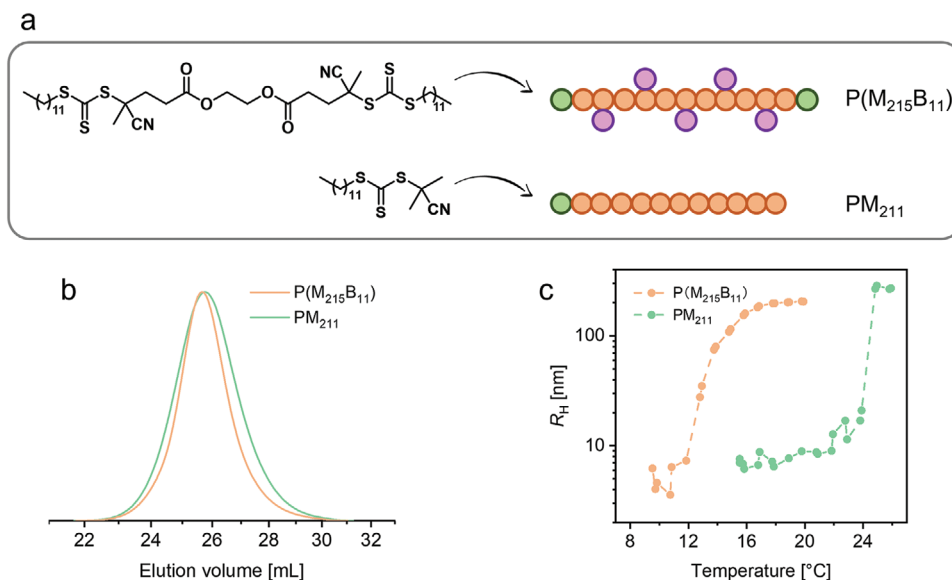


Figure 1. a) Linear polymers obtained from different CTAs; b) SEC curves of P(M₂₁₅B₁₁) ($\bar{M}_{n,SEC} = 33.5$ kDa, $\bar{D} = 1.31$) and PM₂₁₁ ($\bar{M}_{n,SEC} = 30.5$ kDa, $\bar{D} = 1.40$) measured with tetrahydrofuran (THF) as the mobile phase; c) evolution of R_H of P(M₂₁₅B₁₁) and PM₂₁₁ in aqueous solutions ($c = 0.05\%$ [w/w]) monitored by DLS during heating.

compared by temperature-dependent dynamic light scattering (DLS) measurements. During the preparation of the solutions, it was already apparent that these two samples have different solubility in water. While PM₂₁₁ could readily be dissolved in water in the absence of a hydrophobic comonomer, the solution of P(M₂₁₅B₁₁) was milk-white turbid at room temperature (23 °C). The turbid solution became immediately transparent and homogeneous in an ice bath. To avoid precipitation above the LCST-type T_{CP} during the DLS measurements, the solutions were diluted to a concentration of 0.05% (w/w) before the measurements. Judging from the results displayed in Figure 1c, both samples were dissolved in the form of unimers with hydrodynamic radii (R_H) smaller than 10 nm below T_{CP} s (which are determined as the onset of the increase in R_H). In comparison with that of the homopolymer, the T_{CP} of P(M₂₁₅B₁₁) is clearly lower due to the hydrophobic nature of the integrated BTPEMA.

2.2. Polymerization and Characterization of the Graft Copolymer

After preparation of the backbone under green light irradiation, blue light was employed to activate the TTC-groups, resulting in the growth of PDMA side chains. The monomodal SEC curve with \bar{D} of 1.32 confirms successful chain extension (Figure S5, Supporting Information). The well-defined graft copolymer PM₂₁₅(PD₃₁)₁₃ was then dissolved in water to investigate its thermoresponsive behavior. For the nomenclature of the graft copolymer, “(PD₃₁)₁₃” denotes that from the 13 TTC-functions along every chain, 13 PDMA segments with a degree of polymerization (DP) of 31 were synthesized. The DP was calculated based on α (Figure S6, Supporting Information).

In the presence of the hydrophilic PDMA side chains, the graft copolymer became soluble in water at room temperature. The result of the following DLS measurement ($c = 0.1\%$ [w/w]) is shown

in Figure 2a. Surprisingly, the chains of PM₂₁₅(PD₃₁)₁₃ underwent a reversible two-step LCST transition in pure water between 15 and 60 °C. During heating, two pronounced increases in R_H took place at 25 and 50 °C, respectively. The sample could be redissolved after cooling. The first T_{CP} of the copolymer is close to the T_{CP} of PM₂₁₁. However, the second T_{CP} was utterly unexpected as homo-PDMA is highly water-soluble at normal pressure and was reported to have a T_{CP} up to about 200 °C in superheated water.^[30,34]

The two-step LCST transition was not observed in the DLS result of the diblock copolymer, PM₂₁₁-*b*-PD₃₇₅, which was synthesized from PM₂₁₁ under the same blue light. As shown in Figure 2b, the R_H started increasing drastically from about 30 °C. The measurement was stopped at 40 °C because the solution ($c = 0.1\%$ [w/w]) became rather inhomogeneous and no reasonable DLS data could be measured. After taking the sample out of the instrument, macroscopic precipitation was observed. This intense phase separation implies that the aggregates formed above the T_{CP} were unstable even with a long hydrophilic PDMA block. Considering that the diblock and the graft copolymer possess similar comonomer ratios, it can be envisaged that the possible reason for the two-step transition of PM₂₁₅(PD₃₁)₁₃ is its branched structure.

The unique two-step LCST transition of the graft copolymer was also confirmed by turbidimetry straightforwardly. Because the turbidimetry is not as sensitive as the DLS measurement but allows continuous stirring, the concentration of the sample solution was increased to 1% (w/w). As depicted in Figure 2c, the transmittance of the solution descended abruptly to almost 0% at about 39 °C. When enlarging the area between 40 and 75 °C, an additional drop in the transmittance can be observed. The higher T_{CP} s observed in the result of turbidimetry compared with the DLS result can be attributed to the higher heating rate. The obtained values of transmittance can also be

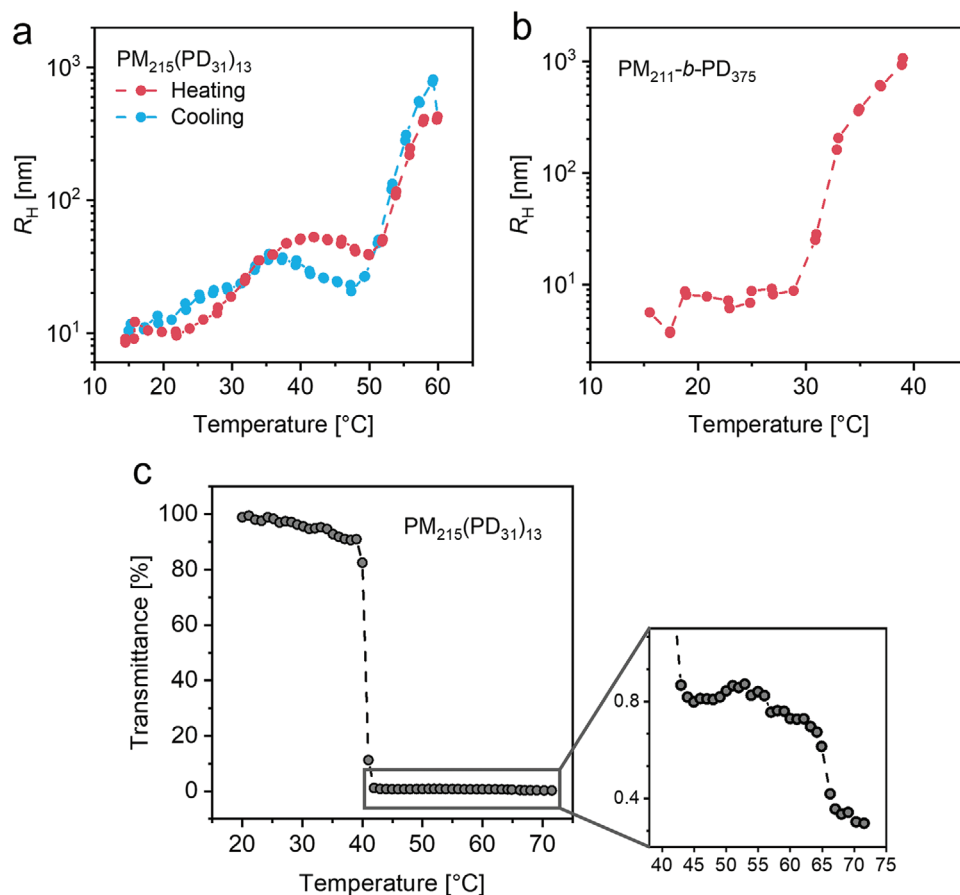


Figure 2. Evolution of R_H of a) $PM_{215}(PD_{31})_{13}$ and b) $PM_{211}\text{-}b\text{-}PD_{375}$ in aqueous solutions ($c = 0.1\%$ [w/w]) monitored by DLS; c) left: temperature dependence of the transmittance measured for the aqueous solution of $PM_{215}(PD_{31})_{13}$ ($c = 1\%$ [w/w]); right: enlarged image of the result of turbidimetry.

converted to absorbance (Figure S7, Supporting Information), which reveals a clearer two-step transition. Despite the promising results, the fundamental cause for the double thermoresponsiveness could not be well explained yet. Therefore, to get more insights into such behavior, temperature-variable $^1\text{H-NMR}$ measurements were performed.

Figure 3a shows the standard $^1\text{H-NMR}$ spectrum of $PM_{215}(PD_{31})_{13}$ in D_2O at ambient temperature, wherein the signals of most interest to the temperature-variable measurements are highlighted. The peaks between 3.40 and 4.05 ppm (peaks A and B) belong to the $PMEO_2MA$ backbone, and those between 2.35 and 3.35 ppm (peaks C and D) result from the PDMA side chains. The normalized temperature-dependent $^1\text{H-NMR}$ spectra are displayed in Figure 3b. The solution was heated from 30 to 55 $^{\circ}\text{C}$ with a temperature step of 5 $^{\circ}\text{C}$. It is obvious that the peaks from the backbone and the side chains were sharper and more intense at low temperatures. Besides, all the peaks except the solvent peak (HDO at 4.79 ppm) shifted to the lower field at high temperatures, which is in accordance with the observation in the literature.^[35]

The decline of the signals reflects the dehydration of polymeric chains during the LCST transitions.^[36] The dehydration processes of the $PMEO_2MA$ backbone and PDMA side chains can be analyzed individually by integrating the respective signal intensities

(i.e., I_{A+B} and I_{C+D}) at different temperatures, which helps elucidate the reason for the two-step LCST transition shown in Figure 2. To this end, it is necessary to introduce the parameter, phase separation degree p , which is defined as^[37]

$$p = 1 - I/I_0,$$

where I and I_0 represent the integrated signal intensities (I_{A+B} or I_{C+D}) at a target temperature and at 30 $^{\circ}\text{C}$, respectively. The calculated values are plotted in Figure 3c. Between 30 and 35 $^{\circ}\text{C}$, the phase separation degrees of both $PMEO_2MA$ and PDMA increased significantly, corresponding to the first LCST transition. Based on this result, it cannot be told whether the backbone or the side chains collapsed first. However, considering that PDMA is much more hydrophilic than $PMEO_2MA$, it is quite logical to infer that the first phase transition was driven by the dehydration of $PMEO_2MA$. Once the first T_{CP} was reached, the $PMEO_2MA$ backbone should turn hydrophobic and start aggregating, resulting in weaker resonant peaks in the $^1\text{H-NMR}$ spectrum. Meanwhile, the formation of the micelles with hydrophobic $PMEO_2MA$ cores could immobilize the attached PDMA side chains (Figure 3d). Additionally, although PDMA chains are still expected to form the hydrophilic shells above the first T_{CP} , the local density of the PDMA chains in a micelle should become higher than that in the

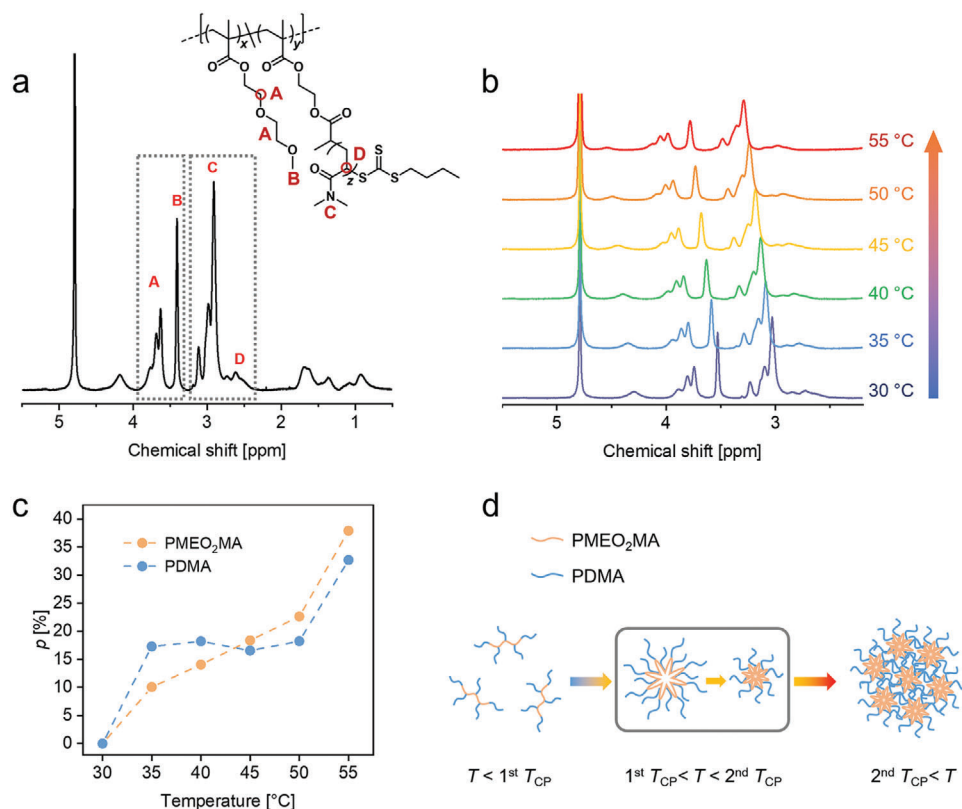


Figure 3. a) Standard $^1\text{H-NMR}$ spectrum of $\text{PM}_{215}(\text{PD}_{31})_{13}$ in D_2O measured at ambient temperature. The signals relevant for the temperature-variable measurements are highlighted in the dashed boxes (end groups and PDMA blocks at α - and ω -terminals of the backbone are not shown); b) normalized $^1\text{H-NMR}$ spectra of $\text{PM}_{215}(\text{PD}_{31})_{13}$ in D_2O at different temperatures; c) calculated phase separation degrees p of PMEO_2MA and PDMA at different temperatures; d) assumed self-assembling process of the copolymer chains.

free chain, especially in the area near the core. The number of water molecules around the side chains thus became less. These factors led to a certain degree of phase separation of PDMA in D_2O below 35°C .

Between 35 and 50°C , the phase separation degree of PMEO_2MA kept increasing gradually, implying continuous expelling of water from the core. This observation can be explained by the mechanism of the LCST transition of PMEO_2MA . Due to the hydrophilic ether oxygen groups in the oxyethylene brushes, the cores formed after the rapid LCST transition were relatively loose.^[35] Since the backbones were surrounded by a considerable number of hydrophilic PDMA arms, further agglomeration was prevented. In those separated micelles, the cores could slowly contract with the increase of temperature. This assumption is also supported by the slight decrease in R_{H} in the DLS result between 40 and 50°C (Figure 2a). On the other hand, the phase separation degree of PDMA was relatively constant in this temperature range, indicating that the shrinkage of the cores hardly influenced the hydration state of the shells. When the sample solution was heated above 50°C , the phase separation degrees of PMEO_2MA and PDMA climbed rapidly again, corresponding well to the second T_{CP} shown in the DLS result. The contraction of PMEO_2MA could cause the disruption of the balance between hydrophilic and hydrophobic interactions at the second T_{CP} . The PDMA chains were no longer capable of stabilizing the particles. Hydrophobic interactions in $-\text{N}(\text{CH}_3)_2$ moieties of the PDMA

chains might be triggered, facilitating the formation of larger clusters and accelerating the dehydration of PMEO_2MA cores in turn.^[30]

The whole assumed double thermoresponsive behavior of the graft copolymer was illustrated in Figure 3d. The driving force of both T_{CP} s can basically be attributed to the dehydration of PMEO_2MA . Thanks to the branched structure of the graft copolymer, hydrophobic cores formed by the backbones could be stabilized by the hydrophilic side chains between two T_{CP} s, causing the emergence of an intermediate state in which amphiphilic micelles could be formed. As the presented $\text{PMEO}_2\text{MA-g-PDMA}$ shows two separate LCST transitions in water, it can nicely be compared with another double thermoresponsive system, POEGMA-g-PNIPAM , investigated in our recent research.^[29] Figure 4 shows their different self-assembling behaviors in dilute aqueous solutions. In the case of $\text{PMEO}_2\text{MA-g-PDMA}$, PMEO_2MA backbone starts aggregating first at a lower temperature, leading to the formation of star-like micelles, while the side chains collapse at a higher temperature. The sequence of transitions of POEGMA-g-PNIPAM is reversed. Hence, flower-like micelles are formed between two T_{CP} s. Another important difference is that the amphiphilic micelles formed by $\text{PMEO}_2\text{MA-g-PDMA}$ above the first T_{CP} are relatively loose, whereas the PNIPAM side chains from POEGMA-g-PNIPAM tend to form denser cores due to additional intra- and interchain hydrogen bonding, which were evidenced by the disappearance of the PNIPAM

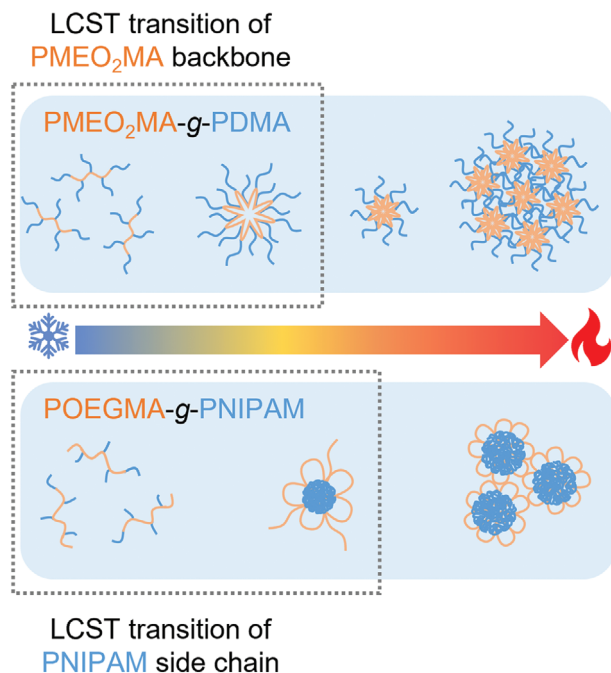


Figure 4. Comparison between the self-assembling behaviors of PMEO₂MA-g-PDMA presented in this work (top) and POEGMA-g-PNIPAM (bottom, effect of the end group is not considered) in the dilute aqueous solutions.^[29]

signal in the ¹H-NMR spectrum at high temperatures.^[29] Apart from the micellar morphologies, the positions of chain ends are different in the micelles of these two systems, which may lead to different application possibilities. TTC-groups of PMEO₂MA-g-PDMA are around the surfaces of the micelles above the first T_{CP} . After converting the TTC-groups to other functionalities (e.g., PDS-groups), it is possible to attach the formed micelles to specific surfaces before triggering the second T_{CP} . On the contrary, the TTC-groups of POEGMA-g-PNIPAM are located in the cores. After end-group modification, the cores of micelles can be chemically cross-linked to form stable nanogels.^[38]

2.3. End-Group Modification and Cross-Linking of the Graft Copolymer

After investigating its thermoresponsive behavior as free chains, PMEO₂MA-g-PDMA was modified for chemical cross-linking. By performing aminolysis in the presence of DTP, the copolymer chains were endowed with the ability to connect with thiol-based cross-linkers (Figure 5a). According to the SEC result shown in Figure 5b, the molecular weight distribution of the graft copolymer was slightly broadened after modification, which most likely resulted from the undesired oxidation of thiol groups during aminolysis.^[39] Since the probable oxidation just caused disulfides and the goal of the modification was cross-linking, the modified sample was totally acceptable and could be regarded as the precursor for a hydrogel.

After purification, the sample appeared pale yellow, indicating that a small portion of TTC-groups was retained. The ultraviolet-visible (UV-vis) spectra displayed in Figure 5c verified this infer-

ence. The absorbance of the TTC-groups at about 308 nm is still observable in the spectrum after aminolysis. The conversion of TTC-groups was then quantitatively determined through the ¹H-NMR spectrum of the modified sample (Figure S8, Supporting Information). The calculated conversion was about 76%, meaning that there were 10 PDS-groups in every chain on average. Although the conversion was not complete, the number of PDS-groups was sufficient for the following cross-linking.

A difunctional thiol-based cross-linker, 2,2'-(ethylenedioxy)diethanethiol (EDT), was employed for cross-linking (Figure 5d). Owing to the superior thiol-reactivity of the PDS-groups, a free-standing gel comprising disulfide bridges was obtained in a few minutes after adding EDT at room temperature.

2.4. Swelling Ratio and Redox-Sensitive Degradation of the Hydrogel

After drying, the swelling rate of the PMEO₂MA-PDMA hydrogel at room temperature was determined by gravimetry. As shown in Figure 6a, the sample absorbed water promptly when immersed in a water bath. After 30 min, the swelling became slower. The sample was almost in a fully swollen state after 2 h and exhibited excellent water capacity. Since the hydrogel was built of thermoresponsive copolymer chains, the absorbed water would be expelled again at high temperatures. Figure 6b shows its deswelling behavior. When it was warmed up, the swollen sample showed a significant contraction between 30 and 40 °C, which corresponds well with the LCST transition of PMEO₂MA. Unlike in the solvents, the chains in the network were constrained and the internal interactions were more complicated. No separate micelles could be formed. It is thus not surprising that only one phase transition occurred. The sample was in a steady state at higher temperatures. In comparison with that of the POEGMA-PNIPAM hydrogel,^[29] the phase transition of the hydrogel presented herein occurred in a temperature range closer to body temperature, which could be an advantage for the biomedical applications.

Eventually, the on-demand dissolution of this covalently cross-linked hydrogel was tested in a reducing environment. As the free graft copolymer chains were water-soluble at room temperature, the degradation was performed in a DL-dithiothreitol (DTT) aqueous solution (Figure 7a). The dissolved polymeric chains during this reaction were monitored by UV-vis spectra of the solution. As depicted in Figure 7b, a small peak at about 308 nm belonging to the embedded TTC-groups appeared within 30 min after immersing the sample in the DTT solution. After 60 min, the absorbance became more intense and meanwhile, the volume of the hydrogel sample in the reaction vial was observed to be much smaller. The last measurement of UV-vis spectroscopy was conducted after 90 min. At this time point, the pieces of the hydrogel sample could no longer be observed, and the solution looked homogeneous. The UV-vis spectrum shows that the absorbance increased further, which is in accordance with the visual observation.

The dissolved chains with multiple thiol functions could be cross-linked again in the presence of an oxidant. Figure 7c shows a reversible sol-gel transition of the thiol-terminated copolymer

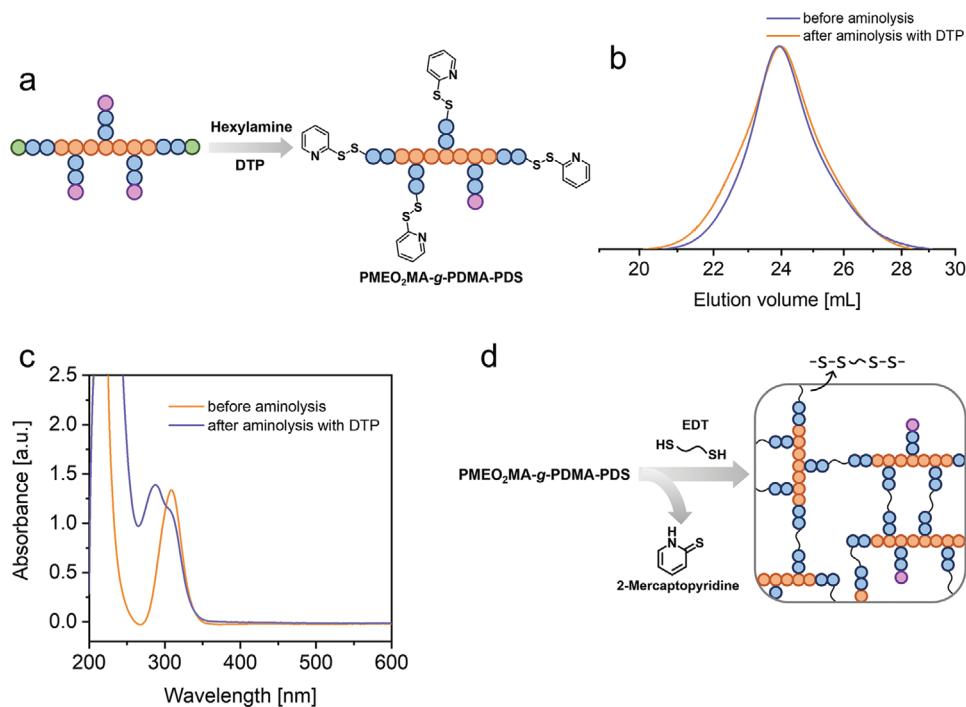


Figure 5. a) Schematic illustration of the aminolysis of the copolymer; b) SEC curves measured before aminolysis ($\bar{M}_{n,SEC} = 59.4$ kDa, $\bar{D} = 1.32$) and after aminolysis in the presence of DTP ($\bar{M}_{n,SEC} = 62.5$ kDa, $\bar{D} = 1.35$) with *N,N*-dimethylacetamide (DMAc) as the mobile phase; c) UV-vis spectra measured before and after aminolysis. The samples were dissolved in ethanol; d) cross-linking reaction between the modified graft copolymer, $\text{PMEO}_2\text{MA-g-PDMA-PDS}$, and the cross-linker, EDT.

chains. After dissolving the hydrogel in a small quantity of the DTT aqueous solution, drops of the hydrogen peroxide (H_2O_2) solution were added and a free-standing gel was formed instantly. The chains could react either with each other or with the free EDT molecules during this process, generating redox-sensitive disulfide linkages again. The pale yellow color seen in the photograph was from the TTC-groups. By adding more DTT into the vial, the hydrogel was redissolved. The homogeneous solution appeared almost colorless because of dilution.

3. Conclusion

In summary, $\text{PMEO}_2\text{MA-g-PDMA}$ was successfully synthesized via successive photoiniferter RAFT polymerization in a grafting-from approach. The graft copolymer was water-soluble at room temperature. During heating and cooling, the copolymer aqueous solution exhibited a reversible two-step LCST transition. Between the two T_{CP} s, stable micelles with PMEO_2MA cores and PDMA shells could be formed due to the branched structure. However, the cores carried on expelling water with the increase of temperature in this range, leading to the disruption of the balance between hydrophilic and hydrophobic interactions at the second T_{CP} . At higher temperatures, both PMEO_2MA and PDMA became substantially more dehydrated and larger aggregates were formed.

By treating the $\text{PMEO}_2\text{MA-g-PDMA}$ copolymer with an amine and DTP simultaneously, an adequate number of TTC-groups were converted to PDS-groups. After adding a dithiol-based cross-linker, a hydrogel with satisfying water absorbency at room

temperature was obtained. The thermoresponsive sample underwent deswelling between 30 and 40 °C. In the presence of the disulfide-reducing agent, DTT, the hydrogel was completely dissolved in an aqueous solution. The obtained thiol-terminated copolymer could further undergo a reversible redox-sensitive sol-gel transition.

It can be envisioned that the presented synthetic route eases the preparation of multifunctional polymers for various applications. By tailoring the backbone and the side chains of the graft copolymer, advanced self-assembling properties in suitable solvents can be realized. After a facile chain modification, “smart” polymer networks with combined advantages, like stimuli-responsiveness and redox-sensitive degradability, become accessible.

4. Experimental Section

Materials: CPDTC (abcr, 97%), CDTPA (abcr, 97%), *N,N'*-dicyclohexylcarbodiimide (DCC, Sigma-Aldrich, 99%), 4-(dimethylamino)pyridine (DMAP, Sigma-Aldrich, 99%), ethylene glycol (Merck, 99%), DTP (TCI, 98%), EDT (Sigma-Aldrich, 95%), hexylamine (Sigma-Aldrich, 99%), DTT (TCI, 98%), H_2O_2 (VWR, 30%). BTPEMA was synthesized according to the literature.^[32] All the solvents were used as received. MEO_2MA (Sigma-Aldrich, 95%) and DMA (Sigma-Aldrich, 99%) were passed through activated basic alumina prior to the polymerizations.

Synthesis of DiCTA: CDTPA (1.20 g, 2.97 mmol), ethylene glycol (0.09 g, 1.45 mmol), DCC (0.74 g, 3.59 mmol), and DMAP (0.02 g, 0.15 mmol) were dissolved in tetrahydrofuran (THF, 9 mL) and the reaction mixture was stirred at room temperature for 24 h. After removal of the solvent, the crude product was purified by column chromatography

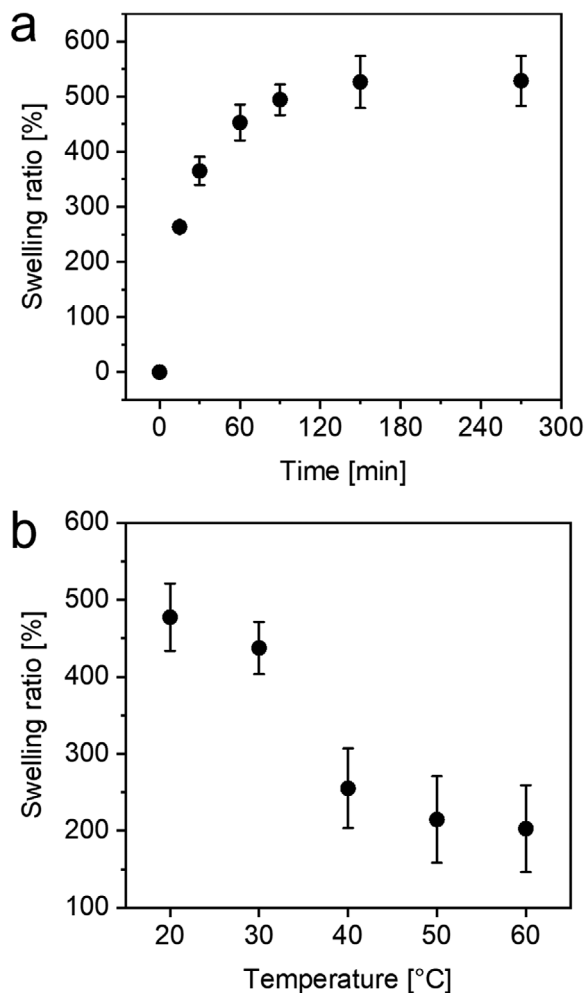


Figure 6. a) Swelling rate of the P(MEO₂MA-r-BTPEMA) hydrogel at room temperature; b) temperature dependence of the swelling ratio of the hydrogel sample.

using hexane/ethyl acetate (5/2 [v/v]) as the mobile phase to give a yellow oil (0.82 g, 68% yield). ¹H-NMR spectroscopy in deuterated chloroform (ppm) (Figure S1, Supporting Information): 0.88 (t, 6H); 1.27 (m, 36H); 1.69 (m, 4H); 1.89 (s, 6H); 2.30–2.80 (m, 8H); 3.33 (t, 4H); 4.32 (s, 4H).

Procedure for the Polymerization of Backbone: In the photoiniferter RAFT polymerization of P(MEO₂MA-r-BTPEMA), MEO₂MA, BTPEMA, and DiCTA ([MEO₂MA]/[BTPEMA]/[DiCTA] = 380/20/1) were dissolved in 1,4-dioxane (DOX) in a polymerization vial. For the determination of monomer conversion, dimethylformamide (DMF) was added as an internal standard. The total solid (DiCTA plus the monomers) concentration was 20% (w/w). The reaction solution was degassed with nitrogen gas for 15 min and then placed in an oil bath at 70 °C under green light irradiation (515 nm) of 1.13 mW cm⁻². After 150 min, the polymerization was stopped by removing the light source and cooling in an ice bath. The conversion was then determined through the decline of the monomer signals in the ¹H-NMR spectra of the reaction mixture. The polymer was precipitated in an excess amount of *n*-hexane and redissolved in THF. The purification was repeated three times. The final product was dried under vacuum at 40 °C.

Procedure for the Polymerization of P(MEO₂MA-g-PDMA Graft Copolymer: In the photoiniferter RAFT polymerization of P(MEO₂MA-g-PDMA, DMA and the backbone ([DMA]/[P(MEO₂MA-r-BTPEMA)] = 780/1, [DMA]/[TTC] = 60/1) were dissolved in DOX in a polymerization vial. For

the determination of monomer conversion, DMF was added as an internal standard. The total solid (P[MEO₂MA-r-BTPEMA] plus DMA) concentration was 15% (w/w). The reaction solution was degassed with nitrogen gas for 15 min and then placed in an oil bath at 70 °C under blue light irradiation (467 nm) of 3.86 mW cm⁻². After 90 min, the polymerization was stopped by removing the light source and cooling in an ice bath. The conversion was also determined through the ¹H-NMR spectra of the reaction mixture. The polymer was precipitated in an excess amount of diethyl ether and redissolved in THF. The purification was repeated three times. The final product was dried under vacuum at room temperature.

Postpolymerization Modification and Cross-Linking of the Graft Copolymer: P(MEO₂MA-g-PDMA ($\bar{M}_{n,th}$ = 85.6 kDa, 13 TTC-groups per chain) (585 mg, 0.089 mmol TTC-groups) and DTP (984 mg, 50-fold molar excess with respect to TTC) were dissolved in 10 mL DOX. The solution was purged with nitrogen gas for 25 min to remove oxygen. Afterward, 0.1 mL of the hexylamine solution (0.6 mL hexylamine dilute in 2 mL DOX) (2.5-fold molar excess with respect to TTC) was added. The reaction mixture was further degassed for 5 min and then stirred overnight at room temperature. After precipitation in diethyl ether (4 times), a pale yellow PDS-functionalized polymer, P(MEO₂MA-g-PDMA-PDS, was recovered.

The modified graft copolymer was cross-linked according to a previous research.^[29] In brief, 150 mg P(MEO₂MA-g-PDMA-PDS ($\bar{M}_{n,th}$ = 85.0 kDa, 0.018 mmol PDS-groups) were dissolved in DMF (c = 25% [w/w]). 0.03 mL of the EDT solution (0.1 mL EDT dilute in 2 mL DMF) (0.017 mmol thiol-groups) was added and mixed at room temperature. The gel-formation was checked by a tube inversion test. A free-standing gel was observed in a few minutes. The gel was then immersed in THF for purification.

Degradation of the Hydrogel: A piece of dried sample (10 mg) was swollen in water before the experiment. The fully swollen sample was immersed in 2 mL DTT aqueous solution (10×10^{-3} M) and then put into a shaker at room temperature. A UV-vis spectrum of the solution was measured every 30 min until the hydrogel was completely dissolved.

Sol-Gel Transition of the Hydrogel: 25 mg of the dried hydrogel were dissolved in 0.2 mL DTT solution (10×10^{-3} M) in a glass vial. H₂O₂ solution was added dropwise into the vial and a free-standing gel was observed. Afterward, DTT solution was added slowly to redissolve the gel.

Analytics: NMR Spectroscopy: Standard ¹H-NMR spectra were measured with a BRUKER AVANCE II 400 MHz at ambient temperature. For the measurement of temperature-variable ¹H-NMR spectra, 2 mg polymer were dissolved in 0.7 mL D₂O and stirred for 24 h. The spectra were recorded with an increment of 5 °C and normalized by the integrated intensity of the HDO peak.

SEC: For P(MEO₂MA-r-BTPEMA) and homo-P(MEO₂MA), THF was used as the eluent with a flow rate of 1.0 mL min⁻¹ at 30 °C. The measurements were performed on an AGILENT 1260 INFINITY system with PSS SDV separation columns and a refractive index (RI) detector. For the graft copolymers, DMAc with 0.1 M LiCl was used as the mobile phase at a flow rate of 0.8 mL min⁻¹. The measurements were conducted with PSS GRAM columns at a temperature of 50 °C. To determine the molecular weight distributions of the polymers, the obtained SEC curves were calibrated by narrowly distributed poly(methyl methacrylate) (PMMA) standards.

UV-vis Spectroscopy: The UV-vis spectra were measured with spectrophotometer UV5 from METTLER TOLEDO at ambient temperature.

DLS Measurements: The polymer samples were dissolved in Milli-Q water and stirred for 24 h before the measurements. The measurements were conducted on an ALV/CGS-3 Compact Goniometer-System containing an ALV/LSE-5004 Multiple Tau Digital Correlator and an Nd:YAG laser (532 nm, 400 mW). The measuring angle was kept at 90° for every measurement. The duration of each measurement was set to 60 s. The viscosity and RI of water at each temperature were corrected in the ALV Digital Correlator Software automatically. The solutions were heated or cooled in a toluene bath. The temperature step of heating and cooling processes was controlled at 1 °C for linear polymers or 2 °C for the copolymers by a Julabo F25 thermostat. The temperature accuracy was set to 1 °C. The obtained DLS data were fitted based on a cumulant approach with a program written by Felix Lauterbach.^[40]

Turbidimetry: The polymer sample was completely dissolved in Milli-Q water. The temperature dependence of the transmittance of the solution

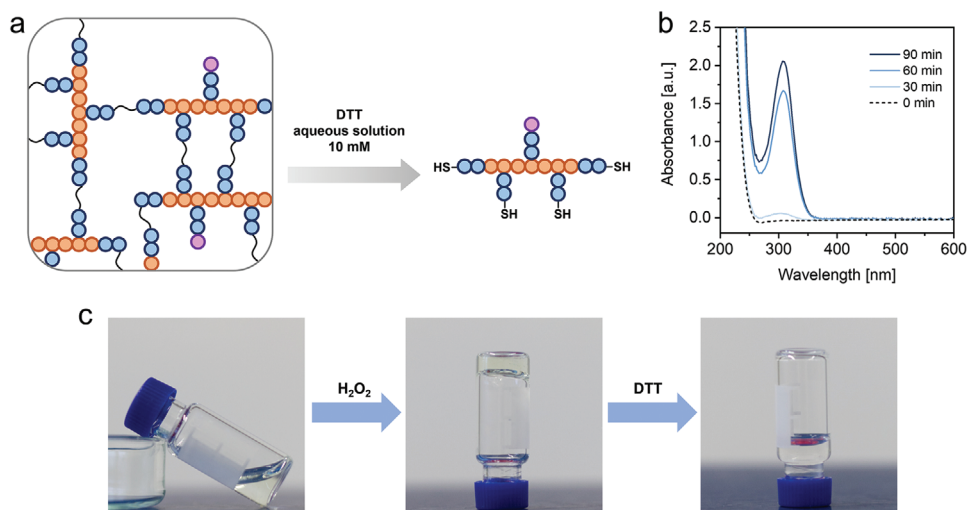


Figure 7. a) Schematic illustration of the degradation of the hydrogel in a DTT aqueous solution; b) UV-vis spectra of the DTT aqueous solution measured every 30 min during the degradation; c) a reversible sol-gel transition in the presence of an oxidant and a reductant.

was recorded on spectrophotometer UV5 at 600 nm during heating. The temperature step was controlled at 1 °C by a thermostat accessory CuveT (METTLER TOLEDO).

Determination of the Swelling Rate of the Hydrogel: The determination was accomplished gravimetrically. A piece of dried sample (30 mg) was immersed in deionized water at room temperature. The sample was taken out of water after a certain period and carefully dried with a soft precision wipe. The swollen sample was weighed and then immersed in water again. The swelling ratio of the hydrogel was determined as

$$\text{Swelling ratio} = (W_s - W_d)/W_d,$$

where W_s means the weight of the swollen hydrogel and W_d represents the weight of the dry sample. The procedure was performed until the weight of the swollen sample barely changed. The test was repeated three times.

Determination of the Temperature Dependence of the Swelling Ratio: A piece of dried sample (26 mg) was immersed in deionized water overnight before the test. The swollen sample was then immersed in water at each target temperature for 30 min. The surface of the wet sample taken out of the water bath was quickly dried with a soft precision wipe. The swelling ratio at each target temperature was then calculated. The test was repeated three times.

Supporting Information

Supporting Information is available from the Wiley Online Library or from the author.

Acknowledgements

The work was financially supported by Universität Hamburg, the Research Training Group NANOHYBRID (GRK 2536/1) funded by the Deutsche Forschungsgemeinschaft (DFG) and a collaborative project funded by the Helmholtz Association and Russian Science Foundation (grant number HRSF-0075). The authors would like to thank the NMR department for the temperature-dependent measurements and Martin Kehden for his help with the SEC measurements.

Open access funding enabled and organized by Projekt DEAL.

Conflict of Interest

The authors declare no conflict of interest.

Data Availability Statement

The data that support the findings of this study are available in the supplementary material of this article.

Keywords

degradable thermoresponsive hydrogels, LCST transitions, photoiniferter RAFT polymerization, sol-gel transitions, thermoresponsive graft copolymers

Received: February 18, 2022

Revised: March 28, 2022

Published online:

- [1] O. Wichterle, D. Lím, *Nature* **1960**, *185*, 117.
- [2] I. Willner, *Acc. Chem. Res.* **2017**, *50*, 657.
- [3] J. L. Drury, D. J. Mooney, *Biomaterials* **2003**, *24*, 4337.
- [4] W. Hu, Z. Wang, Y. u Xiao, S. Zhang, J. Wang, *Biomater. Sci.* **2019**, *7*, 843.
- [5] Z. Xu, W. Liu, *Chem. Commun.* **2018**, *54*, 10540.
- [6] P. Biais, M. Engel, O. Colombani, T. Nicolai, F. Stoffelbach, J. Rieger, *Polym. Chem.* **2021**, *12*, 1040.
- [7] M. Mohamadhoseini, Z. Mohamadnia, *Polym. Chem.* **2021**, *12*, 5679.
- [8] G. Zhang, L. Lv, Y. Deng, C. Wang, *Macromol. Rapid Commun.* **2017**, *38*, 1700018.
- [9] M. Onoda, T. Ueki, R. Tamate, A. M. Akimoto, C. C. Hall, T. P. Lodge, R. Yoshida, *ACS Macro Lett.* **2018**, *7*, 950.
- [10] V. Pertierra, C. Pin-Barre, C. Rivera, C. Pellegrino, J. Laurin, D. Gígenes, T. Trimailla, *Biomacromolecules* **2019**, *20*, 149.
- [11] Z. Zhang, N. Corrigan, A. Bagheri, J. Jin, C. Boyer, *Angew. Chem., Int. Ed.* **2019**, *58*, 17954.

- [12] A. Bagheri, C. Bainbridge, J. Jin, *ACS Appl. Polym. Mater.* **2019**, *1*, 1896.
- [13] J. Zhu, W. K. Tan, X. Song, Z. Gao, Y. Wen, C. N. Ong, C. S. Loh, S. Swarup, J. Li, *ACS Sustainable Chem. Eng.* **2020**, *8*, 9425.
- [14] S.-Y. Choh, D. Cross, C. Wang, *Biomacromolecules* **2011**, *12*, 1126.
- [15] R. T. C. Cleophas, M. Riool, H. (L.) C. Quarles Van Ufford, S. A. J. Zaat, J. A. W. Kruijtzter, R. M. J. Liskamp, *ACS Macro Lett.* **2014**, *3*, 477.
- [16] P. Chakma, Z. A. Digby, J. Via, M. P. Shulman, J. L. Sparks, D. Konkolewicz, *Polym. Chem.* **2018**, *9*, 4744.
- [17] J. Liang, B. B. Karakoçak, J. J. Struckhoff, N. Ravi, *Biomacromolecules* **2016**, *17*, 4064.
- [18] V. Delplace, P. E. B. Nickerson, A. Ortin-Martinez, A. E. G. Baker, V. A. Wallace, M. S. Shoichet, *Adv. Funct. Mater.* **2020**, *30*, 1903978.
- [19] D. D. Mckinnon, D. W. Domaille, J. N. Cha, K. S. Anseth, *Adv. Mater.* **2014**, *26*, 865.
- [20] J. Collins, M. Nadgorny, Z. Xiao, L. A. Connal, *Macromol. Rapid Commun.* **2017**, *38*, 1600760.
- [21] X. Ma, T. Xu, W. Chen, H. Qin, B. o Chi, Z. Ye, *Carbohydr. Polym.* **2018**, *179*, 100.
- [22] J.-F. Lutz, K. Weichenhan, Ö. Akdemir, A. Hoth, *Macromolecules* **2007**, *40*, 2503.
- [23] Z. Q.i Liu, Z. Wei, X.v L. Zhu, G. Y. Huang, F. Xu, J. H. Yang, Y. Osada, M. Zrínyi, J. H. Li, Y. M. Chen, *Colloids Surf., B* **2015**, *128*, 140.
- [24] M. M. Perera, N. Ayres, *Polym. Chem.* **2020**, *11*, 1410.
- [25] P. Mostafalu, G. Kiaee, G. Giatsidis, A. Khalilpour, M. Nabavinia, M. R. Dokmeci, S. Sonkusale, D. P. Orgill, A. Tamayol, A. Khademhosseini, *Adv. Funct. Mater.* **2017**, *27*, 1702399.
- [26] A. Navaei, D. Truong, J. Heffernan, J. Cutts, D. Brafman, R. W. Sirianni, B. Vernon, M. Nikkhah, *Acta Biomater.* **2016**, *32*, 10.
- [27] L.i Liu, S. Jiang, Y. Sun, S. Agarwal, *Adv. Funct. Mater.* **2016**, *26*, 1021.
- [28] K. Fukumori, Y. Akiyama, Y. Kumashiro, J. Kobayashi, M. Yamato, K. Sakai, T. Okano, *Macromol. Biosci.* **2010**, *10*, 1117.
- [29] J. Xu, V. Abetz, *Soft Matter* **2022**, *18*, 2082.
- [30] F. Fischer, D. Zufferey, R. Tahoces, *Polym. Int.* **2011**, *60*, 1259.
- [31] J.-F. Lutz, A. Hoth, *Macromolecules* **2006**, *39*, 893.
- [32] S. Shanmugam, J. Cuthbert, T. Kowalewski, C. Boyer, K. Matyjaszewski, *Macromolecules* **2018**, *51*, 7776.
- [33] J. Xu, V. Abetz, *Macromol. Rapid Commun.* **2021**, *42*, 2000648.
- [34] J. Rieger, W. Zhang, F. Stoffelbach, B. Charleux, *Macromolecules* **2010**, *43*, 6302.
- [35] S. Sun, P. Wu, *Macromolecules* **2013**, *46*, 236.
- [36] J. Spěvák, *Curr. Opin. Colloid Interface Sci.* **2009**, *14*, 184.
- [37] J. Spěvák, J. Dybal, L. Starovoytova, A. Zhigunov, Z. Sedláková, *Soft Matter* **2012**, *8*, 6110.
- [38] J.a-H. Ryu, R. T. Chacko, S. Jiwanich, S. Bickerton, R. P. Babu, S. Thayumanavan, *J. Am. Chem. Soc.* **2010**, *132*, 17227.
- [39] X.-P. Qiu, F. M. Winnik, *Macromolecules* **2007**, *40*, 872.
- [40] F. Lauterbach, *PhD Thesis*, Universität Hamburg **2020**.

Chapter 4

Unpublished Results

This chapter includes the results of some preliminary studies of this work and some further investigations extended from the publications in Chapter 3. First, in Section 4.1, suitable reaction conditions for photoiniferter RAFT polymerization were explored during the investigations on the diblock copolymer PMMA-*b*-POEGMA at the early stage of this work. Next, Section 4.2 discusses the unusual solution behavior of PNAGA, which is related to Publication 1. At last, Section 4.3 extends the investigation in Publication 2, highlighting the influence of the end-group on LCST transitions.

4.1 Investigations on PMMA-*b*-POEGMA

In the literature, the thermoresponsive behavior of PMMA-*b*-PNIPAM aqueous solutions has been intensively investigated.^[184-187] As a potential alternative to PNIPAM,^[146] POEGMA also features an LCST-type T_{CP} in aqueous solutions. The thermoresponsive behavior of the diblock copolymer, PMMA-*b*-POEGMA, is thus also worth investigating. All the polymer samples in this section were synthesized via photoiniferter RAFT polymerization. Before fabricating the diblock copolymer, some efforts were made to explore the influences of different factors on the photoiniferter RAFT polymerization. As a result, suitable reaction conditions were successfully found. More importantly, a better understanding of the photoiniferter strategy was achieved through the analytical results.

4.1.1 Screening the Reaction Conditions

In order to obtain well-defined diblock copolymers with narrowly distributed molecular weights and high end-group fidelity as fast as possible, various factors should be considered when optimizing the polymerization conditions. In this work, the optimization was focused on four factors: light intensity, reaction temperature, the target monomer conversion α , and the choice of CTAs.

The optimization was performed based on the polymerization of MMA. Regarding the CTA choice for the photoiniferter RAFT polymerization, 4-cyano-4-[(dodecylsulfanylthiocarbonyl)sulfanyl]pentanoic acid (CDTPA) and 4-cyanopentanoic acid dithiobenzoate (CPADB) with different Z-groups were tested and compared as they have both been proven to be able to provide good control for the conventional RAFT polymerization of methacrylates.^[57] The ultraviolet–visible (UV–vis) spectra of these two CTAs reveal their different absorption bands in the visible light region (**Figure 4.1**), which also reflect their different colors. While the CDTPA is a yellow powder, CPADB looks pink. Thus, their influences on the visible-light-induced polymerization are of great interest. Herein, visible light LEDs with wavelengths in the regions of blue and green were exploited. Their emission spectra are also shown in **Figure 4.1**. The polymerization optimization then started with CDTPA as the CTA.

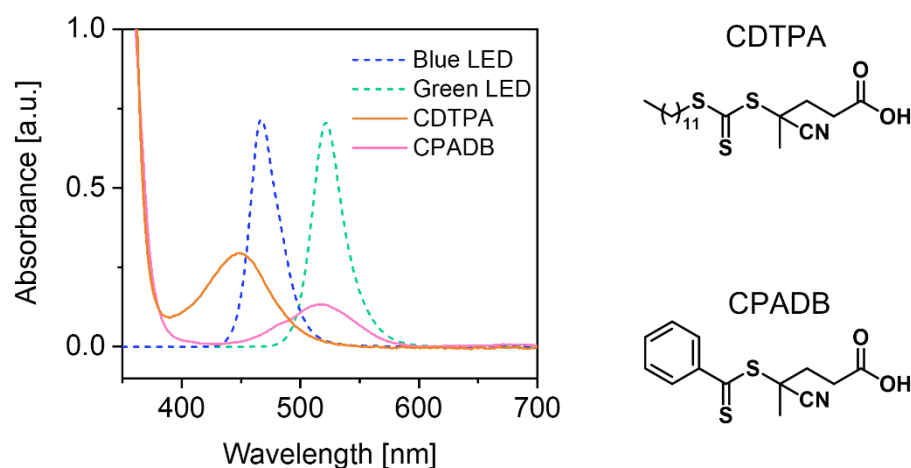


Figure 4.1. UV–vis spectra of the CTAs (CDTPA and CPADB) and the emission spectra of blue and green LEDs. The CTAs were dissolved in DOX ($c = 10$ mM).

Influence of Light Intensity

In this part, a series of photoiniferter RAFT polymerizations of MMA was performed. Previous research has already reported that compared with blue light, green light provides better control over the polymerization of MMA mediated by CDTPA.^[69] Thus, green LEDs (515 nm) were used here as the light source. In order to understand the influence of the light intensities, other factors were kept constant. The solvent for the polymerizations was DOX, which features a relatively high polarity and can thus elevate the polymerization rate. DOX is also miscible with most organic solvents so that the synthesized PMMA could easily be purified by precipitation in a poor solvent, like *n*-hexane. Moreover, the moderate boiling point eases the evaporation of the residual DOX in the products. The solid concentration (CTA plus monomer) of the reaction mixture was kept at 25% (w/w) so that the mixture after the polymerization was neither too viscous to handle nor too dilute for the precipitation. The target DP of every polymerization was 100. In order to shorten the reaction time, all the polymerizations discussed in this part were heated to 70 °C in an oil bath. The reactions were stopped after 300 min.

After determining the conditions mentioned above, the polymerizations were performed under three light intensities: 2.27 mW cm⁻², 1.13 mW cm⁻², and 0.56 mW cm⁻². The size exclusion chromatography (SEC) results of the purified PMMA are shown in **Table 4.1**. It can be observed that the higher intensity led to a faster polymerization rate (higher α), which is in accordance with the results in the literature.^[188] However, the dispersity (\mathcal{D}) of the product was significantly improved when the intensity was reduced from 2.27 mW cm⁻² to 1.13 mW cm⁻². Meanwhile, the sacrifice in α , which was determined by ¹H-NMR, was still acceptable. A further intensity reduction to 0.56 mW cm⁻² hardly affected the \mathcal{D} . Therefore, 1.13 mW cm⁻², a moderate light intensity, was the best choice among these three options.

Table 4.1 Analytical results of the PMMA samples polymerized under different light intensities.

Light intensity [mW cm ⁻²]	α [%] ^{a)}	$\bar{M}_{n,SEC}$ [kDa] ^{b)}	\mathcal{D} ^{c)}
2.27	90	6.2	1.47
1.13	86	5.8	1.22
0.56	78	5.6	1.25

^{a)}Determined through the decline of monomer signals in the ¹H-NMR spectra with the reference signal of *N,N*-dimethylformamide (DMF); ^{b,c)}number average molecular weight and \mathcal{D} determined by SEC in tetrahydrofuran (THF) relative to the PMMA standard.

Influence of Temperature

After deciding the light intensity, the influence of temperature was investigated. **Table 4.1** shows the PMMA samples synthesized at a temperature of 70 °C. In this part, the temperature was lowered to 50 °C. After 300 min under the green light of 1.13 mW cm⁻², α of 70% was reached. The D of the polymer was measured to be 1.30, which was slightly larger than that of the sample synthesized at a higher temperature. As a higher reaction temperature results in a higher rate of polymerization and still a satisfying molecular distribution, the subsequent polymerizations were conducted at 70 °C.

Influence of Monomer Conversion

In order to suppress the formation of dead chains, α must also be carefully controlled because the probability of termination increases as the monomer concentration decreases during the polymerization.^[189] On the other hand, α should be as high as possible to avoid wasting a large number of monomers, especially if the synthesis of the monomers requires massive effort. Therefore, three PMMA samples with different α were synthesized to estimate the upper limit of α . The α was controlled through the reaction time, i.e., a lower α was achieved by shortening the reaction time. A straightforward way to examine these PMMA samples' livingness was to perform chain extensions from them and then measure the SEC traces before and after chain extensions. The monomer used for the chain extensions here was also MMA for simplicity. Consequently, polymer samples, PMMA-*b*-PMMA with two PMMA blocks, were yielded. The SEC results measured with tetrahydrofuran (THF) as the mobile phase are shown in **Figure 4.2**. All the curves of PMMA samples are relatively narrow. However, a flat shoulder can already be discovered in the SEC trace of PMMA-*b*-PMMA when α of the first block reached 70% (**Figure 4.2b**). The shoulder became more evident when α of the first block increased to 85% (**Figure 4.2a**), indicating the increase in "dead" chains in the PMMA sample. When α was lowered to 58%, a clean monomodal SEC curve of PMMA-*b*-PMMA could be measured (**Figure 4.2c**). The corresponding reaction time for the first block was 180 min.

The molecular weight distribution may affect the properties of polymers, including thermoresponsiveness.^[190] Therefore, it is necessary to keep the livingness of the chains at a high level. To this end, α was kept between 50% and 60% in the following polymerizations of methacrylic monomers.

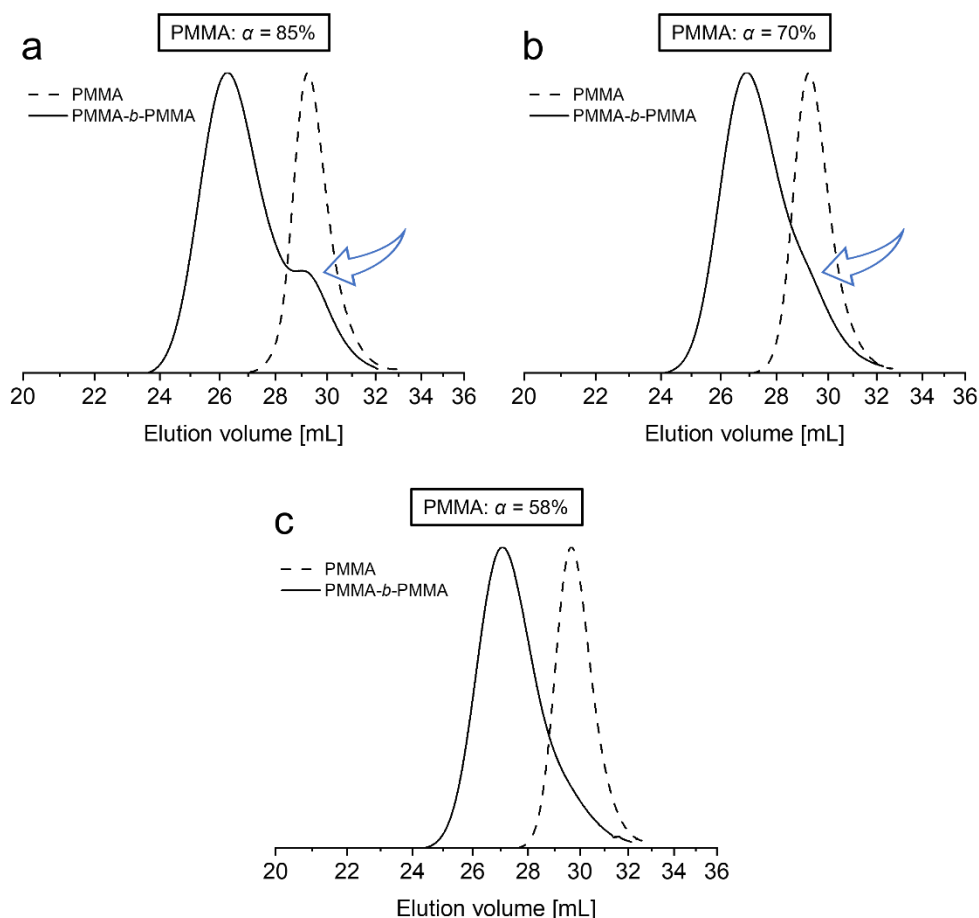


Figure 4.2. SEC traces of PMMA and PMMA-*b*-PMMA obtained after chain extensions. The polymerizations of the first PMMA block were stopped at different α : (a) 85%, (b) 70%, (c) 58%. Blue arrows indicate the shoulders observed in the traces.

Influence of CTAs

As mentioned above, both CDTPA and CPADB are good candidates for the thermally initiated RAFT polymerization of MMA. Through the previous experiments, suitable reaction conditions had been found for the photoiniferter RAFT polymerization with CDTPA. Hence, CDTPA was simply replaced with CPADB in this part to examine the influence of the CTAs on the polymerization.

Surprisingly, under the same reaction conditions (1.13 mW cm^{-2} , $70 \text{ }^\circ\text{C}$), the polymerization rate with CPADB was quite slow. After 180 min, the α of MMA was only about 13%. As such a significant difference between CDTPA and CPADB was not reported in the thermally initiated RAFT polymerization, the reason behind this slower rate should be correlated with the photolysis process. Thus, the light

intensity was increased to 2.27 mW cm^{-2} for CPADB afterward. The α was monitored during the polymerization. The result is plotted in **Figure 4.3a**. With the help of higher light intensity, the polymerization rate was still not ideal but became acceptable. After 420 min, α reached about 50%. However, even though it was stopped at a relatively low α , the polymerization still caused a considerable number of dead chains, which is revealed by the bimodal SEC curve of PMMA-*b*-PMMA (**Figure 4.3b**). Lastly, the blue LED, whose emission spectrum is shown in **Figure 4.1**, was adopted to initiate the polymerization. The light intensity was set to 3.86 mW cm^{-2} . Still, almost no α ($< 5\%$) was obtained after 9 h.

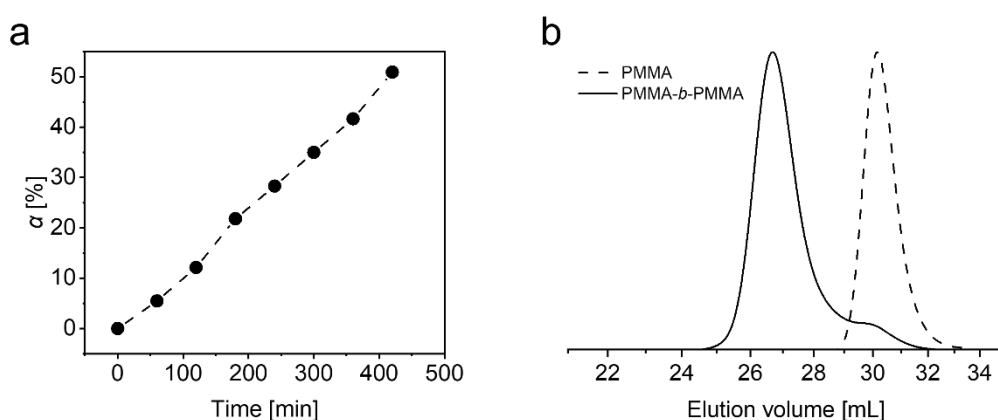


Figure 4.3. (a) α determined every 60 min during the polymerization of the first PMMA block with CPADB; (b) SEC traces of the polymer samples before and after the chain extension.

The slower polymerization rate resulting from CPADB was unexpected, as the absorbance of CPADB solution in the green light region is even higher than that of CDTPA solution with the same concentration (**Figure 4.1**). The possible reason for this phenomenon could be the lower quantum yield and inefficient photolysis of CPADB.^[191] Recently, the Z-group of CTA has been reported to have a significant impact on photolysis.^[192] The absorbance of CPADB in the blue light region is even lower than in the green light region. The blue LED was thus insufficient for the photolysis even with higher light intensity. Considering the sluggish initiation and a high ratio of dead chains in the product, CPADB was not preferred for the photoiniferter RAFT polymerization in this work.

To sum up, suitable reaction conditions for the polymerization of MMA were found at this stage. CDTPA was proven to be able to provide good control over the

molecular weight distribution under a moderate light intensity (1.13 mW cm^{-2}). The reaction mixture could be heated to $70 \text{ }^\circ\text{C}$ to speed up the polymerization. In addition, the reaction time should be carefully controlled so that the final α was between 50% and 60%. Although the optimization was only implemented for MMA, it should be much easier now to adapt the reaction conditions for similar methacrylates. For other monomers that can be polymerized via photoiniferter RAFT under visible light irradiation, the tests shown in this section can also be a meaningful guideline.

4.1.2 Synthesis of PMMA-*b*-POEGMA

After finding the suitable reaction conditions for the polymerization of MMA, a thermoresponsive diblock copolymer, PMMA-*b*-POEGMA, was prepared. PMMA block with a DP of 53 was synthesized first. Its SEC curve in **Figure 4.4** (dashed line) shows a narrow molecular weight distribution ($\mathcal{D} = 1.18$). Through calibration with PMMA standards, the number average molecular weight $\bar{M}_{n,\text{SEC}} = 5.2 \text{ kDa}$ is obtained, which agrees well with expectation. The PMMA block was then extended with POEGMA. The DP of the second block was 100. The applied reaction conditions were similar to those for the PMMA block. The experimental details can be found in Section 4.1.4. The SEC curve clearly shifts to the left after chain extension (**Figure 4.4**). The curve of the diblock copolymer is broadened probably due to the worse solubility of POEGMA compared with PMMA. However, the \mathcal{D} of 1.34 is still acceptable.

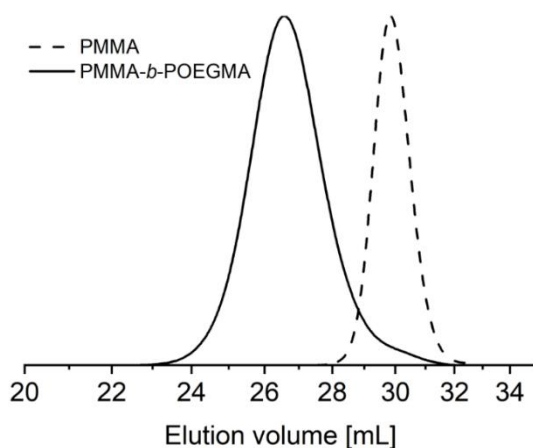


Figure 4.4. SEC traces of PMMA ($\bar{M}_{n,\text{SEC}} = 5.2 \text{ kDa}$, $\mathcal{D} = 1.18$) and PMMA-*b*-POEGMA ($\bar{M}_{n,\text{SEC}} = 24.8 \text{ kDa}$, $\mathcal{D} = 1.34$).

4.1.3 Thermoresponsive Behavior of PMMA-*b*-POEGMA

Because of the short hydrophobic PMMA block and the relatively long POEGMA block, the copolymer could be dissolved in water without ultrasonication at room temperature (**Figure 4.5a**). The transparent polymer solution ($c = 1\%$ [w/w]) became immediately turbid in a water bath at $70\text{ }^{\circ}\text{C}$. After cooling, the solution turned transparent again. The visual turbidimetry reveals clearly a reversible LCST transition.

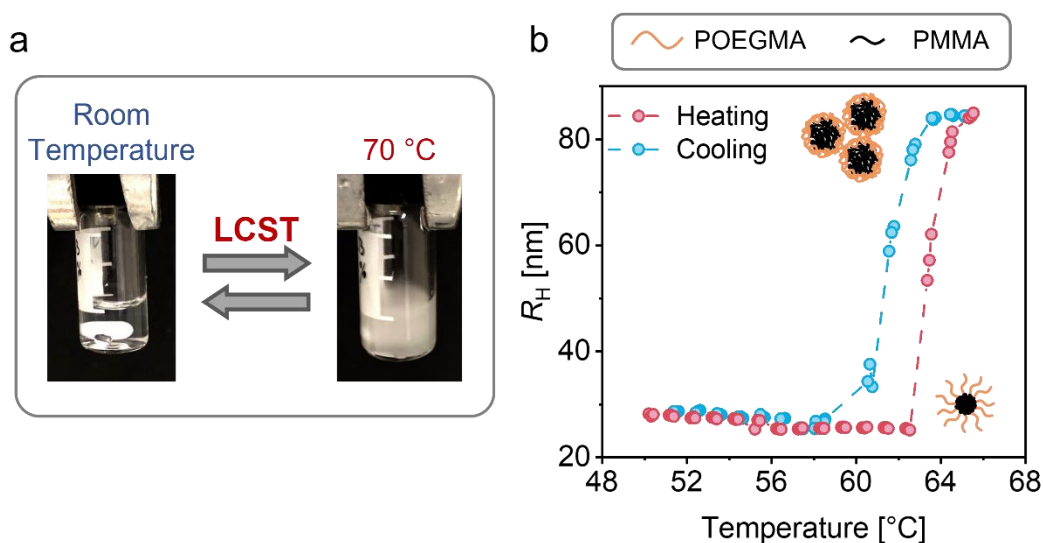


Figure 4.5. (a) Visual turbidimetry for a PMMA-*b*-POEGMA aqueous solution ($c = 1\%$ [w/w]); (b) evolution of R_H of PMMA-*b*-POEGMA in an aqueous solution ($c = 0.1\%$ [w/w]) recorded by DLS. The solution was gradually heated from $50\text{ }^{\circ}\text{C}$ to $65\text{ }^{\circ}\text{C}$ and then cooled.

Subsequently, the polymer solution was diluted to 0.1% (w/w) for the temperature-dependent DLS measurement. **Figure 4.5b** shows the evolution of R_H of the diblock copolymer during the heating and cooling processes. A leap in R_H can be observed in the heating curve. In this work, all the LCST-type T_{CP} s are determined as the onsets of the increase in R_H . Therefore, the T_{CP} of the diblock copolymer is about $62\text{ }^{\circ}\text{C}$. The R_H of the sample could return to the initial state after the cooling process despite small hysteresis. Interestingly, although both blocks were hydrophobic above the T_{CP} , no macroscopic precipitation was caused by the phase transition. According to the DLS result, the increase in R_H has almost stopped at $65\text{ }^{\circ}\text{C}$. The largest R_H in the measurement was under 90 nm . The relatively compact dimension of the aggregates could be attributed to the carboxyl

group at the chain end. The hydrophilic R-group from CDTPA could hinder the further aggregation and stabilize the particles above the T_{CP} , which is similar to the phenomenon described in Publication 2 in Chapter 3.

4.1.4 Experimental Section

Materials

CDTPA (abcr, 97%), CPADB (abcr, 97%), deuterated chloroform ($CDCl_3$, Sigma Aldrich, 100%). All the solvents were used as received. MMA (Sigma Aldrich, 99%) and OEGMA (Sigma Aldrich, $\bar{M}_n = 300$ Da) were passed through activated basic alumina prior to the polymerizations.

Polymerization of PMMA Block

CDTPA and MMA ($[MMA]/[CDTPA] = 100/1$) were dissolved in DOX in a glass vial. The solid concentration (CDTPA plus MMA) of the reaction mixture was 25% (w/w). A small amount of *N,N*-dimethylformamide (DMF) was added as an internal standard for determining the conversion. The solution was degassed with nitrogen for 15 min. The polymerization was then started at 70 °C under green light irradiation (515 nm) of 1.13 mW cm⁻² (a photograph of the experimental setup can be found in the supporting information in Section 7.2). The polymerization was stopped after removing the light source and cooling in an ice bath. Drops of the solution were taken and diluted with $CDCl_3$ to determine the conversion through ¹H-NMR spectroscopy. The result was about 53%. PMMA was then purified through precipitation in excess *n*-hexane three times. The yellow powder was then dried under vacuum at 40 °C for 24 h.

Polymerization of PMMA-*b*-POEGMA

PMMA and OEGMA ($[OEGMA]/[PMMA] = 200/1$) were dissolved in DOX in a glass vial. The solid concentration (PMMA plus OEGMA) of the reaction mixture was reduced to 15% (w/w) to lower the viscosity. A small amount of DMF was added as an internal standard for determining the conversion. The solution was degassed with nitrogen for 15 min and then put into an oil bath at 70 °C under green light irradiation (515 nm) of 1.13 mW cm⁻². The polymerization was stopped after removing the light source and cooling in an ice bath. Drops of the solution were taken and diluted with $CDCl_3$ to determine the conversion through ¹H-NMR

spectroscopy. The result was around 50%. The diblock copolymer was then purified through precipitation in excess *n*-hexane three times. The sticky product was then dried under vacuum at 40 °C for 24 h.

Analytcs

UV–vis. The UV–vis spectra were recorded with spectrophotometer UV5 from METTLER TOLEDO at ambient temperature.

NMR spectroscopy. ¹H-NMR spectra were recorded with BRUKER AVANCE II 400 MHz at ambient temperature.

SEC. For all polymers studied in this section, THF was used as the eluent. The instrument setup of the AGILENT 1260 INFINITY system is described in Publication 2 in Chapter 3. All the data were calibrated with narrowly distributed PMMA standards.

Visual turbidimetry. The PMMA-*b*-POEGMA sample was dissolved in Milli-Q® water overnight (*c* = 1% [w/w]). The transparent solution was heated in a water bath and cooled at room temperature.

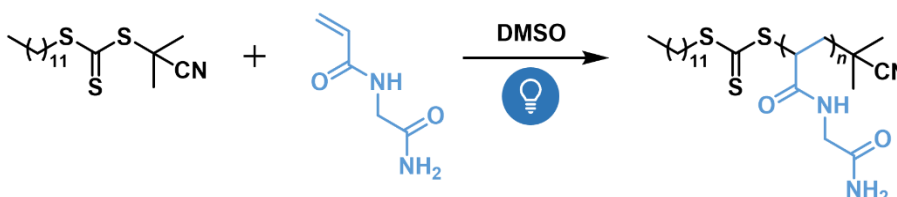
DLS. The measurements were performed by using an ALV/CGS-3 Compact Goniometer-System mentioned in Publication 2 in Chapter 3. The solution was heated and cooled with a temperature step of 1 °C. Three measurements were conducted at every temperature. The data were evaluated using a program written by Felix Lauterbach based on a cumulant approach.^[193]

4.2 Solution Behavior of PNAGA

As mentioned in Section 1.1.3, PNAGA is well-known for its hydrogen bonding-based UCST behavior in pure water. Compared with PMAAm investigated in Publication 1 in Chapter 3, PNAGA has the advantage of being soluble in the organic solvent dimethyl sulfoxide (DMSO).^[194] Hence, the study on PNAGA was conducted and presented in this section, although the synthesis of NAGA was time-consuming.

4.2.1 Synthesis of PNAGA

The PNAGA investigated in this work was prepared by photoiniferter RAFT polymerization in DMSO with 2-cyano-2-propyl dodecyl trithiocarbonate (CPDTC) as the CTA. As already demonstrated in the literature, blue light irradiation should be more suitable for polymerizing acrylates and acrylamides.^[69] Thus, blue LEDs were used as the light source (**Scheme 4.1**). The polymerization was stopped when the monomer conversion reached 60%. The experimental details can be found in Section 4.2.3.



Scheme 4.1. Photoiniferter RAFT polymerization of NAGA in DMSO under blue light irradiation.

After polymerization, PNAGA with a DP of 95 was obtained. The SEC measurements are often very challenging for UCST polymers due to their limited solubility in common solvents. Fortunately, as PNAGA is soluble in DMSO, the molecular weight distribution of the synthesized sample can be analyzed by SEC with DMSO as the mobile phase. The result is shown in **Figure 4.6**. The \bar{D} smaller than 1.30 implies that the polymerization was well controlled.

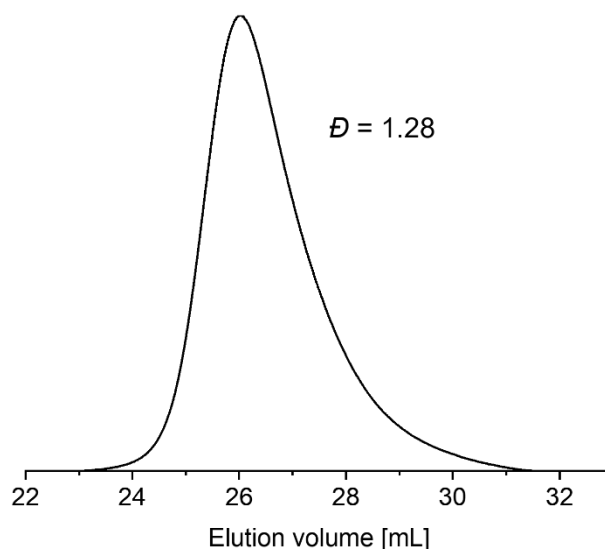


Figure 4.6. SEC trace of PNAGA ($\bar{M}_{n,SEC} = 22.0$ kDa, $\bar{D} = 1.28$) measured with DMSO as the mobile phase.

4.2.2 PNAGA Aqueous Solutions

The well-defined PNAGA was then dispersed in water ($c = 1\%$ [w/w]) to examine its solubility. The sample was stirred at $70\text{ }^{\circ}\text{C}$ for one hour in order to homogenize the mixture. After cooling to room temperature, a turbid solution could be obtained, indicating that PNAGA was insoluble in water at room temperature (**Figure 4.7a**). The solution was then heated to $70\text{ }^{\circ}\text{C}$ again and can be observed to become less turbid. However, it was still whitish, suggesting that the polymer was not completely dissolved even at a high temperature and a clean UCST transition was absent. This result is a bit surprising, as the PNAGA with a DP of approximately 200 was reported to have a UCST-type T_{CP} of around $20\text{ }^{\circ}\text{C}$.^[195] The T_{CP} of PNAGA was also found to be DP-dependent. A lower DP usually means a lower T_{CP} .^[196] Given that the DP of the PNAGA presented herein is 95, the sample was expected to have a UCST-type T_{CP} lower than $20\text{ }^{\circ}\text{C}$. A possible reason for the unanticipated insolubility even at $70\text{ }^{\circ}\text{C}$ could be the dodecyl group at the ω -terminal. The hydrophobic end-group could lead to the formation of aggregates and hamper the UCST transition. However, as shown in Section 4.1.3, a transparent solution ($c = 1\%$ [w/w]) can still be obtained even with a short hydrophobic block. The turbid solution shown in **Figure 4.7a** at $70\text{ }^{\circ}\text{C}$ suggests the worse solubility of PNAGA block in comparison with the POEGMA block.

Although no UCST transition was visually observed, the PNAGA solution still exhibited turbidity variation during heating. The chains should be more hydrophilic at high temperatures since the solution became less turbid. In order to get more insights into the solution behavior, a DLS measurement was conducted. The aqueous solution was diluted to 0.1% (w/w) before the measurement. The results during the cooling and heating processes are shown in **Figure 4.7b**. At 20 °C, the measured R_H was about 48 nm. The relatively large size of the particles implies that PNAGA was insoluble, which is in accordance with the visual observation. Interestingly, the R_H was even larger at 60 °C, i.e., when PNAGA was supposed to become more hydrophilic. Moreover, the variation in R_H during cooling and heating was reversible and occurred gradually.

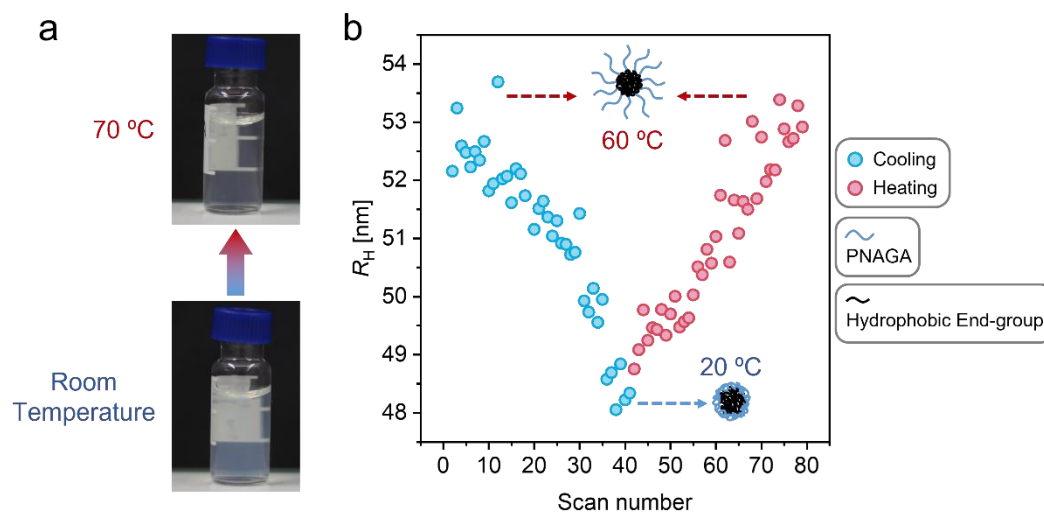


Figure 4.7. (a) Visual turbidimetry for a PNAGA aqueous solution ($c = 1\%$ [w/w]); (b) evolution of R_H of PNAGA in a dilute aqueous solution ($c = 0.1\%$ [w/w]) recorded by DLS during heating and cooling. The solution was gradually cooled from 60 °C to 20 °C and then heated to 60 °C again.

According to these results, it can be imagined that the particles might exist as isolated micelles with PNAGA shells and cores formed by hydrophobic dodecyl end-groups in this dilute solution. At high temperatures, PNAGA shells were more hydrophilic and thus stretched to a greater degree. As temperature decreased, the shells turned less hydrophilic and collapsed. However, as reflected by the decline of R_H , no agglomeration of the micelles occurred in association with the dehydration of the shells. A similar solution behavior was reported in a previous

study concerning a diblock copolymer of PAPy and PS in the literature.^[74] This unusual behavior can be mainly attributed to the high glass transition temperature (T_g) and relatively short chain length of the shell-forming block. Like PAPy, PNAGA has a high T_g (around 186 °C),^[45] reflecting its low chain mobility. With the relatively low DP, entanglements of the shells were not favored, preventing the formation of the aggregates. The gradual R_H transition is also related to the densely packed micellar structure. Due to the confined free volume in the shells, water molecules cannot be absorbed or expelled by PNAGA freely.^[74] A thermosensitive instead of a thermoresponsive behavior is thus observed in **Figure 4.7**.

4.2.3 Experimental Section

Materials

CPDTC (abcr, 97%), NAGA was synthesized according to the literature,^[17] deuterium oxide (D_2O , Sigma Aldrich, 100%). All the other solvents were used as received.

Polymerization of NAGA

CPDTC and NAGA ([NAGA]/[CPDTC] = 150/1) were dissolved in DMSO in a glass vial. The solid concentration (CPDTC plus NAGA) of the reaction mixture was 25% (w/w). A small amount of DMF was added as an internal standard for determining the conversion. The solution was degassed with nitrogen for 15 min. The polymerization was then started at 70 °C under blue light irradiation (467 nm) of 3.86 mW cm⁻² (a photograph of the experimental setup can be found in the supporting information in Section 7.3). The polymerization was stopped after removing the light source and cooling in an ice bath. Drops of the solution were taken and diluted with D_2O to determine the conversion through ¹H-NMR spectroscopy. The result was about 63%. PNAGA was then purified through precipitation in excess methanol. The yellow powder was then dried under vacuum at 40 °C for 24 h.

Analytics

SEC. 2 mg PNAGA were dissolved in 1 mL eluent (DMSO with 0.1 M LiCl) at 70 °C before the measurement. The measurement was conducted with PSS GRAM

columns at 70 °C. The flow rate of the eluent was 0.8 mL min⁻¹. The system was equipped with a refractive index (RI) detector. The data were calibrated with narrowly distributed PMMA standards.

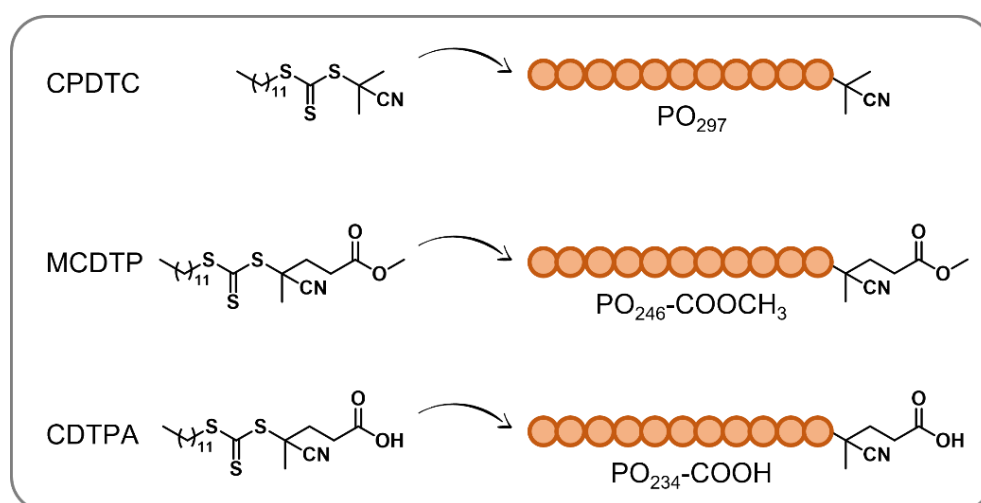
Visual turbidimetry. PNAGA was dispersed in Milli-Q® water ($c = 1\%$ [w/w]) and vigorously stirred overnight at room temperature. The mixture was then heated to 70 °C and stirred for another hour. Afterward, the solution was cooled to room temperature. In order to observe the turbidity variation, the solution was heated to 70 °C again.

DLS. The measurements were performed by using an ALV/CGS-3 Compact Goniometer-System mentioned in Publication 2 in Chapter 3. The solution was heated or cooled with a temperature step of 2 °C. Two measurements were conducted at every temperature. The data were evaluated using a program written by Felix Lauterbach based on a cumulant approach.^[193]

4.3 Influence of the End-group: Further Investigations

4.3.1 POEGMAs with Different Chain Ends

Publication 2 in Chapter 3 compares the LCST-type thermoresponsive behaviors of polymers with and without a carboxyl end-group. Besides CPDTC and CDTPA, another CTA, methyl 4-cyano-4-(dodecylthiocarbonothioylthio)pentanoate (MCDTP), joined the comparison in this section (**Scheme 4.2**). Homopolymers POEGMAs (PO_{297} , PO_{246} -COOCH₃, and PO_{234} -COOH) were synthesized with these three CTAs under green light irradiation. The subscripts in the sample names denote the DP calculated from conversion. Different from CDTPA, MCDTP brought an ester group with a short alkyl group to the α -terminal of the polymer. Due to the lack of a hydrogen donor and the dissociation ability in water, ester groups are less hydrophilic than carboxyl groups, which may make a significant difference in the chains' thermoresponsive behavior.



Scheme 4.2. Homo-POEGMAs synthesized with different CTAs. The polymers have similar DP but different end-groups at the α -terminal.

The obtained POEGMAs were first characterized by SEC measurements. As reflected by the results in **Figure 4.8**, the $\bar{M}_{n,SEC}$ of PO_{246} -COOCH₃ and PO_{234} -COOH are comparable, while the $\bar{M}_{n,SEC}$ of PO_{297} is slightly higher. The molecular weight distributions of the three samples are all relatively narrow ($D \leq 1.40$), suggesting successful photoiniferter RAFT polymerization.

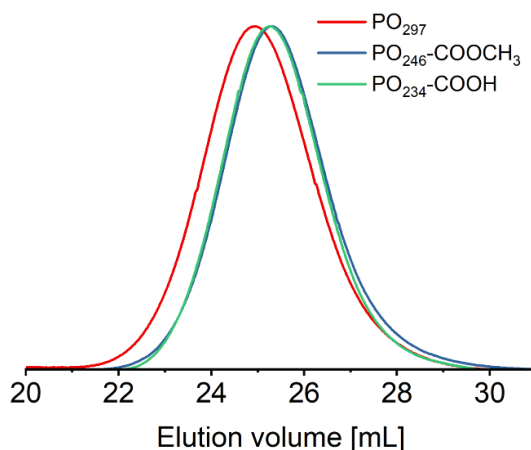


Figure 4.8. SEC traces measured for PO₂₉₇ ($\bar{M}_{n,SEC} = 40.9$ kDa, $\mathcal{D} = 1.40$), PO₂₄₆-COOCH₃ ($\bar{M}_{n,SEC} = 33.8$ kDa, $\mathcal{D} = 1.39$), and PO₂₃₄-COOH ($\bar{M}_{n,SEC} = 38.8$ kDa, $\mathcal{D} = 1.30$).

The well-defined POEGMAs were then dissolved in pure water for temperature-dependent DLS measurements. The solutions were heated with a temperature step of 1 °C. According to the results in **Figure 4.9**, all three polymers exhibited a rapid increase in R_H during heating, corresponding to the LCST transitions. The T_{CP} of PO₂₉₇ in the solution was around 62 °C, while the T_{CP} s of PO₂₄₆-COOCH₃ and PO₂₃₄-COOH were around 64 °C. The slightly lower T_{CP} of PO₂₉₇ could be attributed to its longer chain length. Thus, the T_{CP} was hardly affected by the nature of the end-group, which agrees well with the observation in Publication 2.

When it comes to the size of polymer aggregates formed above T_{CP} , the influence of the hydrophilic carboxyl group cannot be ignored. The massive difference between the DLS curves of PO₂₉₇ and PO₂₃₄-COOH is anticipated and agrees well with the phenomenon described in Publication 2 (**Figure 4.9a** and **Figure 4.9c**). The underlying mechanism is proposed in that publication. Interestingly, by simply replacing the carboxyl group with an ester group, the DLS result of the polymer became similar to that of PO₂₉₇. As shown in **Figure 4.9b**, the R_H of PO₂₄₆-COOCH₃ stayed relatively constant above T_{CP} and was significantly larger than that of the aggregates formed by PO₂₃₄-COOH. No contraction of the particles occurred. This result indicates that the ester group is not hydrophilic enough to hinder the aggregation. However, the R_H of PO₂₄₆-COOCH₃ (about 660 nm) is still smaller than that of PO₂₉₇ (about 880 nm) above T_{CP} , which could again be ascribed to the different chain lengths.

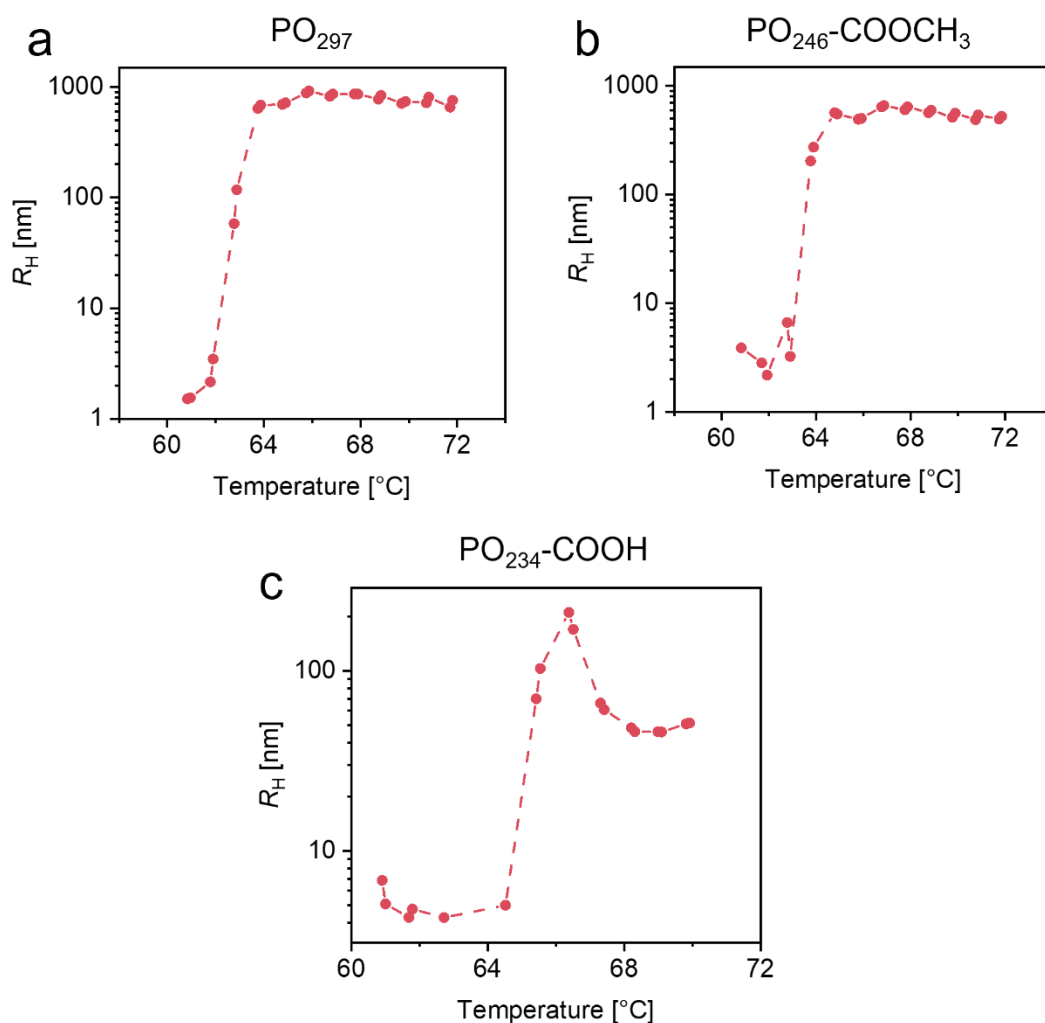


Figure 4.9. Evolution of R_H of (a) PO_{297} , (b) $\text{PO}_{246}\text{-COOCH}_3$, and (c) $\text{PO}_{234}\text{-COOH}$ in aqueous solutions ($c = 0.1\%$ [w/w]) recorded by DLS during heating.

These DLS results also suggest that although the DLS results of the polymers obtained from CPDTC and MCDTP are similar, CPDTC should still be a better choice if a hydrophobic end-group is required because the ester group from MCDTP can undergo hydrolysis in water, especially at high temperatures. The generated carboxyl group from hydrolysis may cause an immense change in the sample's thermoresponsive behavior, as indicated by **Figure 4.9**. Such a problem can be avoided by using CPDTC as the CTA.

4.3.2 Experimental Section

Materials

CPDTC (abcr, 97%), MCDTP (abcr, 90%), CDTPA (abcr, 97%). OEGMA (Sigma Aldrich, $\bar{M}_n = 300$ Da) was passed through activated basic alumina prior to the polymerizations.

Polymerization of OEGMA

In a typical photoiniferter RAFT polymerization of OEGMA, OEGMA and CTA were ($[\text{OEGMA}]/[\text{CTA}] = 390/1$) were dissolved in DOX in a glass vial. The solid concentration (CTA plus OEGMA) of the reaction mixture was 15% (w/w). A small amount of DMF was added as an internal standard for determining the conversion. The solution was degassed with nitrogen for 15 min and then put into an oil bath at 70 °C under green light irradiation (515 nm) of 1.13 mW cm⁻². The polymerization was stopped after removing the light source and cooling in an ice bath. The polymer was then purified through precipitation in excess *n*-hexane three times. The product was dried under vacuum at 40 °C for 24 h.

Analytcs

SEC. For all polymers studied in this section, THF was used as the eluent. The instrument setup of the AGILENT 1260 INFINITY system is described in Publication 2 in Chapter 3. All the data were calibrated with narrowly distributed PMMA standards.

DLS. The measurements were performed by using an ALV/CGS-3 Compact Goniometer-System mentioned in Publication 2 in Chapter 3. The solution was heated or cooled with a temperature step of 1 °C. Two measurements were conducted at every temperature. The data were evaluated using a program written by Felix Lauterbach based on a cumulant approach.^[193]

Chapter 5

Discussion

This chapter summarizes the findings in the last two chapters. In general, this work involved two polymer chain architectures, linear block copolymers and graft copolymers. The compositions of the copolymers were carefully selected, leading to the observation of UCST–LCST and LCST–LCST transitions in aqueous solutions. In addition, an efficient route to multifunctional hydrogels was developed with the thermoresponsive graft copolymers as precursors. The crucial features of the investigated polymers will be reviewed in Section 5.1. The chapter also includes a section (Section 5.2) discussing possible projects for future study.

5.1 Review of the Investigated Polymers

In Publication 1, nonionic diblock copolymers exhibiting both UCST and LCST transitions in pure water were successfully synthesized through green-light-induced photoiniferter RAFT polymerization. The results in Section 4.1.1 served as a guideline for selecting reaction conditions. The LCST block is the random copolymer of MEO₂MA and OEGMA (P[MEO₂MA-*r*-OEGMA]) obtained through simultaneous copolymerization. Its LCST-type T_{CP} can easily be tuned by varying the comonomer ratio. The UCST block was synthesized through chain extension in water with a commercially available nonionic monomer MAAm. The kinetics study implies that the polymerizations were well controlled. As their LCST-type T_{CPS} are higher than the UCST-type T_{CPS} , the diblock copolymer samples can be dissolved in dilute aqueous solutions between two T_{CPS} . Below UCST-type and above LCST-type T_{CPS} , polymeric aggregates with reversed core-shell structures can be formed in the solutions.

Publication 2 and 3 reported LCST–LCST graft copolymers. The backbones and side chains of the copolymers were synthesized successively through photoiniferter RAFT, with the switch of light wavelengths. The kinetics study and SEC measurements helped verify the effectiveness of this convenient approach. The wide choice of commercially available LCST monomers offered much freedom for the design of backbones and side chains. Consequently, the double thermoresponsiveness of the graft copolymers with different compositions could be deeply investigated in these two publications.

Copolymer POEGMA-*g*-PNIPAM is presented in Publication 2. The PNIPAM side chains aggregated first during heating in polymer aqueous solutions due to the lower T_{CP} , leading to the formation of flower-like micelles. However, the aggregation number of the micelles was limited because of the intrachain interaction of the branched structure. The POEGMA backbones were responsible for the second T_{CP} . Moreover, according to the results shown in Publication 2 and Section 4.3, it can be concluded that hydrophilic carboxyl groups brought by the CTA can hinder the LCST-induced aggregation of the synthesized linear and graft polymers immensely. Hence, the role of the end-group should not be ignored when it comes to the selection of CTAs for synthesizing LCST polymers.

The thermoresponsive behavior of the graft copolymer, PMEO₂MA-*g*-PDMA, shown in Publication 3 was totally different from that of POEGMA-*g*-PNIPAM. Although homo-PDMA is excellently water-soluble and not thermoresponsive at normal pressure, the graft copolymer aqueous solution exhibited surprisingly two separated T_{CP} s. The PMEO₂MA backbone aggregated first during heating, forming hydrophobic cores. The PDMA side chains could stabilize the formed particles in a specific temperature range, i.e., before the second T_{CP} . With the continuous contraction of the PMEO₂MA cores above the first T_{CP} , the balance between hydrophobic and hydrophilic interactions was disrupted at the second T_{CP} . A schematic comparison between the self-assembly behaviors of POEGMA-*g*-PNIPAM and PMEO₂MA-*g*-PDMA is provided in Publication 3.

The purpose of using the photoiniferter RAFT approach introduced in Publication 2 and 3 is not only to fabricate intriguing double thermoresponsive polymer chains but also to offer suitable precursors for multifunctional hydrogels. The merit of the TTC-groups randomly distributed along the graft copolymer chains was adequately extracted in this work. Through aminolysis in the presence of DTP, the TTC-groups can easily be converted into PDS-groups, enabling

efficient crosslinking with thiol-based crosslinkers under mild conditions. The yielded hydrogel was thoroughly analyzed in Publication 3. At room temperature, it can absorb a considerable amount of water. As it is based on a thermoresponsive graft copolymer, the hydrogel can expel the absorbed water in a specific temperature range. Moreover, the hydrogel's redox-sensitive degradability originating from the disulfide linkages was tested in that publication. The result fits superbly with the expectation.

5.2 Outlook

The PMAAm block in Publication 1 was successfully synthesized in homogeneous aqueous solutions between the UCST- and LCST-type T_{CP} s. However, the synthetic method still has room for improvement. This procedure needs the prediction of the UCST-type T_{CP} at first. Second, the LCST-type T_{CP} should be high enough to provide a sufficiently wide region between two T_{CP} s to ease the control of the polymerization temperature. Third, as the T_{CP} s depend on concentration and chain length, it is important to control the reaction time and solution concentration. With a high concentration, the UCST-type T_{CP} could be higher than the reaction temperature, leading to the formation of aggregates or even precipitation. With a low concentration, however, the polymerization will be prolonged. Due to these limitations, it would be interesting to find a suitable condition for the heterogeneous RAFT polymerization of the PMAAm block. Considering that the MAAm monomer is excellently water-soluble and PMAAm is water-insoluble below T_{CP} , it might be possible to perform chain extension via photoiniferter PISA in dispersion with the POEGMA block as a stabilizer. Since the photoiniferter approach does not involve a thermal initiator, the reaction temperature can theoretically be flexibly chosen, provided that it is below the UCST-type T_{CP} . Although the low temperature can reduce the propagation rate, the acceleration effect offered by PISA processes may be able to make up for this sacrifice.

Regardless of the synthetic approach, the UCST-LCST behavior of POEGMA-*b*-PMAAm shown in Publication 1 is quite inspiring. Schizophrenic triblock polymers can be looked forward to based on those promising results of diblock copolymers. It might be possible to synthesize a symmetric triblock polymer

consisting of POEGMA and PMAAm with a symmetric CTA like DiCTA used in Publication 3. The thermoresponsive behavior of the triblock copolymer in concentrated solutions, for instance, reversible sol-gel transition, could then be explored.

The synthetic strategy presented in Publication 2 and 3 for graft copolymers and networks may be valuable for further study. For example, it can help design a well-defined graft copolymer combining UCST and LCST. The monomer, NAGA, shown in Section 4.2 might be a proper choice. Besides thermoresponsive polymers, polymers exhibiting other stimuli-responsiveness like pH-responsiveness can also be considered for backbones or side chains. Regarding the chains' self-assembling behaviors, this thesis focuses on dilute aqueous solutions. The properties of their concentrated aqueous solutions could also be an exciting topic for future work. With a suitable concentration, a sol-gel transition may be observed when side chains become hydrophobic. Rheological measurements can be recommended when dealing with concentrated solutions. In addition, TTC-groups are eligible anchoring groups for gold surfaces.^[197, 198] It may be possible to use the graft copolymer with multiple TTC-groups to functionalize gold nanoparticles directly.

In Publication 2 and 3, the degradability of the network resulting from the disulfide bonds is demonstrated. In the research of other groups, disulfide links have also been reported to impart self-healing functionality to networks.^[199-203] This potential advantage may be worth exploring in future work and make the presented crosslinking strategy more appealing. Although this thesis only discusses hydrogels, lipophilic networks can also benefit from this facile crosslinking strategy.

In conclusion, the work presented in this thesis still has a high "livingness". Many exciting topics in different directions may be extended from this work's outcomes. Hopefully, the proposed route to stimuli-responsive polymers and hydrogels can inspire polymer chemists to develop more application-oriented "smart" materials.

Chapter 6

References

- [1] J. S. Scarpa, D. D. Mueller, I. M. Klotz, *J. Am. Chem. Soc.* **1967**, *89*, 6024.
- [2] Y. Cao, C. Zhang, W. Shen, Z. Cheng, L. Yu, Q. Ping, *J. Control. Release* **2007**, *120*, 186.
- [3] X. An, A. Zhu, H. Luo, H. Ke, H. Chen, Y. Zhao, *ACS Nano* **2016**, *10*, 5947.
- [4] F. Doberenz, K. Zeng, C. Willems, K. Zhang, T. Groth, *J. Mater. Chem. B.* **2020**, *8*, 607.
- [5] S. Ohya, Y. Nakayama, T. Matsuda, *J Artif Organs* **2004**, *7*, 181.
- [6] M. Yang, Y. Ding, L. Zhang, X. Qian, X. Jiang, B. Liu, *J. Biomed. Mater. Res.* **2007**, *81*, 847.
- [7] G.-F. Luo, W.-H. Chen, X.-Z. Zhang, *ACS Macro Lett.* **2020**, *9*, 872.
- [8] W. Sun, P. Wu, *Phys. Chem. Chem. Phys.* **2018**, *20*, 20849.
- [9] A. Bordat, T. Boissenot, J. Nicolas, N. Tsapis, *Adv. Drug Deliv. Rev.* **2019**, *138*, 167.
- [10] C. Zhao, Z. Ma, X. X. Zhu, *Prog. Polym. Sci.* **2019**, *90*, 269.
- [11] R. Liu, M. Fraylich, B. R. Saunders, *Colloid. Polym. Sci.* **2009**, *287*, 627.
- [12] T. Yamano, N. Higashi, T. Koga, *Macromol. Rapid Commun.* **2020**, *41*, 1900550.
- [13] Q. Li, A. P. Constantinou, T. K. Georgiou, *J Polym Sci.* **2020**, *59*, 230.
- [14] J. F. Lutz, *J. Polym. Sci., Part A: Polym. Chem.* **2008**, *46*, 3459.
- [15] C. R. Becer, S. Hahn, M. W. M. Fijten, H. M. L. Thijs, R. Hoogenboom, U. S. Schubert, *J. Polym. Sci., Part A: Polym. Chem.* **2008**, *46*, 7138.
- [16] G. Vancoillie, D. Frank, R. Hoogenboom, *Prog. Polym. Sci.* **2014**, *39*, 1074.
- [17] J. Seuring, F. M. Bayer, K. Huber, S. Agarwal, *Macromolecules* **2011**, *45*, 374.
- [18] Z. Xu, W. Liu, *Chem. Commun.* **2018**, *54*, 10540.
- [19] Z. Zhang, H. Li, S. Kasmi, S. Van Herck, K. Deswarte, B. N. Lambrecht, R. Hoogenboom, L. Nuhn, B. G. De Geest, *Angew. Chem. Int. Ed.* **2019**, *58*, 7866.
- [20] J. Seuring, S. Agarwal, *Macromol. Rapid Commun.* **2012**, *33*, 1898.

- [21] R. J. Young, P. A. Lovell, "Introduction to Polymers", 3rd edition, CRC Press, Boca Raton, **2011**, p. 310.
- [22] Q. Zhang, C. Weber, U. S. Schubert, R. Hoogenboom, *Mater. Horiz.* **2017**, *4*, 109.
- [23] C. Boutris, E. G. Chatzi, C. Kiparissides, *Polymer* **1997**, *38*, 2567.
- [24] K. Van Durme, G. Van Assche, B. Van Mele, *Macromolecules* **2004**, *37*, 9596.
- [25] B. A. Pineda-Contreras, F. Liu, S. Agarwal, *J. Polym. Sci., Part A: Polym. Chem.* **2014**, *52*, 1878.
- [26] A. Halperin, M. Kroger, F. M. Winnik, *Angew. Chem. Int. Ed.* **2015**, *54*, 15342.
- [27] A. J. Staverman, J. H. van Santen, *Recl. Trav. Chim. Pays-Bas* **1941**, *60*, 76.
- [28] A. J. Staverman, *Recl. Trav. Chim. Pays-Bas* **1941**, *60*, 640.
- [29] M. L. Huggins, *J. Chem. Phys.* **1941**, *9*, 440.
- [30] M. L. Huggins, *Ann. N.Y. Acad. Sci.* **1942**, *43*, 1.
- [31] P. J. Flory, *J. Chem. Phys.* **1941**, *9*, 660.
- [32] P. J. Flory, *J. Chem. Phys.* **1942**, *10*, 51.
- [33] P. C. Hiemenz, T. P. Lodge, "Polymer Chemistry", 2nd edition, CRC Press, Boca Raton, **2007**, p. 279.
- [34] M. Bercea, M. Cazacu, B. A. Wolf, *Macromol. Chem. Phys.* **2003**, *204*, 1371.
- [35] B. A. Wolf, *Macromol. Chem. Phys.* **2003**, *204*, 1381.
- [36] S. Stryuk, B. A. Wolf, *Macromol. Chem. Phys.* **2003**, *204*, 1948.
- [37] Y. Maeda, T. Higuchi, I. Ikeda, *Langmuir* **2000**, *16*, 7503.
- [38] I. Ortiz de Solorzano, K. K. Bejagam, Y. An, S. K. Singh, S. A. Deshmukh, *Soft Matter* **2020**, *16*, 1582.
- [39] L. Tavagnacco, E. Zaccarelli, E. Chiessi, *Phys. Chem. Chem. Phys.* **2018**, *20*, 9997.
- [40] S. A. Deshmukh, S. K. Sankaranarayanan, K. Suthar, D. C. Mancini, *J. Phys. Chem. B* **2012**, *116*, 2651.
- [41] A. B. Lowe, C. L. McCormick, *Chem. Rev.* **2002**, *102*, 4177.
- [42] Y.-J. Shih, Y. Chang, *Langmuir* **2010**, *26*, 17286.
- [43] P. Mary, D. D. Bendejacq, M.-P. Labeau, P. Dupuis, *J. Phys. Chem. B* **2007**, *111*, 7767.
- [44] J. Seuring, S. Agarwal, *Macromol. Chem. Phys.* **2010**, *211*, 2109.
- [45] J. Seuring, S. Agarwal, *Macromolecules* **2012**, *45*, 3910.
- [46] D. H. Solomon, E. Rizzardo, P. Cacioli, "Polymerization process and polymers produced thereby", **1986**, US4581429A.
- [47] M. K. Georges, R. P. N. Veregin, P. M. Kazmaier, G. K. Hamer, *Macromolecules* **1993**, *26*, 2987.
- [48] G. Moad, E. Rizzardo, *Macromolecules* **1995**, *28*, 8722.

- [49] B. B. Wayland, G. Poszmik, S. L. Mukerjee, M. Fryd, *J. Am. Chem. Soc.* **1994**, *116*, 7943.
- [50] M. Kato, M. Kamigaito, M. Sawamoto, T. Higashimura, *Macromolecules* **1995**, *28*, 1721.
- [51] J.-S. Wang, K. Matyjaszewski, *J. Am. Chem. Soc.* **1995**, *117*, 5614.
- [52] J. Chiefari, Y. K. Chong, F. Ercole, J. Krstina, J. Jeffery, T. P. T. Le, R. T. A. Mayadunne, G. F. Meijs, C. L. Moad, G. Moad, E. Rizzardo, S. H. Thang, *Macromolecules* **1998**, *31*, 5559.
- [53] M. Semsarilar, V. Abetz, *Macromol. Chem. Phys.* **2021**, *222*, 2000311.
- [54] G. Moad, E. Rizzardo, S. H. Thang, *Aust. J. Chem.* **2006**, *59*, 669.
- [55] G. Moad, E. Rizzardo, S. H. Thang, *Aust. J. Chem.* **2005**, *58*, 379.
- [56] G. Moad, E. Rizzardo, S. H. Thang, *Aust. J. Chem.* **2009**, *62*, 1402.
- [57] G. Moad, E. Rizzardo, S. H. Thang, *Aust. J. Chem.* **2012**, *65*, 985.
- [58] M. Benaglia, J. Chiefari, Y. K. Chong, G. Moad, E. Rizzardo, S. H. Thang, *J. Am. Chem. Soc.* **2009**, *131*, 6914.
- [59] J. Gardiner, I. Martinez-Botella, J. Tsanaksidis, G. Moad, *Polym. Chem.* **2016**, *7*, 481.
- [60] M. Hendrich, P. Vana, *Macromol. Mater. Eng.* **2017**, *302*, 1700018.
- [61] S. Perrier, *Macromolecules* **2017**, *50*, 7433.
- [62] J. Xu, S. Shanmugam, N. A. Corrigan, C. Boyer, "Catalyst-Free Visible Light-Induced RAFT Photopolymerization", in *Controlled Radical Polymerization: Mechanisms*, 2015, p. 247.
- [63] X. Tian, J. Ding, B. Zhang, F. Qiu, X. Zhuang, Y. Chen, *Polymers* **2018**, *10*, 318.
- [64] T. Otsu, *J. Polym. Sci., Part A: Polym. Chem.* **2000**, *38*, 2121.
- [65] J. D. Coyle, *Tetrahedron* **1985**, *41*, 5393.
- [66] L. Lu, H. Zhang, N. Yang, Y. Cai, *Macromolecules* **2006**, *39*, 3770.
- [67] T. G. McKenzie, Q. Fu, E. H. H. Wong, D. E. Dunstan, G. G. Qiao, *Macromolecules* **2015**, *48*, 3864.
- [68] S. Z. Zard, *Angew. Chem. Int. Ed. Engl.* **1997**, *36*, 672.
- [69] S. Shanmugam, J. Cuthbert, T. Kowalewski, C. Boyer, K. Matyjaszewski, *Macromolecules* **2018**, *51*, 7776.
- [70] J. Lalevée, N. Blanchard, M. El-Roz, X. Allonas, J. P. Fouassier, *Macromolecules* **2008**, *41*, 2347.
- [71] M. Y. Khan, M.-S. Cho, Y.-J. Kwark, *Macromolecules* **2014**, *47*, 1929.
- [72] H. Zhou, J. A. Johnson, *Angew. Chem. Int. Ed.* **2013**, *52*, 2235.
- [73] S. Muthukrishnan, E. H. Pan, M. H. Stenzel, C. Barner-Kowollik, T. P. Davis, D. Lewis, L. Barner, *Macromolecules* **2007**, *40*, 2978.
- [74] F. Lauterbach, V. Abetz, *Soft Matter* **2020**, *16*, 2321.
- [75] T. Eckert, V. Abetz, *J Polym Sci.* **2020**, *58*, 3050.

- [76] J. Li, C. Ding, Z. Zhang, X. Pan, N. Li, J. Zhu, X. Zhu, *Macromol. Rapid Commun.* **2017**, *38*, 1600482.
- [77] R. G. W. Norrish, E. F. Brookman, *Proc. R. Soc. Lond. A* **1939**, *171*, 147.
- [78] F. R. Mayo, F. M. Lewis, *J. Am. Chem. Soc.* **1944**, *66*, 1594.
- [79] H. De Brouwer, M. A. J. Schellekens, B. Klumperman, M. J. Monteiro, A. L. German, *J. Polym. Sci., Part A: Polym. Chem.* **2000**, *38*, 3596.
- [80] K. Matyjaszewski, M. J. Ziegler, S. V. Arehart, D. Greszta, T. Pakula, *J. Phys. Org. Chem.* **2000**, *13*, 775.
- [81] C. P. Easterling, Y. Xia, J. Zhao, G. E. Fanucci, B. S. Sumerlin, *ACS Macro Lett.* **2019**, *8*, 1461.
- [82] S. Eggers, V. Abetz, *Polymers* **2017**, *9*, 668.
- [83] J. Rieger, *Macromol. Rapid Commun.* **2015**, *36*, 1458.
- [84] X. Wang, Z. An, *Macromol. Rapid Commun.* **2019**, *40*, 1800325.
- [85] W. J. Zhang, C. Y. Hong, C. Y. Pan, *Macromol. Rapid Commun.* **2019**, *40*, 1800279.
- [86] F. D'Agosto, J. Rieger, M. Lansalot, *Angew. Chem. Int. Ed.* **2020**, *59*, 8368.
- [87] N. An, X. Chen, J. Yuan, *Polym. Chem.* **2021**, *12*, 3220.
- [88] M. R. Hill, R. N. Carmean, B. S. Sumerlin, *Macromolecules* **2015**, *48*, 5459.
- [89] S. Eggers, F. Lauterbach, V. Abetz, *Polymer* **2016**, *107*, 357.
- [90] X. Jiang, X. Jiang, G. Lu, C. Feng, X. Huang, *Polym. Chem.* **2014**, *5*, 4915.
- [91] P. Zhao, M. Deng, Y. Yang, J. Zhang, Y. Zhang, *Macromol. Rapid Commun.* **2021**, *42*, 2100424.
- [92] J. Xu, S. Shanmugam, C. Fu, K. F. Aguey-Zinsou, C. Boyer, *J. Am. Chem. Soc.* **2016**, *138*, 3094.
- [93] H. Shinoda, K. Matyjaszewski, *Macromol. Rapid Commun.* **2001**, *22*, 1176.
- [94] G. Li, H. Wang, H. Zheng, R. Bai, *J. Polym. Sci., Part A: Polym. Chem.* **2010**, *48*, 1348.
- [95] D. Mortisen, M. Peroglio, M. Alini, D. Eglin, *Biomacromolecules* **2010**, *11*, 1261.
- [96] C. Xiao, D. Lu, S. Xu, L. Huang, *Starch/Stärke* **2011**, *63*, 209.
- [97] F. Ullah, M. B. Othman, F. Javed, Z. Ahmad, H. Md. Akil, *Mater. Sci. Eng. C* **2015**, *57*, 414.
- [98] M. Shibata, T. Terashima, T. Koga, *Macromolecules* **2021**, *54*, 5241.
- [99] A. A. A. Smith, C. L. Maikawa, H. Lopez Hernandez, E. A. Appel, *Polym. Chem.* **2021**, *12*, 1918.
- [100] Z. Feng, H. Zuo, W. Gao, N. Ning, M. Tian, L. Zhang, *Macromol. Rapid Commun.* **2018**, *39*, 1800138.
- [101] M. Mohamadhoseini, Z. Mohamadnia, *Polym. Chem.* **2021**, *12*, 5679.
- [102] G. Zhang, L. Lv, Y. Deng, C. Wang, *Macromol. Rapid Commun.* **2017**, *38*, 1700018.

- [103] W. Fu, B. Zhao, *Polym. Chem.* **2016**, *7*, 6980.
- [104] Y. Huang, P. Yong, Y. Chen, Y. Gao, W. Xu, Y. Lv, L. Yang, R. L. Reis, R. P. Pirraco, J. Chen, *RSC Adv.* **2017**, *7*, 28711.
- [105] A. P. Constantinou, N. F. Sam-Soon, D. R. Carroll, T. K. Georgiou, *Macromolecules* **2018**, *51*, 7019.
- [106] A. P. Constantinou, K. Zhang, B. Somuncuoğlu, B. Feng, T. K. Georgiou, *Macromolecules* **2021**, *54*, 6511.
- [107] Y. Chen, Y. Gao, L. P. da Silva, R. P. Pirraco, M. Ma, L. Yang, R. L. Reis, J. Chen, *Polym. Chem.* **2018**, *9*, 4063.
- [108] V. Pertici, C. Pin-Barre, C. Rivera, C. Pellegrino, J. Laurin, D. Giges, T. Trimaille, *Biomacromolecules* **2019**, *20*, 149.
- [109] D. Cao, X. Zhang, M. D. Akabar, Y. Luo, H. Wu, X. Ke, T. Ci, *Artif. Cells Nanomed. Biotechnol.* **2019**, *47*, 181.
- [110] M. A. Ward, T. K. Georgiou, *J. Polym. Sci., Part A: Polym. Chem.* **2013**, *51*, 2850.
- [111] A. P. Constantinou, T. K. Georgiou, *Polym. Chem.* **2016**, *7*, 2045.
- [112] H. Jung, S.-E. Gang, J.-M. Kim, T.-Y. Heo, S. Lee, E. Shin, B.-S. Kim, S.-H. Choi, *Macromolecules* **2020**, *53*, 10339.
- [113] K. Wu, X. Chen, S. Gu, S. Cui, X. Yang, L. Yu, J. Ding, *Macromolecules* **2021**, *54*, 7421.
- [114] P. Biais, M. Engel, O. Colombani, T. Nicolai, F. Stoffelbach, J. Rieger, *Polym. Chem.* **2021**, *12*, 1040.
- [115] A. Vidyasagar, S. H. Ku, M. Kim, M. Kim, H. S. Lee, T. R. Pearce, A. V. McCormick, F. S. Bates, E. Kokkoli, *ACS Macro Lett.* **2017**, *6*, 1134.
- [116] B. D. Monnery, R. Hoogenboom, *Polym. Chem.* **2019**, *10*, 3480.
- [117] A. P. Constantinou, B. Zhan, T. K. Georgiou, *Macromolecules* **2021**, *54*, 1943.
- [118] G. Moad, E. Rizzardo, S. H. Thang, *Polym. Int.* **2011**, *60*, 9.
- [119] A. Postma, T. P. Davis, G. Moad, M. S. O'Shea, *Macromolecules* **2005**, *38*, 5371.
- [120] W. Sriprom, C. Neto, S. Perrier, *Soft Matter* **2010**, *6*, 909.
- [121] J. J. Lessard, L. F. Garcia, C. P. Easterling, M. B. Sims, K. C. Bentz, S. Arencibia, D. A. Savin, B. S. Sumerlin, *Macromolecules* **2019**, *52*, 2105.
- [122] Y. K. Chong, G. Moad, E. Rizzardo, S. H. Thang, *Macromolecules* **2007**, *40*, 4446.
- [123] M. Dietrich, M. Glassner, T. Gruending, C. Schmid, J. Falkenhagen, C. Barner-Kowollik, *Polym. Chem.* **2010**, *1*, 634.
- [124] A. Favier, B. Luneau, J. Vinas, N. Laissaoui, D. Giges, D. Bertin, *Macromolecules* **2009**, *42*, 5953.

- [125] A. J. Inglis, S. Sinnwell, T. P. Davis, C. Barner-Kowollik, M. H. Stenzel, *Macromolecules* **2008**, *41*, 4120.
- [126] R. T. A. Mayadunne, E. Rizzardo, J. Chiefari, J. Krstina, G. Moad, A. Postma, S. H. Thang, *Macromolecules* **2000**, *33*, 243.
- [127] P. J. Roth, C. Boyer, A. B. Lowe, T. P. Davis, *Macromol. Rapid Commun.* **2011**, *32*, 1123.
- [128] D. L. Patton, M. Mullings, T. Fulghum, R. C. Advincula, *Macromolecules* **2005**, *38*, 8597.
- [129] X.-P. Qiu, F. M. Winnik, *Macromolecules* **2007**, *40*, 872.
- [130] W. Shen, Q. Qiu, Y. Wang, M. Miao, B. Li, T. Zhang, A. Cao, Z. An, *Macromol. Rapid Commun.* **2010**, *31*, 1444.
- [131] X.-P. Qiu, F. M. Winnik, *Macromol. Rapid Commun.* **2006**, *27*, 1648.
- [132] B. Yu, J. W. Chan, C. E. Hoyle, A. B. Lowe, *J. Polym. Sci., Part A: Polym. Chem.* **2009**, *47*, 3544.
- [133] J. M. Spruell, B. A. Levy, A. Sutherland, W. R. Dichtel, J. Y. Cheng, J. F. Stoddart, A. Nelson, *J. Polym. Sci., Part A: Polym. Chem.* **2009**, *47*, 346.
- [134] J. W. Chan, B. Yu, C. E. Hoyle, A. B. Lowe, *Chem. Commun.* **2008**, 4959.
- [135] H. Willcock, R. K. O'Reilly, *Polym. Chem.* **2010**, *1*, 149.
- [136] P. J. Roth, D. Kessler, R. Zentel, P. Theato, *Macromolecules* **2008**, *41*, 8316.
- [137] J. Xu, L. Tao, C. Boyer, A. B. Lowe, T. P. Davis, *Macromolecules* **2010**, *43*, 20.
- [138] C. Boyer, V. Bulmus, T. P. Davis, *Macromol. Rapid Commun.* **2009**, *30*, 493.
- [139] V. H. Dao, N. R. Cameron, K. Saito, *Polym. Chem.* **2017**, *8*, 6834.
- [140] J. Su, *Gels* **2018**, *4*, 72.
- [141] P. Chakma, Z. A. Digby, J. Via, M. P. Shulman, J. L. Sparks, D. Konkolewicz, *Polym. Chem.* **2018**, *9*, 4744.
- [142] M. Arslan, R. Sanyal, A. Sanyal, *Polym. Chem.* **2020**, *11*, 1763.
- [143] H. W. Ooi, K. S. Jack, A. K. Whittaker, H. Peng, *J. Polym. Sci., Part A: Polym. Chem.* **2013**, *51*, 4626.
- [144] J.-F. Lutz, A. Hoth, *Macromolecules* **2006**, *39*, 893.
- [145] N. Audureau, C. Veith, F. Coumes, T. P. T. Nguyen, J. Rieger, F. Stoffelbach, *Macromol. Rapid Commun.* **2021**, *42*, 2100556.
- [146] J.-F. Lutz, O. Akdemir, A. Hoth, *J. Am. Chem. Soc.* **2006**, *128*, 13046.
- [147] N. Lucht, S. Eggers, V. Abetz, *Polym. Chem.* **2017**, *8*, 1196.
- [148] S. Eggers, T. Eckert, V. Abetz, *J. Polym. Sci., Part A: Polym. Chem.* **2018**, *56*, 399.
- [149] Y. Kotsuchibashi, M. Ebara, T. Aoyagi, R. Narain, *Polymers* **2016**, *8*, 380.
- [150] C. Pietsch, U. Mansfeld, C. Guerrero-Sanchez, S. Hoeppeener, A. Vollrath, M. Wagner, R. Hoogenboom, S. Saubern, S. H. Thang, C. R. Becer, J. Chiefari, U. S. Schubert, *Macromolecules* **2012**, *45*, 9292.

- [151] Q. Zhang, J.-D. Hong, R. Hoogenboom, *Polym. Chem.* **2013**, *4*, 4322.
- [152] Q. Li, C. Gao, S. Li, F. Huo, W. Zhang, *Polym. Chem.* **2014**, *5*, 2961.
- [153] F. D. Jochum, P. J. Roth, D. Kessler, P. Theato, *Biomacromolecules* **2010**, *11*, 2432.
- [154] H. Gehan, C. Mangeney, J. Aubard, G. Lévi, A. Hohenau, J. R. Krenn, E. Lacaze, N. Félidj, *J. Phys. Chem. Lett.* **2011**, *2*, 926.
- [155] M. Toma, U. Jonas, A. Mateescu, W. Knoll, J. Dostalek, *J. Phys. Chem. C* **2013**, *117*, 11705.
- [156] C. M. Papadakis, P. Müller-Buschbaum, A. Laschewsky, *Langmuir* **2019**, *35*, 9660.
- [157] N. S. Vishnevetskaya, V. Hildebrand, B.-J. Niebuur, I. Grillo, S. K. Filippov, A. Laschewsky, P. Müller-Buschbaum, C. M. Papadakis, *Macromolecules* **2016**, *49*, 6655.
- [158] N. S. Vishnevetskaya, V. Hildebrand, B.-J. Niebuur, I. Grillo, S. K. Filippov, A. Laschewsky, P. Müller-Buschbaum, C. M. Papadakis, *Macromolecules* **2017**, *50*, 3985.
- [159] N. S. Vishnevetskaya, V. Hildebrand, M. A. Dyakonova, B.-J. Niebuur, K. Kyriakos, K. N. Raftopoulos, Z. Di, P. Müller-Buschbaum, A. Laschewsky, C. M. Papadakis, *Macromolecules* **2018**, *51*, 2604.
- [160] N. S. Vishnevetskaya, V. Hildebrand, N. M. Nizardo, C. H. Ko, Z. Di, A. Radulescu, L. C. Barnsley, P. Müller-Buschbaum, A. Laschewsky, C. M. Papadakis, *Langmuir* **2019**, *35*, 6441.
- [161] T. Jiang, V. Aseyev, J. Niskanen, S. Hietala, Q. Zhang, H. Tenhu, *Macromolecules* **2020**, *53*, 8267.
- [162] H. Zhang, X. Tong, Y. Zhao, *Langmuir* **2014**, *30*, 11433.
- [163] F. Käfer, F. Liu, U. Stahlschmidt, V. Jérôme, R. Freitag, M. Karg, S. Agarwal, *Langmuir* **2015**, *31*, 8940.
- [164] C. Cummings, H. Murata, R. Koepsel, A. J. Russell, *Biomacromolecules* **2014**, *15*, 763.
- [165] Q. Zhao, W. Zou, Y. Luo, T. Xie, *Sci. Adv.* **2016**, *2*, e1501297.
- [166] X. Li, X. Cai, Y. Gao, M. J. Serpe, *J. Mater. Chem. B* **2017**, *5*, 2804.
- [167] Z. Hu, X. Zhang, Y. Li, *Science* **1995**, *269*, 525.
- [168] D. Kim, H. S. Lee, J. Yoon, *Sci. Rep.* **2016**, *6*, 20921.
- [169] J. Zheng, P. Xiao, X. Le, W. Lu, P. Théato, C. Ma, B. Du, J. Zhang, Y. Huang, T. Chen, *J. Mater. Chem. C* **2018**, *6*, 1320.
- [170] T.-a. Asoh, M. Matsusaki, T. Kaneko, M. Akashi, *Adv. Mater.* **2008**, *20*, 2080.
- [171] Y. Tan, D. Wang, H. Xu, Y. Yang, W. An, L. Yu, Z. Xiao, S. Xu, *Macromol. Rapid Commun.* **2018**, *39*, 1700863.
- [172] Y. Yang, Y. Tan, X. Wang, W. An, S. Xu, W. Liao, Y. Wang, *ACS Appl. Mater. Interfaces* **2018**, *10*, 7688.

- [173] D. Kim, E. Lee, H. S. Lee, J. Yoon, *Sci. Rep.* **2015**, *5*, 7646.
- [174] H. Y. Lee, Y. Cai, S. Bi, Y. N. Liang, Y. Song, X. M. Hu, *ACS Appl. Mater. Interfaces* **2017**, *9*, 6054.
- [175] M. Wu, Y. Shi, R. Li, P. Wang, *ACS Appl. Mater. Interfaces* **2018**, *10*, 39819.
- [176] J.-G. Park, W. Benjamin Rogers, S. Magkiriadou, T. Kodger, S.-H. Kim, Y.-S. Kim, V. N. Manoharan, *Opt. Mater. Express* **2017**, *7*, 253.
- [177] M. Chen, L. Zhou, Y. Guan, Y. Zhang, *Angew. Chem. Int. Ed.* **2013**, *52*, 9961.
- [178] L. Tang, L. Wang, X. Yang, Y. Feng, Y. Li, W. Feng, *Prog. Mater. Sci.* **2021**, *115*, 100702.
- [179] S. Wang, W. Gao, X. Y. Hu, Y. Z. Shen, L. Wang, *Chem. Commun.* **2019**, *55*, 4137.
- [180] P. Mostafalu, G. Kiaee, G. Giatsidis, A. Khalilpour, M. Nabavinia, M. R. Dokmeci, S. Sonkusale, D. P. Orgill, A. Tamayol, A. Khademhosseini, *Adv. Funct. Mater.* **2017**, *27*, 1702399.
- [181] M. Mackiewicz, J. Romanski, E. Drozd, B. Gruber-Bzura, P. Fiedor, Z. Stojek, M. Karbarz, *Int. J. Pharm.* **2017**, *523*, 336.
- [182] Y. Zhan, M. Gonçalves, P. Yi, D. Capelo, Y. Zhang, J. Rodrigues, C. Liu, H. Tomás, Y. Li, P. He, *J. Mater. Chem. B* **2015**, *3*, 4221.
- [183] Y. J. Kim, M. Ebara, T. Aoyagi, *Angew. Chem. Int. Ed.* **2012**, *51*, 10537.
- [184] T. Tang, V. Castelletto, P. Parras, I. W. Hamley, S. M. King, D. Roy, S. Perrier, R. Hoogenboom, U. S. Schubert, *Macromol. Chem. Phys.* **2006**, *207*, 1718.
- [185] C.-H. Ko, C. Henschel, G. P. Meledam, M. A. Schroer, P. Müller-Buschbaum, A. Laschewsky, C. M. Papadakis, *Macromolecules* **2021**, *54*, 384.
- [186] C.-H. Ko, C. Henschel, G. P. Meledam, M. A. Schroer, R. Guo, L. Gaetani, P. Müller-Buschbaum, A. Laschewsky, C. M. Papadakis, *Macromolecules* **2021**, *54*, 5825.
- [187] C. Geiger, J. Reitenbach, L. P. Kreuzer, T. Widmann, P. Wang, R. Cubitt, C. Henschel, A. Laschewsky, C. M. Papadakis, P. Müller-Buschbaum, *Macromolecules* **2021**, *54*, 3517.
- [188] B. Cabannes-Boué, Q. Yang, J. Lalevée, F. Morlet-Savary, J. Poly, *Polym. Chem.* **2017**, *8*, 1760.
- [189] D. J. Keddie, *Chem. Soc. Rev.* **2014**, *43*, 496.
- [190] S. Xu, F. J. Trujillo, J. Xu, C. Boyer, N. Corrigan, *Macromol. Rapid Commun.* **2021**, *42*, 2100212.
- [191] T. G. McKenzie, L. P. d. M. Costa, Q. Fu, D. E. Dunstan, G. G. Qiao, *Polym. Chem.* **2016**, *7*, 4246.
- [192] M. L. Allegranza, N. De Alwis Watuthanthrige, Y. Wang, G. A. Garcia, H. Ren, D. Konkolewicz, *Polym. Chem.* **2020**, *11*, 6129.

-
- [193] F. Lauterbach, PhD thesis, Universität Hamburg, **2020**.
- [194] J. Seuring, PhD Thesis, University of Marburg, **2012**.
- [195] W. Sun, Z. An, P. Wu, *Macromolecules* **2017**, *50*, 2175.
- [196] T. N. Tran, S. Piogé, L. Fontaine, S. Pascual, *Macromol. Rapid Commun.* **2020**, *41*, 2000203.
- [197] A.-S. Duwez, P. Guillet, C. Colard, J.-F. Gohy, C.-A. Fustin, *Macromolecules* **2006**, *39*, 2729.
- [198] C. Rossner, P. Vana, *Angew. Chem. Int. Ed.* **2014**, *53*, 12639.
- [199] J. Canadell, H. Goossens, B. Klumperman, *Macromolecules* **2011**, *44*, 2536.
- [200] M. Pepels, I. Filot, B. Klumperman, H. Goossens, *Polym. Chem.* **2013**, *4*, 4955.
- [201] S. Nevejans, N. Ballard, J. I. Miranda, B. Reck, J. M. Asua, *Phys. Chem. Chem. Phys.* **2016**, *18*, 27577.
- [202] S. Y. An, S. M. Noh, J. K. Oh, *Macromol. Rapid Commun.* **2017**, *38*, 1600777.
- [203] Y. Wang, Q. Chen, M. Chen, Y. Guan, Y. Zhang, *Polym. Chem.* **2019**, *10*, 4844.

Chapter 7

Appendix

7.1 Author Contributions to the Publications

1) Nonionic UCST-LCST Diblock Copolymers with Tunable Thermoresponsiveness Synthesized via PhotoRAFT Polymerization.

Jingcong Xu and Volker Abetz

Macromol. Rapid Commun. **2021**, *42*, 2000648.

DOI: 10.1002/marc.202000648

Jingcong Xu (J.X.): Conceptualization, Investigation, Validation, Visualization, Writing - original draft.

Volker Abetz (V.A.): Conceptualization, Supervision, Funding acquisition, Writing - review & editing.

2) Double thermoresponsive graft copolymers with different chain ends: feasible precursors for covalently crosslinked hydrogels.

Jingcong Xu and Volker Abetz

Soft Matter **2022**, *18*, 2082–2091.

DOI: 10.1039/d1sm01692j

J.X.: Conceptualization, Investigation, Validation, Visualization, Writing - original draft.

V.A.: Conceptualization, Supervision, Funding acquisition, Writing - review & editing.

3) Synthesis of a Degradable Hydrogel Based on a Graft Copolymer with Unexpected Thermoresponsiveness.

Jingcong Xu and Volker Abetz

Macromol. Chem. Phys. **2022**, 2200058.

DOI: 10.1002/macp.202200058

J.X.: Conceptualization, Investigation, Validation, Visualization, Writing - original draft.

V.A.: Conceptualization, Supervision, Funding acquisition, Writing - review & editing.

7.2 Supporting Information of Publication 1

The supporting information is reprinted with permission from J. Xu and V. Abetz, *Macromol. Rapid Commun.* **2021**, *42*, 2000648 – published by Wiley-VCH GmbH.



Supporting Information

for *Macromol. Rapid Commun.*, DOI: 10.1002/marc.202000648

Nonionic UCST–LCST Diblock Copolymers with Tunable
Thermoresponsiveness Synthesized via PhotoRAFT
Polymerization

Jingcong Xu and Volker Abetz*

Supporting Information

Nonionic UCST–LCST Diblock Copolymers with Tunable Thermoresponsiveness Synthesized via PhotoRAFT Polymerization

*Jingcong Xu, and Volker Abetz**

This supporting information provides details of polymerization procedures, SEC, NMR, UV-Vis, transmittance measurements and DLS data

Materials

1,4-dioxane (Grüssing, 99%), 2-Cyano-2-propyl dodecyl trithiocarbonate (CPDTC, abcr, 97%), *n*-hexane (VWR, 95%), tetrahydrofuran (THF, VMR, 99.5%), dimethylformamide (DMF, Grüssing, 100%), methacrylamide (MAAm, Sigma Aldrich, 98%), deuterated chloroform (CDCl₃, Sigma Aldrich, 100%) and deuterium oxide (D₂O, Sigma Aldrich, 100%) were used as received. Di(ethylene glycol) methyl ether methacrylate (MEO₂MA, Sigma Aldrich, 95%) and oligo(ethylene glycol) methacrylate (OEGMA, Sigma Aldrich, $\bar{M}_n = 500$ Da) were passed through activated basic alumina prior to the polymerizations.

Analytical methods

Nuclear magnetic resonance (NMR) spectroscopy: ¹H-NMR spectra were recorded with a BRUKER AVANCE III 300 instrument at a temperature of 300 K. Samples were dissolved in CDCl₃ or D₂O. CHCl₃ and H₂O-signals were used as references, respectively. The ¹H-NMR data were processed with the program MestReNova.

Size exclusion chromatography (SEC): SEC measurements were conducted on an AGILGENT 1260 INFINITY system including an isocratic SECcurity pump, an autosampler, a PSS SDV (styrene-divinylbenzene copolymer network) precolumn (8 × 50 mm, particle size: 5 μm), three PSS SDV separation columns (8 × 300mm, particle size: 5 μm, pore size:

10^3 \AA , 10^5 \AA , and 10^6 \AA) and a refractive index (RI) detector. THF was used as the mobile phase with a flow rate of 1.0 mL min^{-1} at $30 \text{ }^\circ\text{C}$. The system was calibrated with narrowly distributed poly(methyl methacrylate) (PMMA) standards.

Ultraviolet-visible spectroscopy (UV-Vis): The UV-Vis spectra were recorded with a spectrophotometer UV5 from METTLER TOLEDO at room temperature. The sample was measured from 190 to 1100 nm. The scan time was 10 s.

End-group analysis of macro-RAFTs: Number average molecular weights of the macro-RAFTs were calculated by comparing the absorbance coefficient of the polymers with that of the model RAFT agent methyl 2-(butylsulfanylthiocarbonylsulfanyl)-2-methyl propionate ($\epsilon_{\text{CH}_2\text{Cl}_2} = 10400 \text{ L mol}^{-1} \text{ cm}^{-1}$).^[2] Measurements were done in CH_2Cl_2 . The cuvette path length was 10 mm.

Transmittance measurement: Measurements were performed on a spectrophotometer UV5 at 700 nm. The samples were dissolved in Milli-Q[®] water. The heating rate was manually kept at about $2 \text{ }^\circ\text{C}$ every 2 min with a thermostat accessory CuveT from METTLER TOLEDO.

Dynamic light scattering (DLS)

Preparation of the aqueous solutions of macro-RAFTs: 2 mg of the polymer were dissolved in 2 mL Milli-Q[®] water. The solution was stirred at room temperature at least overnight and then filtered through a microporous (200 nm) regenerated cellulose filter prior to the measurement.

Preparation of the aqueous solutions of diblock copolymers: 10 mg of the polymer were dissolved in 2 mL Milli-Q[®] water. The solution was stirred at room temperature for at least 1 h. The homogeneous hazy solution was then stirred at 60 °C for half an hour. The yielded transparent solution was then cooled in a cold water bath immediately and filtered through a microporous (200 nm) regenerated cellulose filter without delay.

Measurement: Temperature-dependent DLS measurements were performed by using an ALV/CGS-3 Compact Goniometer-System with an ALV/LSE-5004 Multiple Tau Digital Correlator and a Nd:YAG laser (532 nm, 400 mW). The measuring angle was 90 °C for all measurements. The duration of every measurement was 60 s. The viscosity and refractive index of water at each temperature were automatically corrected in the ALV Digital Correlator Software 3.0. The sample in a quartz glass vial was put into a toluene bath. The cooling and heating procedure of the toluene bath was controlled by a Julabo F25 thermostat, whose temperature accuracy was set to 1 °C. The DLS results were evaluated by using a program written by Felix Lauterbach based on a cumulant approach.^[1] The intensity correlation function ($g_2(\tau)$) was fitted with the function:

$$g_2(\tau) = B + \beta \exp(-2\bar{\Gamma}\tau) \left(1 + \frac{\mu_2}{2!} \tau^2 - \frac{\mu_3}{3!} \tau^3 + \dots \right)^2 \quad (1)$$

where B represents the baseline, β denotes the stretching factor, $\bar{\Gamma}$ is the mean decay rate, μ_2 , and μ_3 are the cumulants. The hydrodynamic radius R_H is calculated through the Stokes-Einstein equation:

$$R_H = \frac{k_B T q^2}{6\pi\eta\bar{\Gamma}} \quad (2)$$

where k_B is the Boltzmann constant, T is the temperature, q is the scattering vector and η is the viscosity. Additional CONTIN analysis was conducted for the diblock copolymers.

PhotoRAFT polymerization

Experimental set-up: A green LED strip consisting of 300 LEDs was stuck to the inner side of an aluminum cylinder with a diameter of about 16.5 cm (Figure S 1). The light intensity was controlled by a switching power supply PS3005N from QJE. The light intensity was characterized by a S120UV photodiode sensor head from Thorlabs.

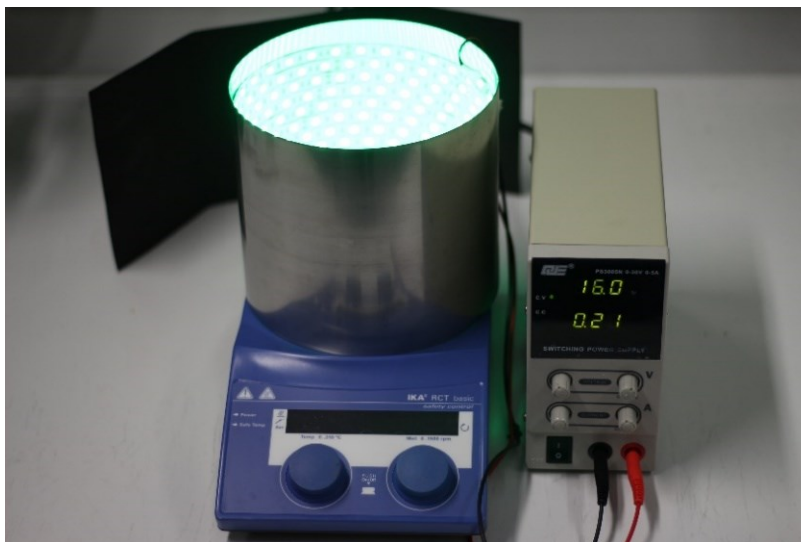


Figure S 1. Experimental set-up for photoRAFT polymerizations.

General polymerization procedure and kinetic study of P(MEO₂MA-*r*-OEGMA): In a typical photoRAFT polymerization of P(MEO₂MA-*r*-OEGMA), CPDTC, MEO₂MA, OEGMA and DMF as an internal standard for conversion calculation were dissolved in 1,4-dioxane in a polymerization vial. The total solid (RAFT agent and the monomers) concentration was kept at 20% (*w/w*). The polymerization vial was purged with N₂ for 15 min and the reaction was subsequently carried out at 60 °C under green light irradiation of 1.12 mW cm⁻² and under constant agitation. During the polymerization, aliquots of the reaction mixture were taken every 1 h and directly diluted with deuterated chloroform to determine monomer conversions through ¹H-NMR spectra. The polymerization was stopped by exposing the mixture to air and cooling with an ice bath. The polymer was then purified through precipitation in an excess amount of *n*-hexane four times. The purified product was dried in vacuo at 40 °C for 24 h.

General polymerization procedure and kinetic study of P(MEO₂MA-*r*-OEGMA)-*b*-PMAAm: In a typical photoRAFT polymerization of diblock copolymers, macro-RAFT, MAAm and DMF as an internal standard for conversion calculation were dissolved in Milli-

Q[®] water in a polymerization vial. The total solid concentration was kept at 10% (w/w). The polymerization vial was purged with N₂ for 15 min. The reaction was subsequently carried out at a previously selected temperature under green light irradiation of 4.55 mW cm⁻² and under constant agitation. During the polymerization, aliquots of the reaction mixture were taken every 1 h and directly diluted with deuterium oxide to determine monomer conversions through ¹H-NMR spectra. The polymerization was stopped by exposing the mixture to air and cooling with an ice bath. After dilution with a large amount of deionized water, the polymer was then purified through dialysis in deionized water for 3 days.

UV-Vis analysis

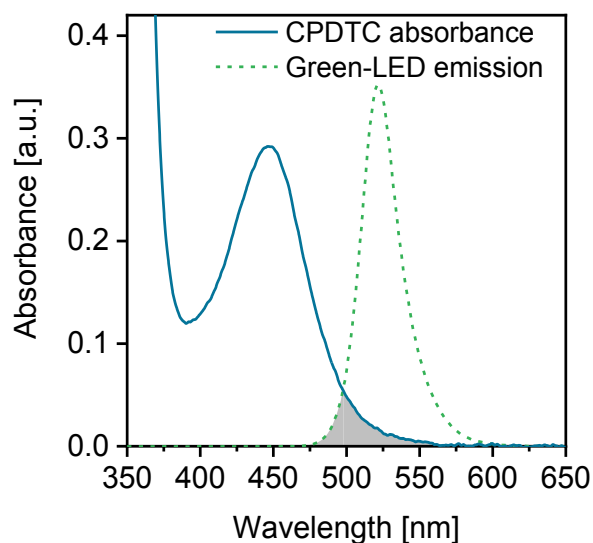


Figure S 2. The absorption spectrum of CPDTC (blue) measured by UV-Vis spectroscopy, which overlaps with the emission spectrum of the used green LED (green) in the marked range (grey) of the wavelengths. The peak of the emission spectrum is at about 522 nm.

SEC characterization

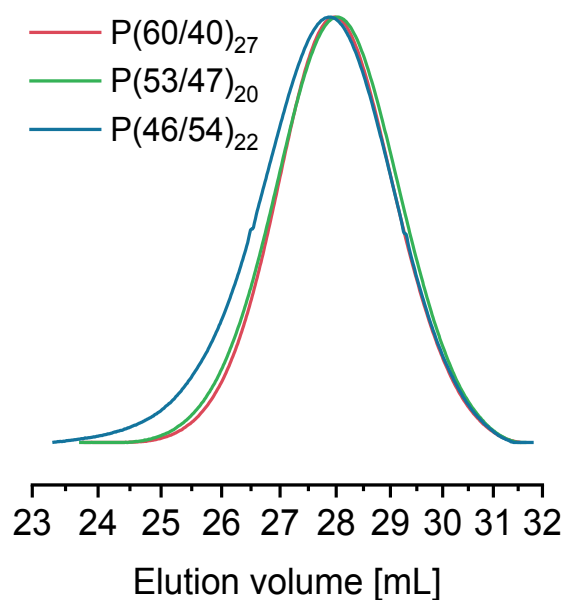


Figure S 3. SEC curves of three macro-RAFTs recorded by a refractive index (RI) detector with THF as eluent.

NMR analysis

Determination of the total conversions of MEO₂MA and OEGMA: The total conversions (α) of MEO₂MA and OEGMA were calculated through the decline of the proton signals from the monomers in the reaction mixture (Figure S 4):

$$\alpha = \left(1 - \frac{I_{m_1} + I_{m_1'}}{I_{m_0} + I_{m_0'}}\right) \times 100\% \quad (3)$$

I_{m_0} and $I_{m_0'}$ are the signal integrals at the beginning of the polymerization, while I_{m_1} and $I_{m_1'}$ are those in the end.

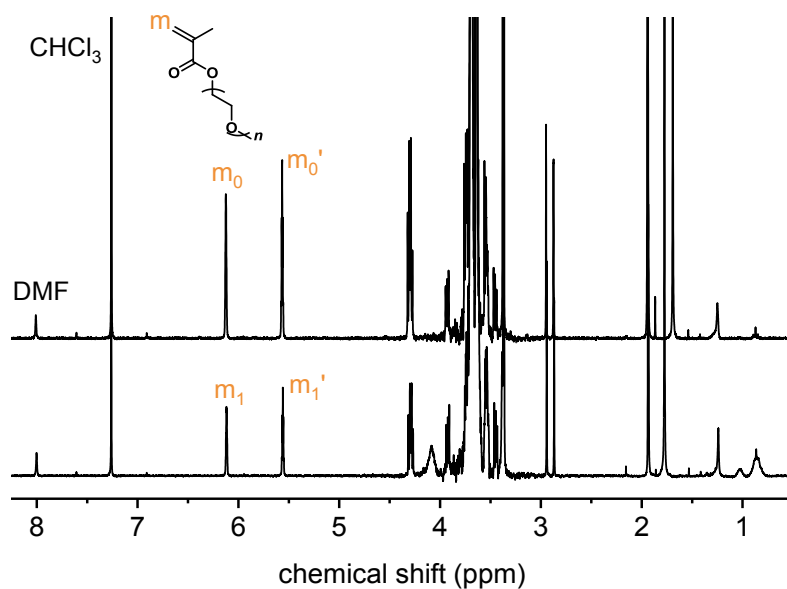


Figure S 4. Typical ¹H-NMR spectra of the reaction mixtures at the beginning of the polymerization (top) and at the end of the polymerization (bottom). The protons used for the conversion calculation are assigned to the signals.

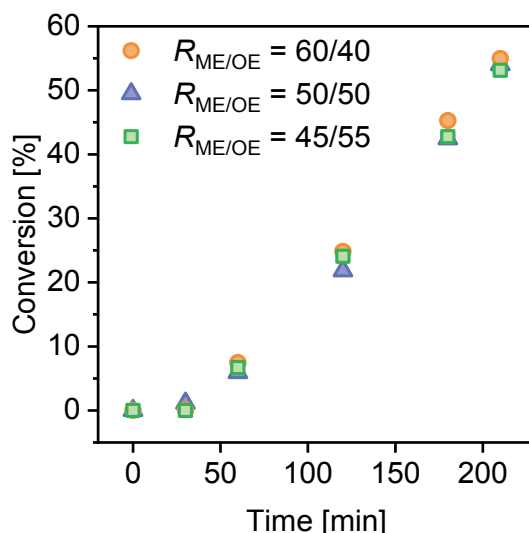


Figure S 5. Total monomer conversions of polymerizations with different feed comonomer ratios ($R_{ME/OE}$) versus time. All the polymerizations were carried out with a theoretical maximum degree of polymerization (DP_{max}) of 50.

Once the final α after the polymerization is calculated, the theoretical molecular weight of the polymer can be calculated as follows:

$$\bar{M}_{n,th} = \alpha \left(\frac{[MEO_2MA]_0}{[CPDTC]_0} M_{MEO_2MA} + \frac{[OEGMA]_0}{[CPDTC]_0} M_{OEGMA} \right) + M_{CPDTC} \quad (4)$$

$[MEO_2MA]_0$ and $[OEGMA]_0$ are the initial concentrations of the monomers. $[CPDTC]_0$ is the initial concentration of the RAFT agent. M_{MEO_2MA} , M_{OEGMA} and M_{CPDTC} are the molecular weights of the monomers and RAFT agent, respectively.

Determination of the ratio between MEO₂MA and OEGMA ($F_{ME/OE}$) in a macro-RAFT:

With a ¹H-NMR spectrum of a macro-RAFT shown in Figure S 6, $F_{ME/OE}$ can be calculated by solving the following equations:

$$I_A = 2N_{MEO_2MA} + 2N_{OEGMA} \quad (5)$$

$$I_B = 6N_{MEO_2MA} + 34N_{OEGMA} \quad (6)$$

$I_{A/B}$ are the signal integrals. N_{MEO_2MA} and N_{OEGMA} are the numbers of the repeating units of two monomers in a macromolecule, respectively.

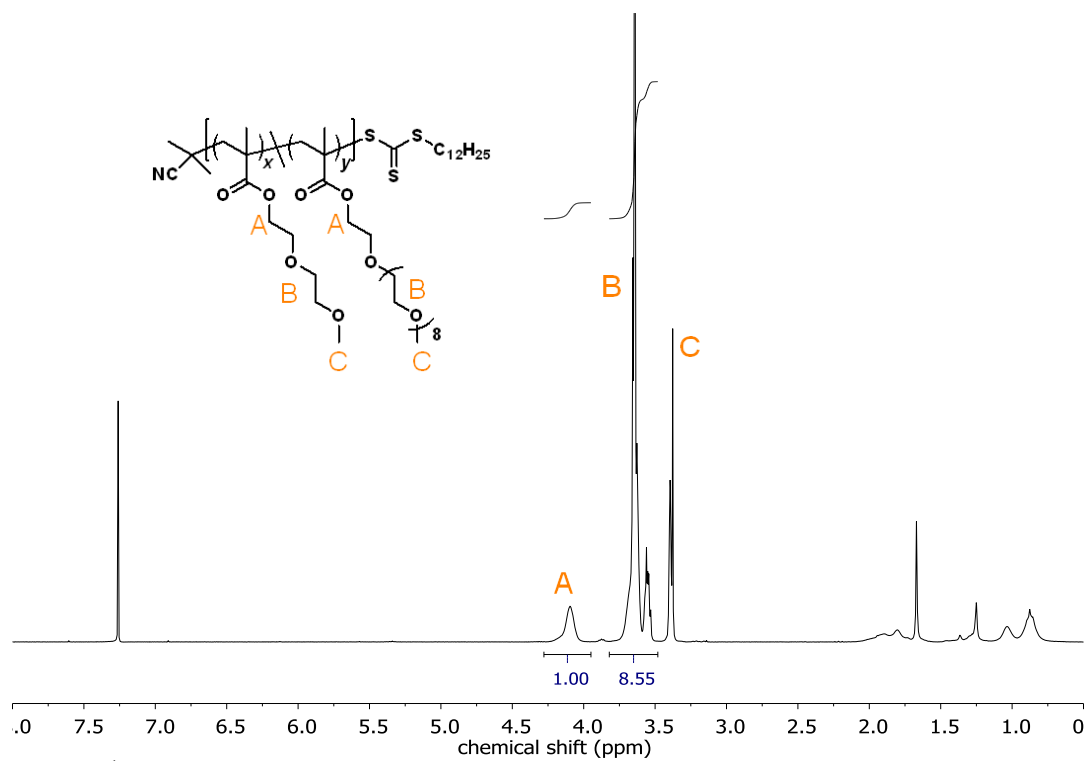


Figure S 6. $^1\text{H-NMR}$ spectrum of $\text{P}(60/40)_{27}$ in CDCl_3 with the assignment of the proton signals in the side chains.

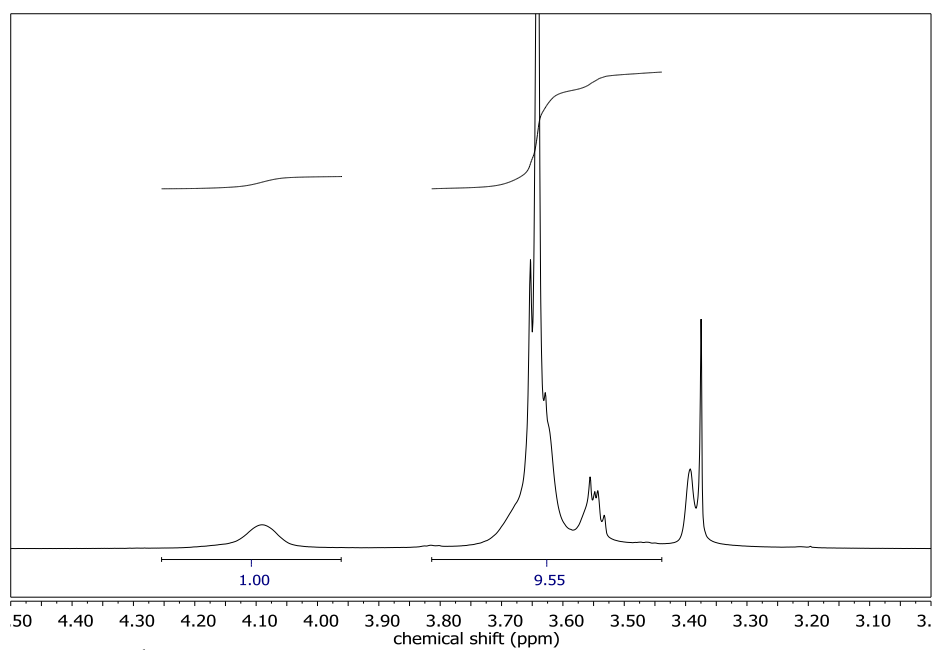


Figure S 7. Enlarged $^1\text{H-NMR}$ spectrum of $\text{P}(53/47)_{20}$ in CDCl_3 .

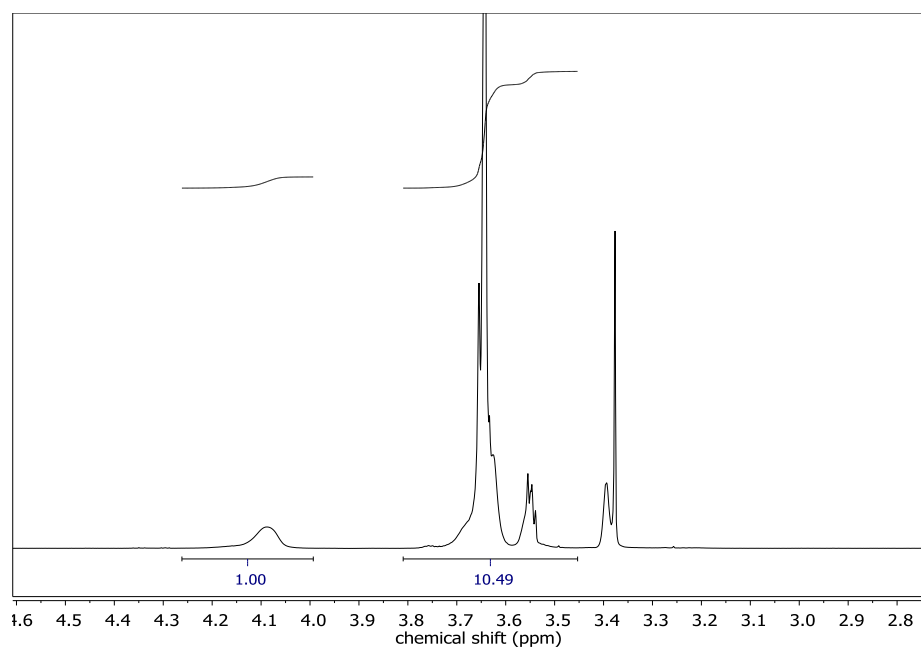


Figure S 8. Enlarged $^1\text{H-NMR}$ spectrum of $\text{P}(46/54)_{22}$ in CDCl_3 .

Determination of the conversion of MAAm: The signals of the vinylic protons in MAAm in D_2O are at 5.4–5.9 ppm. Therefore, the conversion of MAAm can also be calculated with Equation 3. The theoretical molecular weight of $\text{P}(\text{MEO}_2\text{MA-}r\text{-OEGMA})\text{-}b\text{-PMAAm}$ can then be calculated as follows:

$$\bar{M}_{n,\text{th}}(\text{diblock}) = \alpha \frac{[\text{MAAm}]_0}{[\text{macro-RAFT}]_0} M_{\text{MAAm}} + \bar{M}_{n,\text{th}}(\text{macro-RAFT}) \quad (7)$$

Typical $^1\text{H-NMR}$ spectrum of a diblock copolymer: the sample was dissolved in D_2O at $60\text{ }^\circ\text{C}$. The turbid solution was then measured at 300 K . Although the block of PMAAm was not completely soluble in D_2O at low temperatures, signals from its methyl group (d) between 0.90 ppm and 1.40 ppm can still be observed.

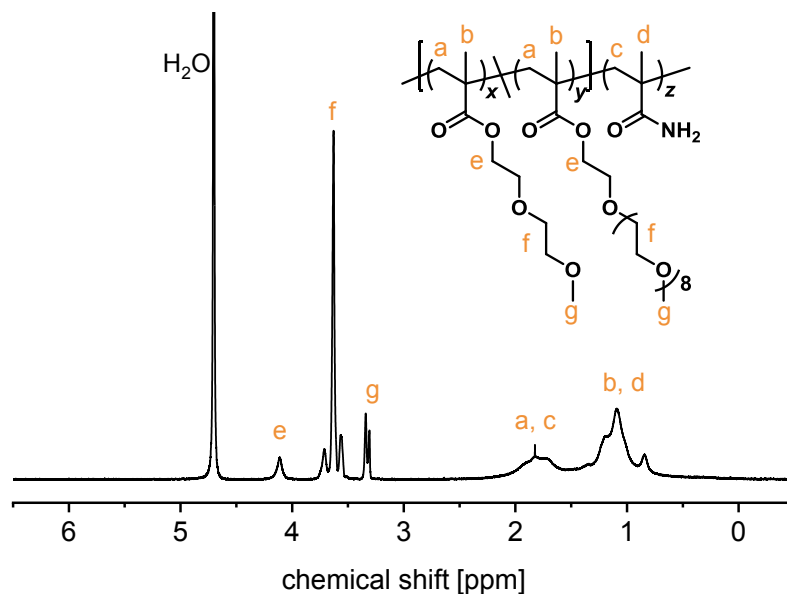


Figure S 9. Typical $^1\text{H-NMR}$ spectrum of a diblock copolymer in D_2O with the assignment of the proton signals.

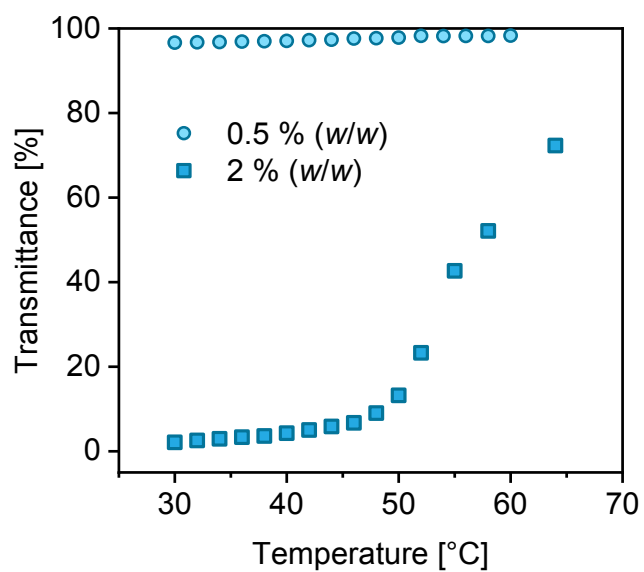
Transmittance measurements of P(60/40)₂₇-*b*-PMAAm₄₄₀

Figure S 10. Heating processes of the transmittance measurements of the aqueous solutions with different concentrations.

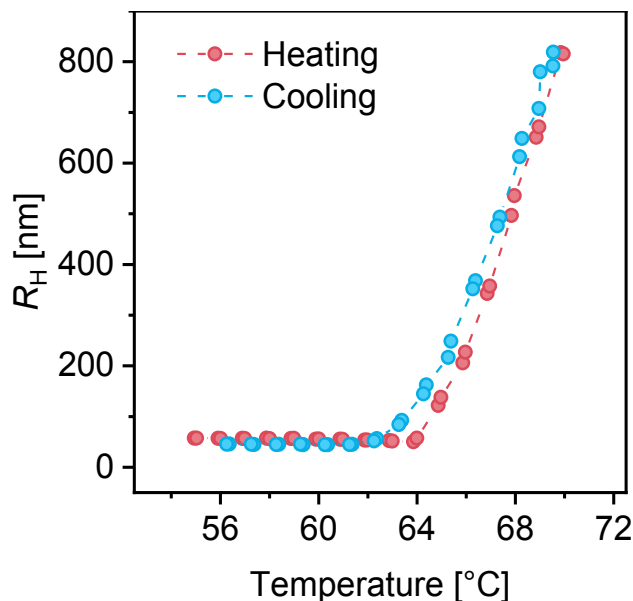
Full heating–cooling cycle of LCST transition of P(MEO₂MA-*r*-OEGMA)

Figure S 11. Evolution of hydrodynamic radius (R_H) of P(60/40)₂₇ in an aqueous solution ($c = 0.1\%$ (w/w)) obtained by DLS measurements. The sample was heated from 55 °C to 70 °C and then cooled to 55 °C again. The temperature step was 1 °C and two measurements were conducted at each temperature.

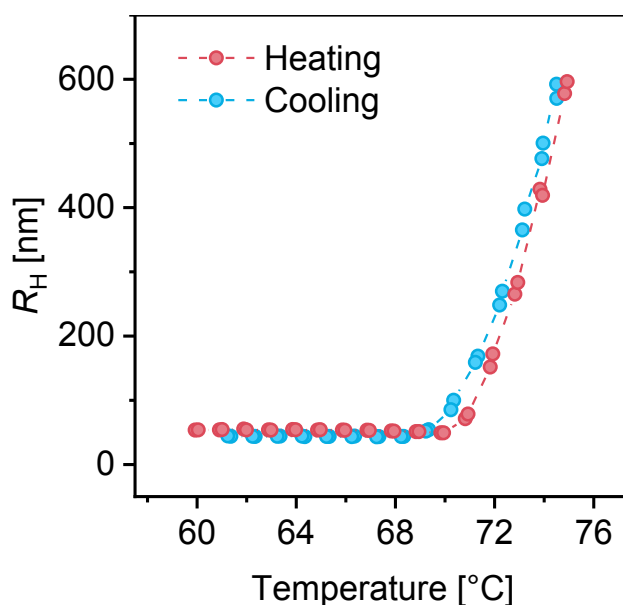


Figure S 12. Evolution of hydrodynamic radius (R_H) of P(53/47)₂₀ in an aqueous solution ($c = 0.1\%$ (w/w)) obtained by DLS measurements. The sample was heated from 60 °C to 75 °C and then cooled to 60 °C again. The temperature step was 1 °C and two measurements were conducted at each temperature.

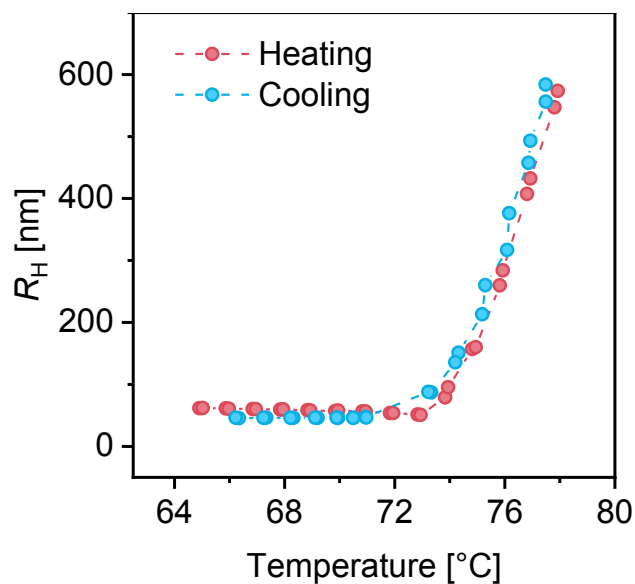


Figure S 13. Evolution of hydrodynamic radius (R_H) of P(46/54)₂₂ in an aqueous solution ($c = 0.1\%$ (w/w)) obtained by DLS measurements. The sample was heated from 65 °C to 78 °C and then cooled to 65 °C again. The temperature step was 1 °C and two measurements were conducted at each temperature.

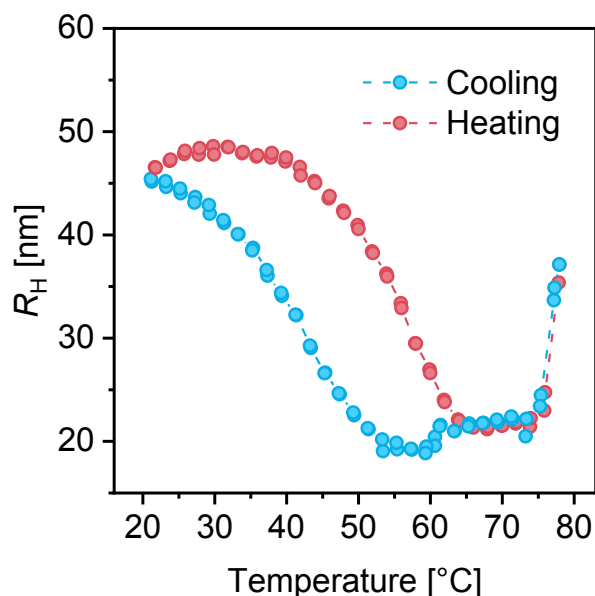
Full cooling–heating–cooling cycle of UCST-LCST transitions of P(MEO₂MA-*r*-OEGMA)-*b*-PMAAm

Figure S 14. Evolution of hydrodynamic radius (R_H) of P(53/47)₂₀-*b*-PMAAm₃₅₂ in an aqueous solution ($c = 0.5\%$ (w/w)) obtained by DLS measurements. The measurement started with a cooling process from 60 °C to 20 °C, followed by a heating process till 78 °C. Lastly, the solution was cooled to 60 °C. The temperature step was 2 °C and two measurements were conducted at each temperature.

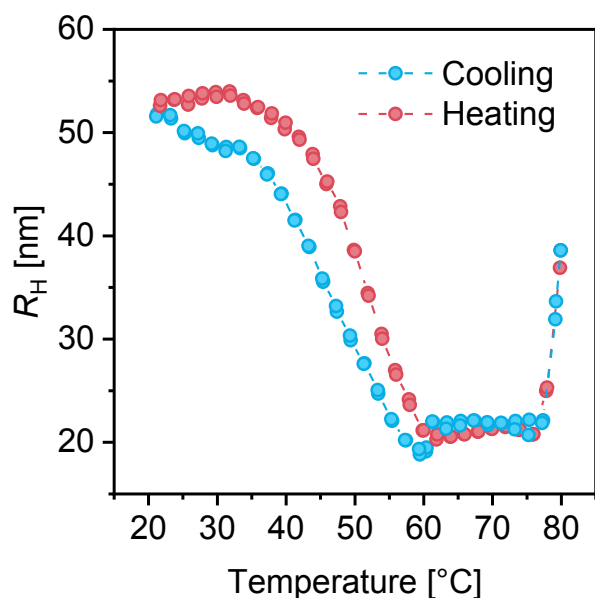


Figure S 15. Evolution of hydrodynamic radius (R_H) of P(46/54)₂₂-*b*-PMAAm₃₆₁ in an aqueous solution ($c = 0.5\%$ (w/w)) obtained by DLS measurements. The measurement started with a cooling process from 60 °C to 20 °C, followed by a heating process till 80 °C. Lastly, the solution was cooled to 60 °C. The temperature step was 2 °C and two measurements were conducted at each temperature.

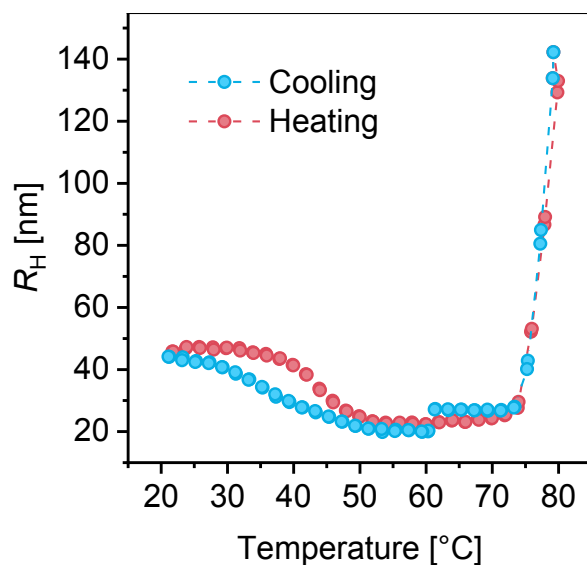


Figure S 16. Evolution of hydrodynamic radius (R_H) of P(46/54)₂₂-*b*-PMAAm₂₉₆ in an aqueous solution ($c = 0.5\%$ (w/w)) obtained by DLS measurements. The measurement started with a cooling process from 60 °C to 20 °C, followed by a heating process till 80 °C. Lastly, the solution was cooled to 60 °C. The temperature step was 2 °C and two measurements were conducted at each temperature.

Size distributions of the diblock copolymers in aqueous solutions at representative temperatures

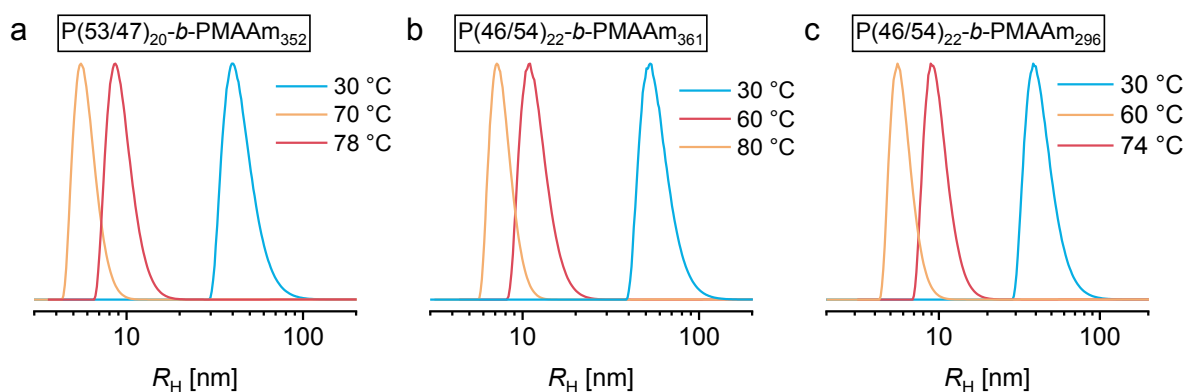


Figure S 17. Intensity-weighted size distributions of the diblock copolymers in aqueous solutions ($c = 0.5\%$ (w/w)) at representative temperatures obtained from DLS measurements. The DLS data were fitted by CONTIN analysis.

References

- [1] F. Lauterbach, Advances in RAFT polymerization process design and analysis, Ph.D. Thesis, University of Hamburg, Hamburg, June 2020.
- [2] K. Skrabania, A. Miasnikova, A. M. Bivigou-Koumba, D. Zehm, A. Laschewsky, *Polym. Chem.* **2011**, 2, 2074.

7.3 Supporting Information of Publication 2

The supporting information is reprinted with permission from J. Xu and V. Abetz, *Soft Matter* **2022**, *18*, 2082–2091 – published by The Royal Society of Chemistry.

Supplementary Information

Double thermoresponsive graft copolymers with different chain ends: feasible precursors for covalently crosslinked hydrogels

Jingcong Xu, and Volker Abetz*

1. Experimental set-up

An LED strip was stuck to the inner side of an aluminum cylinder with a diameter of about 16.5 cm (Fig. S1). The light intensity and wavelength were changed by a remote control. The light intensity was characterized by a S120UV photodiode sensor head from Thorlabs. The positions of the oil bath and the polymerization vial in the reactor were kept as constant as possible for every polymerization to ensure a satisfying reproducibility.

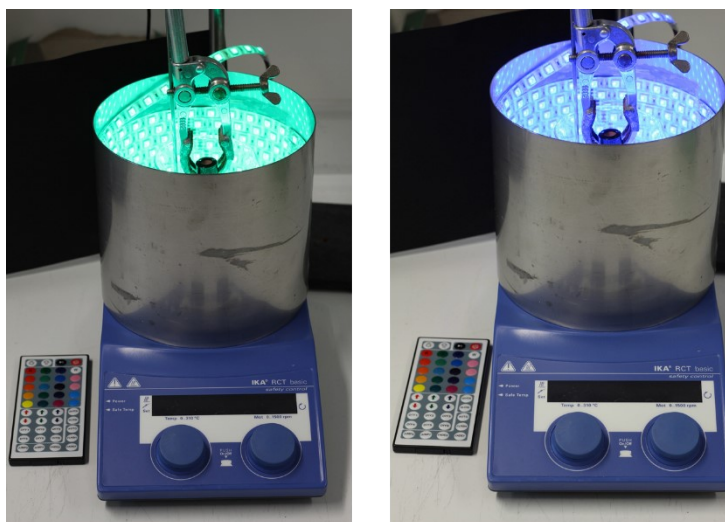


Fig. S1 Experimental set-up for photoiniferter RAFT polymerizations.

2. NMR analysis

2.1 Determination of the total conversion of OEGMA and BTPEMA

The total conversion (α) of OEGMA and BTPEMA was calculated through the decline of the proton signals from the monomers in the reaction mixture (Fig. S2):

$$\alpha = \left(1 - \frac{I_{O_1+B_1} + I_{O_1'+B_1'}}{I_{O_0+B_0} + I_{O_0'+B_0'}} \right) \times 100\% \quad (1)$$

$I_{O_0+B_0}$ and $I_{O_0'+B_0'}$ are the signal integrals at the beginning of the polymerization, while $I_{O_1+B_1}$ and $I_{O_1'+B_1'}$ are those in the end.

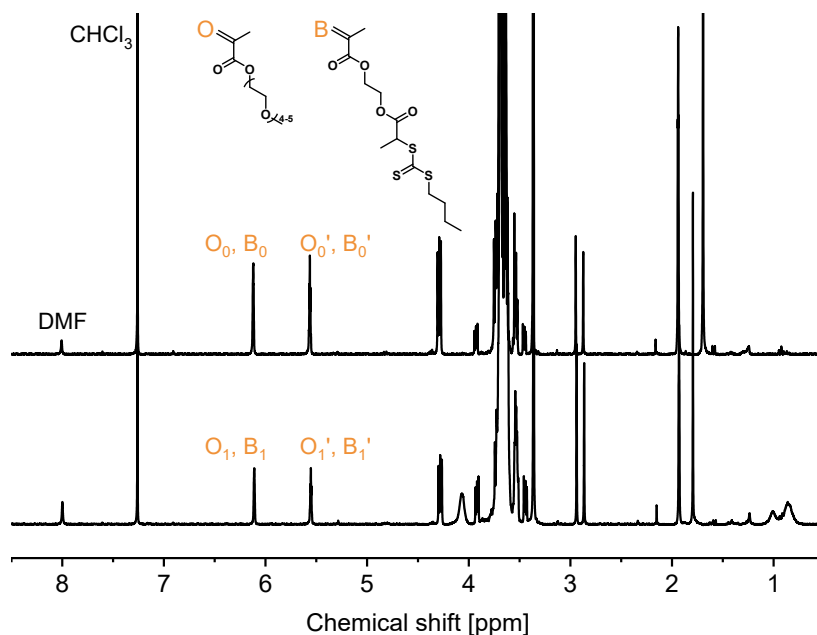


Fig. S2 Typical ^1H -NMR spectra of the reaction mixtures at the beginning of the polymerization (top) and at the end of the polymerization (bottom). The protons used for the conversion calculation are assigned to the signals.

Once α after the polymerization is calculated, the theoretical molecular weight of the statistical copolymer can be calculated as follows:

$$\bar{M}_{n,th} = \alpha \left(\frac{[\text{OEGMA}]_0}{[\text{RAFT}]_0} M_{\text{OEGMA}} + \frac{[\text{BTPEMA}]_0}{[\text{RAFT}]_0} M_{\text{BTPEMA}} \right) + M_{\text{RAFT}} \quad (2)$$

$[\text{OEGMA}]_0$ and $[\text{BTPEMA}]_0$ are the initial concentrations of the monomers. $[\text{RAFT}]_0$ is the initial concentration of the RAFT agent. M_{OEGMA} , M_{BTPEMA} , and M_{RAFT} are the molecular weights of the monomers and RAFT agent, respectively.

2.2 Determination of the conversion of NIPAM

The conversion of NIPAM was also calculated through the decline of the proton signal from the monomer in the reaction mixture (**Fig. S3**):

$$\alpha = \left(1 - \frac{I_{N_1}}{I_{N_0}}\right) \times 100\% \quad (3)$$

I_{N_0} is the signal integral at the beginning of the polymerization, while I_{N_1} is that in the end.

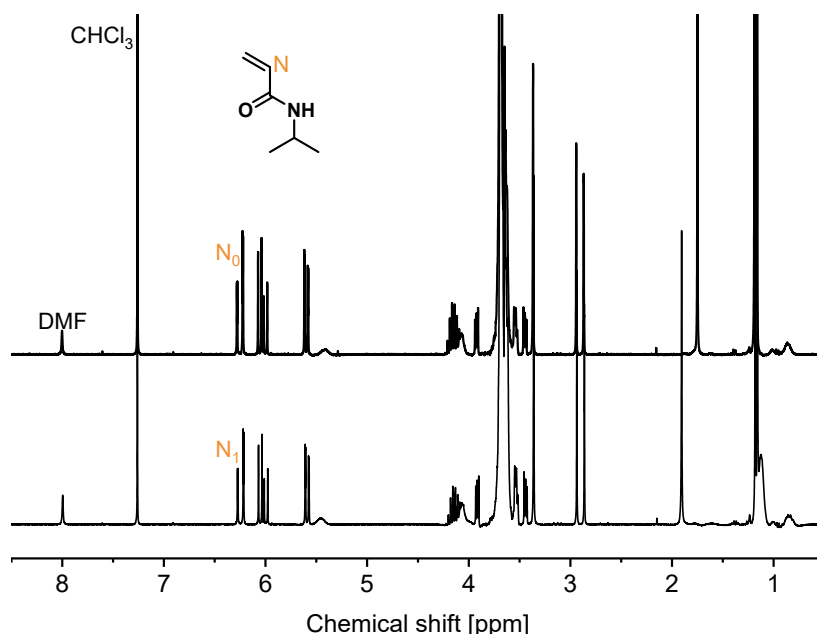


Fig. S3 Typical ^1H -NMR spectra of the reaction mixtures at the beginning of the polymerization (top) and at the end of the polymerization (bottom). The proton used for the conversion calculation is assigned to the signals.

Once α after the polymerization is calculated, the theoretical molecular weight of the graft copolymer can be calculated as follows:

$$\bar{M}_{n,th} = \alpha \frac{[\text{NIPAM}]_0}{[\text{backbone}]_0} M_{\text{NIPAM}} + \bar{M}_{n,th(\text{backbone})} \quad (4)$$

2.3 Determination of the molar ratio between OEGMA and BTPEMA

With the ^1H -NMR spectra of the statistical copolymers shown in **Fig. S4** and **Fig. S5**, the molar ratios (OEGMA/BTPEMA) in two backbones can be calculated by the signal integrals I_A and I_B :

$$\frac{\text{OEGMA}}{\text{BTPEMA}} = \frac{I_B/3}{I_A} \quad (5)$$

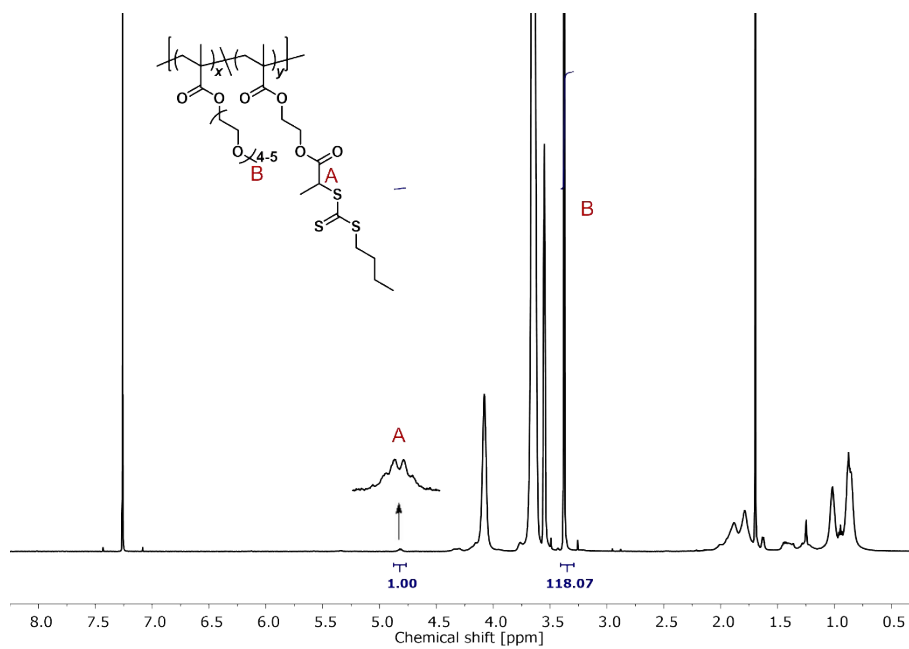


Fig. S4 ¹H-NMR spectrum of P(O₂₄₅B₆) in CDCl₃ with the assignment of the proton signals (chain ends of the backbone are not shown here).

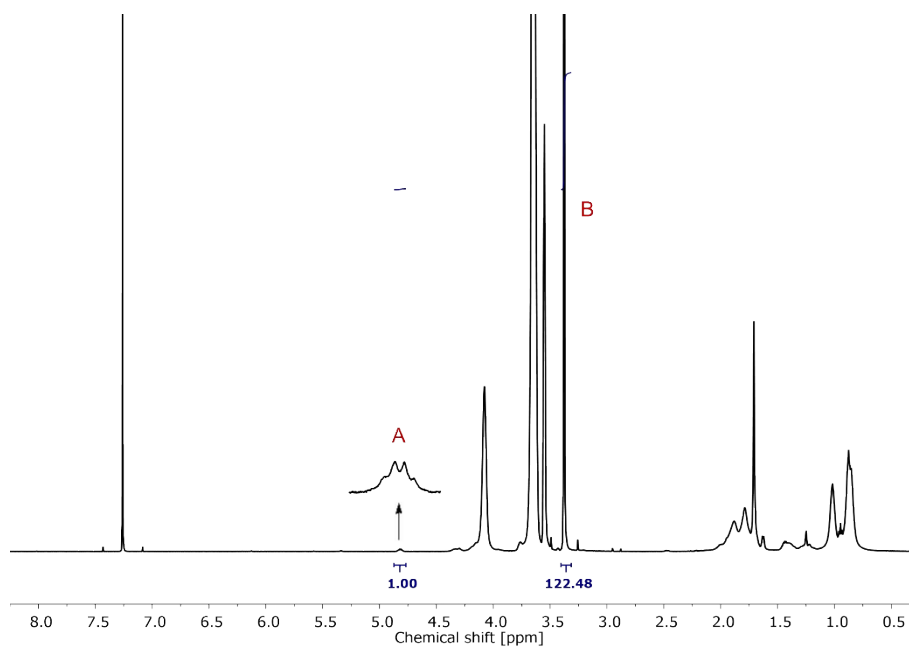


Fig. S5 ¹H-NMR spectrum of P(O₂₃₄B₆)-COOH in CDCl₃.

2.4 Determination of the molar ratio between OEGMA and NIPAM

With the $^1\text{H-NMR}$ spectra of the graft copolymers shown in **Fig. S6** and **Fig. S7**, the molar ratios (OEGMA/NIPAM) in two graft copolymers can be calculated by solving the following equations:

$$I_{A+C} = \text{NIPAM} + 2 \times \text{OEGMA} \quad (6)$$

$$I_B = 3 \times \text{OEGMA} \quad (7)$$

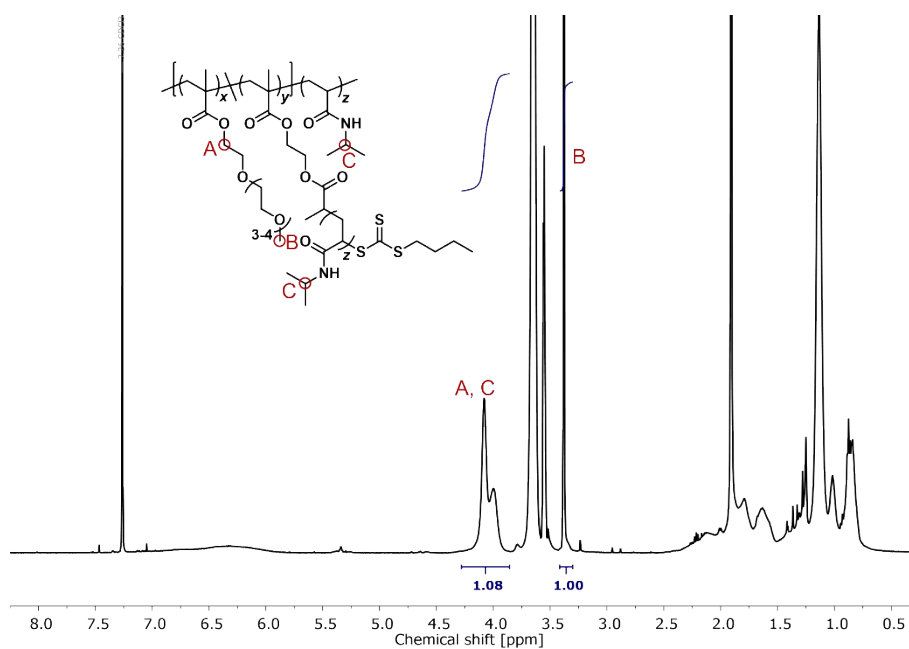


Fig. S6 $^1\text{H-NMR}$ spectrum of $\text{PO}_{245}(\text{PN}_{40})_7$ in CDCl_3 with the assignment of the proton signals (chain ends of the backbone are not shown here).

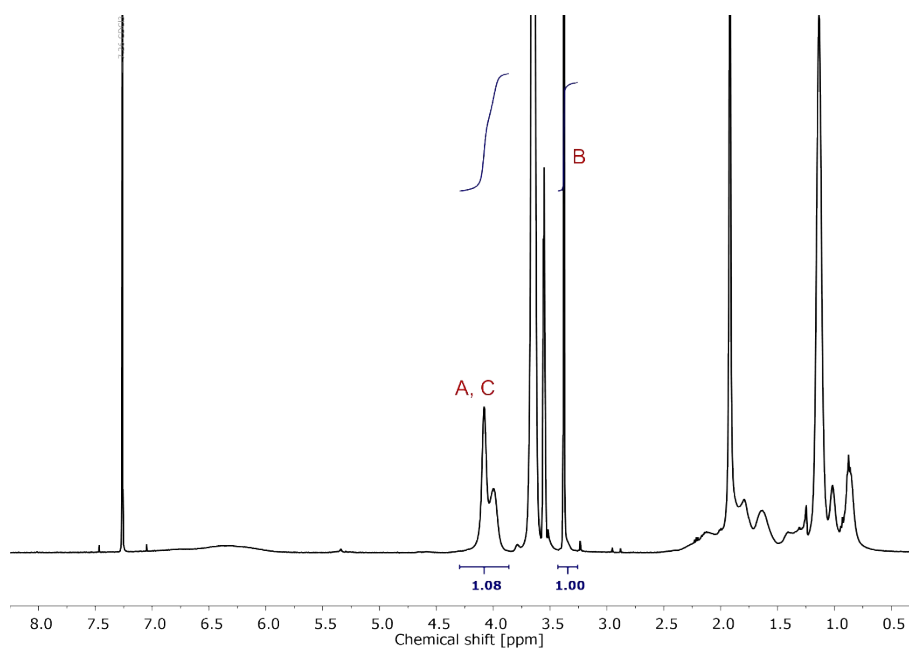


Fig. S7 $^1\text{H-NMR}$ spectrum of $\text{PO}_{234}(\text{PN}_{43})_7\text{-COOH}$ in CDCl_3 .

3. Kinetic study of chain extension

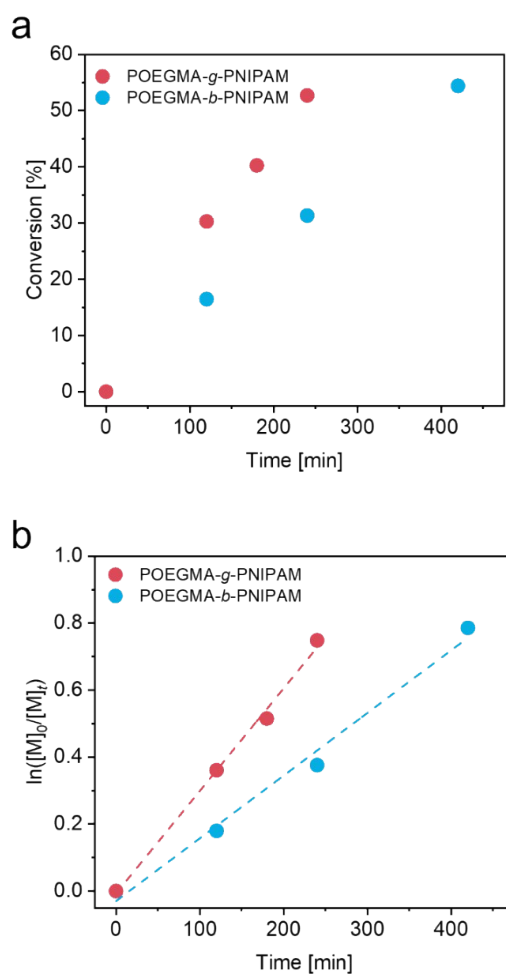


Fig. S8 (a): Monomer conversions of chain extensions from $\text{PO}_{234}\text{-COOH}$ and $\text{P}(\text{O}_{234}\text{B}_6)\text{-COOH}$. A block copolymer and a graft copolymer were supposed to be obtained, respectively; (b): pseudo first-order kinetics plots of both chain extensions.

4. Static light scattering (SLS) measurements

The aqueous solution of PO₂₃₄(PN₄₃)₇-COOH with a fixed concentration ($c = 0.1\%$ [w/w]) was measured at 25 °C and 40 °C by SLS. The range of the scattering angles of the measurements was from 30° to 150° with a step of 10°. The results are shown in **Fig. S9**.

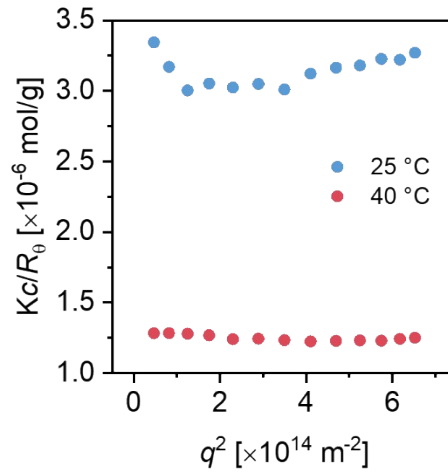


Fig. S9 SLS data of the aqueous solution of PO₂₃₄(PN₄₃)₇-COOH ($c = 0.1\%$ [w/w]) at two different temperatures.

The weight average molecular weights (\bar{M}_w) at both temperatures were estimated by the partial Zimm approach:

$$\frac{Kc}{R_\theta} = \frac{1}{\bar{M}_w} \left(1 + \frac{R_g^2 q^2}{3} \right) \quad (8)$$

where K , c , R_θ , R_g , and q are the optical constant, concentration, difference in the Rayleigh ratio between the polymer solution and the solvent, radius of gyration, and scattering vector, respectively.

According to the SLS results, the absolute \bar{M}_w of the formed micelles ($\bar{M}_{w,agg}$) at 40 °C was about 784 kDa. The absolute \bar{M}_w of the unimers ($\bar{M}_{w,uni}$) dissolved at 25 °C was about 324 kDa. The deviation from the theoretical value could be attributed to the inaccurate concentration, but it has no influence on the estimation of the aggregation number ($N_{agg} = \bar{M}_{w,agg}/\bar{M}_{w,uni}$).

5. Cumulant approach for evaluation of dynamic light scattering (DLS) data

In the DLS measurements, the obtained intensity correlation function ($g_2(\tau)$) for one size distribution was fitted with the following standard function:

$$g_2(\tau) = B + \beta \exp(-2\bar{\Gamma}\tau) \left(1 + \frac{\mu_2}{2!}\tau^2 - \frac{\mu_3}{3!}\tau^3 + \dots \right)^2 \quad (9)$$

where B represents the baseline, β denotes the stretching factor (contrast), $\bar{\Gamma}$ is the mean decay rate, μ_2 , and μ_3 are the cumulants. The hydrodynamic radius R_H is calculated through the Stokes-Einstein equation:

$$R_H = \frac{k_B T q^2}{6\pi\eta\bar{\Gamma}} \quad (10)$$

where k_B is the Boltzmann constant, T is the temperature, q is the scattering vector and η is the viscosity.

For two size distributions, the data were fitted with the sum of two exponential decay functions:

$$g_2(\tau) = B + \beta \left(\sum_{i=1}^2 f_i \exp(-\bar{\Gamma}_i \tau) \left(1 + \frac{\mu_{2,i}}{2!}\tau^2 - \frac{\mu_{3,i}}{3!}\tau^3 + \dots \right) \right)^2 \quad (11)$$

where f_i represents the fraction of different particle species. The hydrodynamic radius $R_{H,i}$ of each specie is calculated through the Stokes-Einstein equation:

$$R_{H,i} = \frac{k_B T q^2}{6\pi\eta\bar{\Gamma}_i} \quad (12)$$

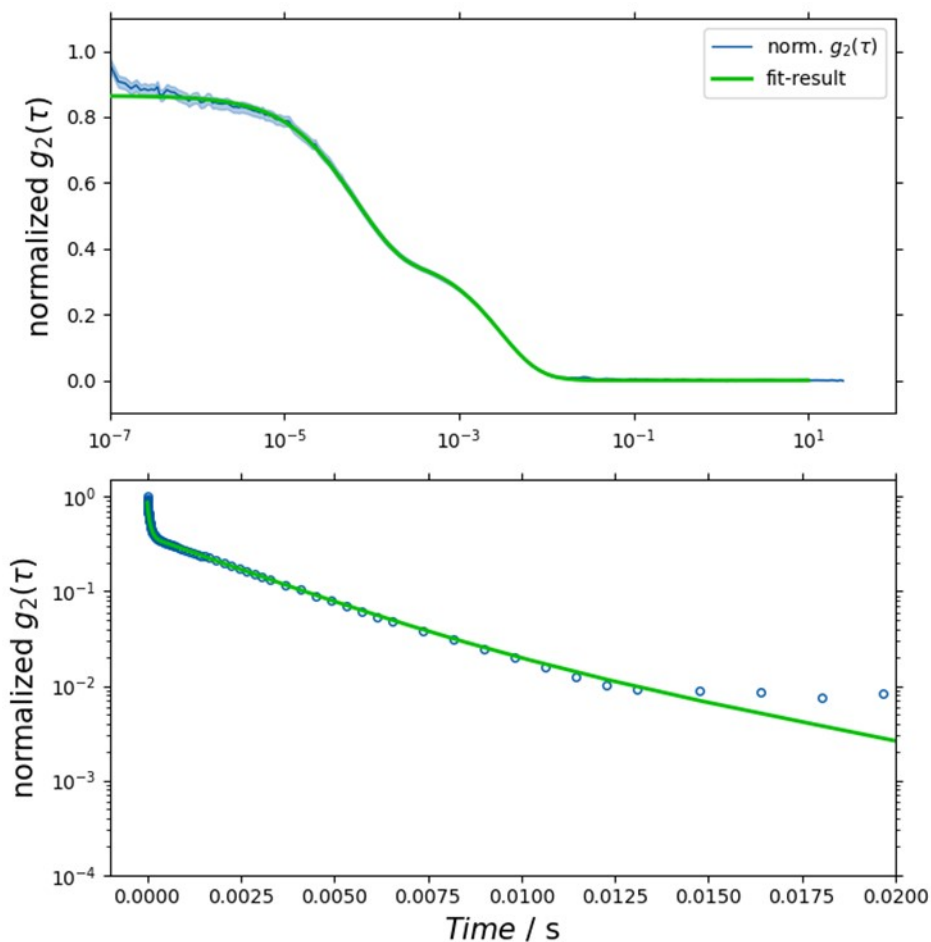


Fig. S10 DLS data of $\text{PO}_{245}(\text{PN}_{40})_7$ at 40 °C (blue curve) and fit result by using Equation 11 (green curve).

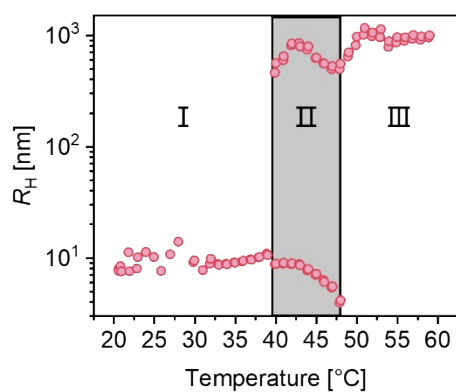


Fig. S11 Evolution of R_H of $\text{PO}_{218}(\text{PN}_{32})_7$ in a dilute aqueous solution ($c = 0.05\%$ [w/w]) during heating followed by DLS.

7.4 Supporting Information of Publication 3

The supporting information is reprinted with permission from J. Xu and V. Abetz, *Macromol. Chem. Phys.* **2022**, 2200058 – published by Wiley-VCH GmbH.

[M]acro-
molecular
Chemistry and Physics

Supporting Information

for *Macromol. Chem. Phys.*, DOI 10.1002/macp.202200058

Synthesis of a Degradable Hydrogel Based on a Graft Copolymer with Unexpected Thermoresponsiveness

*Jingcong Xu and Volker Abetz**

Supporting Information

Synthesis of a Degradable Hydrogel Based on a Graft Copolymer with Unexpected Thermoresponsiveness

Jingcong Xu and Volker Abetz

1. Analytic Results of DiCTA

1.1 $^1\text{H-NMR}$ Spectrum of DiCTA

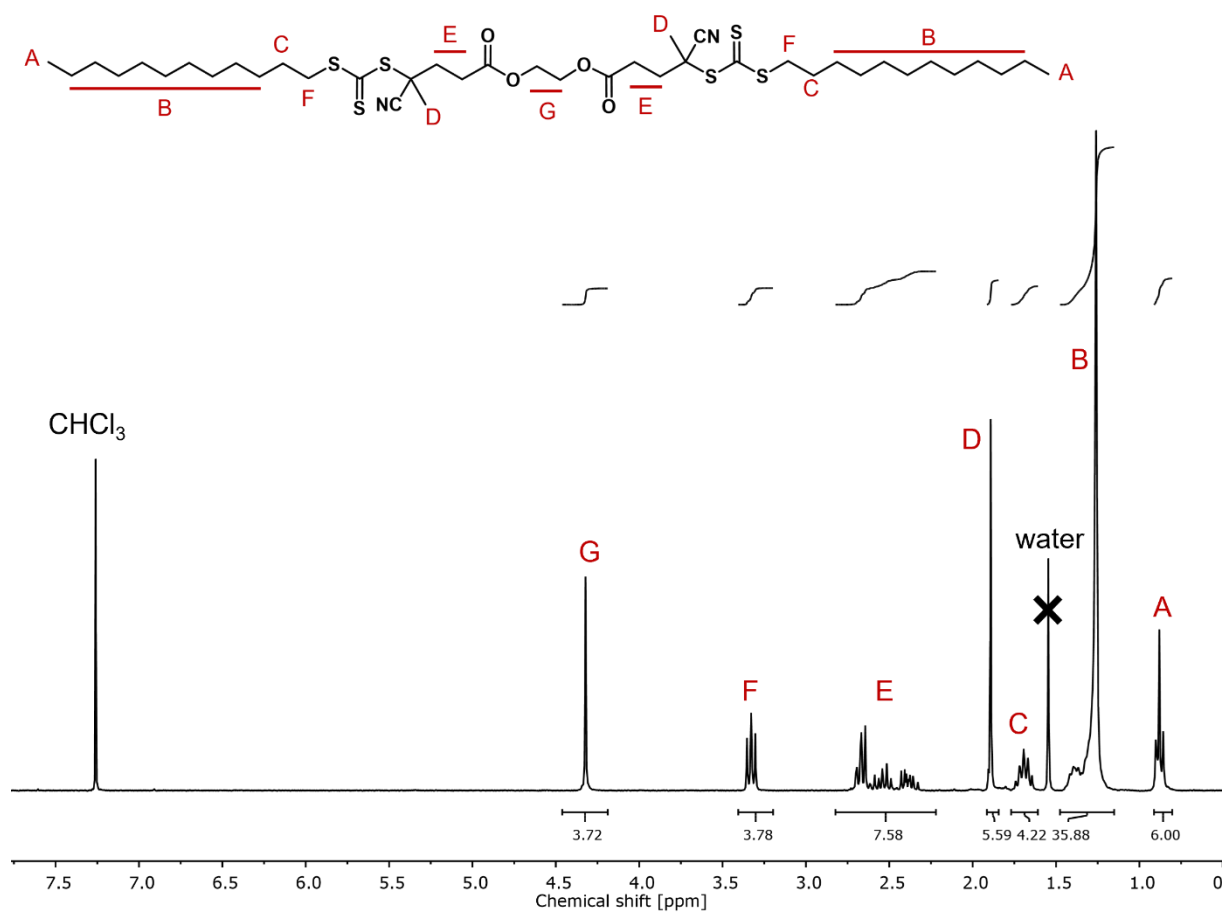


Figure S1. $^1\text{H-NMR}$ spectrum of DiCTA in CDCl_3 with the assignment of the proton signals.

1.2 UV-vis Spectra of the Chain Transfer Agents

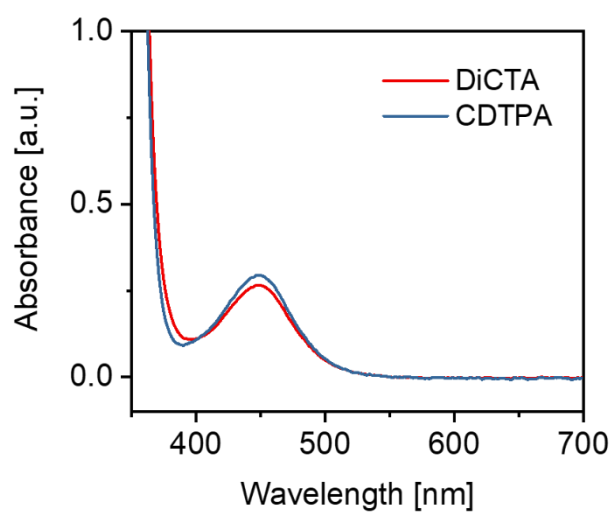


Figure S2. UV-vis spectra of the chain transfer agents. The samples were dissolved in 1,4-dioxane before the measurements.

2. Polymerization of the Backbone

2.1 Calculation of Total Conversion of MEO₂MA and BTPEMA

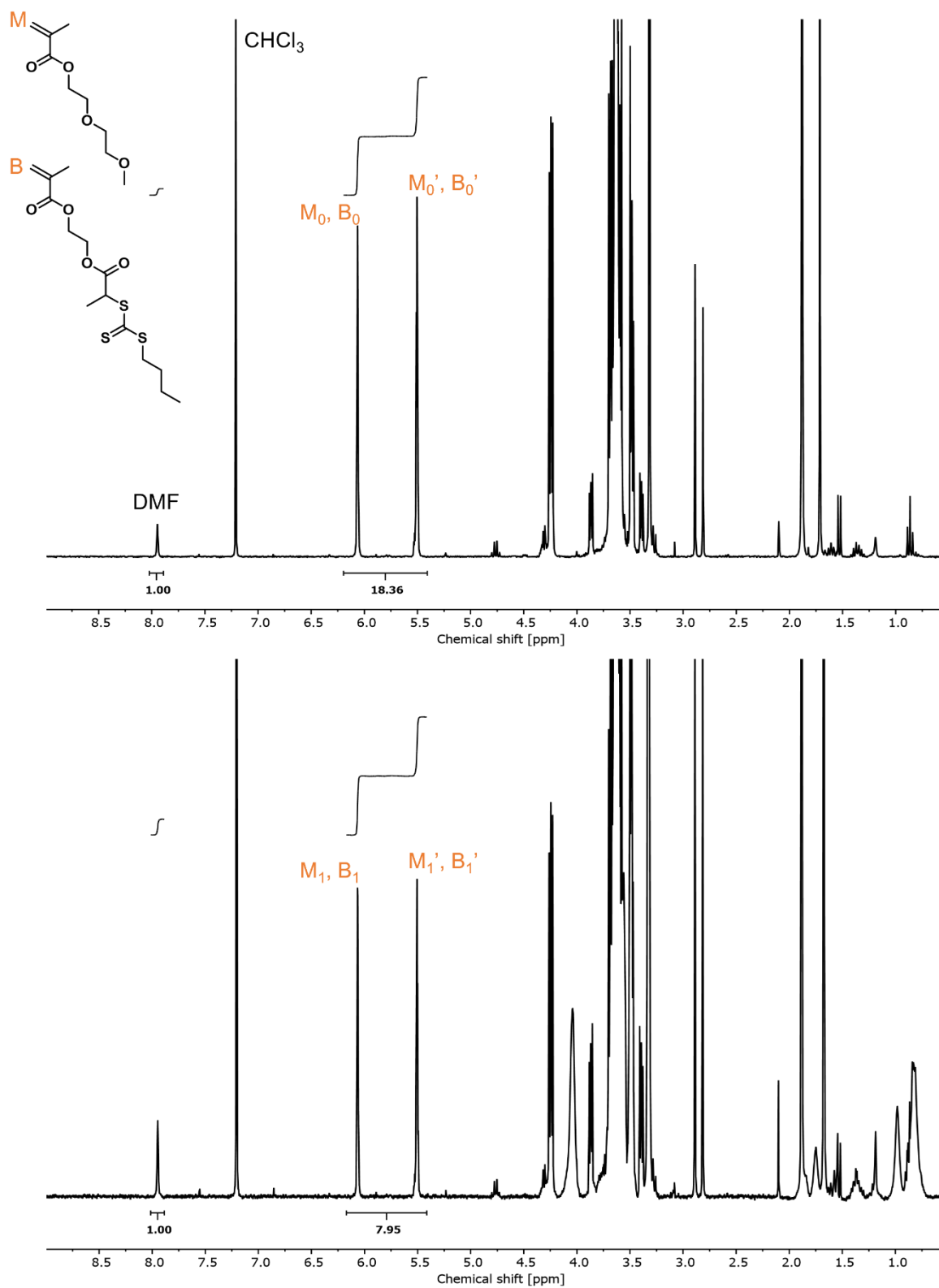


Figure S3. ¹H-NMR spectra of the reaction mixtures at the beginning of the polymerization (top) and the end of the polymerization (bottom). The protons used for the conversion calculation are assigned to the signals.

The total conversion (α) of MEO₂MA and BTPEMA was calculated through the decline of the proton signals from the monomers in the reaction mixture (**Figure S3**):

$$\alpha = \left(1 - \frac{I_{M_1+B_1} + I_{M_{1'}+B_{1'}}}{I_{M_0+B_0} + I_{M_{0'}+B_{0'}}} \right) \times 100\% \approx 57\% \quad (1)$$

The theoretical molecular weight of the random copolymer (backbone) can then be calculated as follows:

$$\bar{M}_{n,th} = \alpha \left(\frac{[MEO_2MA]_0}{[DiCTA]_0} M_{MEO_2MA} + \frac{[BTPEMA]_0}{[DiCTA]_0} M_{BTPEMA} \right) + M_{DiCTA} \quad (2)$$

[MEO₂MA]₀ and [BTPEMA]₀ are the initial concentrations of the monomers. [DiCTA]₀ is the initial concentration of DiCTA. M_{MEO_2MA} , M_{BTPEMA} , and M_{DiCTA} are the molecular weights of the monomers and DiCTA, respectively. The result is around 45.4 kDa.

2.2 Determination of the Molar Ratio between MEO₂MA and BTPEMA ($F_{M/B}$) in P(MEO₂MA-*r*-BTPEMA)

With the ¹H-NMR spectrum of P(M₂₁₅B₁₁) shown in **Figure S4**, the molar ratio $F_{M/B}$ can be estimated by the signal integrals I_A and I_B :

$$F_{M/B} = \frac{I_A/3}{I_B} \quad (3)$$

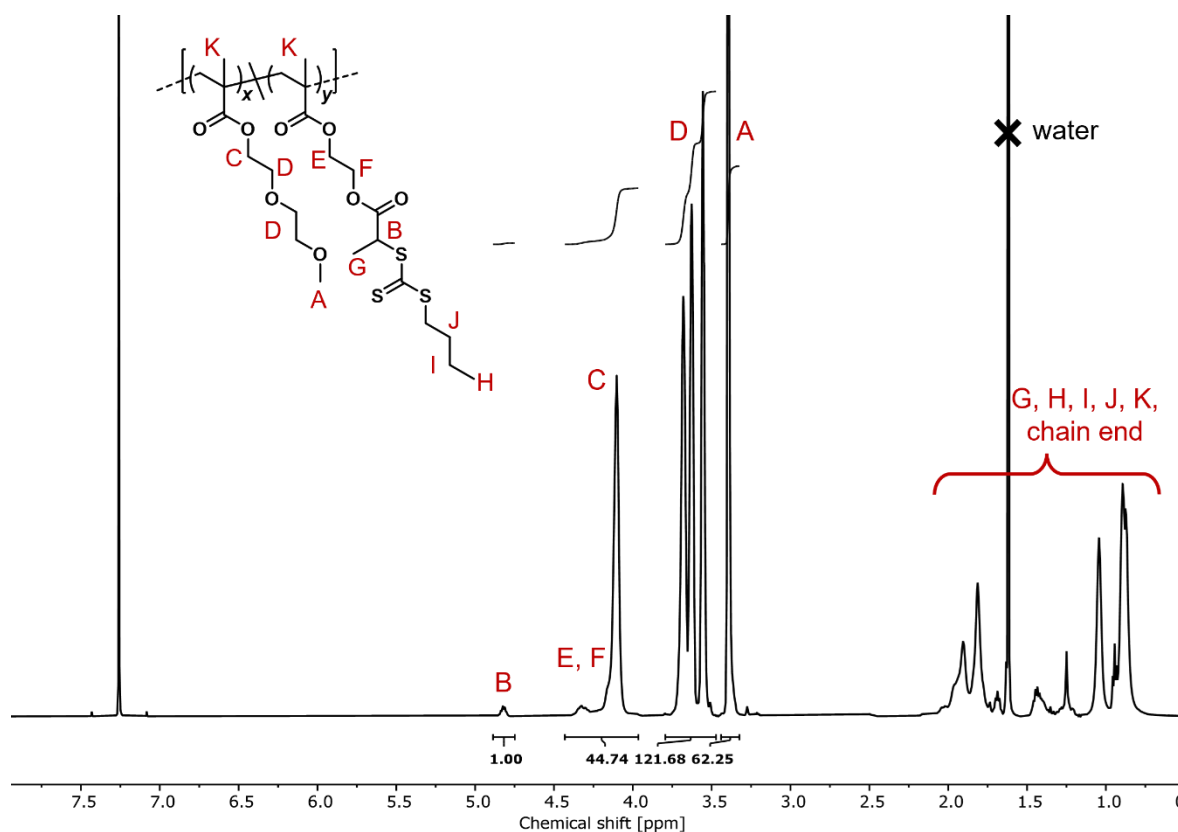


Figure S4. ¹H-NMR spectrum of P(M₂₁₅B₁₁) in CDCl₃ with the assignment of the proton signals (chain ends of the backbone are not shown here).

Table S1. Variation of $F_{M/B}$ with monomer conversion.

Monomer Conversion [%]	$F_{M/B}$
26	22/1
37	21/1
56	21/1
66	21/1
71	20/1

3. Polymerization of the Side Chains

3.1 SEC Curve of the Graft Copolymer

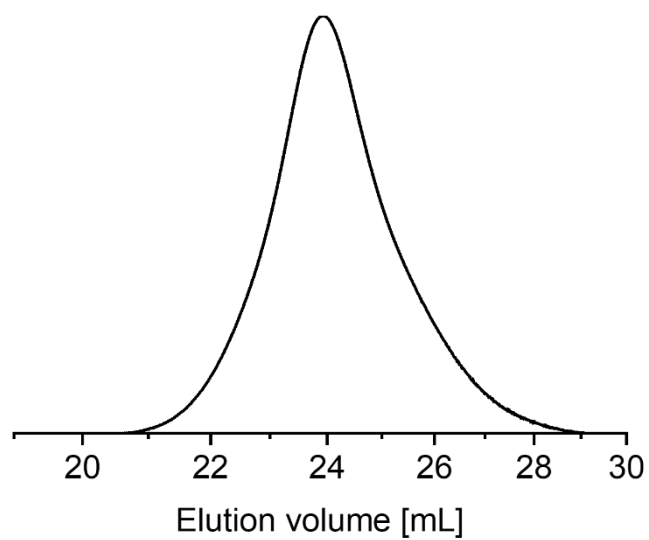


Figure S5. SEC curve of the graft copolymer ($\bar{M}_{n,SEC} = 59.4$ kDa, $D = 1.32$) measured with DMAc as the mobile phase.

3.2 Calculation of Conversion of DMA

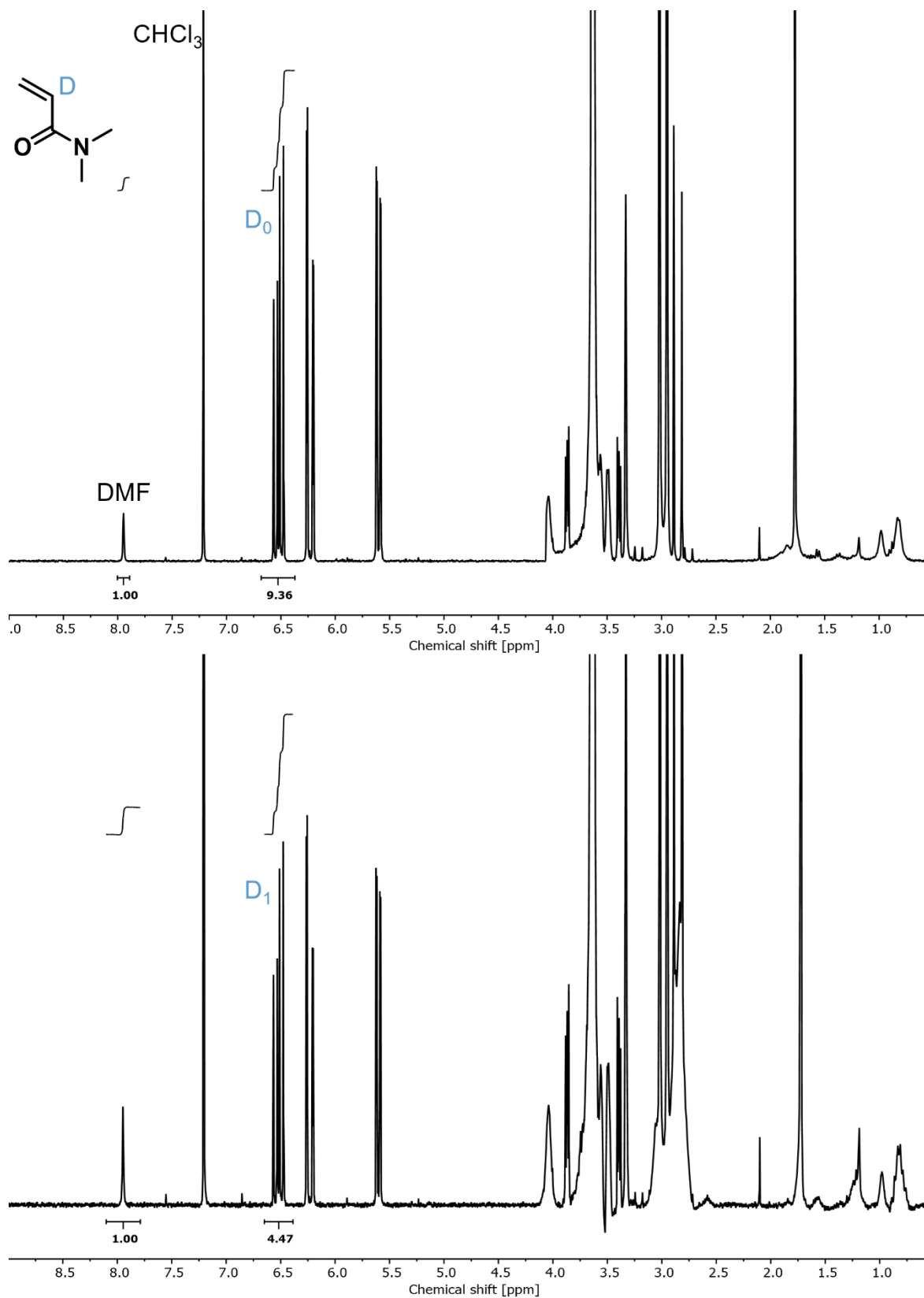


Figure S6. $^1\text{H-NMR}$ spectra of the reaction mixtures at the beginning of the polymerization (top) and the end of the polymerization (bottom). The proton used for the conversion calculation is assigned to the signals.

The conversion of DMA was also calculated through the decline of the proton signal from the monomer in the reaction mixture (**Figure S6**):

$$\alpha = \left(1 - \frac{I_{D_1}}{I_{D_0}}\right) \times 100\% \approx 52\% \quad (4)$$

The theoretical molecular weight of the graft copolymer can then be calculated as follows:

$$\bar{M}_{n,th} = \alpha \frac{[DMA]_0}{[backbone]_0} M_{DMA} + \bar{M}_{n,th(backbone)} \quad (5)$$

The result is around 85.6 kDa.

4. Turbidimetry

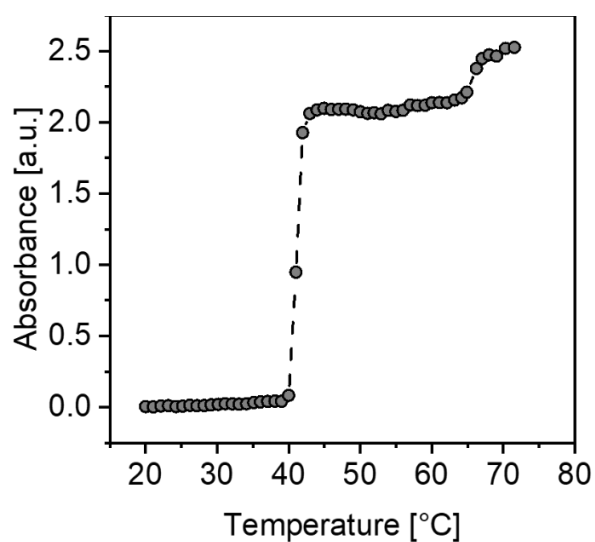


Figure S7. Result of turbidimetry of the $PM_{215}(PD_{31})_{13}$ aqueous solution.

5. Conversion of End-group Modification

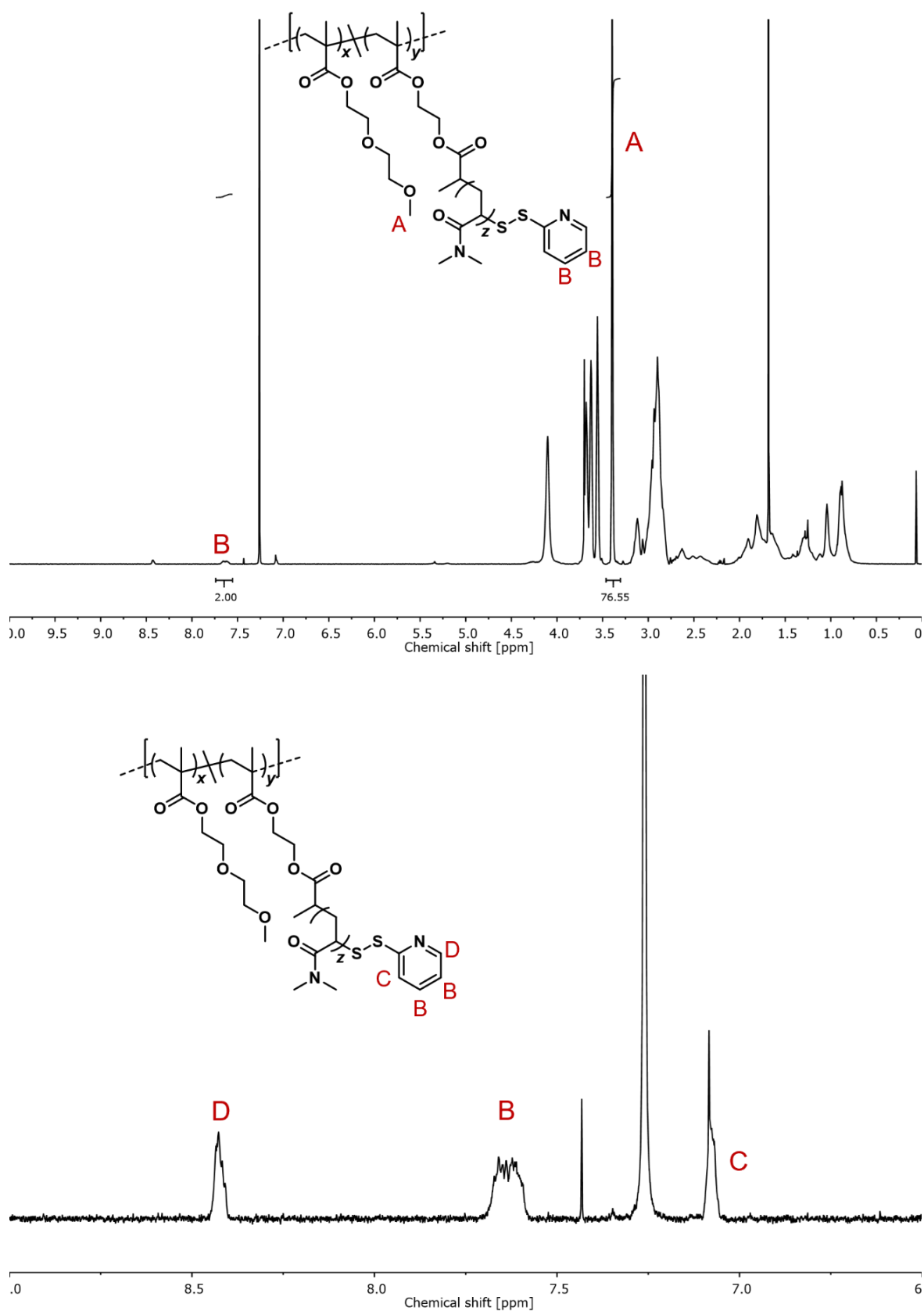


Figure S8. Top: $^1\text{H-NMR}$ spectrum of $\text{P(MEO}_2\text{MA-g-PDMA-PDS)}$ in CDCl_3 with the assignment of the proton signals (end-groups and PDMA blocks at α - and ω -terminals of the backbone are not shown here); bottom: enlarged image of the NMR measurement.

$$Conversion = 100\% \times \left(\frac{I_B/2}{I_A/3} \right) / \left(\frac{1}{19} \right) \quad (6)$$

where I_A and I_B are the signal integrals of MEO₂MA and PDS-group, respectively, 1/19 is the original molar ratio between BTPEMA and MEO₂MA.

6. Cumulant Approach for Evaluation of Dynamic Light Scattering (DLS) Data

After the DLS measurements, the obtained intensity correlation function ($g_2(\tau)$) was fitted with the following function:








$$g_2(\tau) = B + \beta \exp(-2\bar{\Gamma}\tau) \left(1 + \frac{\mu_2}{2!} \tau^2 - \frac{\mu_3}{3!} \tau^3 + \dots \right)^2 \quad (7)$$






where B represents the baseline, β means the stretching factor (contrast), $\bar{\Gamma}$ is the mean decay rate, μ_2 , and μ_3 are the cumulants. The hydrodynamic radius R_H was calculated through the Stokes-Einstein equation:






$$R_H = \frac{k_B T q^2}{6\pi\eta\bar{\Gamma}} \quad (8)$$

where k_B is the Boltzmann constant, T is the temperature, q is the scattering vector, and η is the viscosity.


7.5 Used Hazardous Substances According to GHS

substance	symbol	hazard statements	precautionary statements
acetone (Merck, 99 %)		EUH066, 225, 319, 336	210, 233, 240, 241, 242, 243, 264, 280, 303+361+353, 305+351+338, 337+313, 370+378, 403+235, 501
activated basic aluminum oxide (Merck, 99 %)		222, 229, 319, 336	210, 251, 305+351+338, 405, 410+412, 501
4-cyano-4- [(dodecylsulfanylthiocarbonyl)sulfanyl]pentanoic acid (abcr, 97%)		302	—
4-cyano-4- (dodecylthiocarbonothioylthio)pentanoate (abcr, 90%)		315, 319, 302	—
2-cyano-2-propyl dodecyl trithiocarbonate (abcr, 97%)		302	—
4-cyanopentanoic acid dithiobenzoate (abcr, 97%)		317	280
deuterated chloroform (Sigma Aldrich, 100%)		302, 315, 350, 373	201, 202, 260, 264, 280, 281, 301+312, 305+352, 308, 313, 321, 330, 332, 313, 362, 405, 501

substance	symbol	hazard statements	precautionary statements
deuterium oxide (Sigma Aldrich, 100%)	—	—	—
<i>N,N'</i> -dicyclohexylcarbodiimide (Sigma Aldrich, 99%)		302, 311, 317, 318	280, 301+312+330, 302+352+312, 305+351+338+310
di(ethylene glycol) methyl ether methacrylate (Sigma Aldrich, 95%)		315, 317, 319, 335	280, 302+352, 305+351+338
<i>N,N</i> -dimethylacrylamide (Sigma Aldrich, 99 %)		302, 312, 330	260, 304+340, 320, 330, 405, 501
4-(dimethylamino)pyridine (Sigma Aldrich, 99%)		301+331, 310, 315, 318, 370, 411	262, 273, 280, 301+310, 302+352+310, 305+351+338
<i>N,N</i> -dimethylformamide (Grüssing, 100%)		312, 319, 332, 360d	201, 202, 261, 264, 380, 381, 302+352, 304+340, 305+351+338, 308+313, 312+ 322, 337+313, 363, 405, 501

substance	symbol	hazard statements	precautionary statements
1,4-dioxane (Grüssing, 99%)		EUH019, EUH066, 225, 319, 335, 351	201, 202, 210, 240, 241, 242, 243, 261, 264, 280, 281, 303+361+353, 304+340, 305+351+338, 308+313, 312, 337+313, 370+378, 403+233, 403+235, 405, 501
2,2'-dithiodipyridine (TCI, 98%)	—	—	—
DL-dithiothreitol (TCI, 98%)		302, 315, 318	264, 270, 280, 301+312, 302+352, 305+351+338
ethanol (VWR, 99.8 %)		225	210, 233, 240, 241, 242, 243, 280, 303+361+353, 370+378, 403+235, 501
2,2'-(ethylenedioxy)diethanethiol (Sigma Aldrich, 95%)		301, 332, 410	261, 264, 270, 273, 301+310, 304+340+312
ethylene glycol (Merck, 99%)		302, 373	260, 264, 270, 301+312, 314, 501

substance	symbol	hazard statements	precautionary statements
<i>n</i> -hexane (VWR, 95%)		225, 304, 315, 336, 361f, 373, 411	201, 202, 210, 233, 240, 241, 242, 243, 260, 264, 273, 280, 281, 301+310, 302+352, 303+361+353, 303+313, 370+378, 391, 403+235, 405, 501
hexylamine (Sigma Aldrich, 99%)		226, 301+311, 314, 411	210, 273, 280, 303+361+353, 304+340+310, 305+351+338
hydrogen peroxide (VWR, 30%)		318, 412	273, 280, 305+351+338, 501
<i>N</i> -isopropylacrylamide (TCl, 98%)		302, 318	264, 270, 280, 301+312, 305+351+338, 501
methacrylamide (Sigma Aldrich, 98%)		302, 319, 335, 371, 373	260, 264, 270, 301+312, 305+351+338, 308+311
methyl methacrylate (Sigma Aldrich, 99%)		225, 315, 317, 335	210, 233, 240, 241, 280, 303+361+353
oligo(ethylene glycol) methacrylate (Sigma Aldrich)		315	264, 280, 302+352, 332+313, 362+364
silica gel (Macherey Nagel, 100 %)		373	260, 314, 501

substance	symbol	hazard statements	precautionary statements
tetrahydrofuran (VMR, 99.5%)		EUH019, 225, 319, 335, 351	201, 202, 210, 233, 240, 241, 242, 243, 260, 264, 280, 281, 302+352, 303+361+353, 304+340, 305+351+338, 308+313, 337+313, 370+378, 403+235, 405, 501

Chapter 8

Acknowledgements

In this chapter, I would like to thank all the people who gave me support and encouragement over the past years.

Many thanks to Volker Abetz for giving me the chance to start my Ph.D. study in the beautiful city of Hamburg. Under his supervision, I was influenced by his passion for science and always felt motivated. All the scientific discussions with him were delightful and provided me with meaningful suggestions. Meanwhile, he respected all my ideas, trusted me and gave me sufficient freedom of investigation arrangement. His rich experience also helped me learn a lot about the scientific community. Moreover, I cannot thank him enough for his support beyond the scope of science. Since 2020, the global pandemic has changed many things in this world. For me, 2021 was particularly challenging. I really appreciate that Volker was always there for me. Without his support and understanding, I could not have finished the Ph.D. work smoothly.

I would also like to thank Horst Weller for agreeing to become the second referee of this dissertation very quickly. I sincerely appreciate the time he spends evaluating this work.

I show my gratitude to Sigrid Zeckert for her highly efficient support in appointment management and other administrative affairs. I am thankful to Felix Lauterbach for inspiring discussions and teaching me DLS measurement at the beginning of this work. His program for evaluating DLS results is an essential tool for all my publications. Many thanks to Tilman Eckert for teaching me photoiniferter RAFT and discussing with me about thermoresponsive polymers. I am furthermore grateful to Birgit Hankiewicz for teaching me SLS measurement patiently and showing me CONTIN analysis.

I am genuinely grateful to the NMR team of the Chemistry Department of Universität Hamburg for a large number of measurements. I am thankful to Martin Kehden for timely SEC measurements and chemical purchases.

Special thanks to the members of office 363, Tilman Eckert and Philipp Haida. Their company made me never feel alone during my study and kept me thinking positively even in challenging times. Additionally, sharing the laboratory with Philipp was pretty relaxing all the time. I would also like to thank Iklima Oral, who is always kind and available for suggestions and discussions.

I am truly thankful to Tilman Eckert, Siraphat Weerathaworn, Sabrina Tamm, Sascha Lemich, Philipp Haida, and Iklima Oral for reading this dissertation before submission and giving me valuable comments and advice.

I would like to express my deep appreciation to all my other present and former coworkers in the Abetz group. Andreas Meyer, Niklas Lucht, Stephan Hinrichs, Margarethe Fritz, Florian Klein, Merlina Thiessen, Maria Weißpflog, Melanie Benken, Ulf König, they were wonderful to me from the first day and always willing to offer help. It was an honor for me to work with them.

I appreciate Universität Hamburg for the financial support during this Ph.D. study.

Last but not least, I would like to thank my family members who constantly gave me solid mental support, even though they were physically very far from me. Their understanding and comfort allowed me to calm down and stay focused on what I was doing. I express my best thanks to my mother, SUN Jingfang. Although you left this world in 2021, your selflessness, kindness, optimism, courage, and diligence will keep inspiring me. You also taught me how to face reality and take things rationally. I will always keep you in my heart.

Chapter 9

Declaration on Oath

I hereby declare on oath, that I have written the present dissertation by my own and have not used other than the acknowledged resources and aids. The submitted written version corresponds to the version on the electronic storage medium. I hereby declare that I have not previously applied or pursued for a doctorate (Ph.D. studies)

09.05.2022, Hamburg

Jingcong Xu
